BIOCHEMICAL, GENETIC AND GENOMIC APPROACHES TO STUDYING SULFUR METABOLISM BY THE HYPERTHERMOPHILIC ARCHAEON *PYROCOCCUS FURIOSUS*

by

STEPHANIE LOUISE BRIDGER

(Under the Direction of MICHAEL W. W. ADAMS)

ABSTRACT

The availability of a highly efficient genetic system in the model hyperthermophilic archaeon, *Pyrococcus furiosus*, has greatly improved our ability to study its physiology and metabolism. This work describes the genome sequencing of the genetically-tractable strain of *P. furiosus*, COM1, and the characterization of deletion strains of key sulfur responsive proteins, namely NSR1, MBX1, and SIP1. The COM1 genome revealed a surprisingly large number of changes compared to that of the *P. furiosus* NCBI reference sequence, including chromosomal rearrangements, deletions, and single base changes in both coding and potential regulatory regions. However, in spite of all the genomic changes only a few phenotypic differences could be observed in COM1 compared to its parental strain. COM1 was used to generate deletions of the genes encoding for the cytoplasmic NADPH-dependent coenzyme-A sulfur oxidoreductase (NSR), the membrane-bound oxidoreductase (MBX) and the sulfur-induced protein A (SipA). Characterization of NSR1 revealed a non-essential role for NSR in S^0 reduction, unlike MBX, which was shown to play a critical role in S^0 reduction and energy conservation. Transcriptional analyses revealed a probable role for NSR in maintaining the thiol-redox balance of the cell and modulating the activity of the redox-dependent S^0-response regulator, SurR.

INDEX WORDS: Archaea, *Pyrococcus furiosus*, metabolism, elemental sulfur, sulfide, CoA, CoA disulfide, redox, NSR, MBX, SipA, SurR, COM1, competence, genome sequencing, IS elements, DNA microarray.

BIOCHEMICAL, GENETIC AND GENOMIC APPROACHES TO STUDYING SULFUR METABOLISM BY THE HYPERTHERMOPHILIC ARCHAEON *PYROCOCCUS FURIOSUS*

by

STEPHANIE LOUISE BRIDGER

B.S., North Carolina State University, 2003

A Dissertation Submitted to the Graduate Faculty of The University of Georgia in Partial Fulfillment of the Requirements for the Degree

DOCTOR OF PHILOSOPHY

ATHENS, GEORGIA

2012

BIOCHEMICAL, GENETIC AND GENOMIC APPROACHES TO STUDYING SULFUR METABOLISM BY THE HYPERTHERMOPHILIC ARCHAEON *PYROCOCCUS FURIOSUS*

by

STEPHANIE LOUISE BRIDGER

Major Professor: Michael W. W. Adams

Committee: Michael K. Johnson
Robert J. Maier
William N. Lanzilotta

Electronic Version Approved:

Maureen Grasso
Dean of the Graduate School
The University of Georgia
May 2012

DEDICATION

To my grandmother, Grammie, I know you would have loved to have seen me graduate.

Thank you for all you taught me about life, love, and independence.

You are greatly loved and missed.

ACKNOWLEDGEMENTS

First, I would like to acknowledge and thank all of the people who have contributed to my personal and scientific development both prior to, and during my graduate career in the Biochemistry and Molecular Biology Department at the University of Georgia. Without your guidance and/or support the work presented herein would not have been possible.

A special thanks to my major professor, Dr. Mike Adams, for the outstanding opportunity, advice and direction you have given me throughout this process and to my committee members, Drs. Rob Maier, Mike Johnson, and Bill Lanzilotta for their assistance. I would also like to acknowledge my undergraduate mentor and teacher, Dr. Bob Kelly at North Carolina State University, for the biotech research and teaching experiences he provided me and for encouraging me to go to graduate school. Other former teachers who helped inspire my interests in science and math were my organic chemistry professor at N.C. State, Dr. Kay Sandberg, and my Sanderson High School teachers Sharon Cooke (physics) and June Blackwell (mathematics).

To the members of the Adams lab, you guys are the best!!! Thank you for the countless hours you spent with me, whether it was at the bench sharing your practical knowledge and expertise in experimental design or techniques, in the coffee room in discussing science and/or providing support and encouragement when experiments were not going well, or teaching me how to use computer programs! You all have, in one way or another, contributed to the work described in the chapters that follow. Particular recognition goes to: Gerti Schut, Farris Poole, Angeli Mennon, Andrew Lancaster, Gina Lipscomb, Sonya Clarkson, Chris Hopkins, Corey Smith, Matt Keller, Sanjeev Chandrayan, Michael Thorgersen, Mirko Basen and Bret Dillard.

Also, special thanks to Peter Horanyi and Jeff Habel (Wang lab) for helping me with experiments and projects during my first years of grad school!

Lastly, but perhaps most importantly, I would like to thank my family and friends, who have played an essential role in keeping me motivated throughout this very long process. To my Mom and Dad, thank your unwavering love and support, without you none of this is possible. To my brother and good friend, Rob, I am so lucky to have you in my life. You encourage, support, and challenge me every day, thank you! Also, to my Uncle Johnny and Aunt Janet, thank you for keeping up with me and checking in to see how things were going. To my most wonderful and supportive boyfriend, Robert, I am extremely grateful to have you in my life. I know you only got to see the end of this long journey and had to endure all the long hours that went into the completion of this work, but I thank you for always listening, even when you had no idea what I was talking about, and for taking such good care of me. To my friends, scientific and otherwise, thank you for always making me laugh and for reminding me that there is a life outside of science! Special recognition goes to: Teresa Pieper, April Harper, Andrea Lafera, Kathy Perry, Eric Kaufman, Jarrod Barnes, Joey Farkas, Peter and Lisa Horanyi, Quentin Florence, Jeff Habel, and Brian Spencer.

TABLE OF CONTENTS

LIST OF TABLES

Page

LIST OF FIGURES

Page

CHAPTER 1

INTRODUCTION AND LITERATURE REVIEW

Archaea were first discovered in 1977 by Carl Woese and colleagues (96) at the same time fundamental methods for sequencing nucleic acids emerged (32). Woese constructed an evolutionary tree of life based on small-subunit ribosomal RNA (rRNA) sequences that divided organisms into three distinct domains: the bacteria, the eukaryotes, and the archaebacteria (now called archaea) (96, 97). In contrast to eukaryotes, both bacteria and archaea are prokaryotes, cells lacking a nucleus or other organelles; however, the phylogenetic tree reveals a closer relationship between archaea and eukaryotes than bacteria (Figure 1.1).

Archaea have many unique properties and harbor a mosaic of bacterial and eukaryotic traits. Unique archaeal features include but are not limited to their ability to thrive at temperature above 95°C (33), a membrane structure containing isoprenoid tetraether lipids (70), and a lack of any discovered chlorophyll based photosynthesis. Similarities with bacteria include: morphology (33), genome organization (33), mechanisms of gene regulation (35), and the majority of operational proteins such as metabolic enzymes, membrane receptors, and transporters (52). In contrast, nearly all informational proteins involved in DNA replication, transcription and translation are more similar to eukaryotic species (10, 14, 35).

Over the past three decades an enormous amount of interest has surrounded the study of archaea, their evolutionary history, cellular machinery, and metabolic diversity. Archaea are renowned for their love of extremely harsh habitats including: high-salt (halophiles), high and low pH (alkaliphiles and acidophiles), and high and low temperatures (hyperthermophiles and psychrophiles) (33); however recent environmental analyses of microbial diversity have revealed that archaea are surprisingly abundant in ‘normal’ environments including waters and

soils (79). Technological advances in microbial cultivation, molecular biology, whole genome sequencing, comparative genomics, and the development of reverse genetics tools for targeted gene mutations have greatly improved our understanding of these fascinating microorganisms and revealed numerous industrial applications for their robust enzymes.

ARCHAEA

Phylogeny.

Based on 16S rRNA the archaeal domain is split into two major phyla, the Euryarchaeota and the Crenarchaeota (97). The Euryarchaeota are named after a Greek word meaning wide, for having the greatest phenotypic diversity including methanogens, halophiles, and some thermoacidophiles and hyperthermophiles (including *Pyrococcus furiosus*, which will be the focus of the next section). The Crenarchaeota were originally named due to their more limited detection in hyperthermophilic ($\geq$ 80°C) environments after the Greek word meaning spring (33). This was based on the hypothesis that the Last Universal Common Ancestor (LUCA) was a hyperthermophile. Since then, Crenarchaeota have been detected in numerous environmental samples and estimated to account for nearly 20% of the marine picoplankton worldwide (43). Shortly after the genomics revolution began, a third phylum, the Korarchaeota, was suggested to include a large group of environmental sequences that branched between that of the Euryarchaeota and Crenarchaeota (8). More recently, sequencing of addition environmental isolates has lead to the proposal of two more main phyla, the Thaumarchaeota and 'Aigarchaeota' (19). Thaumarchaeota have been found to be quite abundant in freshwater, soil, ocean, and hot spring environments and some of their members are capable of ammonia oxidation (75), which was previously thought to be restricted to bacteria (85).

Cell Structure/Machinery.

Archaea can be difficult to distinguish from bacteria because their shapes and sizes are quite similar; however some archaea have morphologies not found in bacteria including: the square

shaped euryarchaeon *Haloarcula* and the irregular cocci in some hyperthermophiles such as the crenarchaeon *Pyrodictium abyssi*.

The outermost cell wall component of all archaea and many bacteria is termed the surface layer (S-layer). The S-layer is typically composed of a single protein or glycoprotein species whose subunits self-assemble into large two-dimentsional crystalline lattices of which up to 70% is composed of pores between the sizes of 2-8 nm (5, 30, 48, 87). Post-translational modifications are known to occur in S-layer proteins, including phosphorylation, sulfonation, and glycosylation of amino acid residues (29). The biological importance of the S-layer is thought to be environment specific and it has been shown to function as a structural scaffold, a molecular sieve, and a matrix for the anchoring of exoenzymes (30, 48). In archaea the S-layer is anchored to the cytoplasmic membrane by prenyl-groups or transmembrane domains, and presumably act to immobilize lipids and proteins (5).

The cytoplasmic membrane functions as a selective barrier between the cytoplasm and the external environment, which controls the movement of solutes (ions and nutrients) into or out of the cell (51). The permeability of the membrane is restricted due to the need for specific transporters required for the transfer of hydrophilic solutes (or ions) from the aqueous phase through the apolar interior of the membrane (5). Bacterial and eukaryotic membranes contain lipids in which two acyl chains are linked to glycerol via ester bonds and are organized in a bilayer. In contrast, archaeal membranes contain predominantly ether lipids in which fully saturated isoprenoid chains are ether-linked to glycerol or another alcohol (49). These tetraether lipids span the membrane giving it a monolayer type of organization (5, 38, 49). Membrane proteins embedded in lipids account for up to 60% (w/w) of the mass of prokaryotic membranes and are involved in energy transducing processes and solute transport systems.

A typical archaeal genome consists of a single circular DNA molecule of approximately 1-3 mega base pairs (Mb) (17). Similar to that of bacteria, genes are clustered into operons and are coexpressed as polycistronic transcripts. A few examples of eukaryotic-like introns have

been reported in archaeal lineages. In addition to chromosomal DNA, plasmid DNA has been reported in all groups of the hyperthermophilic archaea (17). Most of the Euryarchaeota (including *Pyrococcus*) contain homologues of eukaryotic histones H3 and H4, which are small DNA-binding proteins that compact genomic DNA (6). These histones are distinct from that of eukaryotes in oligomeric structure (tetramers compared to octamers, respectively), they bind less tightly, and they lack the N-terminal and C-terminal 'tails' that are targets for methylation, acetylation, and phosphorylation in eukaryotes (6). This suggests that chromatin remodeling is not used as a mode of gene regulation in archaea (77).

Archaeal information systems (DNA replication, recombination and repair, transcription, and translation) are far more complex than bacteria, but yet simplified versions of eukaryotic systems. In *Pyrococcus* species, the origin of replication has been found to be highly conserved with clusters of eukaryotic-like DNA replication genes around it (73). However, despite harboring eukaryotic DNA replication machinery, *Pyrococcus* species replicate their chromosome bi-directionally like bacteria (73). Proteins that catalyze homologous recombination and double-stranded break repair have been well studied in archaea including Mre11, Rad50 and RadA which are conserved between archaea and eukaryotes, and Hjc, NurA and HerA which are unique to archaea (95). The core archaeal transcription machinery is also eukaryotic-like and consists of a RNA polymerase (RNAP) II-like transcriptase and two transcription initiation factors, TATA-binding protein (TBP) and transcription factor B (TFB) (13). However, the majority of known archaeal transcriptional regulators are more similar to that of bacteria (35). The core translational machinery in archaea (rRNAs) is also eukaryotic in nature and translation initiation uses methionine instead of N-formylmethionine like bacteria (6).

Genome Evolution.

The mechanisms of chromosome structure and evolution in archaea are still being explored; however, they are thought to be similar to that of bacteria due to the high degree of resemblance between their genome organizations. However, most bacterial and archaeal

genomes exhibit no synteny and very little conservation in their gene order. This observation is in agreement with rapid genomic evolution by recombination (41). DNA replication has been linked to constrictions in chromosomal rearrangements observed among both bacteria and archaea. In bacteria, the terminus of DNA replication is known to be a hot spot for recombination (69), as was shown for two *Pyrococcus* species, *P. abyssi* and *P. horikoshii*. The main rearrangement between the two *Pyrococcus* genomes occurred symmetrically to the axis formed between the origin and the terminus of replication (99). In addition to these genome rearrangements, recombination events have been linked to insertion sequence (IS) elements in several archaeal genomes (20).

Insertion sequences are small (<2.5-kb) simple, and self-directed segments of DNA capable of inserting at multiple sites in a target molecule (67). IS elements were initially identified during studies of model bacterial genetic systems by their ability to generate mutations as a result of their translocation. Now studied in prokaryotes and eukaryotes alike, IS elements have been shown to play key roles in genome evolution and organization by participating in the acquisition of accessory genes, plasmid integration, and chromosome rearrangements (67). IS elements are especially abundant in *S. solfataricus* and *Halobacterium* NRC1 (27). Comparison of three Pyrococcus species suggests that a family of IS elements, only present in *P. furiosus*, has been involved in most chromosomal rearrangements observed (55, 66). In *Pyrococcus* and *Sulfolobus*, chromosomal rearrangements linked to IS element occur preferentially in the limit of one replichore (the half chromosome comprised between the origin and terminus of replication), suggesting a principle of genome organization that is not yet understood (20, 99).

Genetics.

The ability to make genetic manipulations significantly contributes to our ability to study the physiology and metabolism of any model organism. Developing genetics systems in archaea has been particularly challenging due not only to extreme growth requirements, but also the lack of selectable markers (59). Typical antibiotic selection strategies used in bacteria are mostly

ineffective due to the differences in molecular informational systems as described above. In addition, for hyperthermophiles, the instability of drugs at high temperatures is also a problem. However, despite these technical difficulties genetics systems have been developed for representatives of all major groups of archaea (59) (Figure 1.2). One of the first archaeal hyperthermophiles for which genetic manipulations were reported was a close relative of *P. furiosus*; *Thermococcus kodakarensis (83)*, and based on this model a genetics system has recently been developed for *P. furiosus* (62). The following chapters will describe studies on *P. furiosus*, specifically chapter 2 will describe the genome sequencing of the recently selected genetically-tractable strain of *P. furiosus* and the involvement of IS elements in its genome evolution, and chapters 3 and 4 will focus on understanding the mechanism by which *P. furiosus* utilizes elemental sulfur as a terminal electron acceptor in anaerobic respiration through the biochemical characterization of targeted gene knockouts and transcriptional analyses. The next section of this chapter will introduce *P. furiosus*; describe how its genetics system was developed and what is known about how sulfur influences its metabolism.

PYROCOCCUS FURIOSUS

Pyrococcus furiosus is a member of the well-studied branch of the Euryarchaeota, the *Thermococcales*, and was one of the first hyperthermophiles to be discovered (31). It was originally isolated by Karl Stetter and coworkers off the coast of Vulcano Italy from the sediments of a shallow marine hydrothermal vent. As shown in Figure 1.3, *P. furiosus* is coccoid in shape, possesses monopolar flagella, and ranges in size from 0.8 to 2.5 μm in diameter. *P. furiosus* is an anaerobic heterotrophic hyperthermophile that grows optimally at 100°C and is capable of utilizing a wide range of poly- and oligosaccharides and peptides as carbon sources for growth. Since its discovery *P. furiosus* has become a model organism in the hyperthermophilic archaea and extensive work has been done to elucidate its biochemical pathways (1-4). *P. furiosus* was the first *Pyrococcus* species to have its genome sequenced

(78), and since the genome sequences of four other closely related species have become available (25, 42, 44, 56), thus enabling comparative genomic analyses (22, 55, 99). Also, a whole genome DNA microarray is available for *P. furiosus* (88-91, 94), allowing genome-wide transcription analyses under different growth conditions. The most recent advancement in the study of this model hyperthermophile is the ability to make genetic manipulations. During the process of developing this genetic system for *P. furiosus* a variant in the lab strain population was discovered that is highly efficient for the uptake and recombination of exogenous DNA (62). This genetically-tractable strain, COM1, has therefore become the new platform for which future studies including gene knockouts, overexpression strains, and the development of additional genetic tools will be based. Therefore it is critical to define this new strain at the chromosomal level for anticipated molecular manipulations. In the following, Chapter 2 describes the genome sequencing of COM1 and discusses differences compared with the *P. furiosus* reference genome (NCBI).

Development of Genetic System (COM1).

As shown in Figure 1.4, two selection strategies were used to generate a targeted gene knockout of a uracil biosynthetic enzyme, orotidine-5'-monophosphate (OMP) decarboylase (*pyrF*; PF1114) in *P. furiosus*. First, the thermostable drug, simvastatin, was used to select for integration of a *pyrF* deletion plasmid (based on homologous recombination within a 1-kb region up- or downstream) at the *pyrF* locus on the *P. furiosus* chromosome by overexpressing a key enzyme in the biosynthesis of isoprenoid membrane lipids, 3-hydroxy-3-methylglutaryl coenzyme A (HMG-CoA) reductase (under the control of the glutamate dehydrogenase (*gdh*) promoter), which confers resistance to simvastatin (53, 71). Counterselection for removal of plasmid DNA and deletion of the *pyrF* gene was obtained by a second selection strategy using a pyrimidine analog, 5-fluoroorotic acid (5-FOA), which is converted to a toxic product (fluorodeoxyuridine) in cells with a wild-type *pyrF* gene (16, 83). Remarkably, the transformation frequency of the resulting strain (Δ*pyrF*) was orders of magnitude higher than in

the wild-type strain and was thus named COM1, for competent strain (62). In addition to uptake of circular plasmid DNA, the same competence was observed with linear DNA. It is unknown what changes in COM1, whether it is in DNA uptake, homologous recombination, or a yet unknown mechanism, confer this dramatic difference in transformation efficiency (62).

The COM1 strain has now been used to generate markerless deletion mutants of the *P. furiosus* cytoplasmic hydrogenases (SHI and SHII; (62)) and an overexpression strain of a catalytically-active sub-complex of *P. furiosus* hydrogenase has been generated that produces approximately 100 times the level of native hydrogenase with an affinity tag for rapid protein purification (40). In addition, a more robust genetics method has been developed that allows for selection on complex growth media for agmatine auxotrophy, which has been used to generate a tagged version of the native cytoplasmic hydrogenase (21). In the following, Chapter 3 describes the construction and characterization of three deletion strains generated to study the metabolism of sulfur by *P. furiosus*.

Sugar Metabolism.

As introduced, *P. furiosus* is capable of utilizing a wide range of poly- and oligosaccharides as carbon sources for growth and produces organic acids (primarily acetate), carbon dioxide (CO_2), hydrogen (H_2), and small amounts of alanine and ethanol (24, 31, 84). These sugars include, but are not limited to, disaccharides (maltose and cellobiose; (50, 93)) and complex carbohydrates (starch, chitin and laminarin; (34, 50, 93)), but not monosaccharides (glucose). Degradation of these different α- and β-linked sugars is accomplished via several intracellular and extracellular enzymes including: α-amylases, amylopullulanase, cyclodextrin glucanotransferase, β-glucosidases, β-galactosidase, β-mannosidase, endo-β-1,3-glucanase and so on (9, 28, 36, 47, 57, 93). So far three ATP-binding cassette (ABC) sugar transporters have been characterized in *P. furiosus* and include: maltose/trehalose transporter (Mal-I), maltodextrin transporter (Mal-II), and the cellobiose transport system (CBT). The degradation of glucose to acetate occurs via a modified Embden-Meyerhof glycolytic pathway (80, 81, 92).

The hexokinase and phosphofructokinase enzymes in this pathway are ADP- rather than ATP-dependent compared to typical EM pathways (46). The classical glycolytic enzymes, glyceraldehyde-3-phosphate dehydrogenase (GAPDH) and phosphoglycerate kinase (PGK), are replaced by a single ferredoxin-linked enzyme, glyceraldehyde-3-phosphate ferredoxin oxidoreductase (GAPOR) (72). This converts glyceraldehyde-3-phosphate to glycerate-3-phosphate without the generation of ATP via substrate-level phosphorylation. The other oxidation step in the conversion of glucose to acetate is also coupled to the reduction of ferredoxin (Fd), and is catalyzed by pyruvate ferredoxin oxidoreductase (POR) (15). Therefore, ATP (2 per mol glucose) is only generated in the final step by the two acetate producing acetyl-CoA synthetases (ACS I & II; (68)). Consequently, all of the reductant is generated in glycolysis is reduced Fd, and no NADPH is formed. As shown in Figure 1.5, this reduced Fd then serves as the electron donor for the membrane-bound hydrogenase (MBH), which evolves H_2 in an energy-conserving manner via a proton motive force (82).

During growth on sugars, *P. furiosus* is a facultative sulfur reducer and can utilize elemental sulfur as a terminal electron acceptor in anaerobic respiration, producing H_2S instead of H_2 (1, 31, 89). Its ability to grow well in both the presence and absence of sulfur on maltose is somewhat unique among archaeal hyperthermophiles and therefore is why *P. furiosus* is a good platform for studying the effects of sulfur on metabolism.

Sulfur Metabolism.

Sulfur can be found in a range of valance states from the highly reduced sulfide (-2) to the most oxidized form sulfate (+6), and can act as an electron donor for oxidation or an electron acceptor for reduction in biology (39, 86). Sulfur forms highly covalent bonds and little energy exchange is involved going from an electrophile as in a disulfide, to a nucleophile as in a thiol. Thus sulfur makes and breaks bonds easily (11, 39). Elemental sulfur (S^0) is an insoluble yellow powder that predominates in the form of an 8-membered ring and can be hydrothermally formed as an oxidation product of sulfide weathering or biologically formed as a product of

sulfide oxidation by microorganisms (39, 86). Sulfide is present in a variety of forms, as bisulfide ion (HS^-) at neutral pH, as sulfide ion (S^{2-}) at alkaline pH, and as hydrogen sulfide (H_2S) at low pH. H_2S is the only form that is volatile and has a characteristic rotten egg smell. Dissolved sulfides react strongly with base and transition metal ions to form insoluble sulfide minerals, the most prominent of which are iron sulfides that make anoxic sediments black (11, 86). The solubility of S^0 in water at 25°C is very low (5μg l^{-1}) and at higher temperatures is not known, however, probably considerably higher than at 25°C. Polysulfide is formed by dissolving S^0 powder in an aqueous sulfide solution as shown in the reaction below (39):

$$nS^\circ + HS^- \rightarrow S^{2-}_{n+1} + H^+$$

The S_8-ring is cleaved by a nucleophilic attack of the HS^- ion, where the maximum amount of S^0 that can be dissolved is nearly equivalent to the sulfide concentration (11). Therefore, in the hydrothermal environments where the concentration of exogenous sulfide is high, the amount of polysulfide and colloidal sulfur (solid S^0 in suspension) present is at a constant equilibrium.

In *P. furiosus* S^0 reduction, like H_2 production, has been proposed to be a mechanism for disposing of excess reductant (31, 84); however, it is not known if S° reduction is an energy conserving process like H_2 production (82). The S^0 reduction system of the mesophilic bacterium *Wolinella succinogenes* is generally accepted as a model system for anaerobic S^0 respiration in which H_2S production is coupled to energy conservation (39). *W. succinogenes* uses H_2 or formate as the electron donor and their oxidation is linked through cytochrome *b* and quinones to a membrane bound, molybdopterin-containing sulfur reductase (26). A similar S^0-reducing respiratory system has been characterized in other autotrophs, including the hyperthermophilic bacterium *Aquifex aeolicus* (37) and the hyperthermoacidophilic archaeon *Acidianus ambivalens* (54), and it appears to be present in the H_2-oxidizing hyperthermophilic archaea, *Pyrodictium brockii* (76) and *Pyrodictium abyssi* (45). However, S° reduction by heterotrophic hyperthermophiles, such as *P. furiosus*, is poorly understood and proceeds via a

different mechanism of S^0 reduction than that found in the autotrophic species. *Pyrococcus* genome sequences do not contain obvious homologs of the molybdenum-containing sulfur reductase of *W. succinogenes* or *A. ambivalens* (7), and there are also no reports of the presence of quinones or cytochromes in these organisms. Three enzymes from *P. furiosus* have been previously reported to possess S^0 reductase activity *in vitro* including the two cytoplasmic hydrogenases (64) and a sulfide dehydrogenase (65). However, both the activity and the expression of the two hydrogenases dramatically decreased in cells grown in the presence of S^0 (1, 90). Similarly, the sulfide dehydrogenase is now thought to function *in vivo* as a ferredoxin:NADPH oxidoreductase (FNOR) (63), and the expression of its gene is related to the carbon source rather than S^0 (88). Consequently, none of these three enzymes are likely to play a role in S^0 reduction *in vivo*.

Transcriptional Regulation of Hydrogen and Sulfur Metabolism.

As mentioned earlier, the basal transcriptional apparatus in archaea is eukaryotic-like however most archaeal regulatory transcription factors characterized so far are bacterial-like repressors and only a few activators are known (35). Some archaeal regulatory factors have been shown to be regulated by small effector molecules including: metal ions such as Fe^{2+}, Mn^{2+}, or Ni^{2+} (Mdr1 of Archaeoglobus fulgidus; (12)), amino acids such as lysine (LysM of Sulfolobus solfataricus; (18)), metabolic intermediates such as 2-oxoglutarate (NrpR of Methanococcus maripaludis; (60)), and various sugars including: maltose, trehalose, sucrose, maltodextrin, and glucose (TrmB and TrmB-like of *P. furiosus*; (58)). Recently the first example of an archaeal redox-responsive transcriptional regulator was discovered in *P. furiosus*, SurR, and has been shown act both as an activator and repressor, controlling hydrogen and S^0 metabolism (Figure 1.6) (61, 98).

The S^0 response regulator, SurR, was initially discovered following a transcriptional study on the affects of S^0 addition to *P. furiosus* (see Appendix A for full details; (89)) which identified a set of primary S^0 response genes that appeared to be intimately involved with both

H_2 and H_2S production. The operon encoding the H_2-evolving membrane-bound hydrogenase (MBH) was shown to be dramatically down-regulated within ten minutes of S^0 addition (89) and was therefore chosen as the target for transcription factor discovery in *P. furiosus* (61). Utilizing ~200 bp of the MBH promoter and ~100 bp of the first ORF in the operon, *mbh1* (PF1423), as bait, the SurR protein was captured in a DNA-affinity assay from S^0-grown cell extracts and has since been elegantly characterized at the molecular and structural level. SurR is a sequence-specific DNA-binding protein that recognizes the consensus motif $GTTn_3AAC$ (and additional extended motifs) and can both activate and repress transcription depending on the position of the SurR binding site relative to the basal transcriptional elements. Structural studies showed that SurR contains winged helix-turn-helix (HTC) DNA-binding domains and a CxxC motif adjacent to the recognition helix. Oxidization of the cysteine residues caused a conformation change which disrupted the typical tri-helical bundle of the HTH domain and prevented DNA-binding *in vitro* (98). In addition, the DNA-binding ability of SurR was shown to be reversible, where oxidation by colloidal S^0 (100-500 μM) completely eliminated sequence-specific binding and excess of the reductant DTT almost completely reversed the effect *in vitro* (but not the reductants cysteine, sodium dithionite, and sodium sulfide). Therefore, the CxxC motif in SurR represents a regulatory redox switch comparable to those described in bacteria (OxyR of *Escherichia coli* and Spx of *Bacillus subtilis*) whose transcription is governed by direct sensing of redox conditions (23, 74). In *P. furiosus* it is unclear what the actual physiological effector(s) are that modulate the SurR redox switch and whether it is reversible via chemical or enzymatic means in vivo. It has been proposed that either colloidal S^0 or polysulfide species are the *in vivo* effectors for SurR.

A search of the *P. furiosus* genome revealed that SurR binding motifs appear upstream of most of the ORFs indentified in the *P. furiosus* primary S^0 response including the NADPH-dependent S^0 oxidoreductase (NSR) and the membrane-bound oxidoreductase (MBX), but not the secondary S^0 response, which includes the S^0-induced protein A (SipA). Elucidating the

physiological role of these three key sulfur responsive proteins is the focus of chapter 3, while chapters 4 will discuss potential implications for one of these proteins in acting as a redox sensor involved in the SurR response.

RESEARCH OBJECTIVES

The overall goal of this research was to define the genome sequence of the recently selected genetically-tractable strain of *P. furiosus*, COM1, and utilize this new genetic system to further advance our understanding of S^0 metabolism by *P. furiosus*. Prior to 2007, the mechanism of S^0 reduction by heterotrophic hyperthermophilic archaea, such as *Pyrococcus* and *Thermococcus* species, was completely unknown. In the appendix, the work which describes the initial characterization of the novel S^0 reducing system in *P. furiosus* is described. In the following, Chapter 2 describes the genome sequencing of the COM1 strain and a discussion on the differences compared to the published NCBI reference sequence and involvement of IS elements in the genome evolution. Chapter 3 focuses on the characterization of targeted gene knockouts of three key players in S^0 metabolism including: a cytoplasmic NADPH sulfur oxidoreductase (NSR), a membrane-bound oxidoreductase complex (MBX), and the sulfur-induced protein A (SipA). Chapter 4 utilizes whole genome DNA microarrays to further investigate the physiological role of NSR by analyzing transcriptional differences in the deletion strain (NSR1) in both the presence and absence of S^0.

REFERENCES

1. **Adams, M. W., J. F. Holden, A. L. Menon, G. J. Schut, A. M. Grunden, C. Hou, A. M. Hutchins, F. E. Jenney, Jr., C. Kim, K. Ma, G. Pan, R. Roy, R. Sapra, S. V. Story, and M. F. Verhagen.** 2001. Key role for sulfur in peptide metabolism and in regulation of three hydrogenases in the hyperthermophilic archaeon *Pyrococcus furiosus*. J Bacteriol **183:**716-24.
2. **Adams, M. W. W., and R. M. Kelly.** 2001. Hyperthermophilic Enzymes, Pt A, vol. 330. Academic Press, San Diego, CA.
3. **Adams, M. W. W., and R. M. Kelly.** 2001. Hyperthermophilic Enzymes, Pt B, vol. 331. Academic Press, San Diego, CA.
4. **Adams, M. W. W., and R. M. Kelly.** 2001. Hyperthermophilic Enzymes, Pt C, vol. 334. Academic Press, San Diego, CA.
5. **Albers, S. V., J. L. van de Vossenberg, A. J. Driessen, and W. N. Konings.** 2000. Adaptations of the archaeal cell membrane to heat stress. Front Biosci **5:**D813-20.
6. **Allers, T., and M. Mevarech.** 2005. Archaeal genetics - the third way. Nat Rev Genet **6:**58-73.
7. **Altschul, S. F., T. L. Madden, A. A. Schaffer, J. Zhang, Z. Zhang, W. Miller, and D. J. Lipman.** 1997. Gapped BLAST and PSI-BLAST: a new generation of protein database search programs. Nucleic Acids Res **25:**3389-402.
8. **Barns, S. M., C. F. Delwiche, J. D. Palmer, and N. R. Pace.** 1996. Perspectives on archaeal diversity, thermophily and monophyly from environmental rRNA sequences. Proc Natl Acad Sci U S A **93:**9188-93.
9. **Bauer, M. W., E. J. Bylina, R. V. Swanson, and R. M. Kelly.** 1996. Comparison of a beta-glucosidase and a beta-mannosidase from the hyperthermophilic archaeon *Pyrococcus furiosus*. Purification, characterization, gene cloning, and sequence analysis. J Biol Chem **271:**23749-55.

10. **Beattie, T. R., and S. D. Bell.** 2011. Molecular machines in archaeal DNA replication. Curr Opin Chem Biol **15:**614-9.

11. **Beinert, H.** 2000. A tribute to sulfur. Eur J Biochem **267:**5657-64.

12. **Bell, S. D., S. S. Cairns, R. L. Robson, and S. P. Jackson.** 1999. Transcriptional regulation of an archaeal operon *in vivo* and *in vitro*. Mol Cell **4:**971-82.

13. **Bell, S. D., and S. P. Jackson.** 2001. Mechanism and regulation of transcription in archaea. Curr Opin Microbiol **4:**208-13.

14. **Benelli, D., and P. Londei.** 2011. Translation initiation in Archaea: conserved and domain-specific features. Biochem Soc Trans **39:**89-93.

15. **Blamey, J. M., and M. W. Adams.** 1993. Purification and characterization of pyruvate ferredoxin oxidoreductase from the hyperthermophilic archaeon *Pyrococcus furiosus*. Biochim Biophys Acta **1161:**19-27.

16. **Boeke, J. D., F. LaCroute, and G. R. Fink.** 1984. A positive selection for mutants lacking orotidine-5'-phosphate decarboxylase activity in yeast: 5-fluoro-orotic acid resistance. Mol Gen Genet **197:**345-6.

17. **Bohlke, K., F. M. Pisani, M. Rossi, and G. Antranikian.** 2002. Archaeal DNA replication: spotlight on a rapidly moving field. Extremophiles **6:**1-14.

18. **Brinkman, A. B., S. D. Bell, R. J. Lebbink, W. M. de Vos, and J. van der Oost.** 2002. The *Sulfolobus solfataricus* Lrp-like protein LysM regulates lysine biosynthesis in response to lysine availability. J Biol Chem **277:**29537-49.

19. **Brochier-Armanet, C., S. Gribaldo, and P. Forterre.** 2011. Spotlight on the *Thaumarchaeota*. ISME J **6:**227-30.

20. **Brugger, K., P. Redder, Q. She, F. Confalonieri, Y. Zivanovic, and R. A. Garrett.** 2002. Mobile elements in archaeal genomes. FEMS Microbiol Lett **206:**131-41.

21. **Chandrayan, S. K., P. M. McTernan, R. C. Hopkins, J. Sun, F. E. Jenney, Jr., and M. W. Adams.** 2012. Engineering Hyperthermophilic Archaeon *Pyrococcus furiosus* to Overproduce Its Cytoplasmic [NiFe]-Hydrogenase. J Biol Chem **287:**3257-64.

22. **Chinen, A., I. Uchiyama, and I. Kobayashi.** 2000. Comparison between *Pyrococcus horikoshii* and *Pyrococcus abyssi* genome sequences reveals linkage of restriction-modification genes with large genome polymorphisms. Gene **259:**109-21.

23. **Choi, H., S. Kim, P. Mukhopadhyay, S. Cho, J. Woo, G. Storz, and S. E. Ryu.** 2001. Structural basis of the redox switch in the OxyR transcription factor. Cell **105:**103-13.

24. **Chou, C. J., K. R. Shockley, S. B. Conners, D. L. Lewis, D. A. Comfort, M. W. Adams, and R. M. Kelly.** 2007. Impact of substrate glycoside linkage and elemental sulfur on bioenergetics of and hydrogen production by the hyperthermophilic archaeon *Pyrococcus furiosus*. Appl Environ Microbiol **73:**6842-53.

25. **Cohen, G. N., V. Barbe, D. Flament, M. Galperin, R. Heilig, O. Lecompte, O. Poch, D. Prieur, J. Querellou, R. Ripp, J. C. Thierry, J. Van der Oost, J. Weissenbach, Y. Zivanovic, and P. Forterre.** 2003. An integrated analysis of the genome of the hyperthermophilic archaeon *Pyrococcus abyssi*. Mol Microbiol **47:**1495-512.

26. **Dietrich, W., and O. Klimmek.** 2002. The function of methyl-menaquinone-6 and polysulfide reductase membrane anchor (PsrC) in polysulfide respiration of *Wolinella succinogenes*. Eur J Biochem **269:**1086-95.

27. **Diruggiero, J., D. Dunn, D. L. Maeder, R. Holley-Shanks, J. Chatard, R. Horlacher, F. T. Robb, W. Boos, and R. B. Weiss.** 2000. Evidence of recent lateral gene transfer among hyperthermophilic archaea. Mol Microbiol **38:**684-93.

28. **Driskill, L. E., M. W. Bauer, and R. M. Kelly.** 1999. Synergistic interactions among beta-laminarinase, beta-1,4-glucanase, and beta-glucosidase from the hyperthermophilic archaeon *Pyrococcus furiosus* during hydrolysis of beta-1,4-, beta-1,3-, and mixed-linked polysaccharides. Biotechnol Bioeng **66:**51-60.

29. **Eichler, J., and M. W. Adams.** 2005. Posttranslational protein modification in Archaea. Microbiol Mol Biol Rev **69:**393-425.

30. **Engelhardt, H.** 2007. Are S-layers exoskeletons? The basic function of protein surface layers revisited. J Struct Biol **160:**115-24.

31. **Fiala, G., and K. Stetter.** 1986. *Pyrococcus furiosus* sp. nov. represents a novel genus of marine heterotrophic archaebacteria growing optimally at 100°C. Arch Microbiol **145:**56-61.

32. **Forterre, P.** 1997. Archaea: what can we learn from their sequences? Curr Opin Genet Dev **7:**764-70.

33. **Forterre, P., C. Brochier, and H. Philippe.** 2002. Evolution of the Archaea. Theor Popul Biol **61:**409-22.

34. **Gao, J., M. W. Bauer, K. R. Shockley, M. A. Pysz, and R. M. Kelly.** 2003. Growth of hyperthermophilic archaeon *Pyrococcus furiosus* on chitin involves two family 18 chitinases. Appl Environ Microbiol **69:**3119-28.

35. **Geiduschek, E. P., and M. Ouhammouch.** 2005. Archaeal transcription and its regulators. Mol Microbiol **56:**1397-407.

36. **Gueguen, Y., W. G. Voorhorst, J. van der Oost, and W. M. de Vos.** 1997. Molecular and biochemical characterization of an endo-beta-1,3- glucanase of the hyperthermophilic archaeon *Pyrococcus furiosus*. J Biol Chem **272:**31258-64.

37. **Guiral, M., P. Tron, C. Aubert, A. Gloter, C. Iobbi-Nivol, and M. T. Giudici-Orticoni.** 2005. A membrane-bound multienzyme, hydrogen-oxidizing, and sulfur-reducing complex from the hyperthermophilic bacterium *Aquifex aeolicus*. J Biol Chem **280:**42004-15.

38. **Hanford, M. J., and T. L. Peeples.** 2002. Archaeal tetraether lipids: unique structures and applications. Appl Biochem Biotechnol **97:**45-62.

39. **Hedderich, R., O. Klimmek, A. Kroger, R. Dirmeier, M. Keller, and K. O. Stetter.** 1998. Anaerobic respiration with elemental sulfur and with disulfides. Fems Microbiology Reviews **22:**353-381.

40. **Hopkins, R. C., J. Sun, F. E. Jenney, Jr., S. K. Chandrayan, P. M. McTernan, and M. W. Adams.** 2011. Homologous expression of a subcomplex of *Pyrococcus furiosus* hydrogenase that interacts with pyruvate ferredoxin oxidoreductase. PLoS One **6:**e26569, Oct 24 (epub).

41. **Huynen, M. A., and P. Bork.** 1998. Measuring genome evolution. Proc Natl Acad Sci U S A **95:**5849-56.

42. **Jun, X., L. Lupeng, X. Minjuan, P. Oger, W. Fengping, M. Jebbar, and X. Xiang.** 2011. Complete genome sequence of the obligate piezophilic hyperthermophilic archaeon *Pyrococcus yayanosii* CH1. J Bacteriol **193:**4297-8.

43. **Karner, M. B., E. F. DeLong, and D. M. Karl.** 2001. Archaeal dominance in the mesopelagic zone of the Pacific Ocean. Nature **409:**507-10.

44. **Kawarabayasi, Y., M. Sawada, H. Horikawa, Y. Haikawa, Y. Hino, S. Yamamoto, M. Sekine, S. Baba, H. Kosugi, A. Hosoyama, Y. Nagai, M. Sakai, K. Ogura, R. Otsuka, H. Nakazawa, M. Takamiya, Y. Ohfuku, T. Funahashi, T. Tanaka, Y. Kudoh, J. Yamazaki, N. Kushida, A. Oguchi, K. Aoki, and H. Kikuchi.** 1998. Complete sequence and gene organization of the genome of a hyper-thermophilic archaebacterium, *Pyrococcus horikoshii* OT3. DNA Res **5:**55-76.

45. **Keller, M., and R. Dirmeier.** 2001. Hydrogen-sulfur oxidoreductase complex from *Pyrodictium abyssi*. Methods Enzymol **331:**442-51.

46. **Kengen, S. W., F. A. de Bok, N. D. van Loo, C. Dijkema, A. J. Stams, and W. M. de Vos.** 1994. Evidence for the operation of a novel Embden-Meyerhof pathway that involves ADP-dependent kinases during sugar fermentation by *Pyrococcus furiosus*. J Biol Chem **269:**17537-41.

47. **Kengen, S. W., E. J. Luesink, A. J. Stams, and A. J. Zehnder.** 1993. Purification and characterization of an extremely thermostable beta-glucosidase from the hyperthermophilic archaeon *Pyrococcus furiosus*. Eur J Biochem **213:**305-12.

48. **Kinns, H., and S. Howorka.** 2008. The surface location of individual residues in a bacterial S-layer protein. J Mol Biol **377:**589-604.

49. **Koga, Y., and H. Morii.** 2007. Biosynthesis of ether-type polar lipids in archaea and evolutionary considerations. Microbiol Mol Biol Rev **71:**97-120.

50. **Koning, S. M., W. N. Konings, and A. J. Driessen.** 2002. Biochemical evidence for the presence of two alpha-glucoside ABC-transport systems in the hyperthermophilic archaeon *Pyrococcus furiosus*. Archaea **1:**19-25.

51. **Konings, W. N., S. V. Albers, S. Koning, and A. J. Driessen.** 2002. The cell membrane plays a crucial role in survival of bacteria and archaea in extreme environments. Antonie Van Leeuwenhoek **81:**61-72.

52. **Koonin, E. V., A. R. Mushegian, M. Y. Galperin, and D. R. Walker.** 1997. Comparison of archaeal and bacterial genomes: computer analysis of protein sequences predicts novel functions and suggests a chimeric origin for the archaea. Mol Microbiol **25:**619-37.

53. **Lam, W. L., and W. F. Doolittle.** 1989. Shuttle vectors for the archaebacterium *Halobacterium volcanii*. Proc Natl Acad Sci U S A **86:**5478-82.

54. **Laska, S., F. Lottspeich, and A. Kletzin.** 2003. Membrane-bound hydrogenase and sulfur reductase of the hyperthermophilic and acidophilic archaeon *Acidianus ambivalens*. Microbiology **149:**2357-71.

55. **Lecompte, O., R. Ripp, V. Puzos-Barbe, S. Duprat, R. Heilig, J. Dietrich, J. C. Thierry, and O. Poch.** 2001. Genome evolution at the genus level: comparison of three complete genomes of hyperthermophilic archaea. Genome Res **11:**981-93.

56. **Lee, H. S., S. S. Bae, M. S. Kim, K. K. Kwon, S. G. Kang, and J. H. Lee.** 2011. Complete genome sequence of hyperthermophilic *Pyrococcus* sp. strain NA2, isolated from a deep-sea hydrothermal vent area. J Bacteriol **193:**3666-7.

57. **Lee, H. S., K. R. Shockley, G. J. Schut, S. B. Conners, C. I. Montero, M. R. Johnson, C. J. Chou, S. L. Bridger, N. Wigner, S. D. Brehm, F. E. Jenney, Jr., D. A. Comfort, R. M. Kelly, and M. W. Adams.** 2006. Transcriptional and biochemical analysis of starch metabolism in the hyperthermophilic archaeon *Pyrococcus furiosus*. J Bacteriol **188:**2115-25.

58. **Lee, S. J., M. Surma, W. Hausner, M. Thomm, and W. Boos.** 2008. The role of TrmB and TrmB-like transcriptional regulators for sugar transport and metabolism in the hyperthermophilic archaeon *Pyrococcus furiosus*. Arch Microbiol **190:**247-56.

59. **Leigh, J. A., S. V. Albers, H. Atomi, and T. Allers.** 2011. Model organisms for genetics in the domain Archaea: methanogens, halophiles, *Thermococcales* and *Sulfolobales*. FEMS Microbiol Rev **35:**577-608.

60. **Lie, T. J., G. E. Wood, and J. A. Leigh.** 2005. Regulation of nif expression in *Methanococcus maripaludis*: roles of the euryarchaeal repressor NrpR, 2-oxoglutarate, and two operators. J Biol Chem **280:**5236-41.

61. **Lipscomb, G. L., A. M. Keese, D. M. Cowart, G. J. Schut, M. Thomm, M. W. Adams, and R. A. Scott.** 2009. SurR: a transcriptional activator and repressor controlling hydrogen and elemental sulphur metabolism in *Pyrococcus furiosus*. Mol Microbiol **71:**332-49.

62. **Lipscomb, G. L., K. Stirrett, G. J. Schut, F. Yang, F. E. Jenney, Jr., R. A. Scott, M. W. Adams, and J. Westpheling.** 2011. Natural competence in the hyperthermophilic archaeon *Pyrococcus furiosus* facilitates genetic manipulation: construction of markerless deletions of genes encoding the two cytoplasmic hydrogenases. Appl Environ Microbiol **77:**2232-8.

63. **Ma, K., and M. W. Adams.** 2001. Ferredoxin:NADP oxidoreductase from *Pyrococcus furiosus*. Methods Enzymol **334:**40-5.

64. **Ma, K., and M. W. Adams.** 2001. Hydrogenases I and II from *Pyrococcus furiosus*. Methods Enzymol. **331:**208-16.

65. **Ma, K., and M. W. Adams.** 1994. Sulfide dehydrogenase from the hyperthermophilic archaeon *Pyrococcus furiosus*: a new multifunctional enzyme involved in the reduction of elemental sulfur. J Bacteriol **176:**6509-17.

66. **Maeder, D. L., R. B. Weiss, D. M. Dunn, J. L. Cherry, J. M. Gonzalez, J. DiRuggiero, and F. T. Robb.** 1999. Divergence of the hyperthermophilic archaea *Pyrococcus furiosus* and *P. horikoshii* inferred from complete genomic sequences. Genetics **152:**1299-305.

67. **Mahillon, J., and M. Chandler.** 1998. Insertion sequences. Microbiol Mol Biol Rev **62:**725-74.

68. **Mai, X., and M. W. Adams.** 1996. Purification and characterization of two reversible and ADP-dependent acetyl coenzyme A synthetases from the hyperthermophilic archaeon *Pyrococcus furiosus*. J Bacteriol **178:**5897-903.

69. **Makino, S., and M. Suzuki.** 2001. Bacterial genomic reorganization upon DNA replication. Science **292:**803.

70. **Matsumi, R., H. Atomi, A. J. Driessen, and J. van der Oost.** 2011. Isoprenoid biosynthesis in Archaea--biochemical and evolutionary implications. Res Microbiol **162:**39-52.

71. **Matsumi, R., K. Manabe, T. Fukui, H. Atomi, and T. Imanaka.** 2007. Disruption of a sugar transporter gene cluster in a hyperthermophilic archaeon using a host-marker system based on antibiotic resistance. J Bacteriol **189:**2683-91.

72. **Mukund, S., and M. W. Adams.** 1991. The novel tungsten-iron-sulfur protein of the hyperthermophilic archaebacterium, *Pyrococcus furiosus*, is an aldehyde ferredoxin

oxidoreductase. Evidence for its participation in a unique glycolytic pathway. J Biol Chem **266:**14208-16.

73. **Myllykallio, H., and P. Forterre.** 2000. Mapping of a chromosome replication origin in an archaeon: response. Trends Microbiol **8:**537-9.

74. **Nakano, S., K. N. Erwin, M. Ralle, and P. Zuber.** 2005. Redox-sensitive transcriptional control by a thiol/disulphide switch in the global regulator, Spx. Mol Microbiol **55:**498-510.

75. **Pester, M., C. Schleper, and M. Wagner.** 2011. The *Thaumarchaeota*: an emerging view of their phylogeny and ecophysiology. Curr Opin Microbiol **14:**300-6.

76. **Pihl, T. D., L. K. Black, B. A. Schulman, and R. J. Maier.** 1992. Hydrogen-oxidizing electron transport components in the hyperthermophilic archaebacterium *Pyrodictium brockii*. J Bacteriol **174:**137-43.

77. **Reeve, J. N.** 2003. Archaeal chromatin and transcription. Mol Microbiol **48:**587-98.

78. **Robb, F. T., D. L. Maeder, J. R. Brown, J. DiRuggiero, M. D. Stump, R. K. Yeh, R. B. Weiss, and D. M. Dunn.** 2001. Genomic sequence of hyperthermophile, *Pyrococcus furiosus*: implications for physiology and enzymology. Methods Enzymol **330:**134-57.

79. **Robertson, C. E., J. K. Harris, J. R. Spear, and N. R. Pace.** 2005. Phylogenetic diversity and ecology of environmental Archaea. Curr Opin Microbiol **8:**638-42.

80. **Ronimus, R. S., and H. W. Morgan.** 2003. Distribution and phylogenies of enzymes of the Embden-Meyerhof-Parnas pathway from archaea and hyperthermophilic bacteria support a gluconeogenic origin of metabolism. Archaea **1:**199-221.

81. **Sakuraba, H., and T. Ohshima.** 2002. Novel energy metabolism in anaerobic hyperthermophilic archaea: A modified Embden-Meyerhof pathway. J. Biosci. Bioeng. **93:**441-448.

82. **Sapra, R., K. Bagramyan, and M. W. Adams.** 2003. A simple energy-conserving system: proton reduction coupled to proton translocation. Proc Natl Acad Sci USA **100:**7545-50.

83. **Sato, T., T. Fukui, H. Atomi, and T. Imanaka.** 2003. Targeted gene disruption by homologous recombination in the hyperthermophilic archaeon *Thermococcus kodakaraensis* KOD1. J Bacteriol **185:**210-20.

84. **Schicho, R. N., K. Ma, M. W. Adams, and R. M. Kelly.** 1993. Bioenergetics of sulfur reduction in the hyperthermophilic archaeon *Pyrococcus furiosus*. J Bacteriol **175:**1823-30.

85. **Schleper, C., and G. W. Nicol.** 2010. Ammonia-oxidising archaea--physiology, ecology and evolution. Adv Microb Physiol **57:**1-41.

86. **Schlesinger, W. H.** 2005. Anaerobic Metabolism: Linkages to Trace Gases and Aerobic Processes, Biogeochemistry: Treatise on Geochemistry, vol. 8. Elsevier Science.

87. **Schuster, B., and U. B. Sleytr.** 2000. S-layer-supported lipid membranes. J Biotechnol **74:**233-54.

88. **Schut, G. J., S. D. Brehm, S. Datta, and M. W. Adams.** 2003. Whole-genome DNA microarray analysis of a hyperthermophile and an archaeon: *Pyrococcus furiosus* grown on carbohydrates or peptides. J Bacteriol **185:**3935-47.

89. **Schut, G. J., S. L. Bridger, and M. W. Adams.** 2007. Insights into the metabolism of elemental sulfur by the hyperthermophilic archaeon *Pyrococcus furiosus*: characterization of a coenzyme A- dependent NAD(P)H sulfur oxidoreductase. J Bacteriol **189:**4431-41.

90. **Schut, G. J., J. Zhou, and M. W. Adams.** 2001. DNA microarray analysis of the hyperthermophilic archaeon *Pyrococcus furiosus*: evidence for a new type of sulfur-reducing enzyme complex. J Bacteriol **183:**7027-36.

91. **Strand, K. R., C. Sun, T. Li, F. E. Jenney, Jr., G. J. Schut, and M. W. Adams.** 2010. Oxidative stress protection and the repair response to hydrogen peroxide in the hyperthermophilic archaeon *Pyrococcus furiosus* and in related species. Arch Microbiol **192:**447-59.

92. **Verhees, C. H., S. W. Kengen, J. E. Tuininga, G. J. Schut, M. W. Adams, W. M. De Vos, and J. Van Der Oost.** 2003. The unique features of glycolytic pathways in Archaea. Biochem J **375:**231-46.

93. **Voorhorst, W. G., Y. Gueguen, A. C. Geerling, G. Schut, I. Dahlke, M. Thomm, J. van der Oost, and W. M. de Vos.** 1999. Transcriptional regulation in the hyperthermophilic archaeon *Pyrococcus furiosus*: coordinated expression of divergently oriented genes in response to beta-linked glucose polymers. J Bacteriol **181:**3777-83.

94. **Weinberg, M. V., G. J. Schut, S. Brehm, S. Datta, and M. W. Adams.** 2005. Cold shock of a hyperthermophilic archaeon: *Pyrococcus furiosus* exhibits multiple responses to a suboptimal growth temperature with a key role for membrane-bound glycoproteins. J Bacteriol **187:**336-48.

95. **White, M. F.** 2011. Homologous recombination in the archaea: the means justify the ends. Biochem Soc Trans **39:**15-9.

96. **Woese, C. R., and G. E. Fox.** 1977. Phylogenetic structure of the prokaryotic domain: the primary kingdoms. Proc Natl Acad Sci U S A **74:**5088-90.

97. **Woese, C. R., O. Kandler, and M. L. Wheelis.** 1990. Towards a natural system of organisms: proposal for the domains Archaea, Bacteria, and Eucarya. Proc Natl Acad Sci U S A **87:**4576-9.

98. **Yang, H., G. L. Lipscomb, A. M. Keese, G. J. Schut, M. Thomm, M. W. Adams, B. C. Wang, and R. A. Scott.** 2010. SurR regulates hydrogen production in *Pyrococcus furiosus* by a sulfur-dependent redox switch. Mol Microbiol **77:**1111-22.

99. **Zivanovic, Y., P. Lopez, H. Philippe, and P. Forterre.** 2002. *Pyrococcus* genome comparison evidences chromosome shuffling-driven evolution. Nucleic Acids Res **30:**1902-10.

Figure 1.1. Universal phylogenetic tree of life based on 16S rRNA gene sequences. Red lines represent hyperthermophilic lineages. The model hyperthermophilic archaeon, *Pyrococcus furiosus*, is the focus of this work and is highlighted in blue. Modified from (97).

FIGURE 1.1

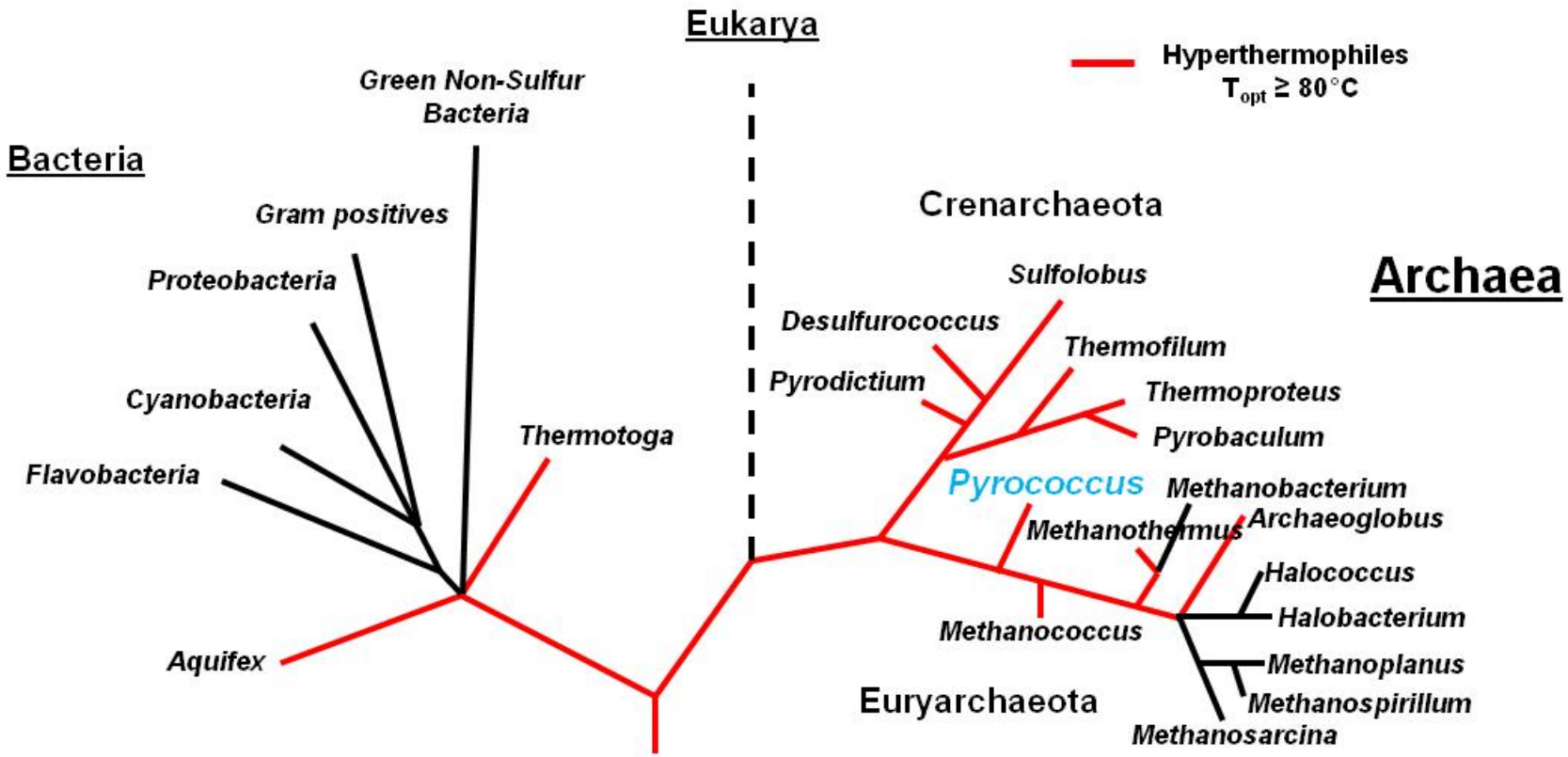
Eukarya
Hyperthermophiles
$T_{opt} \geq 80°C$
Green Non-Sulfur Bacteria
Bacteria
Gram positives
Proteobacteria
Cyanobacteria
Flavobacteria
Thermotoga
Aquifex
Crenarchaeota
Archaea
Sulfolobus
Desulfurococcus
Thermofilum
Pyrodictium
Thermoproteus
Pyrobaculum
Pyrococcus
Methanobacterium
Archaeoglobus
Methanothermus
Halococcus
Halobacterium
Methanococcus
Methanoplanus
Euryarchaeota
Methanospirillum
Methanosarcina

Figure 1.2. Phylogenetic tree showing archaea with genetics systems. Phylogenetic tree based on 16S rRNA gene sequences of a select group of archaeal species within the Euryarchaeota and Crenarchaeota whose genomes are sequenced. Organisms with solid red stars have developed genetics systems, open stars indicate genetics has been applied or there is a potential for genetics, yellow star marks recently developed genetics system in *P. furiosus*. Defining the genome sequence of the genetically-tractable strain of *P. furiosus* (COM1) is the focus of chapter 3. Modified from (59).

FIGURE 1.2

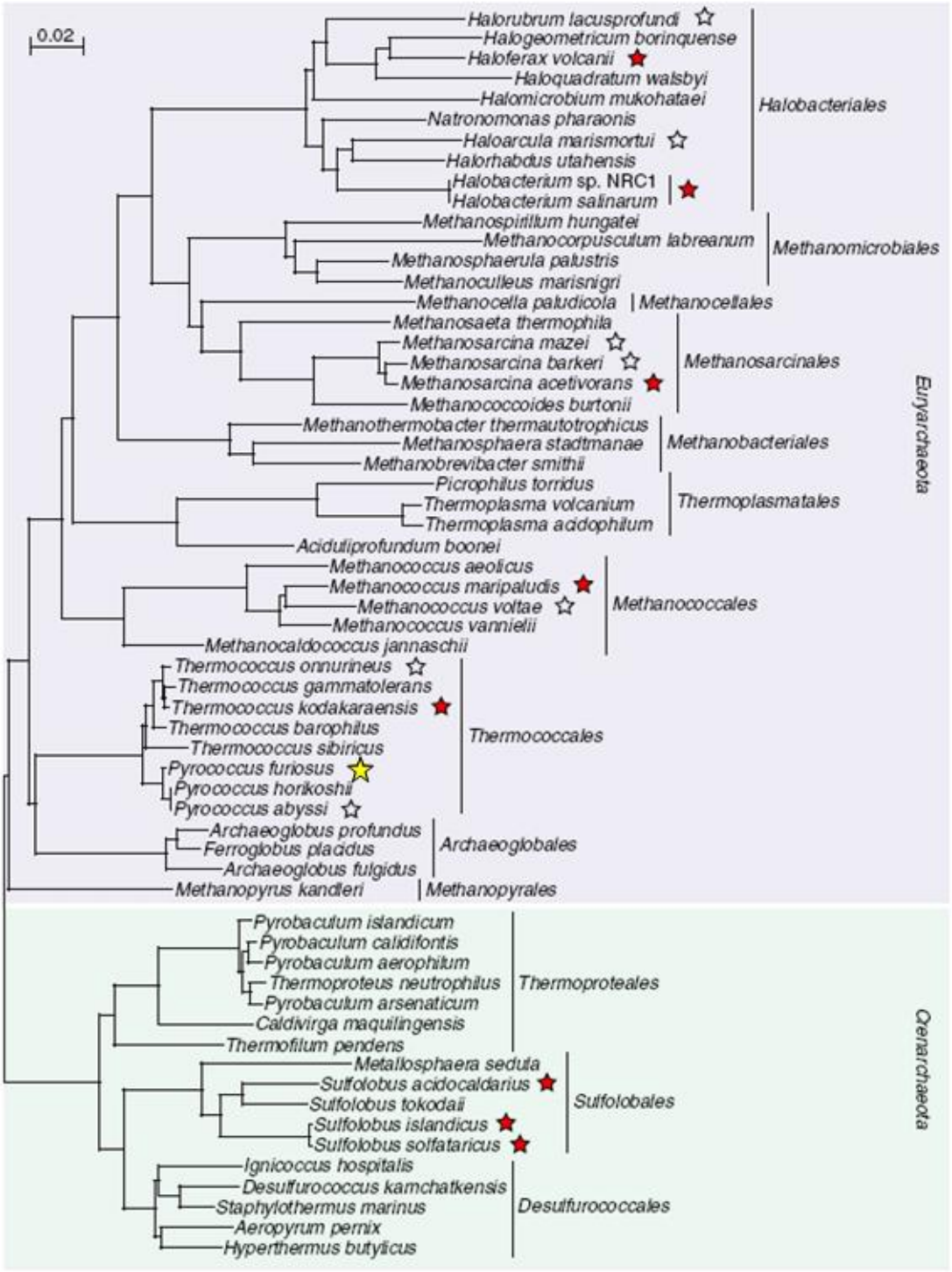
0.02
Halorubrum lacusprofundi
Halogeometricum borinquense
Haloferax volcanii
Haloquadratum walsbyi
Halomicrobium mukohataei
Natronomonas pharaonis
Haloarcula marismortui
Halorhabdus utahensis
Halobacterium sp. NRC1
Halobacterium salinarum
Halobacteriales
Methanospirillum hungatei
Methanocorpusculum labreanum
Methanosphaerula palustris
Methanoculleus marisnigri
Methanomicrobiales
Methanocella paludicola
Methanocellales
Methanosaeta thermophila
Methanosarcina mazei
Methanosarcina barkeri
Methanosarcina acetivorans
Methanococcoides burtonii
Methanosarcinales
Methanothermobacter thermautotrophicus
Methanosphaera stadtmanae
Methanobrevibacter smithii
Methanobacteriales
Picrophilus torridus
Thermoplasma volcanium
Thermoplasma acidophilum
Thermoplasmatales
Aciduliprofundum boonei
Methanococcus aeolicus
Methanococcus maripaludis
Methanococcus voltae
Methanococcus vannielii
Methanococcales
Methanocaldococcus jannaschii
Thermococcus onnurineus
Thermococcus gammatolerans
Thermococcus kodakaraensis
Thermococcus barophilus
Thermococcus sibiricus
Pyrococcus furiosus
Pyrococcus horikoshii
Pyrococcus abyssi
Thermococcales
Archaeoglobus profundus
Ferroglobus placidus
Archaeoglobus fulgidus
Archaeoglobales
Methanopyrus kandleri
Methanopyrales
Euryarchaeota
Pyrobaculum islandicum
Pyrobaculum calidifontis
Pyrobaculum aerophilum
Thermoproteus neutrophilus
Pyrobaculum arsenaticum
Thermoproteales
Caldivirga maquilingensis
Thermofilum pendens
Metallosphaera sedula
Sulfolobus acidocaldarius
Sulfolobus tokodaii
Sulfolobus islandicus
Sulfolobus solfataricus
Sulfolobales
Ignicoccus hospitalis
Desulfurococcus kamchatkensis
Staphylothermus marinus
Aeropyrum pernix
Hyperthermus butylicus
Desulfurococcales
Crenarchaeota

Figure 1.3. Electron micrograph of *Pyrococcus furiosus*. Taken from (31).

FIGURE 1.3

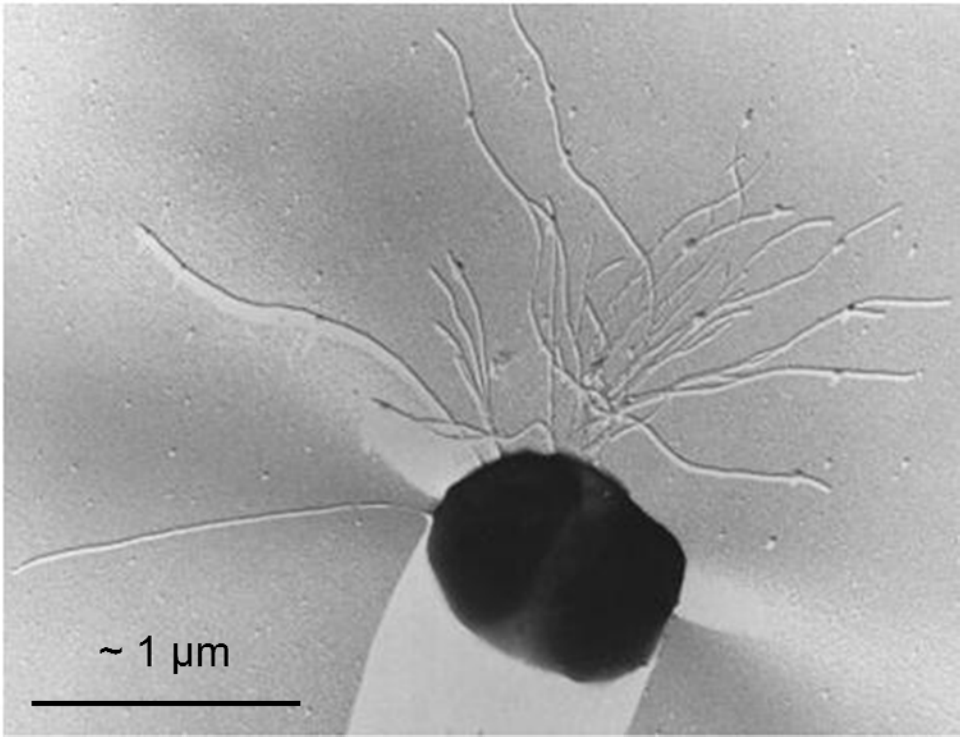

Figure 1.4. Strategy for deleting the *pyrF* gene in *P. furiosus*. This diagram shows genome organization at the *pyrF* locus with the *pyrF* deletion plasmid having 1-kb regions for homologous recombination up- and downstream of *pyrF* and containing the P_{gdh}-*hmg* cassette for selection on simvastatin. Integration of the plasmid can occur at either the up- or downstream *pyrF* flanking regions, generating a simvastatin resistant strain. Loss of the plasmid and *pyrF* gene was accomplished by selection on 5-FOA. Taken from (62).

FIGURE 1.4

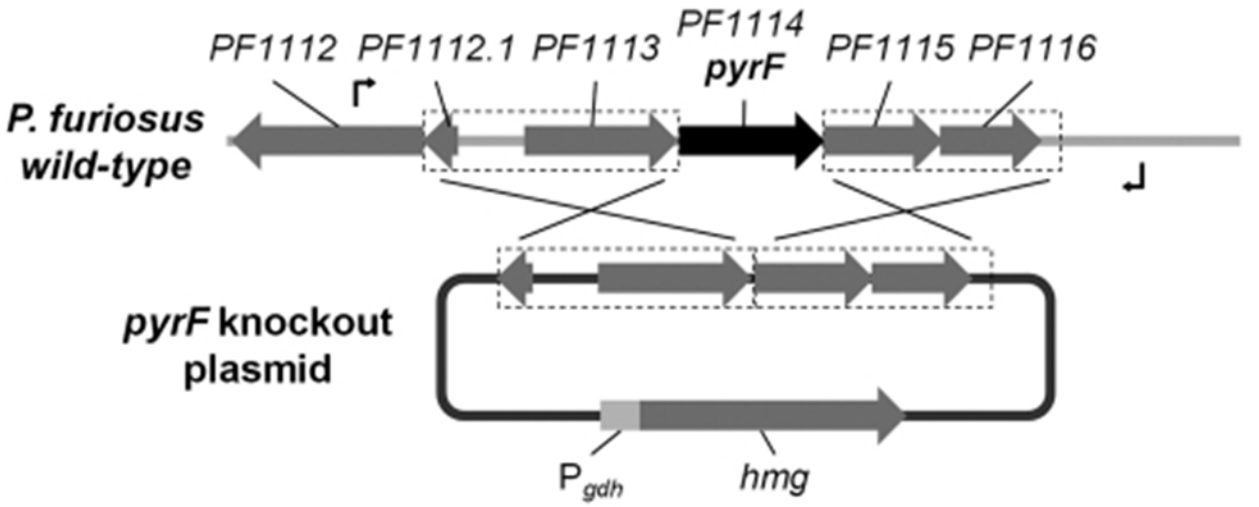

Simvastatin resistance selects for plasmid integration (two orientations)

5-FOA resistance selects for plasmid removal and deletion of *pyrF*

Figure 1.5. Glycolytic pathway in *P. furiosus* linked to hydrogen production. In *P. furiosus* glucose is converted to acetate via a modified Embden-Meyerhof (EM) pathway where all the reductant generated is in the form of reduced ferredoxin (Fd) (Fd-linked enzymes are highlighted in yellow) which serves as electron donor for the membrane-bound hydrogenase (MBH) to evolve hydrogen (H_2). Modified from (92) and (82).

FIGURE 1.5

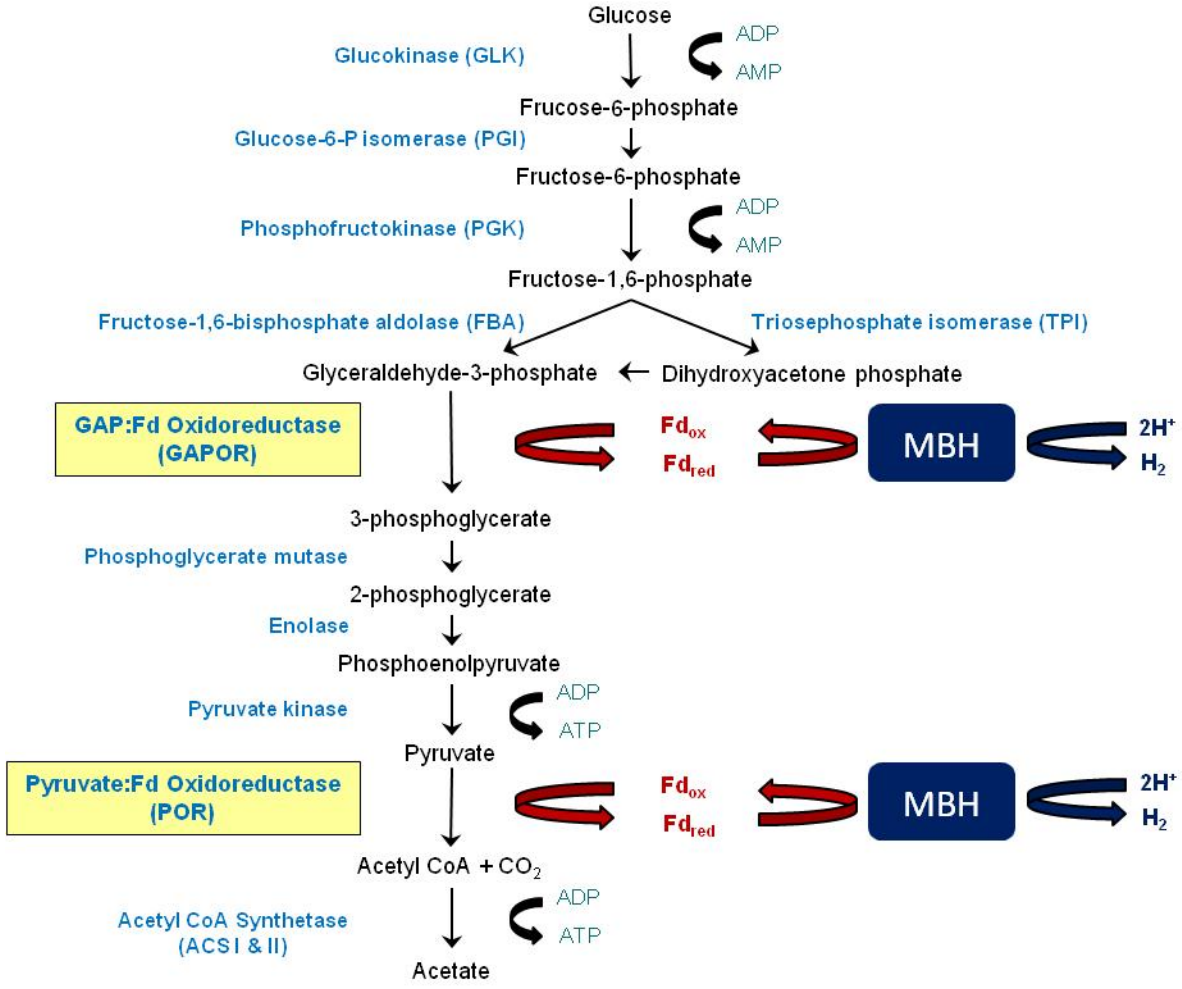
Glucose
Glucokinase (GLK)
ADP
AMP
Frucose-6-phosphate
Glucose-6-P isomerase (PGI)
Fructose-6-phosphate
Phosphofructokinase (PGK)
ADP
AMP
Fructose-1,6-phosphate
Fructose-1,6-bisphosphate aldolase (FBA)
Triosephosphate isomerase (TPI)
Glyceraldehyde-3-phosphate
Dihydroxyacetone phosphate
GAP:Fd Oxidoreductase (GAPOR)
Fdox
Fdred
MBH
2H+
H2
3-phosphoglycerate
Phosphoglycerate mutase
2-phosphoglycerate
Enolase
Phosphoenolpyruvate
Pyruvate kinase
ADP
ATP
Pyruvate
Pyruvate:Fd Oxidoreductase (POR)
Fdox
Fdred
MBH
2H+
H2
Acetyl CoA + CO2
Acetyl CoA Synthetase (ACS I & II)
ADP
ATP
Acetate

Figure 1.6. S^0-dependent redox switch regulates hydrogen and sulfur metabolism in *P. furiosus*. Under H_2 producing conditions (absence of S^0), SurR is in the reduced state ($SurR_{red}$) and is able to bind DNA and activates transcription of hydrogenase related genes, by presumably recruiting the basal transcriptional machinery to the promoter, while simultaneously repressing transcription of primary S^0 response genes, by presumably blocking access to the promoter. However, as soon as S^0 is available, cells switch from producing H_2 to H_2S due at least in part to the oxidative deactivation of SurR ($SurR_{ox}$). It is proposed that either intracellular colloidal S^0 or polysulfide (HS_n^-) oxidize SurR, and once the oxidizing S^0 species are depleted that SurR is converted back to its reduced and active state to promote H_2 production by the cell. Redrawn from (98).

FIGURE 1.6

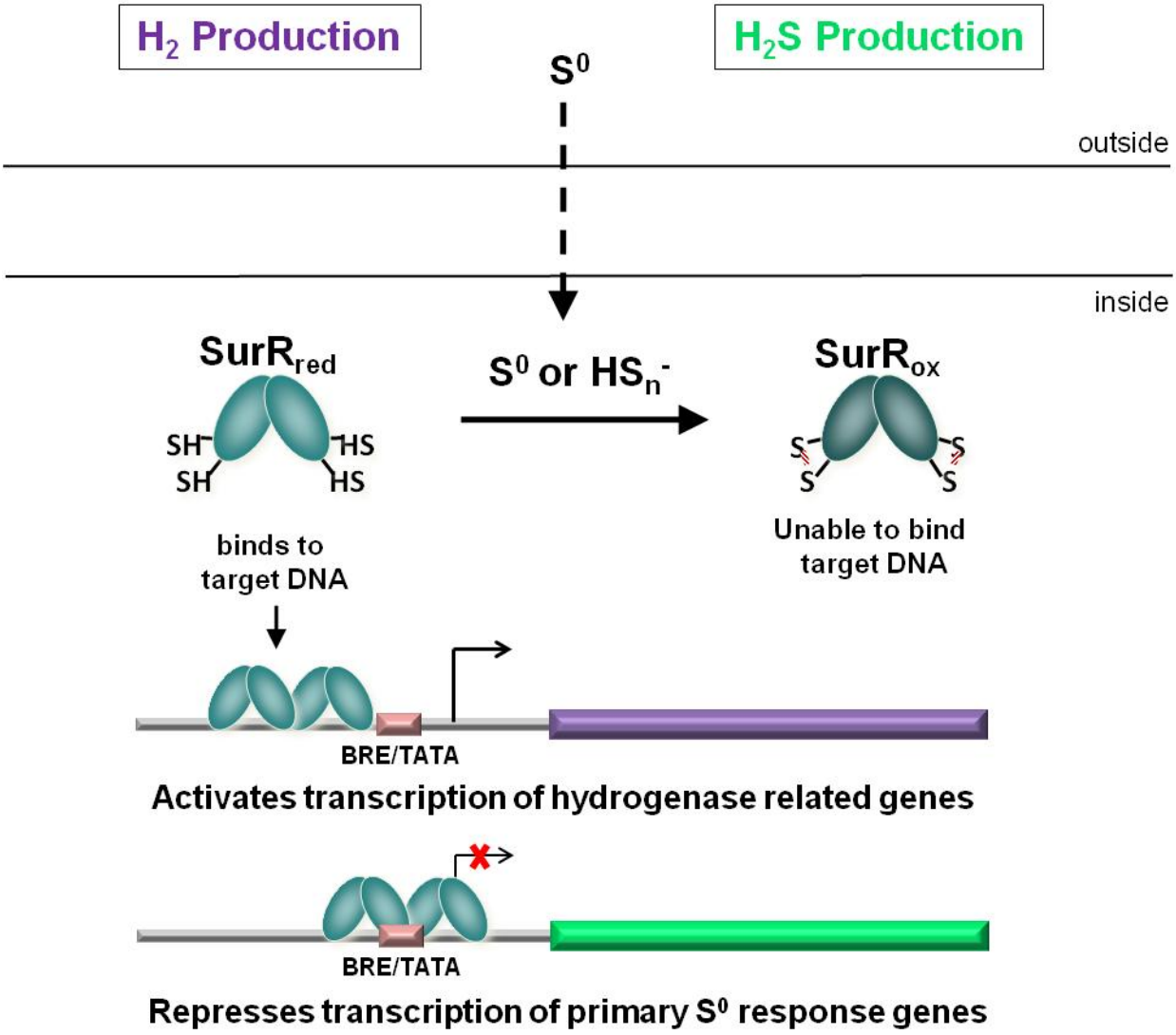
H2 Production
H2S Production
S0
outside
inside
SurRred
SH
SH
HS
HS
S0 or HSn-
SurRox
S
S
S
S
binds to target DNA
Unable to bind target DNA
BRE/TATA
Activates transcription of hydrogenase related genes
BRE/TATA
Represses transcription of primary S0 response genes

CHAPTER 2

GENOME SEQUENCING OF A GENETICALLY-TRACTABLE *PYROCOCCUS FURIOSUS* STRAIN REVEALS A HIGHLY DYNAMIC GENOME[1]

[1] Bridger, S.L.[*], W.A. Lancaster[*], F.L. Poole, 2nd, G.J. Schut, and M.W. Adams. Submitted to *J Bacteriol*, 03/20/2012.
[*] Authors contributed equally to this work

ABSTRACT

The model archaeon *Pyrococcus furiosus* grows optimally near 100°C on carbohydrates and peptides. Its genome sequence (NCBI) was determined twelve years ago. A genetically-tractable strain, COM1, was very recently reported and herein we describe its genome sequence. Of 1,910,278 bp in size, it is 2,013 bp longer (0.1%) than the reference NCBI sequence. The COM1 genome contains numerous chromosomal rearrangements, deletions and single base changes. COM1 also has 45 full or partial insertion elements compared to 35 in the reference NCBI strain and these have resulted in the direct deletion or insertional inactivation of thirteen genes. Another seven genes were affected by chromosomal deletions and are predicted to be non-functional. In addition, the amino acid sequences of another 102 of the 2134 predicted gene products are different in COM1. These changes potentially impacted various cellular functions, including carbohydrate, peptide and nucleotide metabolism, DNA repair, CRISPR-associated defense, transcriptional regulation, membrane transport and growth at 72°C. Hence, the IS-mediated inactivation of riboflavin synthase in COM1 resulted in a riboflavin-requirement for growth. Nevertheless, COM1 grew on cellobiose, malto-oligosaccharides and peptides in complex and minimal media at 98 and 72°C to the same extent as both its parent strain and a new culture collection strain (DSMZ 3638). This was in spite of COM1 lacking several metabolic enzymes, including non-phosphorylating glyceraldehyde-3-phosphate dehydrogenase and beta-glucosidase. The *P. furiosus* genome is therefore of high plasticity and the availability of the COM1 sequence will be critical for the future studies of this model hyperthermophile.

INTRODUCTION

The genus *Pyrococcus* represents a group of obligate anaerobic archaea that grow optimally near 100°C and utilize a wide range of poly- and oligosaccharides and peptides (36). They are found in marine hydrothermal vents and are some of the most well-studied archaea with potential biotechnological applications (2). Complete genome sequences are available for five *Pyrococcus* species (9, 26, 28, 34, 49). Their evolution and genomic diversity has been linked to a high degree of DNA recombination efficiency and the presence of mobile genetic elements (58). These insertion sequences (ISs) are small (<2.5 kb), self-directed segments of DNA capable of inserting at many non-homologous sites in the target DNA (38). Numerous reports have indicated that IS element transposition has led to extensive chromosomal rearrangements and lateral gene transfer (LGT) in the *Pyrococcus* genus (13, 16, 22, 27, 58, 60). For example, environmental isolates of *Pyrococcus* differ in their distribution of IS elements suggesting a high degree of mobility (58), as has been reported for other hyperthermophilic archaea from freshwater vents (40). These genomic features are thought to play a role in the adaptation to rapidly changing environmental conditions (58).

The best characterized of the *Pyrococcus* species is *P. furiosus,* the first to be isolated (19) and the first to have its genome sequenced (49). This organism has been studied by numerous '-omics' based approaches, including transcriptomics by tiling (59) and DNA microarrays (14, 35, 51, 54, 57), comparative genomics (8, 33, 60), proteomics (32, 42), metallomics (11), and structural genomics (25). In many ways it has become one of the model hyperthermophiles, a status recently sustained by the development of a genetic system for the organism (37). This was based on isolation of a variant in a lab strain population, designated COM1, which was highly efficient in taking up and recombining exogenous DNA in both circular and linear forms. The COM1 strain was obtained by targeted gene disruption of the *pyrF* locus (PF1114) using a plasmid designed for double-crossover recombination (37).

The COM1 strain has now been used to generate marked or markerless deletions of a number of genes, either singly or iteratively in the same strain, including those encoding two hydrogenases, a sulfur-reducing system and an iron-sulfur biosynthesis system (4, 37). A stable replicating shuttle vector is also available (18). In addition, recombinant forms have been generated that contain inserted DNA, such as highly-active promoters or protein affinity tags for rapid protein purification (7, 24). For example, an affinity-tagged, catalytically-active, H_2 gas producing sub-complex of *P. furiosus* hydrogenase was produced at approximately 100 times the level of the native hydrogenase (24). A more robust genetic method has also been developed that allows for selection on complex growth media for agmatine auxotrophy, involving a thermostable compound required for polyamine biosynthesis (50). This was used to produce an affinity-tagged (Strep) version of the native form of the cytoplasmic hydrogenase of *P. furiosus* (7).

The development of additional genetic tools for COM1 and its use as a platform for genetic manipulation and metabolic engineering can be anticipated. For such studies the complete genome sequence of this strain is obviously essential for all molecular manipulations. It was also important to determine if the genome sequence of COM1 could reveal any unanticipated phenotypic changes, particularly those affecting its ability to metabolize growth substrates or its requirement for vitamins or cofactors. The genome sequence of COM1 has now been determined and comparison with the published sequence of the *P. furiosus* reference strain ((49); NC_003413) revealed a surprisingly large number of changes. The results of this study have implications not only for the utility of this new genetic system for a well-studied hyperthermophile but also for our understanding of the dynamics of genomic change and maintenance for organisms living both in extreme environments and in the laboratory.

MATERIALS AND METHODS

Strains and growth conditions.

The three *P. furiosus* strains used in this study are termed COM1, which is the genetically tractable strain (37); Parent, which is the lab strain from which COM1 was derived, and DSMZ 3638, which was acquired in October 2010 from the German Collection of Microorganisms and Cell Cultures (Braunshweig, Germany). For genomic DNA isolation (and routine growth studies), cells were grown from a single colony of the COM1 strain, the Parent lab strain population, and the minimally passaged DSMZ strain. They were grown in a complex cellobiose medium as described previously (37) with uracil (20 μM) added to the growth medium of the auxotrophic COM1 strain. Growth experiments to evaluate phenotypes were carried out in biological triplicate in 100 mL serum bottles with 50 mL of complex or defined media with cellobiose, maltose or malto-oligosaccarides as carbon sources at 98°C or 72°C. To obtain cells for enzyme assays, cultures were grown on cellobiose and peptides in a 20 L DCI-Biolafitte BioPro^{TM} Evo Series SIP fermentor and cells were harvested at the end of exponential growth.

DNA sequencing.

Cells for genomic DNA isolation were harvested from a 400 mL stationary phase culture and suspended in 2 mL buffer A (25% sucrose, 50 mM Tris-HCl, 40 mM EDTA pH 7.4) followed by incubation at 37°C for 1 hr with 0.6 mg/mL RNase, 0.2 mg/mL Proteinase K, and 0.25 M EDTA pH 8.0, and then incubation at 65°C for 45 min with 1% SDS, Triton X-100, cetyltrimethylammonium bromide (CTAB), and 0.7M NaCl. Genomic DNA was extracted using phenol:chloroform:isoamyl alcohol (25:24:1, buffered at pH 8), ethanol precipitated and suspended in 10 mM Tris buffer, pH 8.0, to a concentration of ~0.1μg/μl. All genomic sequencing libraries were prepared according to the manufacturer's guidelines. Single-end 454 sequencing of COM1 was performed using a Roche GS FLX titanium pyrosequencer, with a quarter-plate. Illumina sequencing was performed using a single lane on a GAIIx sequencer.

The mate-pair library was constructed with a 2-5 kb protocol. Sanger sequencing of PCR products was used to confirm mutations and genome rearrangements. PCR targets were amplified using PfuTurbo® DNA Polymerase (Stratagene) on a Bio-Rad C1000™ thermal cycler. Products were analyzed on an agarose gel and purified using a StrataPrep PCR Purification Kit (Agilent Technologies).

Genome sequences, assembly and analysis.

De novo hybrid assembly of COM1 single-end 454 and mate-pair Illumina data was performed using the MIRA assembler (version 3.2.1). Illumina library insert size was estimated using Bowtie version 0.12.7 on the NCBI reference *P. furiosus* sequence (NC_003413). Scaffolding of the resulting MIRA-produced contigs was performed using SSPACE version 1.1 in extension mode with the mate-pair Illumina reads. Scaffold regions with ambiguous base calls were PCR amplified and sequenced. Genome block alignments were performed using Progressive Mauve version 2.3.1. Fuzznuc, part of the Emboss toolkit 6.3.1 (48), was used to locate ORFs with exact matches to NCBI-annotated sequences and to sequences derived from a mapped assembly using the *P. furiosus* NCBI genome as a reference. Additional ORFs present in the NCBI annotation that did not have exact matches in the *de novo* assembled chromosome were located using BLAST version 2.2.24 and coordinates determined by visual inspection. In addition to the NCBI gene names, Interpro's Iprscan version 4.8 was used to assign functional annotations to ORFs. Transmembrane domains and signal peptides were predicted using the optional TMHMM and SignalP packages. IS elements were determined using the ISFinder BLAST analysis tool (http://www-is.biotoul.fr/; (52)). The COM1 assembled genome was visualized and annotations corrected using the CLC Genomics Workbench version 6.2. Annotated ORFs were translated using Transeq (EMBOSS toolkit 6.3.1) with Table 11. Needleman-Wunsch global alignments of the translated ORFs with NCBI reference protein sequences were performed using Needle (EMBOSS toolkit 6.3.1). An alignment of the NCBI reference genome (NC_003413) with COM1 was performed using Nucmer version 3.0.7 with a

maximum gap size of 500 and a minimum cluster length of 100. A dot plot of the alignment was created using Mummerplot version 3.5.

Enzyme activities.

Cytoplasmic extracts of each strain were prepared as previously described (42). All steps were carried out under strict anaerobic conditions unless otherwise noted. Non-phosphorylating glyceraldehyde-3-phosphate dehydrogenase (GAPN) activity was measured at 70°C monitoring the rate of NAD(P)H formation at 340 nm (41). β-glucosidase (CelB) activity was measured aerobically in a discontinuous assay with β-D-glucopyranoside-*p*-nitrophenyl as the substrate at 80°C (29). Reaction mixtures contained 50 mM Tris-HCl (pH 7.4) for GAPN and 50 mM sodium phosphate (pH 6.0) for CelB. The Bradford method (3) was used to estimate protein concentrations in cell extracts using bovine serum albumin as the standard.

RESULTS

Genome sequence.

De novo assembly of 5,213,746 total reads of the COM1 genomic DNA resulted in one scaffold of 1,910,278 bp. This is 2,013 bp longer (0.1%) than the NCBI reference sequence for *P. furiosus* (1,908,256 bp) (49). The average coverage of the COM1 scaffold was 32X and 89X for 454 and Illumina reads, respectively.

Genome organization.

Alignment of the COM1 genome sequence with the *P. furiosus* NCBI reference (49) revealed a high overall degree of synteny, with two major inversions (Figure 2.1). Sequence blocks, labeled A to E, were assigned to the COM1 genome based on the organization of the reference sequence (Figures 2.2A and B, respectively) with block A (red colored arrow) starting at PF0001. Block boundaries are located at the sites of IS elements (black tick marks), with the exception of the boundary between blocks A and E, which represents the boundary between the first and last annotated ORFs in the NCBI reference sequence (PF0001 and PF2065). Block A

(red) begins at position 1,497,249 in the COM1 genome sequence and continues through PF0189, followed by block D (blue, PF0390 – PF1603'), block C (green, PF0349 – PF0388), block B (yellow, PF0190 - PF0347), and block E (purple, PF1603'' – PF2065). Relative to the NCBI reference sequence, blocks AE and C are inverted in COM1. The IS elements identified at the boundaries flanking block C were part of the originally annotated sequence (PF0348 and PF0389), whereas the other sites of rearrangement are due to recent IS activity in the intergenic region upstream of PF0190 and within PF1603.

Confirmation of the COM1 genome organization (Figures 2.1 and 2.2A) was obtained by amplifying and sequencing PCR products that spanned the boundaries of each genome block (see Figures S2.1 and S2.2 in the supplemental material). Care was taken to design unique primers not within transposable elements. The chromosomal orientations of the Parent and DSMZ strains were also analyzed. Surprisingly, both the NCBI reference order (Figure 2.2B) and the inverted orientations of blocks AE and C were observed in the COM1 and Parent. Only the inverted order of block C and the reference order of block AE were observed in the DSMZ strain.

IS element activity.

COM1 and the *P. furiosus* reference sequences were annotated for IS elements using ISFinder blast analysis tool (52) with an e-value cut off of $\leq$ 4E-17. The reference sequence contains 29 complete and 6 partial IS elements (Table 2.1), whereas COM1 also contains the same 6 partial sequences in the same relative positions, but the number of complete sequences increased to 39. IS elements represent over 26 kb (1.38%) of the reference genome but over 34 kb (1.79%) of the COM1 genome. Most of the IS elements (80%) identified in both genomes are members of the IS6 family with the remainder representing three other IS families (IS982, IS607 and IS200/IS605, Table 2.1). Species-specific names for the IS elements are based on their origin and include not only ISPfu1-ISPfu5 but also those derived from *Thermococcus* species (ISTko2 and ISTsi3, (52)). The full-length copies of the different ISPfu elements (1-5) have consistent

sizes (781, 782, 933, 1961, and 779 bp, respectively) and possess properties typical of known transposable elements, i.e., putative transposase genes, terminal inverted repeats, and flanking duplicated target sequences. Locations of these IS elements were mapped (Figures 2.2A and B) and it is evident that they are responsible for a large number of genomic changes in COM1 relative to the NCBI sequence. These are summarized in Table 2.2. They include four excisions resulting in the complete or partial deletion of six neighboring genes, seven insertions within seven genes, and nine intergenic insertions potentially affecting regulatory regions upstream of eleven genes. Of these 24 genes, 10 encode conserved hypothetical proteins, 13 are predicted to be in operons, and the predicted cellular location of the gene products are divided between the membrane (7), extracellular (5) and cytoplasmic fractions (12).

Transposases originally annotated in the NCBI reference sequence as PF0013 (ISPfu1), PF0408 (ISPfu1), PF2035 (ISPfu2) and PF0756 (ISPfu2) are deleted in COM1, and these include portions of or complete neighboring genes: PF0012 (39 bp 3' end), PF0407 (41 bp 5' end), PF2034 (41 bp 5' end), and a 1,714 bp region with PF0755 (300 bp deleted at 3' end), PF0757 and PF0758 (deleted), respectively (Table 2.2). The affected neighboring genes are predicted to be non-functional since, in most cases, the deleted region includes the transcriptional start site. Additionally, IS-mediated gene disruptions include PF0061, PF0393, PF0429, PF0823, PF1260, PF1603 and PF2059 and these are also predicted to be non-functional. Nucleotide alignments of each gene are identical to the NCBI reference sequence minus the IS element and duplicated target repeat. However, at the protein-level, the COM1 sequences terminate with premature stop codons ~16 bp into the IS element. An example of IS element gene disruption is shown in Figure 2.3, which compares the gene encoding riboflavin synthase subunit alpha (PF0061). There are some other IS-disrupted genes that have a specific rather than a general predicted function, and these include GAPN, aminopeptidase, and proline permease (Table 2.2), and these are considered further below. Similarly, several intergenic regions were also disrupted by IS elements and may potentially affect the regulation

of genes with specific known or predicted functions, which include alpha-amylase, sugar kinase, trehalose/maltose binding protein, dihydroorotase, methyltransferase, purine permease and cold-induced protein A (57), as shown in Figure 2.4.

In addition to the IS-mediated excisions observed in COM1, there are several genes affected by large chromosomal deletions compared to the reference sequence that appear to be independent of these elements. However, given the obvious recent IS activity, it is impossible to rule out previous IS activity in these regions prior to excision. The coding sequences of the seven genes are partially or completely deleted (Table 2.3) and the encoded proteins are therefore predicted to be non-functional. These include CelB (PF0073), which has a 774 bp deletion at the 3' end resulting in protein length of 214 compared to 472 amino acid residues in the NCBI reference sequence. The other six genes are in a single large chromosomal region (6,238 bp) that includes the genes PF1249-PF1253 (deleted) and PF1254 (904 bp deleted at 5' end). These encode an ABC transporter, a sodium dependent transporter, aromatic aminotransferase II and three hypothetical proteins.

Protein-level genome differences.

In addition to the IS-mediated gene disruptions and large chromosomal deletions observed in COM1, the protein products of 102 of the total 2134 genes in the NCBI reference sequence are disrupted in COM1 at the translational level through non-synonymous mutations. These result in amino acid changes, insertions and deletions introducing premature stop codons and frameshifts producing longer or shorter products with alternate coding sequences. These were subdivided into 36 major changes (Table 2.4) and 66 minor changes (see Table S2.1 in supplemental material) based on the Needleman-Wunsch global alignment identity when compared with the protein sequences in the NCBI reference sequence (49) using ≥ 90% cutoff as a major difference. Since the deletion of the *pyrF* gene (PF1114) is the auxotrophic selectable marker for uracil biosynthesis in the COM1 strain (37), it was omitted from the list of

major differences in Table 2.4 but is included in the complete list of disrupted genes in COM1 relative to the NCBI reference (see Table S2.1 in supplemental material).

In general, although the COM1 genes that fall into the major difference category almost certainly encode nonfunctional proteins, those in the minor difference category could also result in protein products with diminished or abolished functions. Experimental assessment of function would be required for proteins deemed to have minor changes since a single amino acid change could obviously lead to inactivation. Functional annotation of all 102 genes in the reference sequence revealed that 46 of them encode conserved hypothetical proteins (see Table S2.1 in supplemental material). The remaining 56 are predicted to be involved in a wide variety of cellular functions involving carbohydrate and peptide metabolism, DNA repair, CRISPR-associated defense, transcriptional regulation and membrane transport. However, as described above for the IS-mediated disruptions, there are only some affected genes where a specific rather than a general function can be assigned. For example, the major difference category includes two enzymes involved in carbohydrate degradation, β-galactosidase (PF0363) and amylopullulanase (PF1935*; Table 2.4). β-galactosidase in COM1 is predicted to be non-functional as it contains only 32 of the 772 amino acid residues encoded in the NCBI reference sequence due to a single base deletion only 18 bp into the coding sequence creating a premature stop. On the other hand, the gene encoding amylopullulanase was previously reported to have a sequencing error that revealed a gene fusion of PF1934-PF1935 (35). In COM1 we found that the gene fusion results in an even longer protein than previously reported (1,355 compared to 1,114 amino acids, (35)), and is more similar in length to those in other *Pyrococcus* and *Thermococcu*s species. The amylopullulanase in COM1 is therefore expected to be fully functional. In fact, PCR confirmed the same length product for the PF1935* gene in all three strains (DSMZ, Parent, and COM1, data not shown). The COM1 genome sequence also contained the gene fusion between PF1191 and PF1192 previously demonstrated by the native purification of spherical virus-like particles from *P. furiosus* (44).

Phenotypic properties.

The COM1, Parent and DSMZ strains were screened for their ability to grow under various conditions to investigate the predictions of non-functional genes based on the COM1 sequence. For example, both IS and non-IS disruption of gene products or gene regulatory regions (Tables 2.2-2.4) involve β-glucosidase (CelB; PF0073), 4-α-glucanotransferase (PF0272), sugar kinase (PF1738), trehalose/maltose binding protein (PF1739) and GAPN (PF0755). However the growth rates and final cell densities of all three strains, COM1, Parent, and DSMZ, on cellobiose, maltose and malto-oligosaccharides were comparable, with the proviso for COM1 that yeast extract (0.5 g/L) was also added. This was due to the inability of COM1 to synthesize riboflavin due to a non-functional riboflavin synthase (PF0061) (Table 2.2). When riboflavin (0.1 μM) was added, the yeast extract was no longer required. COM1 also grew on a complex peptide-based medium (tryptone, 5 g/L) in the presence of elemental sulfur (2 g/L) to the same extent as the Parent and DSMZ strains, indicating that the disrupted genes in COM1 potentially related to peptide catabolism, including aromatic aminotransferase II (PF1253), proline permease (PF0429) and aminopeptidase (PF2059) (Tables 2.2 and 2.3), do not affect growth on peptides. In addition, all three strains grew well on the defined minimal medium (although COM1 required riboflavin) implying that the function of gene products involved in nucleotide metabolism, such as dihydroorotase (PF0189) and purine permease (PF1240) (Table 2.2), are still fully functional despite upstream IS insertion or not required for growth under these conditions.

A previous study (57) showed that a number of genes are up-regulated when *P. furiosus* is grown at 72°C compared to the optimum near 100°C, the most highly-expressed of which is a membrane glycoprotein termed cold-induced protein A (CipA, (PF0190)). In COM1, *cipA* is not expressed due to the upstream insertion of an IS element (Table 2.2 and Figure 2.4). However, no differences were observed in the ability of the COM1, Parent and DSMZ strains in their abilities to grow at low temperature (72°C, data not shown). In addition, a number of genes

involved in DNA repair, including an uncharacterized RadA domain protein (PF0872), DNA repair helicase Rad3 (PF0933), a 5' to 3' exonuclease NurA (PF1168, (23)), and DNA repair helicase (PF1902) could potentially be inactive in COM1 as they fall into the minor protein-level differences category (see Table S2.1 in supplemental material). However, COM1, Parent and DSMZ showed no significant differences in their ability to recover from exposure to UV or gamma irradiation using conditions previously reported for *P. furiosus* (14). Consequently, in spite of the massive genome rearrangements in COM1 relative to the NCBI reference sequence, and the actual or potential inactivation of more than 120 genes, its ability to grow under various conditions previously used for the Parent strain in the laboratory are unaffected.

Enzyme assays were carried out to determine the effects of 5' end deletion of the gene encoding non-phosphorylating glyceraldehyde-3-phosphate dehydrogenase, GAPN (PF0755), and the 3' end deletion of the gene encoding β-glucosidase (CelB; PF0073). The DSMZ strain was used as a control, as PCR and sequence analyses confirmed that it contained full-length versions of *gapn* and *celB* (data not shown). On the other hand, PCR analysis of the Parent strain revealed a full-length copy of *gapn* but its *celB* contained the same 5' end deletion as that found in COM1. Surprisingly, all attempts to measure GAPN activity in the cell extracts of all three of the strains were unsuccessful, even in the presence of glucose-1-phosphate (1 mM), which is reportedly an activator of the enzyme in *Thermococcus kodakarensis* (41). As expected, the DSMZ strain contained high CelB activity (1.68 μmoles/min/mg at pH 6.0) and this was an order of magnitude greater than that measured in extracts of either the COM1 or Parent strains (0.16 and 0.15 μmoles/min/mg, respectively at pH 6.0).

DISCUSSION

The availability of a highly efficient genetically-tractable strain of *P. furiosus* (COM1) has dramatically expanded the potential to study this model hyperthermophilic species. Its sequence not only defines the genetic platform for these future studies, it has also provided

novel insights into chromosome structure and plasticity. The COM1 sequence assembly and scaffolding indicated the inversion of two large chromosomal segments relative to the published NCBI reference sequence (Figures 2.1 and 2.2). The high rate of chromosomal breakage in hyperthermophilic environments and those where large doses of ionizing radiation are encountered require robust and accurate repair mechanisms (46). *P. furiosus* is able to completely reassemble its chromosome after gamma radiation-induced fragmentation into 30-500 kb fragments with up to 15 chromosomal copies per cell present in the exponential growth phase serving as templates for reassembly (12). This ability, coupled with IS elements scattered throughout the genome that serve as substrates for homologous recombination, is consistent with the observed alterations in genome structure in COM1. A comparative genomics study of three *Pyrococcus* species revealed that the genome of *P. furiosus* exhibits less bias in the preference of co-directionality of transcription with replication than other sequenced organisms at the time (60). Given the ease with which the genome undergoes rearrangement, this is likely necessary to ensure proper transcription of essential genes. In addition, the high degree of operonization in the genome of *P. furiosus* places further constraints on the location of chromosomal shuffling hot spots (59).

IS elements also participate in genome evolution by disrupting gene coding sequences, influencing the expression of genes downstream of insertions (10). Sequencing of the COM1 genome revealed that two IS element types, ISPfu1 and 2 (both of the IS6 family), have been recently active under laboratory conditions and involved in four excisions and fourteen insertions within genes and upstream of genes in potential regulatory regions (Table 2.2). LGT of a bacterial-type composite transposon was previously documented in *P. furiosus* and *T. litoralis* with the acquisition in the former organism of the Mal I ABC transport system for maltose and trehalose (13, 22, 45). Among the seven IS annotated archaeal genomes (30), *P. furiosus* harbors far more IS elements (29 full, 6 partial) than any other member of the *Thermococcales*, but less than a quarter of the IS elements identified in the *S. solfataricus* genome (146 full, 297

partial). In fact, no full-length IS elements have been identified in the genomes of *P. abyssi* or *P. horikoshii*, and only one full length IS element has been identified in *T. kodakarensis* (30).

In addition to IS-mediated disruptions, 102 differences in sequence were observed in the COM1 genome that would lead to gene products differing from those encoded by the published NCBI reference sequence. Some are likely to have been sequencing or assembly errors in the original published NCBI sequence, some could have arisen in the lab strain through random mutagenesis and some may be unique to the COM1 strain. However, these categories are difficult to assess quantitatively. Although the NCBI reference sequence is labeled as the type strain (DSM 3638), the strain that provided the reference sequence (49) was not obtained directly from the DSMZ (Kelly, R. and Robb, F., personal communication). Originally a gift from Dr. Karl Stetter (19), the strain was maintained at 4°C in a laboratory setting with periodic clonal selection for more than 10 years prior to producing DNA for genome sequencing in 1999 (49). Similarly, the strain that gave rise to COM1 (37) was obtained from DSMZ in 2007 and maintained for two years in the laboratory at ambient temperature with multiple transfers on various media. That such conditions can lead to numerous mutations in strains originating from the same isolate is not surprising and is now well established in other organisms. For example, this was recently revealed by a large scale re-sequencing effort of *Bacillus subtilis* strains from multiple laboratories (53), emphasizing the need to maintain a permanent storage capacity within the laboratory setting.

Despite extensive genomic changes in the COM1 strain, including multiple excisions, insertions and protein-level changes, its major metabolic functions have not been disrupted. Select phenotypic properties were examined based on the changes in the COM1 strain but no significant differences in growth under a variety of conditions were detected between it and the Parent and DSMZ strains. However, this analysis did reveal one puzzle and this concerned the glycolytic enzyme, GAPN, whose function should be abolished in COM1 due to the deletion of the transcriptional start site. However, we were unable confirm loss of GAPN activity in cell

extracts of COM1 since the Parent and DSMZ strains, which from sequence analyses should contain a functional GAPN, also lacked this activity. GAPN has been shown to be a key glycolytic enzyme in the related euryarchaeon *T. kodakarensis* since a strain with a targeted gene knockout (Δ*gapN*) was unable to grow on malto-oligosaccharides (41). Similarly, GAPN plays a key glycolytic role in various crenarchaeota, including *Thermoproteus* (5), *Aeropyrum* (47) and *Sulfolobus* species (1, 17). The oxidation of glyceraldehyde-3-phosphate during glycolysis in *P. furiosus* can be catalyzed by the tungsten-containing enzyme, glyceraldehyde-3-phosphate ferredoxin oxidoreductase (GAPOR), which uses ferredoxin rather than NADP as the electron acceptor (43). In *T. kodakarensis* both GAPOR and GAPN are required for growth on sugars (41) but, for unknown reasons, this is not the case in *P. furiosus* as COM1 grew well on maltose, cellobiose and malto-oligosaccharides in the absence of a functional GAPN. COM1 also lacks the gene encoding CelB, but its ability to utilize cellobiose, a β-1,4-linked disaccharide, is not surprising given that there is redundancy in beta-specific glycosidases in *P. furiosus* (15).

One significant phenotypic difference between COM1 and the Parent and DSMZ strains is obviously their ability to be genetically manipulated. The high efficiency in transformation and recombination of COM1 is likely the result of changes in multiple genes but genome sequence comparisons between the strains cannot define the responsible gene(s). One group potentially involved in conferring competence is the disruption of five of the CRISPR-associated (Cas) proteins (Tables 2.2 and 2.4 and see Table S2.1 in supplemental material). This is the most well characterized defense system against invasion by foreign nucleic acids in both archaea and bacteria (20, 39). In *P. furiosus*, Cas6 has been shown to recognize and cleave foreign RNA that match spacer sequences present in the host's CRISPR loci (6, 21). A possible role of these disrupted proteins in conferring competence is intriguing and an obvious target for future research. Other disrupted genes in COM1 that could also play a role in DNA uptake and recombination include 20 membrane transporters, one or more of which could affect membrane

integrity thereby facilitating DNA uptake. Similarly, numerous proteins involved in DNA replication, transcription, and repair are actually or potentially disrupted in COM1 (see Tables 2.2 and 2.4). These include four DNA helicases (PF0085, PF0572, PF0933, PF1902), two RNA helicases (PF0592, PF1120), a DNA primase (PF1725), a cell division control protein (PF1882), an uncharacterized RadA domain protein (PF0872), five putative transcription factors (DNA-binding proteins: PF0054, PF0524, PF0621, PF0710, PF1206), a RNA-binding protein (PF1573), and a 5' to 3' exonuclease NurA (PF1168, (23)). In addition, of the 122 genes disrupted by IS- and non-IS-mediated events in the COM1 strain, 56 of them encode conserved hypothetical proteins, some of which could be partially or solely responsible for the genetic properties of COM1. Clearly, determining how many of these genes directly or indirectly affect competence will not be an easy task.

ACKNOWLEDGEMENTS

We acknowledge the Division of Chemical Sciences, Geosciences, and Biosciences, Office of Basic Energy Sciences of the U.S. Department of Energy through grant DE-FG05-95ER20175 for funding the phenotypic analyses and the ENIGMA project supported by the U. S Department of Energy under Contract No. DE-AC02-05CH11231 for funding the sequencing and data analysis. We thank the UGA Sequencing Facility for 454 sequencing, K. Stirrett and J. Westpheling for providing a sample of COM1 DNA for 454 sequencing, Ryan Weil at the Emory GRA Genomics Core for assistance with Illumina sequencing, Mirko Basen for assistance with low temperature cultures, and Gina Lipscomb for many helpful discussions.

REFERENCES

1. **Albers, S. V., N. K. Birkeland, A. J. Driessen, S. Gertig, P. Haferkamp, H. P. Klenk, T. Kouril, A. Manica, T. K. Pham, P. Ruoff, C. Schleper, D. Schomburg, K. J. Sharkey, B. Siebers, P. Sierocinski, R. Steuer, J. van der Oost, H. V. Westerhoff, P. Wieloch, P. C. Wright, and M. Zaparty.** 2009. SulfoSYS (Sulfolobus Systems Biology): towards a silicon cell model for the central carbohydrate metabolism of the archaeon *Sulfolobus solfataricus* under temperature variation. Biochem Soc Trans **37:**58-64.
2. **Atomi, H.** 2005. Recent progress towards the application of hyperthermophiles and their enzymes. Curr Opin Chem Biol **9:**166-73.
3. **Bradford, M. M.** 1976. A rapid and sensitive method for the quantitation of microgram quantities of protein utilizing the principle of protein-dye binding. Anal Biochem **72:**248-54.
4. **Bridger, S. L., S. M. Clarkson, K. Stirrett, M. B. DeBarry, G. L. Lipscomb, G. J. Schut, J. Westpheling, R. A. Scott, and M. W. Adams.** 2011. Deletion strains reveal metabolic roles for key elemental sulfur-responsive proteins in *Pyrococcus furiosus*. J Bacteriol **193:**6498-504.
5. **Brunner, N. A., H. Brinkmann, B. Siebers, and R. Hensel.** 1998. NAD+-dependent glyceraldehyde-3-phosphate dehydrogenase from *Thermoproteus tenax*. The first identified archaeal member of the aldehyde dehydrogenase superfamily is a glycolytic enzyme with unusual regulatory properties. J Biol Chem **273:**6149-56.
6. **Carte, J., N. T. Pfister, M. M. Compton, R. M. Terns, and M. P. Terns.** 2010. Binding and cleavage of CRISPR RNA by Cas6. RNA **16:**2181-8.
7. **Chandrayan, S. K., P. M. McTernan, R. C. Hopkins, J. Sun, F. E. Jenney, Jr., and M. W. Adams.** 2012. Engineering Hyperthermophilic Archaeon *Pyrococcus furiosus* to Overproduce Its Cytoplasmic [NiFe]-Hydrogenase. J Biol Chem **287:**3257-64.

8. **Chinen, A., I. Uchiyama, and I. Kobayashi.** 2000. Comparison between *Pyrococcus horikoshii* and *Pyrococcus abyssi* genome sequences reveals linkage of restriction-modification genes with large genome polymorphisms. Gene **259:**109-21.

9. **Cohen, G. N., V. Barbe, D. Flament, M. Galperin, R. Heilig, O. Lecompte, O. Poch, D. Prieur, J. Querellou, R. Ripp, J. C. Thierry, J. Van der Oost, J. Weissenbach, Y. Zivanovic, and P. Forterre.** 2003. An integrated analysis of the genome of the hyperthermophilic archaeon *Pyrococcus abyssi*. Mol Microbiol **47:**1495-512.

10. **Craig, N. L., R. Craigie, M. Gellert, and A. M. Lambowitz (ed.).** 2002. Mobile DNA II. American Society for Microbiology, Washington, D.C.

11. **Cvetkovic, A., A. L. Menon, M. P. Thorgersen, J. W. Scott, F. L. Poole, 2nd, F. E. Jenney, Jr., W. A. Lancaster, J. L. Praissman, S. Shanmukh, B. J. Vaccaro, S. A. Trauger, E. Kalisiak, J. V. Apon, G. Siuzdak, S. M. Yannone, J. A. Tainer, and M. W. Adams.** 2010. Microbial metalloproteomes are largely uncharacterized. Nature **466:**779-82.

12. **DiRuggiero, J., J. R. Brown, A. P. Bogert, and F. T. Robb.** 1999. DNA Repair Systems in Archaea: Mementos from the Last Universal Common Ancestor? J Mol Evol **49:**474-84.

13. **Diruggiero, J., D. Dunn, D. L. Maeder, R. Holley-Shanks, J. Chatard, R. Horlacher, F. T. Robb, W. Boos, and R. B. Weiss.** 2000. Evidence of recent lateral gene transfer among hyperthermophilic archaea. Mol Microbiol **38:**684-93.

14. **DiRuggiero, J., N. Santangelo, Z. Nackerdien, J. Ravel, and F. T. Robb.** 1997. Repair of extensive ionizing-radiation DNA damage at 95 degrees C in the hyperthermophilic archaeon *Pyrococcus furiosus*. J Bacteriol **179:**4643-5.

15. **Driskill, L. E., M. W. Bauer, and R. M. Kelly.** 1999. Synergistic interactions among beta-laminarinase, beta-1,4-glucanase, and beta-glucosidase from the hyperthermophilic

archaeon *Pyrococcus furiosus* during hydrolysis of beta-1,4-, beta-1,3-, and mixed-linked polysaccharides. Biotechnol Bioeng **66:**51-60.

16. **Escobar-Paramo, P., S. Ghosh, and J. DiRuggiero.** 2005. Evidence for genetic drift in the diversification of a geographically isolated population of the hyperthermophilic archaeon *Pyrococcus*. Mol Biol Evol **22:**2297-303.

17. **Ettema, T. J., H. Ahmed, A. C. Geerling, J. van der Oost, and B. Siebers.** 2008. The non-phosphorylating glyceraldehyde-3-phosphate dehydrogenase (GAPN) of *Sulfolobus solfataricus*: a key-enzyme of the semi-phosphorylative branch of the Entner-Doudoroff pathway. Extremophiles **12:**75-88.

18. **Farkas, J., D. Chung, M. DeBarry, M. W. Adams, and J. Westpheling.** 2011. Defining components of the chromosomal origin of replication of the hyperthermophilic archaeon *Pyrococcus furiosus* needed for construction of a stable replicating shuttle vector. Appl Environ Microbiol **77:**6343-9.

19. **Fiala, G., and K. Stetter.** 1986. *Pyrococcus furiosus* sp. nov. represents a novel genus of marine heterotrophic archaebacteria growing optimally at 100°C. Arch Microbiol **145:**56-61.

20. **Garrett, R. A., G. Vestergaard, and S. A. Shah.** 2011. Archaeal CRISPR-based immune systems: exchangeable functional modules. Trends Microbiol **19:**549-56.

21. **Hale, C. R., P. Zhao, S. Olson, M. O. Duff, B. R. Graveley, L. Wells, R. M. Terns, and M. P. Terns.** 2009. RNA-guided RNA cleavage by a CRISPR RNA-Cas protein complex. Cell **139:**945-56.

22. **Hamilton-Brehm, S. D., G. J. Schut, and M. W. Adams.** 2005. Metabolic and evolutionary relationships among *Pyrococcus* Species: genetic exchange within a hydrothermal vent environment. J Bacteriol **187:**7492-9.

23. **Hopkins, B. B., and T. T. Paull.** 2008. The *P. furiosus* mre11/rad50 complex promotes 5' strand resection at a DNA double-strand break. Cell **135:**250-60.

24. **Hopkins, R. C., J. Sun, F. E. Jenney, Jr., S. K. Chandrayan, P. M. McTernan, and M. W. Adams.** 2011. Homologous expression of a subcomplex of *Pyrococcus furiosus* hydrogenase that interacts with pyruvate ferredoxin oxidoreductase. PLoS One **6:**e26569, Oct 24 (epub).

25. **Jenney, F. E., Jr., and M. W. Adams.** 2008. The impact of extremophiles on structural genomics (and vice versa). Extremophiles **12:**39-50.

26. **Jun, X., L. Lupeng, X. Minjuan, P. Oger, W. Fengping, M. Jebbar, and X. Xiang.** 2011. Complete genome sequence of the obligate piezophilic hyperthermophilic archaeon *Pyrococcus yayanosii* CH1. J Bacteriol **193:**4297-8.

27. **Kanoksilapatham, W., J. M. Gonzalez, D. L. Maeder, J. DiRuggiero, and F. T. Robb.** 2004. A proposal to rename the hyperthermophile *Pyrococcus woesei* as *Pyrococcus furiosus* subsp. *woesei*. Archaea **1:**277-83.

28. **Kawarabayasi, Y., M. Sawada, H. Horikawa, Y. Haikawa, Y. Hino, S. Yamamoto, M. Sekine, S. Baba, H. Kosugi, A. Hosoyama, Y. Nagai, M. Sakai, K. Ogura, R. Otsuka, H. Nakazawa, M. Takamiya, Y. Ohfuku, T. Funahashi, T. Tanaka, Y. Kudoh, J. Yamazaki, N. Kushida, A. Oguchi, K. Aoki, and H. Kikuchi.** 1998. Complete sequence and gene organization of the genome of a hyper-thermophilic archaebacterium, *Pyrococcus horikoshii* OT3. DNA Res **5:**55-76.

29. **Kengen, S. W., E. J. Luesink, A. J. Stams, and A. J. Zehnder.** 1993. Purification and characterization of an extremely thermostable beta-glucosidase from the hyperthermophilic archaeon *Pyrococcus furiosus*. Eur J Biochem **213:**305-12.

30. **Kichenaradja, P., P. Siguier, J. Perochon, and M. Chandler.** 2010. ISbrowser: an extension of ISfinder for visualizing insertion sequences in prokaryotic genomes. Nucleic Acids Res **38:**D62-8.

31. **Koning, S. M., W. N. Konings, and A. J. Driessen.** 2002. Biochemical evidence for the presence of two alpha-glucoside ABC-transport systems in the hyperthermophilic archaeon *Pyrococcus furiosus*. Archaea **1:**19-25.

32. **Lancaster, W. A., J. L. Praissman, F. L. Poole, 2nd, A. Cvetkovic, A. L. Menon, J. W. Scott, F. E. Jenney, Jr., M. P. Thorgersen, E. Kalisiak, J. V. Apon, S. A. Trauger, G. Siuzdak, J. A. Tainer, and M. W. Adams.** 2011. A computational framework for proteome-wide pursuit and prediction of metalloproteins using ICP-MS and MS/MS data. BMC Bioinformatics **12:**64.

33. **Lecompte, O., R. Ripp, V. Puzos-Barbe, S. Duprat, R. Heilig, J. Dietrich, J. C. Thierry, and O. Poch.** 2001. Genome evolution at the genus level: comparison of three complete genomes of hyperthermophilic archaea. Genome Res **11:**981-93.

34. **Lee, H. S., S. S. Bae, M. S. Kim, K. K. Kwon, S. G. Kang, and J. H. Lee.** 2011. Complete genome sequence of hyperthermophilic *Pyrococcus* sp. strain NA2, isolated from a deep-sea hydrothermal vent area. J Bacteriol **193:**3666-7.

35. **Lee, H. S., K. R. Shockley, G. J. Schut, S. B. Conners, C. I. Montero, M. R. Johnson, C. J. Chou, S. L. Bridger, N. Wigner, S. D. Brehm, F. E. Jenney, Jr., D. A. Comfort, R. M. Kelly, and M. W. Adams.** 2006. Transcriptional and biochemical analysis of starch metabolism in the hyperthermophilic archaeon *Pyrococcus furiosus*. J Bacteriol **188:**2115-25.

36. **Leigh, J. A., S. V. Albers, H. Atomi, and T. Allers.** 2011. Model organisms for genetics in the domain Archaea: methanogens, halophiles, *Thermococcales* and *Sulfolobales*. FEMS Microbiol Rev **35:**577-608.

37. **Lipscomb, G. L., K. Stirrett, G. J. Schut, F. Yang, F. E. Jenney, Jr., R. A. Scott, M. W. Adams, and J. Westpheling.** 2011. Natural competence in the hyperthermophilic archaeon *Pyrococcus furiosus* facilitates genetic manipulation: construction of

markerless deletions of genes encoding the two cytoplasmic hydrogenases. Appl Environ Microbiol **77:**2232-8.

38. **Mahillon, J., and M. Chandler.** 1998. Insertion sequences. Microbiol Mol Biol Rev **62:**725-74.

39. **Makarova, K. S., D. H. Haft, R. Barrangou, S. J. Brouns, E. Charpentier, P. Horvath, S. Moineau, F. J. Mojica, Y. I. Wolf, A. F. Yakunin, J. van der Oost, and E. V. Koonin.** 2011. Evolution and classification of the CRISPR-Cas systems. Nat Rev Microbiol **9:**467-77.

40. **Martusewitsch, E., C. W. Sensen, and C. Schleper.** 2000. High spontaneous mutation rate in the hyperthermophilic archaeon *Sulfolobus solfataricus* is mediated by transposable elements. J Bacteriol **182:**2574-81.

41. **Matsubara, K., Y. Yokooji, H. Atomi, and T. Imanaka.** 2011. Biochemical and genetic characterization of the three metabolic routes in *Thermococcus kodakarensis* linking glyceraldehyde 3-phosphate and 3-phosphoglycerate. Mol Microbiol **81:**1300-12.

42. **Menon, A. L., F. L. Poole, 2nd, A. Cvetkovic, S. A. Trauger, E. Kalisiak, J. W. Scott, S. Shanmukh, J. Praissman, F. E. Jenney, Jr., W. R. Wikoff, J. V. Apon, G. Siuzdak, and M. W. Adams.** 2009. Novel multiprotein complexes identified in the hyperthermophilic archaeon *Pyrococcus furiosus* by non-denaturing fractionation of the native proteome. Mol Cell Proteomics **8:**735-51.

43. **Mukund, S., and M. W. Adams.** 1995. Glyceraldehyde-3-phosphate ferredoxin oxidoreductase, a novel tungsten-containing enzyme with a potential glycolytic role in the hyperthermophilic archaeon *Pyrococcus furiosus*. J Biol Chem **270:**8389-92.

44. **Namba, K., K. Hagiwara, H. Tanaka, Y. Nakaishi, K. T. Chong, E. Yamashita, G. E. Armah, Y. Ono, Y. Ishino, T. Omura, T. Tsukihara, and A. Nakagawa.** 2005. Expression and molecular characterization of spherical particles derived from the

genome of the hyperthermophilic euryarchaeote *Pyrococcus furiosus*. J Biochem **138:**193-9.

45. **Noll, K. M., P. Lapierre, J. P. Gogarten, and D. M. Nanavati.** 2008. Evolution of mal ABC transporter operons in the *Thermococcales* and *Thermotogales*. BMC Evol Biol **8:**7.

46. **Peak, M. J., F. T. Robb, and J. G. Peak.** 1995. Extreme resistance to thermally induced DNA backbone breaks in the hyperthermophilic archaeon *Pyrococcus furiosus*. J Bacteriol **177:**6316-8.

47. **Reher, M., S. Gebhard, and P. Schonheit.** 2007. Glyceraldehyde-3-phosphate ferredoxin oxidoreductase (GAPOR) and nonphosphorylating glyceraldehyde-3-phosphate dehydrogenase (GAPN), key enzymes of the respective modified Embden-Meyerhof pathways in the hyperthermophilic crenarchaeota *Pyrobaculum aerophilum* and *Aeropyrum pernix*. FEMS Microbiol Lett **273:**196-205.

48. **Rice, P., I. Longden, and A. Bleasby.** 2000. EMBOSS: the European Molecular Biology Open Software Suite. Trends Genet **16:**276-7.

49. **Robb, F. T., D. L. Maeder, J. R. Brown, J. DiRuggiero, M. D. Stump, R. K. Yeh, R. B. Weiss, and D. M. Dunn.** 2001. Genomic sequence of hyperthermophile, *Pyrococcus furiosus*: implications for physiology and enzymology. Methods Enzymol **330:**134-57.

50. **Santangelo, T. J., L. Cubonova, and J. N. Reeve.** 2010. *Thermococcus kodakarensis* genetics: TK1827-encoded beta-glycosidase, new positive-selection protocol, and targeted and repetitive deletion technology. Appl Environ Microbiol **76:**1044-52.

51. **Schut, G. J., S. D. Brehm, S. Datta, and M. W. Adams.** 2003. Whole-genome DNA microarray analysis of a hyperthermophile and an archaeon: *Pyrococcus furiosus* grown on carbohydrates or peptides. J Bacteriol **185:**3935-47.

52. **Siguier, P., J. Perochon, L. Lestrade, J. Mahillon, and M. Chandler.** 2006. ISfinder: the reference centre for bacterial insertion sequences. Nucleic Acids Res **34:**D32-6.

53. **Srivatsan, A., Y. Han, J. Peng, A. K. Tehranchi, R. Gibbs, J. D. Wang, and R. Chen.** 2008. High-precision, whole-genome sequencing of laboratory strains facilitates genetic studies. PLoS Genet **4:**e1000139.

54. **Strand, K. R., C. Sun, T. Li, F. E. Jenney, Jr., G. J. Schut, and M. W. Adams.** 2010. Oxidative stress protection and the repair response to hydrogen peroxide in the hyperthermophilic archaeon *Pyrococcus furiosus* and in related species. Arch Microbiol **192:**447-59.

55. **Tran, T. T., P. Dam, Z. Su, F. L. Poole, 2nd, M. W. Adams, G. T. Zhou, and Y. Xu.** 2007. Operon prediction in *Pyrococcus furiosus*. Nucleic Acids Res **35:**11-20.

56. **Ward, D. E., W. M. de Vos, and J. van der Oost.** 2002. Molecular analysis of the role of two aromatic aminotransferases and a broad-specificity aspartate aminotransferase in the aromatic amino acid metabolism of *Pyrococcus furiosus*. Archaea **1:**133-41.

57. **Weinberg, M. V., G. J. Schut, S. Brehm, S. Datta, and M. W. Adams.** 2005. Cold shock of a hyperthermophilic archaeon: *Pyrococcus furiosus* exhibits multiple responses to a suboptimal growth temperature with a key role for membrane-bound glycoproteins. J Bacteriol **187:**336-48.

58. **White, J. R., P. Escobar-Paramo, E. F. Mongodin, K. E. Nelson, and J. DiRuggiero.** 2008. Extensive genome rearrangements and multiple horizontal gene transfers in a population of *Pyrococcus* isolates from Vulcano Island, Italy. Appl Environ Microbiol **74:**6447-51.

59. **Yoon, S. H., D. J. Reiss, J. C. Bare, D. Tenenbaum, M. Pan, J. Slagel, R. L. Moritz, S. Lim, M. Hackett, A. L. Menon, M. W. Adams, A. Barnebey, S. M. Yannone, J. A. Leigh, and N. S. Baliga.** 2011. Parallel evolution of transcriptome architecture during genome reorganization. Genome Res **21:**1892-904.

60. **Zivanovic, Y., P. Lopez, H. Philippe, and P. Forterre.** 2002. *Pyrococcus* genome comparison evidences chromosome shuffling-driven evolution. Nucleic Acids Res **30:**1902-10.

Table 2.1. Comparison of IS element population in *P. furiosus* COM1 strain relative to the NCBI reference sequence.

IS Family	Name	COM1 Genome		NCBI Reference	
		Full	Partial	Full	Partial
IS6	ISPfu1	16	1	8	1
	ISPfu2	13	0	11	0
	ISPfu5	4	0	4	0
IS982	ISPfu3	5	0	5	0
IS607	ISPfu4	1	2	1	2
	ISTko2	0	2	0	2
IS200/IS605	ISTsi3	0	1	0	1
	Total IS elements	39	6	29	6
	Total IS lengths (bp)	32406	1798	24592	1798
	Genome (%)	1.70	0.09	1.29	0.09

ISFinder blast analysis tool (52) was used to annotate IS elements with e-value scores $\leq$ 4E-17 in both the COM1 and NCBI reference genome sequences. Sequence similarity among the members of an IS family and between IS families results in multiple hits at each locus. Only the best BLAST hit was retained for each IS element.

Table 2.2. Genes affected by IS activity in the *P. furiosus* COM1 strain.

IS Element[a]	Affected Gene(s)	Gene Annotation[b]	Length (bp)	Operon Position[c]	Predicted Location[d]
Excisions[e]			**Deletion**		
PF0013 (ISPfu1)	PF0012	hypothetical protein	39 (3' end)		cyt
PF0408 (ISPfu1)	PF0407	<carboxypeptidase-like, regulatory domain>	41 (5' end)	1 of 2	mem
PF0756 (ISPfu2)	PF0755	non-phosphorylating GAPDH (GAPN)	300 (5'end)	4 of 4	cyt
	PF0757	hypothetical protein	complete		cyt
	PF0758	<nucleotide-binding domain (HEPN)>	complete		cyt
PF2035 (ISPfu2)	PF2034	<methyltransferase (TYW3)>	41 (5'end)	1 of 2	cyt
Insertions in ORF[f]			**IS Element**		
ISPfu2	PF0061	riboflavin synthase subunit alpha	782	1 of 4	cyt
ISPfu1	PF0393	[CRISPR-associated protein, Cas6-2 (21)]	781		cyt
ISPfu1	PF0429	proline permease	781		mem
ISPfu1	PF0823	<multi antimicrobial extrusion protein (MatE)>	781	1 of 2	mem
ISPfu1	PF1260	hypothetical protein	781	1 of 2	cyt
ISPfu1	PF1603	Na antiporter	781	1 of 3	mem
ISPfu1	PF2059	aminopeptidase	781	1 of 2	exc
Insertion in Intergenic Regions[g]			**IS Element**		
ISPfu1	PF0189	dihydroorotase	781	3 of 3	cyt
	PF0190	[cold-induced protein A, CipA (57)]			mem
ISPfu1	PF0271	hypothetical protein	781		exc
	PF0272	[4-α-glucanotransferase, (35)]			cyt
ISPfu1	PF0401	methyltransferase	781	4 of 4	exc

ISPfu1	PF1738	sugar kinase	781		cyt
	PF1739	[Mal I transporter, (31)]		1 of 6	exc
ISPfu2	PF_t006	tRNA Glu anticodon TTC	782		
ISPfu2	PF0497	<Winged helix-turn-helix transcription factor>	782	1 of 9	cyt
ISPfu2	PF1239	hypothetical protein	782		mem
	PF1240	purine permease		1 of 2	mem

[a] IS element nomenclature based on ISFinder database (52).
[b] Annotations are NCBI gene names (no brackets) and literature cited ([ ]), except for hypothetical genes, where the best IPR (< >) match is given if available.
[c] Operon predictions from (55) based on NCBI reference sequence.
[d] Predicted cellular location based on predicted TMDs, proteins with ≥ 2 TMDs classified as membrane (mem), proteins with <2 TMDs and a predicted signal peptide using SignalP with the gram-positive model ≥ 0.6 are classified as extracellular (exc), and proteins with <2 TMDs and no predicted signal peptide are classified as cytoplasmic (cyt).
[e] Includes neighboring genes affected by IS excision, either full deletion (complete) or truncation (bp) at the chromosomal-level.
[f] Includes genes disrupted by IS insertion within their open reading frame.
[g] Includes neighboring genes with transcriptional start sites downstream of IS insertion.

Table 2.3. Additional large chromosomal deletions in *P. furiosus* COM1 strain relative to NCBI reference.

Gene	Gene Annotation[b]	Deletion Length (bp)	Operon Position[c]	Predicted Location[d]
PF0073	beta-glucosidase (CelB)	774 of 1,419 (3' end)		cyt
PF1249[h]	ABC transporter	complete	1 of 2	cyt
PF1250	hypothetical protein	complete	2 of 2	exc
PF1251	<alpha-galactosidase, NEW3 domain>	complete	1 of 2	cyt
PF1252	hypothetical protein	complete	2 of 2	mem
PF1253	[aromatic aminotransferase II (56)]	complete		cyt
PF1254	sodium dependent transporter	904 of 1,737 (5' end)	1 of 2	mem

[b] Annotations are NCBI gene names (no brackets) and literature cited ([ ]), except for hypothetical genes, where the best IPR (< >) match is given if available.
[c] Operon predictions from (55) based on NCBI reference sequence.
[d] Predicted cellular location, for explanation see Table 2.2, footnote d.
[h] Adjacent to transposase (PF1248, ISPfu3) in both COM1 and reference sequence.

Table 2.4. Major protein-level genome differences in *P. furiosus* COM1 strain relative to NCBI reference (<90% identity).

Gene	Gene Annotation[b]	Identical Residues (AA)[i]	Alignment Length (AA)[i]	Identity (%)[i]	Operon Position[c]	Predicted Location[d]
PF0054	AsnC family transcriptional regulator	91	155	58.7	6 of 7	cyt
PF0067	cobalt ABC transporter	157	243	64.6	1 of 2	mem
PF0147	potassium channel-like protein	23	205	11.2	2 of 2	cyt
PF0225	N-acetyltransferase	111	201	55.2	1 of 2	cyt
PF0228	hypothetical protein	49	89	55.1	2 of 3	cyt
PF0244	hypothetical protein	38	89	42.7		cyt
PF0314	signal peptidase	58	173	33.5	2 of 3	cyt
PF0334	flagella-like protein	24	194	12.4	2 of 6	exc
PF0351	hypothetical protein	22	285	7.7		cyt
PF0352	[CRISPR-associated protein, Cmr1-2 (21)]	189	451	41.9		cyt
PF0363	beta-galactosidase	11	775	1.4	7 of 7	cyt
PF0423	hypothetical protein	45	117	38.5	1 of 3	cyt
PF0424	hypothetical protein	34	172	19.8	2 of 3	cyt
PF0439	hypothetical protein	297	401	74.1		cyt
PF0472	<class III signal peptide motif>	42	54	77.8	2 of 2	exc
PF0524	<ribbon-helix-helix (Met_repress_like)>	57	72	79.2	1 of 4	cyt
PF0611	hypothetical protein	295	382	77.2		cyt
PF0622	hypothetical protein	7	33	21.2		cyt
PF0710	<transcription repressor DNA-binding>	79	157	50.3	3 of 3	cyt
PF0764	DEXX-box atpase	232	434	53.5		cyt

PF0777	hypothetical protein	191	215	88.8		mem
PF0785.2n	hypothetical protein	148	192	77.1		N/A
PF0873	hypothetical protein	36	196	18.4		cyt
PF0874	membrane dipeptidase	9	379	2.4	1 of 2	cyt
PF0901	hypothetical protein	121	142	85.2		cyt
PF0960	hypothetical protein	15	112	13.4	2 of 2	exc
PF1075	hypothetical protein	3	219	1.4		mem
PF1109	<carbohydrate-binding domain (CARDB)>	959	1132	84.7	1 of 2	exc
PF1113	<tRNA amidotransferease GAD domain>	199	223	89.2	1 of 3	cyt
PF1182	<thioredoxin-like fold>	7	126	5.6		cyt
PF1182.1n	hypothetical protein	53	169	31.4		N/A
PF1206	<nucleic acid-binding, PIN, PH0500>	15	156	9.6	1 of 3	cyt
PF1748	sulfate permease, ABC transporter	321	543	59.1	4 of 6	mem
PF1749	sulfate transport integral membrane protein	10	228	4.4	5 of 6	mem
PF1761	<putative cell wall binding repeat 2>	204	389	52.4	1 of 2	exc
PF1935[j]	amylopullulanase	1114	1355	82.2	3 of 6	exc

[b] Annotations are NCBI gene names (no brackets) and literature cited ([ ]), except for hypothetical genes, where the best IPR (< >) match is given if available.
[c] Operon predictions from (55) based on NCBI reference sequence.
[d] Predicted cellular location, for explanation see Table 2.2, footnote d.
[i] Based on Needleman-Wunsch global alignment with NCBI reference sequence.
[j] A fusioin of PF1934 and PF1935 was previously reported (35). A longer product was found in COM1 which is closer in length to those in other *Pyrococci*.

Figure 2.1. Dot plot of the alignment of the *P. furiosus* NCBI reference sequence (NC_003413) on the x-axis and the *P. furiosus* COM1 strain on the y-axis indicates high overall synteny with two major inversions. Inverted segments in COM1 synonymous with the circular diagram in Figure 2.2 are: block A (1,497,249-1,297,198), block E (1,911,081-1,497,250), and block C (199,582-162,245). The small segment (210,862-211,700) is a result of an IS element insertion between PF0401 and PF0402 in COM1.

FIGURE 2.1

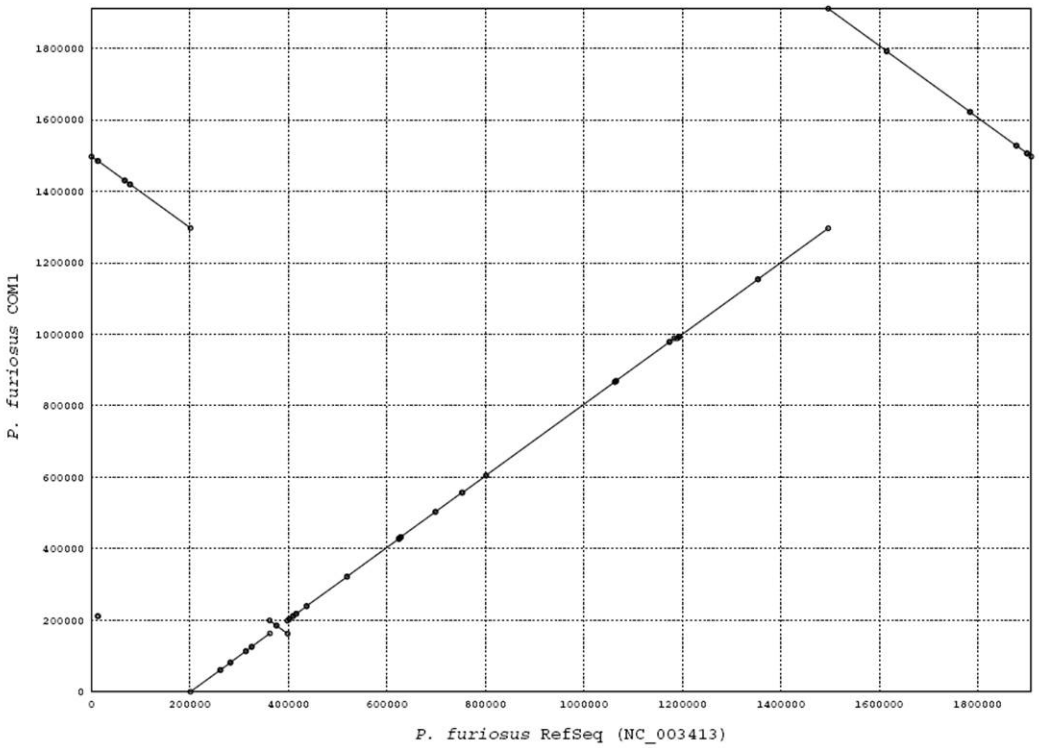
P. furiosus COM1
P. furiosus RefSeq (NC_003413)
0
200000
400000
600000
800000
1000000
1200000
1400000
1600000
1800000

Figure 2.2. COM1 genome organization (panel A) compared to the *P. furiosus* reference sequence (NC_003413, panel B). Black tick marks on the outside of the circular diagrams represent full length IS elements in both genomes, with two additional IS elements located at the boundaries on the COM1 genome between blocks A and D, and B and E. The block boundary between A and E indicates start/end of reference sequence and is just upstream of the origin of replication (ori) in both genomes. PF numbers associated with each block are ordered in the 5' to 3' direction of each arrow: A (red) PF0001 – PF0189, B (yellow) PF0190 – PF0347, C (green) PF0349 – PF0388, D (blue) PF0390 – PF1603', E (purple) PF1603'' – PF2065. PF1603 is disrupted by an IS element in the COM1 genome.

FIGURE 2.2

A

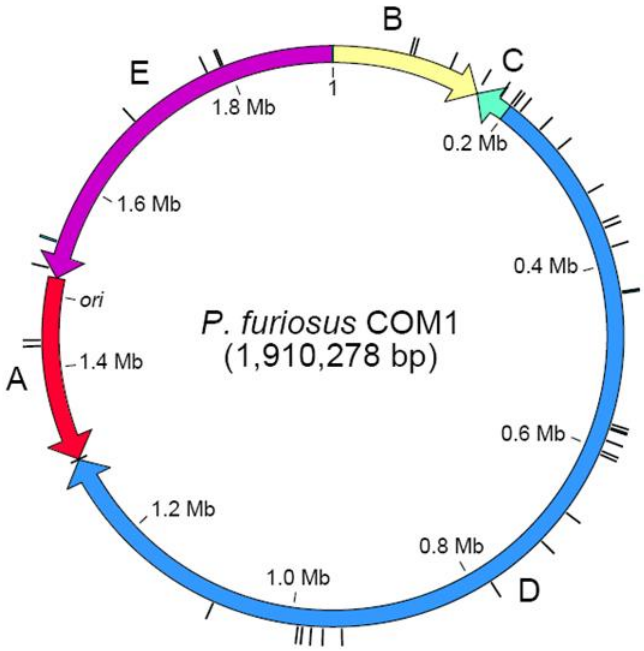
B
C
E
1
1.8 Mb
0.2 Mb
1.6 Mb
0.4 Mb
ori
P. furiosus COM1
(1,910,278 bp)
A
1.4 Mb
0.6 Mb
1.2 Mb
0.8 Mb
1.0 Mb
D

B

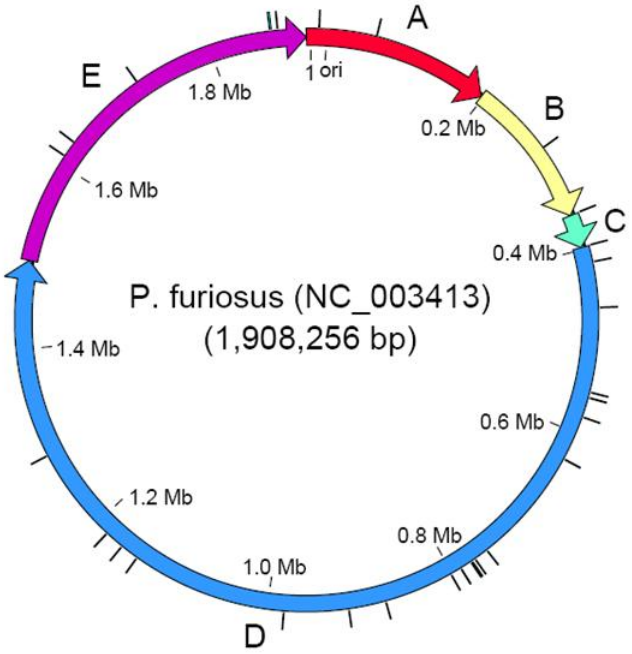
A
E
1 ori
1.8 Mb
0.2 Mb
B
1.6 Mb
C
0.4 Mb
P. furiosus (NC_003413)
(1,908,256 bp)
1.4 Mb
0.6 Mb
1.2 Mb
0.8 Mb
1.0 Mb
D

Figure 2.3. Map of IS element in the riboflavin synthase subunit alpha (PF0061) gene in COM1 strain compared to NCBI reference. IS element is represented by white arrow and flanked by direct repeat sequences (boxed). A single copy of the direct repeat sequence is located at the same position on the gene in the reference sequence. The nucleotide sequence alignment is identical for both genes minus the IS element and additional direct repeat; however, at the protein-level COM1 sequence has premature stop codon (~16 bp into the IS element).

FIGURE 2.3

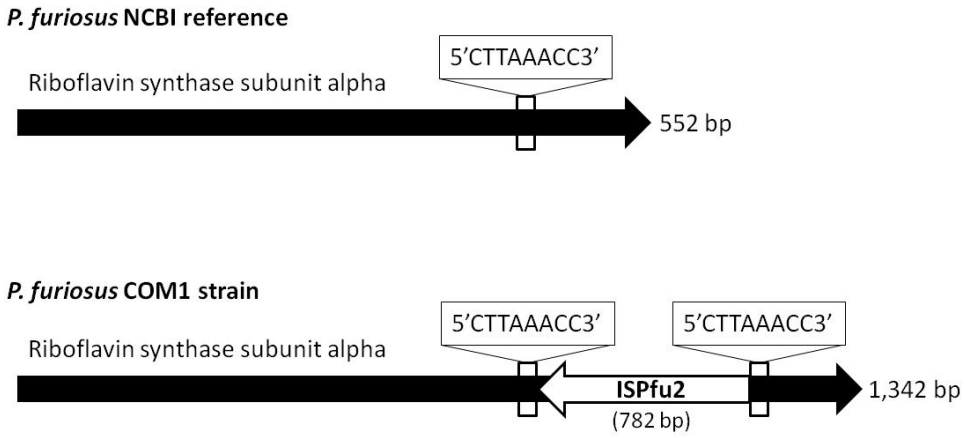
P. furiosus NCBI reference
Riboflavin synthase subunit alpha
5'CTTAAACC3'
552 bp
P. furiosus COM1 strain
Riboflavin synthase subunit alpha
5'CTTAAACC3'
5'CTTAAACC3'
ISPfu2
(782 bp)
1,342 bp

Figure 2.4. Map of IS element upstream of the cold-induced protein A (PF0190) in COM1 strain compared to NCBI reference. IS element is represented by white arrow and flanked by direct repeat sequences (boxed). A single copy of the direct repeat sequence is located at the same position on reference sequence, 34 bp upstream of the PF0190 translational start site. The nucleotide sequence alignment is identical for both upstream regions minus the IS element and additional direct repeat.

FIGURE 2.4

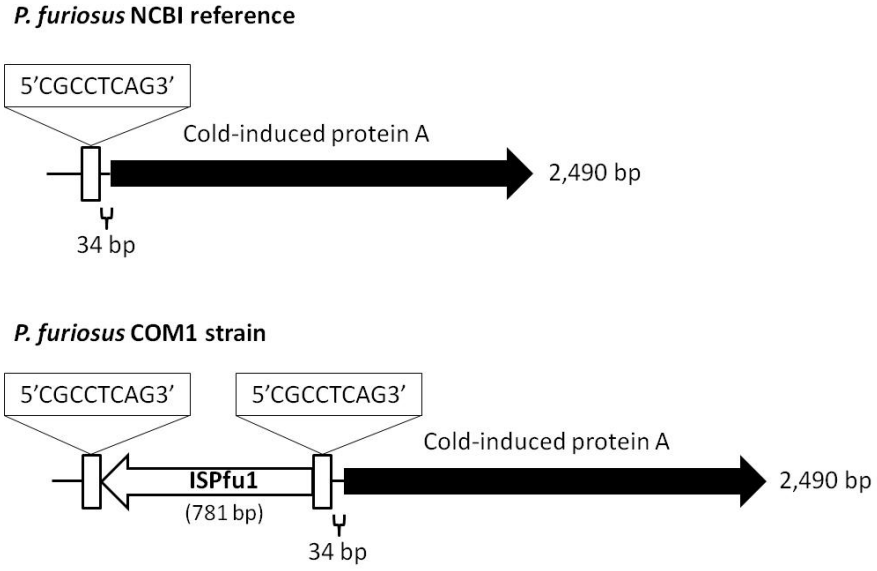
P. furiosus NCBI reference
5'CGCCTCAG3'
Cold-induced protein A
2,490 bp
34 bp
P. furiosus COM1 strain
5'CGCCTCAG3'
5'CGCCTCAG3'
Cold-induced protein A
ISPfu1
(781 bp)
2,490 bp
34 bp

SUPPLEMENTAL MATERIAL

Table S2.1. Disrupted genes in *P. furiosus* COM1 strain relative to NCBI reference. These include genes IS-mediated and IS-independent deletions, major chromosome-level deletions, major (<90% identity) and minor (≥90% identity) protein-level genome differences, and silent mutations.

Gene	Gene Annotation[b]	Identical Residues (AA)[i]	Alignment Length (AA)[i]	Identitiy (%)[i]	Operon Position[c]	Location[d]
PF0002	<YcaO-like>	433	434	99.8	2 of 5	cyt
PF0012[k]	hypothetical protein	252	267	94.4		cyt
PF0036	daunorubicin resistance membrane protein	262	263	99.6	2 of 2	mem
PF0054[m]	AsnC family transcriptional regulator	91	155	58.7	6 of 7	cyt
PF0057	<peptidase M28>	538	551	97.6		cyt
PF0058	dolichol monophosphate mannose synthase	351	352	99.7	1 of 3	mem
PF0061[k]	riboflavin synthase subunit alpha	163	186	87.6	1 of 4	cyt
PF0067[m]	cobalt transport ABC transporter	157	243	64.6	1 of 2	mem
PF0073[l]	beta-glucosidase (CelB)	209	472	44.3		cyt
PF0079	cyclic 2,3-diphospoglycerate-synthetase	430	431	99.8	2 of 2	cyt
PF0085	DNA helicase	1274	1355	94	1 of 2	cyt
PF0122	translation initiation factor IF-2	320	321	99.7	1 of 2	cyt
PF0132	hypothetical protein	486	489	99.4	1 of 2	cyt
PF0147[m]	potassium channel-like protein	23	205	11.2	2 of 2	cyt
PF0179	V-type ATP synthase subunit E	202	203	99.5	7 of 13	cyt
PF0209	ribosomal protein s6 modification protein	271	273	99.3	3 of 3	cyt
PF0220	hexulose-6-phosphate synthase	433	454	95.4		cyt

PF0225[m]	N-acetyltransferase	111	201	55.2	1 of 2	cyt
PF0228[m]	hypothetical protein	49	89	55.1	2 of 3	cyt
PF0244[m]	hypothetical protein	38	89	42.7		cyt
PF0270	alanyl-tRNA synthetase	912	914	99.8		cyt
PF0314[m]	signal peptidase	58	173	33.5	2 of 3	cyt
PF0332	flagellar accessory protein FlaH	203	204	99.5	4 of 4	cyt
PF0334[m]	flagella-like protein	24	194	12.4	2 of 6	exc
PF0351[m]	hypothetical protein	22	285	7.7		cyt
PF0352[m]	[CRISPR-associated protein, Cmr1-2 (21)]	189	451	41.9		cyt
PF0356	beta-galactosidase	481	483	99.6	3 of 3	cyt
PF0357	dipeptide-binding protein	630	631	99.8	1 of 7	mem
PF0360	oligopeptide ABC transporter	323	324	99.7	4 of 7	cyt
PF0363[m]	beta-galactosidase	11	775	1.4	7 of 7	cyt
PF0393[k]	[CRISPR-associated protein, Cas6-2 (21)]	11	241	4.6		cyt
PF0404[n]	<von Willebrand factor, type A (VWA)>	418	418	100	3 of 5	exc
PF0407[k]	<carboxypeptidase-like, regulatory domain>	14	607	2.3	1 of 2	mem
PF0423[m]	hypothetical protein	45	117	38.5	1 of 3	cyt
PF0424[m]	hypothetical protein	34	172	19.8	2 of 3	cyt
PF0429[k]	proline permease	195	493	39.6		mem
PF0439[m]	hypothetical protein	297	401	74.1		cyt
PF0445[n]	galactokinase	352	352	100	3 of 4	cyt
PF0446	NDP-sugar synthase	151	152	99.3	4 of 4	cyt
PF0463	hydrolase related to 2-haloalkanoic acid dehalogenase	233	234	99.6	1 of 5	cyt

PF0472 [m]	<class III signal peptide motif>	42	54	77.8	2 of 2	exc
PF0509	integral membrane glycosyltransferase	673	707	95.2	2 of 4	mem
PF0524 [m]	<ribbon-helix-helix (Met_repress_like)>	57	72	79.2	1 of 4	cyt
PF0534	indolepyruvate oxidoreductase beta	197	214	92.1	3 of 3	cyt
PF0552	arsenical-resistance protein acr3	363	399	91		mem
PF0572	dna2-nam7 helicase family protein	654	655	99.8		cyt
PF0592	ATP-dependent RNA helicase	866	867	99.9	5 of 6	cyt
PF0600	hypothetical protein	354	356	99.4	1 of 3	exc
PF0611 [m]	hypothetical protein	295	382	77.2		cyt
PF0621	<winged helix-turn-helix transcription repressor DNA-binding>	255	283	90.1	2 of 2	exc
PF0622 [m]	hypothetical protein	7	33	21.2		cyt
PF0710 [m]	<transcription repressor DNA-binding>	79	157	50.3	3 of 3	cyt
PF0714	<flavodoxin/nitric oxide synthase>	169	176	96		cyt
PF0755 [k]	non-phosphorylating GAPDH (GAPN)	389	506	76.9	4 of 4	cyt
PF0757 [k]	hypothetical protein	0	0	0		cyt
PF0758 [k]	<nucleotide-binding domain (HEPN)>	0	0	0		cyt
PF0764 [m]	DEXX-box atpase	232	434	53.5		cyt
PF0777 [m]	hypothetical protein	191	215	88.8		mem
PF0782	<polysaccharide biosynthesis protein>	107	109	98.2	1 of 2	mem
PF0785.2n [m]	hypothetical protein	148	192	77.1		N/A
PF0793	hypothetical protein	81	87	93.1	7 of 7	cyt
PF0823 [k]	<multi antimicrobial extrusion protein (MatE)>	115	472	24.4	1 of 2	mem
PF0856	isopentenyl pyrophosphate isomerase	370	394	93.9		cyt

PF0868[n]	NDP-sugar synthase	413	413	100		cyt
PF0871[n]	hypothetical protein	135	135	100	2 of 3	cyt
PF0872	<circadian clock protein KaiC/DNA repair protein RadA>	115	125	92	3 of 3	cyt
PF0873[m]	hypothetical protein	36	196	18.4		cyt
PF0874[m]	membrane dipeptidase	9	379	2.4	1 of 2	cyt
PF0884	hypothetical protein	346	347	99.7	4 of 4	cyt
PF0889[n]	hypothetical protein	325	325	100		exc
PF0901[m]	hypothetical protein	121	142	85.2		cyt
PF0921	ABC transporter	285	305	93.4	1 of 5	cyt
PF0933	DNA repair helicase Rad3	626	647	96.8	3 of 3	cyt
PF0960[m]	hypothetical protein	15	112	13.4	2 of 2	exc
PF0978	<transglutaminase-like domain>	314	328	95.7	7 of 7	exc
PF1030	methionyl-tRNA synthetase	723	724	99.9		cyt
PF1075[m]	hypothetical protein	3	219	1.4		mem
PF1109[m]	<carbohydrate-binding domain (CARDB)>	959	1132	84.7	1 of 2	exc
PF1113[m]	<tRNA amidotransferease GAD domain>	199	223	89.2	1 of 3	cyt
PF1114[o]	orotidine 5'-phosphate decarboxylase	0	0	0	2 of 3	cyt
PF1120	ATP-dependent RNA helicase	723	724	99.9	3 of 4	cyt
PF1121	[CRISPR-associated protein, Cas5t (21)]	229	230	99.6	4 of 4	cyt
PF1130	[CRISPR-associated protein, Cmr1-1 (21)]	325	338	96.2	7 of 7	cyt
PF1131	[CRISPR-associated protein, Cas6 (21)]	263	264	99.6		cyt
PF1159	L-tyrosine decarboxylase	362	387	93.5	2 of 4	cyt
PF1168	[5’ to 3’ exonuclease, NurA (23)]	450	451	99.8	6 of 7	exc

PF1182[m]	<thioredoxin-like fold>	7	126	5.6		cyt
PF1182.1n[m]	hypothetical protein	53	169	31.4		N/A
PF1206[m]	<nucleic acid-binding, PIN, PH0500>	15	156	9.6	1 of 3	cyt
PF1208	beta-mannosidase	509	510	99.8	3 of 3	cyt
PF1225	hypothetical protein	94	95	98.9	2 of 3	cyt
PF1238	ABC transporter	622	632	98.4	2 of 2	cyt
PF1247.1n	hypothetical protein	151	152	99.3		N/A
PF1249[l]	ABC transporter	0	0	0	1 of 2	cyt
PF1250[l]	hypothetical protein	0	0	0	2 of 2	exc
PF1251[l]	<alpha-galactosidase, NEW3 domain>	0	0	0	1 of 2	cyt
PF1252[l]	hypothetical protein	0	0	0	2 of 2	mem
PF1253[l]	[aromatic aminotransferase II (56)]	0	0	0		cyt
PF1254[l]	sodium dependent transporter	270	578	46.7	1 of 2	mem
PF1258	ribose-5-phosphate isomerase A	222	229	96.9	2 of 3	cyt
PF1259	hypothetical protein	106	107	99.1	3 of 3	mem
PF1260[k]	hypothetical protein	183	304	60.2	1 of 2	cyt
PF1268[n]	5-methyltetrahydropteroyltriglutamate--homocysteine S-methyltransferase	309	309	100	3 of 4	cyt
PF1305	hypothetical protein	717	721	99.4	4 of 5	exc
PF1328	ferredoxin-NADP reductase	277	278	99.6	3 of 3	cyt
PF1407	uridylate kinase	224	225	99.6	4 of 4	cyt
PF1433[n]	membrane bound hydrogenase beta	173	173	100	11 of 14	cyt
PF1434[n]	membrane bound hydrogenase alpha	427	427	100	12 of 14	cyt
PF1480	formaldehyde:ferredoxin oxidoreductase wor5	570	633	90	2 of 2	cyt

PF1494	hypothetical protein	190	193	98.4		mem
PF1567	exosome complex RNA-binding protein Rrp42	276	277	99.6	1 of 5	cyt
PF1572	<amino acid-binding ACT (ACT)>	174	175	99.4		cyt
PF1573[n]	<peptidase U62, modulator of DNA gyrase>	455	455	100	1 of 2	cyt
PF1589	<carbohydrate/purine kinase (PfkB)>	250	251	99.6		cyt
PF1603[k]	Na antiporter	185	427	43.3	1 of 3	mem
PF1615	<intein DOD homing endonuclease>	969	970	99.9	4 of 4	cyt
PF1624	hypothetical protein	174	175	99.4		mem
PF1718	tRNA-modifying protein	337	338	99.7		cyt
PF1725	DNA primase	422	452	93.4	2 of 2	cyt
PF1748[m]	system permease, ABC transporter	321	543	59.1	4 of 6	mem
PF1749[m]	sulfate transport membrane protein	10	228	4.4	5 of 6	mem
PF1761[m]	<putative cell wall binding repeat 2>	204	389	52.4	1 of 2	exc
PF1774	iron ABC transporter ATP-binding protein	342	363	94.2		exc
PF1882	cell division protein CDC48	795	796	99.9		cyt
PF1896.1n	hypothetical protein	63	64	98.4		N/A
PF1902	DNA repair helicase	444	447	99.3		cyt
PF1910[n]	oxidoreductase	476	476	100	1 of 2	cyt
PF1935[j m]	amylopullulanase	1114	1355	82.2	3 of 6	exc
PF1971	anaerobic ribonucleoside triphosphate reductase	604	605	99.8	1 of 2	cyt
PF1989	preprotein translocase subunit SecE	60	61	98.4	1 of 6	cyt
PF2000	glycine dehydrogenase subunit 2	494	502	98.4	2 of 2	cyt
PF2034[k]	<methyltransferase (TYW3)>	206	229	90	1 of 2	cyt
PF2059[k]	aminopeptidase	29	567	5.1	1 of 2	exc

[b] Annotations are NCBI gene names (no brackets) and literature cited ([ ]), except for hypothetical genes, where the best IPR (< >) match is given if available.
[c] Operon predictions from (55) based on NCBI reference sequence.
[d] Predicted cellular location based on predicted TMDs, proteins with >= 2 TMDs classified as membrane (mem), proteins with <2 TMDs and a predicted signal peptide using SignalP with the gram-positive model >= 0.6 are classified as extracellular (exc), and proteins with <2 TMDs and no predicted signal peptide are classified as cytoplasmic (cyt).
[i] Based on Needleman-Wunsch global alignment with NCBI reference sequence.
[j] A fusion of PF1934 and PF1935 was previously reported (35). A longer product was found in COM1 which is closer in length to those in other *Pyrococci*.
[k] Genes affected by IS activity (Table 2.2).
[l] Additional large chromosomal deletions (Table 2.3).
[m] Major protein-level genome differences (Table 2.4).
[n] Silent mutation at protein-level.
[o] Auxotrophic strain deletion (37).

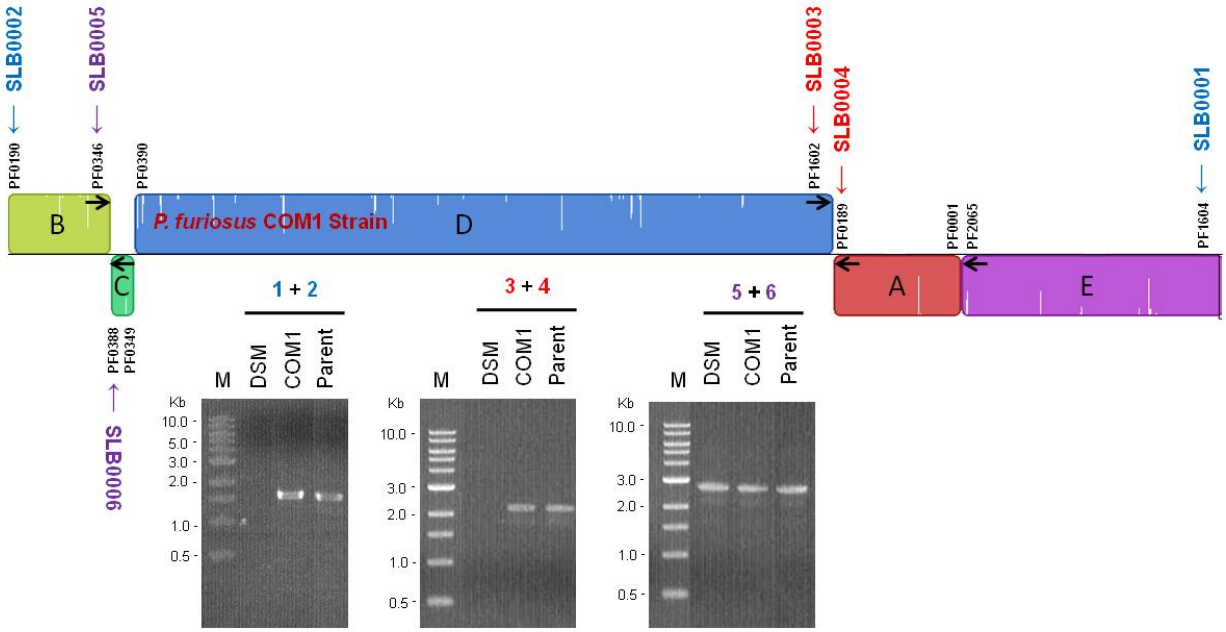

Figure S2.1. PCR confirmation of COM1 genome organization. PCR primers (SLB0001-6) were designed within ORFs up or downstream of block boundaries. PCR products were sequenced and further confirmed COM1 genome rearrangement. Inverted orientations of block C and block AE was also observed in the Parent. Only the inverted order of block C was observed in the DSMZ strain. Primer sequences are as follows: SLB0001 (5'- AGG CTA ATA AGG GTA GGT GG -3‘), SLB0002 (5'- AAG TGG GCT TAC TAA CAT GC -3‘), SLB0003 (5'- ATC TCC ATA TAT TGG GCA GC -3‘), SLB0004 (5'- ACA ACT TCC ATG CTA ATC ACC -3‘), SLB0005 (5'- TCT TAG CCA ATT CTT CGT CG -3’), and SLB0006 (5'- TCT AAC AGG AGT CAC TGC C -3’).

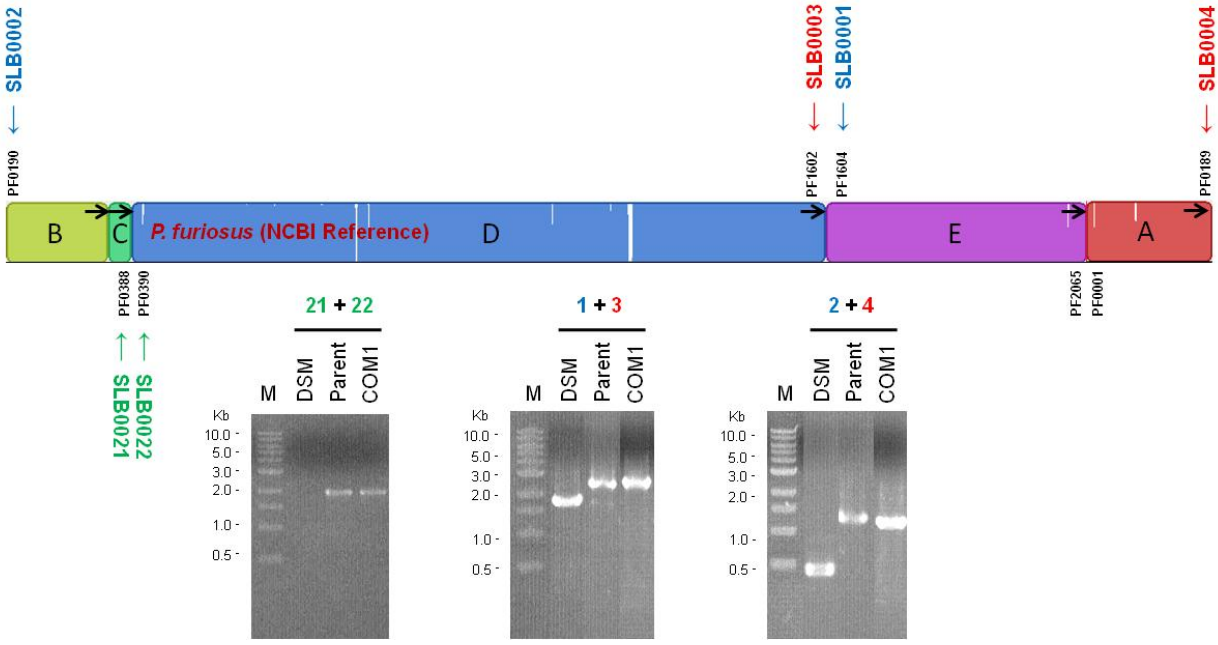

Figure S2.2. PCR analysis of NCBI reference genome organization. PCR primers (SLB0001-4 and 21-22) were designed within ORFs up or downstream of block boundaries. PCR products were sequenced to confirm genome arrangements. NCBI reference arrangement of blocks AE and C were observed in the COM1 and Parent with IS element insertion in amplified products. Only the inverted order of block C (Figure S2.1) and the reference order of block AE were observed in the DSMZ strain. Primer sequences are as follows: SLB0001 (5'- AGG CTA ATA AGG GTA GGT GG -3‘), SLB0002 (5'- AAG TGG GCT TAC TAA CAT GC -3‘), SLB0003 (5'- ATC TCC ATA TAT TGG GCA GC -3‘), SLB0004 (5'- ACA ACT TCC ATG CTA ATC ACC -3‘), SLB0021 (5'- TCA GTA TTG CGA TGA GAG C -3’), and SLB0022 (5'- TCC ATT CTC GAC AAT CTC TCC -3’).

CHAPTER 3

DELETION STRAINS REVEAL METABOLIC ROLES FOR KEY ELEMENTAL SULFUR RESPONSIVE PROTEINS IN *PYROCOCCUS FURIOSUS*[2]

[2] Bridger, S.L., S.M. Clarkson, K. Stirrett, M.B. DeBarry, G.L. Lipscomb, G.J. Schut, J. Westpheling, R.A. Scott, and M.W. Adams. 2011. *J Bacteriol.* 193(23):6498-6504.
Reprinted here with permission from the American Society for Microbiology.

ABSTRACT

Transcriptional and enzymatic analyses of *Pyrococcus furiosus* previously indicated that three proteins play key roles in the metabolism of elemental sulfur (S^0): a membrane-bound oxidoreductase complex (MBX), NADPH sulfur oxidoreductase (NSR), and sulfur-induced protein A (SipA). Deletion strains, referred to as MBX1, NSR1 and SIP1, respectively, have now been constructed by homologous recombination utilizing the uracil auxotrophic COM1 parent (Δ*pyrF*). Growth of all three mutants on maltose was comparable without S^0 but in its presence, growth of MBX1 was greatly impaired while growth of NSR1 and SIP1 was largely unaffected. In the presence of S^0, MBX1 produced little if any sulfide but much more acetate (per unit protein) than the parent strain, demonstrating that MBX plays a critical role in S^0 reduction and energy conservation. In contrast, comparable amounts of sulfide and acetate were produced by NSR1 and the parent strain COM1, indicating that NSR is not essential for energy conservation during S^0 reduction. SIP1 produced the same amount of acetate and more sulfide than its control strain. Differences in the transcriptional response to S^0 in NSR1 suggest that two isoenzymes of sulfide dehydrogenase provide a compensatory NADPH-dependent S^0 reduction system. Genes controlled by the S^0-responsive regulator, SurR, were not as highly regulated in MBX1 and NSR1. That SipA is not essential for growth of S^0-grown cells indicates it is not required for detoxification of metal sulfides as previously suggested, but rather may play a role in iron-sulfur cluster metabolism. A model is proposed for S^0 reduction by *P. furiosus* with roles for MBX and NSR in bioenergetics and for SipA in FeS metabolism.

INTRODUCTION

Pyrococcus furiosus is a hyperthermophilic archaeon that grows optimally near 100°C (5). It utilizes carbohydrates for growth and produces acetate, CO_2 and H_2. When elemental sulfur (S^0) is present, hydrogen sulfide (H_2S) is produced instead of H_2 (1, 5, 22). Transcriptional and biochemical analyses revealed a novel S^0-reducing system found only in the Thermococcales (22) involving two key enzymes: a 13-gene cluster encoding a membrane-bound oxidoreductase (MBX) and a cytoplasmic coenzyme A (CoA)-dependent NADPH sulfur oxidoreductase (NSR), which is proposed to reduce S^0 and produce sulfide intracellularly. MBX was predicted to act as a respiratory ferredoxin NADP oxidoreductase, generating NADPH for NSR and creating an electrochemical gradient to drive ATP synthesis, although this activity could not be verified experimentally (22). The gene cluster encoding MBX is highly similar to that which encodes the H_2-evolving, energy-conserving membrane-bound NiFe-hydrogenase (MBH), except that in MBX the homolog of the catalytic subunit responsible for H_2 production in MBH (*mbxL*, PF1442) lacks two key residues necessary for coordinating a NiFe center (24).

A regulatory transcription factor, S^0-response regulator, SurR, is thought to regulate expression in *P. furiosus* of almost all of the primary S^0-response genes (22) and within 10 min of S^0 addition causes the up-regulation of genes involved in S^0 metabolism and down-regulation of those involved in H_2 metabolism (12). The DNA-binding activity of SurR is modulated by a redox-dependent conformational change whereby SurR is unable to bind DNA in the presence of S^0 (27). Accordingly, expression of the genes encoding both MBX and NSR increase and expression of the operon encoding MBH (as well as those encoding two soluble NiFe-hydrogenases, SHI and SHII), decrease as part of the primary S^0 response (22). SurR also appears to down-regulate expression of an operon (PF1327-PF1328, *sudAB* (12, 22)) that encodes sulfide dehydrogenase I (SuDH I (6, 16)). This catalyzes both the NADPH-dependent reduction of S^0 (6, 16) and the ferredoxin-dependent reduction of NADP (15, 16) *in vitro* hence

its true function is not clear. *P. furiosus* also contains a homolog of SuDH I referred to as SuDH II (PF1910-PF1911, *sudXY* (6)), which is up-regulated during growth on peptides (21).

The secondary response of *P. furiosus* to S^0 addition occurs within 30 min and is independent of SurR. It includes genes involved in iron-sulfur cluster metabolism (22) as well as the most highly expressed gene in S^0-grown cells encoding sulfur-induced protein A or SipA (23). SipA expression is regulated in an iron-dependent manner by sulfide, the product of S^0 reduction (4), as well as by oxidative stress (25, 26). While the function of SipA is not known, it has been proposed to prevent the precipitation of toxic intracellular insoluble metal sulfides (7) by the controlled reaction of sulfide with assimilated iron and by iron released due to oxidative damage to iron sulfur clusters (4).

To provide further insight into the biochemical and physiological roles of these three key S^0 responsive proteins, MBX, NSR and SipA, we have taken advantage of the recently developed genetic system for *P. furiosus* (13) to construct and characterize targeted gene deletions. Their effects on growth and on the expression of genes involved in the primary and secondary responses to S^0 show that MBX plays a critical role in S^0 reduction and energy conservation while the two SuDH isoenzymes appear to compensate for the NADPH-dependent S^0 reduction system in the absence of NSR. The strain lacking SipA grows well with S^0, consistent with a role in iron-sulfur cluster metabolism rather than sulfide detoxification.

MATERIALS AND METHODS

Strains and growth conditions.

P. furiosus strains used or constructed in this study are listed in Table 3.1. All strains were grown in the presence and absence of S^0 with maltose as the primary carbon source. The growth medium was the same as previously reported (1) except that yeast extract was added at 0.5 g/L and uracil (20 μM) was added to the growth media of all auxotrophic strains (COM1, NSR1, and MBX1). Growth experiments to determine the effects of S^0 were carried out in

biological triplicate in 100 mL serum bottles with 50 mL media stirred (300 rpm) at 98°C, with S^0 (Alfa Aesar, Ward Hill, MA) added to a final concentration of 2 g/L. To obtain RNA for QPCR analyses, cultures were grown in a 20 L fermentor (1) and samples (2 L each) were removed before and 30 min after the addition of S^0 as previously described (22).

Construction of gene deletions.

A deletion of *nsr* (PF1186) was constructed with 3 kb flanking regions cloned sequentially into a plasmid, and this plasmid was then used as template to amplify the *nsr* deletion construct with only 1 kb flanking regions and cloned into pGLW015, containing the P_{gdh}*pyrF* cassette for prototrophic selection (13). Therefore the final markerless deletion of *nsr* contains a remnant of the original plasmid multiple cloning site (GCGGCCGCATTTAAATACAAGTATAGCGGAAGA-TATCGGCCGGCC) as a scar. A deletion of *mbxL* (PF1442), was constructed by overlap PCR with 1 kb flanking regions and cloned into pGLW015 (13). A deletion of *sipA* (PF2025) was constructed with 1 kb flanking regions on either side of the P_{gdh}*pyrF* cassette (13) using overlap PCR. Plasmid deletion constructs for *nsr* and *mbxL* were transformed into *P. furiosus* COM1 (Δ*pyrF*) selecting uracil prototrophy on solid defined medium and counter-selected for loss of the plasmid using 5-FOA resistance as previously described (13). The PCR product containing a deletion of *sipA* was transformed directly selecting uracil prototrophy resulting in marker replacement. The pyrF allele in the COM1 strain was restored to wild type by transforming COM1 with a PCR product containing the wild-type *pyrF* (PF1114) allele and ~1 kb flanking regions. DNA was extracted from transformants as previously described (13) and screened for deletion by PCR amplification of the locus using primers outside the homologous flanking regions used to construct the deletions. Isolates containing the deletion were further colony purified by serial passage on solid medium. PCR products amplified from the target regions were sequenced.

Cell protein, H_2S and H_2 analyses.

The Bradford method (2) was routinely used to estimate total cell protein concentrations to monitor cell growth, with bovine serum albumin as a standard. Headspace and media samples (500 µL each) were taken from cultures and transferred anaerobically into the double-vial system for H_2S and H_2 analysis, as previously reported (22). H_2S production was assayed by the methylene blue method (3), and abiotic sulfide production was subtracted from the experimental samples using controls lacking cells. H_2 production was measured with a gas chromatograph (Shimadzu GC-8A).

Acetate measurements.

Samples (1 mL) of *P. furiosus* cultures were centrifuged at 16,000 x *g* for 20 min to pellet cells and the supernatant fraction was acidified with 0.1M H_2SO_4 (final concentration). Acetate concentrations were determined using a Waters 2690 high-performance liquid chromatography (HPLC) separation module equipped with a photodiode array detector. Organic acids were separated on an Aminex HPX-87H column (Bio-Rad) at 23°C using 5 mM H_2SO_4 as the mobile phase at 0.6 mL/min. The specific acetate production for each strain was calculated based on a known acetate standard and divided by the total estimated cell protein (described above) at the endpoint of growth.

RNA isolation and quantitative PCR analyses.

Total RNA was extracted from *P. furiosus* cells using acid-phenol (23) and further purified by a second acid-phenol isolation, Turbo DNase (Ambion, Austin, TX) treatment (30 min, 37°C), and Absolutely RNA cleanup kit (Agilent Technologies, Lexington, MA). cDNA was prepared using the AffinityScript QPCR cDNA Synthesis Kit (Agilent). The genes *pdo* (PF0094), *shIβ* (PF0891), *nsr* (PF1186), *sudB* (PF1328), *shIIβ* (PF1329), *mbhA* (PF1423), *mbxA* (PF1453), *sudY* (PF1911), *sipA* (PF2025), and PF2051 were selected for study, and the constitutively expressed gene encoding the POR gamma subunit (PF0971) was selected as a control. Quantitative PCR (QPCR) experiments were carried out in technical triplicate using an Mx3000P instrument

(Agilent) and the Brilliant SYBR green QPCR master mix (Agilent). The comparative cycle threshold method was used to analyze the resulting data, which are expressed as a ratio of gene expression change (*n*-fold).

RESULTS

Construction and validation of *P. furiosus* deletion strains.

Markerless deletions of *nsr* (NSR1) and *mbxL* (MBX1) and a marker-replaced deletion of *sipA* (SIP1) were constructed in the COM1 background strain (Δ*pyrF*). PCR and sequence analyses confirmed the gene deletions in all three strains (see Figure S3.1 and S3.2 in the supplemental material) and QPCR products of the deleted genes were not detected. The absence of NSR and SipA in the appropriate strain was also confirmed by Western analysis (see Figure S3.3 in the supplemental material).

Effect of S^0 availability on growth of deletion strains.

Growth of the deletion and control strains were compared after three consecutive transfers with standard inocula (1 x 10^7 cells/ml) using a maltose-containing medium with and without 2 g/L S^0. NSR1 and MBX1 were compared to COM1 (Δ*pyrF*) in the presence of 20 µM uracil and SIP1 was compared to the complemented COM1c (Δ*pyrF*::*pyrF*). Growth of MBX1 was similar to that of COM1 in the absence of S^0, but was significantly impaired in the presence of S^0 in both growth rate and final cell yield (Figure 3.1). In contrast, the growth of NSR1 and SIP1 was comparable to that of the control strains in both the presence and absence of S^0, with similar growth rates and final cell yields (Figures 3.1 and 3.2).

Production of H_2S, H_2 and acetate in deletion strains.

Using the appropriate control strains for comparison, the amounts of H_2S, H_2 and acetate produced during growth of the three deletion strains with S^0 were determined. Like COM1, NSR1 produced H_2S at a rate closely following that of cell growth (see Figure S3.4 in the supplemental material). Similarly, H_2S production in COM1c and SIP1 followed cell growth (see

Figure S3.5 in the supplemental material); however, total H_2S (per µg protein) trended higher in SIP1 than COM1c (see Figure S3.6 in the supplemental material). In contrast, given the very low growth rate of MBX1, coupled with the high background of abiotic S^0 reduction, it was not possible to determine if this strain was actively reducing S^0. Interestingly, compared to COM1 and NSR1, which produce little if any H_2 during growth on S^0 (2.3 $\pm$ 2 nmoles H_2 per µg protein), MBX1 did produce appreciable amounts of H_2 (25 $\pm$ 7 nmoles H_2 per µg protein). This is about 14% of that measured when the strains are grown in the absence of S^0 (182 ± 6 nmoles H_2 per µg of protein). Specific production of acetate was calculated for each strain based on the concentration of acetate in the media and total cell protein after 11 hours of growth. Acetate production (per µg cell protein) was similar in COM1, COM1c, NSR1, and SIP1 (152 $\pm$ 11.3 µmoles), but significantly higher in MBX1 (190 $\pm$ 2.7 µmoles).

Effect of S^0 addition on the growth and transcriptional responses of deletion strains.

All strains were challenged by the addition of S^0 near mid-log phase (Figure 3.3). Growth of NSR1, SIP1 and the control strains was affected similarly (Figure 3.3), with a brief stall immediately upon S^0 addition followed by restoration of the initial growth rate within 30 min. However, while growth of MBX1 also stalled briefly upon S^0 addition before resuming within 30 min, an additional growth effect was observed one hour after S^0 addition where the growth rate lagged for one hour before resuming the growth rate observed in the absence of S^0, but for only two hours before reaching stationary phase (Figure 3.3).

Cells of all strains were harvested just before S^0 addition and 30 min after (Figure 3.3), and the transcriptional responses of previously identified S^0-responsive genes (22) and those potentially involved in S^0 metabolism (6) were determined. These included genes whose expression is up-regulated upon addition of S^0, a glutaredoxin-like protein disulfide oxidoreductase (PDO, PF0094), which does not catalyze S^0 reduction (22), and a putative operon consisting of two potential regulators, PF2051 and PF2052 (22). As shown in Figure 3.4,

compared to COM1, most of the S^0-responsive genes exhibited a much smaller change in expression in NSR1 and MBX1. Specifically, gene expression in NSR1 compared to COM1 (Figure 3.4A) was lower for the S^0 up-regulated genes *mbxA* (3 v. 6-fold), PF2051 (2 v. 10-fold) *pdo* (4 v. 7-fold), and *sipA* (4 v. 11-fold), and for the S^0 down-regulated genes *shIβ* (17 v. 95-fold) and shIIβ (193 v. 478-fold). Similarly, gene expression in MBX1 compared to COM1 (Figure 3.4B) was lower for the S^0 up-regulated genes *nsr* (8 v. 14-fold), PF2051 (8 v. 10-fold), *pdo* (3 v. 7-fold), and *sipA* (<2 v. 11-fold), and for the S^0 down-regulated genes *shIβ* (38 v. 95-fold) and *shIIβ* (80 v. 478-fold). In contrast, the degree of S^0 down-regulation of *mbhA* was seemingly unaffected in NSR1 and MBX1 compared to COM1 (13, 12, and 13-fold, respectively). A total of four genes in the MBX operon were examined in the MBX1 strain: *mbxA* (first gene in the MBX operon, PF1453), *mbxK* (upstream of the deleted gene, PF1443), *mbxL* (deleted gene, PF1442), and *mbxN* (downstream of the deleted gene, PF1441). An increase in expression was observed for the genes *mbxA*, *mbxK* and *mbxN* 30 min after S^0 addition (11, 17, and 10-fold respectively), while no gene product was detected for *mbxL*.

An interesting expression pattern was observed for the genes encoding SuDH I (*sudB*) and SuDH II (*sudY*) following S^0 addition in NSR1 and MBX1 (Figure 3.4). In NSR1, the expression of *sudB* upon S^0 addition decreases to a lesser extent (5-fold less) compared to the parent while the expression of *sudY* was 7-fold higher than in the parent. Similarly, in MBX1, the expression of *sudY* was 2-fold higher than in the parent, and the expression of *sudB* actually increased ~2-fold following S^0 addition, compared to an almost order of magnitude decrease in the parent (a difference in expression of ~10 fold between the two strains).

For SIP1, only two of the primary S^0 response genes were differentially expressed 30 minutes after S^0 addition compared to COM1c. These were *pdo*, whose expression increased 7-fold in SIP1, compared to 13-fold in the control strain, and *shIIβ*, whose expression decreased 160-fold in SIP1, compared to 460-fold in the control strain (see Figure S3.7 in the supplemental material).

DISCUSSION

MBX1 exhibited a well-defined phenotype during batch growth in the presence of S^0 with a dramatically lower growth rate and cell yield (Figure 3.1) and produced little if any sulfide, suggesting that the pathway for the disposal of reductant from glycolysis via sulfide production is blocked and that MBX plays an obligatory in mediating electron flow to S^0 (Figure 3.5). The decrease in cell yield observed for MBX1 can be attributed in part to a decrease in respiratory ATP production. In the absence of S^0, the MBH respiratory system is proposed to account for an additional 1.2 mol of ATP per mol of glucose oxidized to acetate and CO_2 (20). Therefore, it would be expected that if the equivalent ion-pumping mechanism was impaired in the MBX1 strain, it would exhibit reduced cell yield due to the loss of ATP synthesis in respiration and only be able to generate ATP via substrate-level phosphorylation for a total of 2 mol ATP rather than 3.2 mol ATP per glucose. Support for this hypothesis was obtained by the finding that MBX1 produced 20% more acetate (per unit protein) than the parent strain or NSR1 during growth on S^0, indicating that MBX1 must oxidize more glucose to acetate to yield the same amount of ATP for cell growth. When challenged in exponential growth by the addition of S^0 (Figure 3.3), MBX1 initially responded in a similar manner to the parent strain but then underwent a one-hour lag phase before cells resumed their previous growth rate for an additional two hours before reaching stationary phase, but at a lower final cell density than the parent. This lag in growth can be explained by the inability of MBX1 to generate a proton gradient for ATP synthesis in the presence of S^0, and the resumption of the growth rate may be due to increased glycolytic flux.

In addition to producing more acetate than the COM1 and NSR1 strains in the presence of S^0, MBX1 also produced about 10-fold more H_2 (per unit protein). The gene expression results (Figure 3.4) also indicate that the soluble hydrogenases, SHI and SHII, are significantly less down-regulated in MBX1 than in the parent and that expression of H_2-producing MBH is seemingly unaffected within 30 min after S^0 addition. Similar results were reported for an Mbx-deficient mutant (MXD1) in related hyperthermophilic archaeaon, *Thermococcus kodakarensis*

(9). In the presence of S^0 the MXD1 strain produced 4-times more H_2 than the wild type strain and an increase in expression of the soluble and membrane-bound hydrogenases was observed (9). Hence, *P. furiosus* MBX1 also appears to retain some ability to dispose of excess reductant as H_2, as well as increasing the glycolytic flux to compensate for decreased ATP production per glucose oxidized. MBX is proposed to oxidize ferredoxin and reduce NADP where the NADPH is used by NSR to reduce S^0 (Figure 3.5). However, for unknown reasons, in *in vitro* assays the membranes of S^0-grown *P. furiosus* cells do not catalyze the ferredoxin-dependent reduction of NADP nor, as discussed below, do they catalyze the direct ferredoxin-dependent reduction of S^0 (22).

NSR is the only S^0-reducing enzyme detected in extracts of S^0-grown *P. furiosus* cells that was not present in cells grown without S^0 and its up-regulation is part of the SuR-mediated primary response (22). However, NSR1 did not exhibit an obvious phenotype (Figure 3.1) and produced sulfide (see Figure S3.4 in the supplemental material) and acetate in amounts comparable to the parent strain, clearly demonstrating that NSR is not essential for growth with S^0. This poses the fundamental question of what reduces S^0 in the absence of NSR. Given the degree of homology between MBX and the ferredoxin-dependent H_2-evolving MBH complex, which can be demonstrated *in vitro* (20), MBX is an obvious candidate to catalyze ferredoxin-dependent S^0 reduction but cell membranes do not catalyze this reaction *in vitro*. On the other hand, NADPH-dependent S^0-reducing SuDH I and SuDH II may be a mechanism to compensate for reduction of S^0 in the absence of NSR. The expression of SuDH I in the presence of S^0 does not decrease as much as in the parent strain (4 v. 9-fold, respectively), and the expression of SuDH II increases by an order of magnitude in NSR1 (10-fold) (Figure 3.4). While SuDH II has not been characterized and the specific activity of SuDH I is much lower than that of NSR in NADPH-dependent S^0 reduction (7 v. 100 µmol sulfide produced/min/mg) (16, 22), the compensatory expression of the two SuDH enzymes could be partially responsible for S^0 reduction in NSR1. It is also possible that S^0 reduction in NSR1 is catalyzed inadvertently by

enzymes that do not normally function to reduce S^0 but do so *in vitro,* including SHI and SHII (17) and pyruvate ferredoxin oxidoreductase (POR) (Schut, G., unpublished data). These enzymes in combination with SuDH I and SuDH II may be able to generate amounts of sulfide in NSR1 comparable to those of the parent strain.

It has been shown that in the absence of S^0, SurR activates transcription of genes necessary for H_2 metabolism and represses those required for growth with S^0 (27). Addition of S^0 leads to SurR oxidation, possibly mediated by either colloidal S^0 or polysulfide, such that it is unable to bind DNA (27). Since the degree of the SurR-mediated gene regulation was up to 80% lower in the MBX1 and NSR1 deletion strains compared to the parent (Figure 3.4), there may be limited amounts of the agent that oxidizes SurR if MBX and NSR are not present. We postulate that NSR contributes to the pool of sulfur species responsible for SurR oxidation and that this NSR activity is dependent on the activity of MBX. However, NSR (and MBX) cannot provide the only source of oxidant for SurR given that growth of NSR1 is indistinguishable from the parent in the presence or absence of S^0 (Figures 3.1 and 3.3). The muted transcriptional responses in MBX1 and NSR1 also suggest that the product of the NSR reaction plays a role in mediating the increase in expression of *sipA* during the secondary response to S^0. It would be logical if one of the S^0-reducing, SurR-regulated enzymes, namely, NSR, not only generated a product (presumably sulfide) that was utilized by SipA but also functioned in controlling its expression.

SipA is unlikely to play an essential role in the detoxification of metal sulfides, as previously proposed (4), as one would predict greatly impaired growth of the SIP1 mutant in the presence of S^0, which was not observed (Figure 3.2). In addition to up-regulation of *sipA* expression, the secondary response to S^0 includes up-regulation of genes involved in iron transport (*feoB*), and iron-sulfur cluster biosynthesis (*sufBD*), and of iron-sulfur-cluster containing enzymes (glutamate synthase (18) and 3-isopropylmalate dehydratase (8)), indicating an increased need for iron-sulfur metabolism under S^0 reducing conditions and that

SipA may be involved in iron-sulfur metabolism. Since some archaea use sulfide, rather than cysteine, as a sulfur source for iron-sulfur cluster biosynthesis (14), NSR might function to enable S^0 to be used, via sulfide, for iron-sulfur cluster synthesis by SipA. This is supported by the increased amount of sulfide produced by SIP1, suggesting that in the absence of SipA, sulfide is no longer incorporated into iron-sulfur clusters. If SipA does synthesize iron-sulfur clusters, a mutant lacking a functional SufBD, the only recognized cluster biosynthetic scaffold in *P. furiosus*, may grow only in the presence of S^0, and such a study is currently in progress. It is unclear why the absence of SipA should influence expression of the SHII genes in response to S^0, but not those of SHI (see Figure S3.7 in the supplemental material).

While this paper was in revision, deletion strains in *T. kodakarensis* of homologs of *nsr* and *mbx,* and also supposedly of *sipA,* were reported (19). The phenotypes of the *nsr* (TS1109) and *mbx* (TS1105) mutants are similar to their *P. furiosus* counterparts, although we did not observe the higher concentrations of H_2 that were produced by the *nsr* mutant. The other *T. kodakarensis* strain is not comparable to *P. furiosus* SIP1 (19) because the deleted genes (TK1260-TK1261) are homologs of an operon encoding putative transcriptional regulators (PF2051-PF2052). In any event, the results with both organisms are consistent with a role of MBX in energy conservation during S^0 reduction and in connecting reduced ferredoxin generated during glycolysis to S^0 reduction by NSR via NADPH. NSR likely reduces colloidal sulfur (22), which exists as both short S^0 chains and S_8 (10, 11), making the end products of S^0 reduction both polysulfide (S_x^{2-}) and hydrogen sulfide (H_2S), as shown in Figure 3.5. The products generated by NSR, which are assumed to be dependent on the NADPH generated by MBX, appear to modulate at least in part SurR activity and SipA expression. We propose that polysulfide oxidizes SurR while sulfide induces SipA expression (Figure 3.5). When MBX is absent, NADPH is not generated, and NSR cannot produce either polysulfide or H_2S. We further propose that in the absence of NSR, a combination of SuDH I and II, and perhaps SHI, SHII and POR, reduce S^0. However, the muted transcriptional response in NSR1 suggests that the

product(s) of SuDH/SH/POR reduction does not modulate SurR activity or SipA regulation. The reason for this is unclear and is the subject of further investigation.

ACKNOWLEDGEMENTS

This research was supported by grants from the Chemical Sciences, Geosciences and Biosciences Division (FG05-95ER20175) and the Office of Biological and Environmental Research (FG02-08ER64690) of the Office of Basic Energy Sciences, Office of Science, U.S. Department of Energy. We thank Michael Thorgersen and Frank Jenney for many helpful discussions and Farris Poole for invaluable technical assistance.

REFERENCES

1. **Adams, M. W., J. F. Holden, A. L. Menon, G. J. Schut, A. M. Grunden, C. Hou, A. M. Hutchins, F. E. Jenney, Jr., C. Kim, K. Ma, G. Pan, R. Roy, R. Sapra, S. V. Story, and M. F. Verhagen.** 2001. Key role for sulfur in peptide metabolism and in regulation of three hydrogenases in the hyperthermophilic archaeon *Pyrococcus furiosus*. J Bacteriol **183:**716-24.
2. **Bradford, M. M.** 1976. A rapid and sensitive method for the quantitation of microgram quantities of protein utilizing the principle of protein-dye binding. Anal Biochem **72:**248-54.
3. **Chen, J. S., and L. E. Mortenson.** 1977. Inhibition of methylene blue formation during determination of the acid-labile sulfide of iron-sulfur protein samples containing dithionite. Anal Biochem **79:**157-65.
4. **Clarkson, S. M., E. C. Newcomer, E. G. Young, and M. W. Adams.** 2010. The elemental sulfur-responsive protein (SipA) from the hyperthermophilic archaeon *Pyrococcus furiosus* is regulated by sulfide in an iron-dependent manner. J Bacteriol **192:**5841-3.
5. **Fiala, G. a. K. O. S.** 1986. *Pyrococcus furiosus* sp. nov. represents a novel genus of marine heterotrophic archaebacteria growing optimally at 100° C. Arch. Microbiol. **145:**56-61.
6. **Hagen, W. R., P. J. Silva, M. A. Amorim, P. L. Hagedoorn, H. Wassink, H. Haaker, and F. T. Robb.** 2000. Novel structure and redox chemistry of the prosthetic groups of the iron-sulfur flavoprotein sulfide dehydrogenase from *Pyrococcus furiosus*; evidence for a [2Fe-2S] cluster with Asp(Cys)3 ligands. J Biol Inorg Chem **5:**527-34.
7. **Hatton, B., and D. Rickard.** 2008. Nucleic acids bind to nanoparticulate iron (II) monosulphide in aqueous solutions. Orig Life Evol Biosph **38:**257-70.

8. **Jang, S., and J. A. Imlay.** 2007. Micromolar intracellular hydrogen peroxide disrupts metabolism by damaging iron-sulfur enzymes. J Biol Chem **282:**929-37.

9. **Kanai, T., R. Matsuoka, H. Beppu, A. Nakajima, Y. Okada, H. Atomi, and T. Imanaka.** 2011. Distinct physiological roles of the three [NiFe]-hydrogenase orthologs in the hyperthermophilic archaeon *Thermococcus kodakarensis*. J Bacteriol **193**:3109-16.

10. **Kleinjan, W. E., A. de Keizer, and A. J. Janssen.** 2005. Kinetics of the chemical oxidation of polysulfide anions in aqueous solution. Water Res **39:**4093-100.

11. **Kleinjan, W. E., de Keizer, A., and Janssen, J.H.** 2003. Biologically produced sulfur. Top Curr Chem **230:**167–188.

12. **Lipscomb, G. L., A. M. Keese, D. M. Cowart, G. J. Schut, M. Thomm, M. W. Adams, and R. A. Scott.** 2009. SurR: a transcriptional activator and repressor controlling hydrogen and elemental sulphur metabolism in *Pyrococcus furiosus*. Mol Microbiol **71:**332-49.

13. **Lipscomb, G. L., K. Stirrett, G. J. Schut, F. Yang, F. E. Jenney, Jr., R. A. Scott, M. W. Adams, and J. Westpheling.** 2011. Natural competence in the hyperthermophilic archaeon *Pyrococcus furiosus* facilitates genetic manipulation: construction of multiple markerless deletions of genes encoding the two cytoplasmic hydrogenases. Appl Environ Microbiol **77**:2232-8.

14. **Liu, Y., M. Sieprawska-Lupa, W. B. Whitman, and R. H. White.** 2010. Cysteine is not the sulfur source for iron-sulfur cluster and methionine biosynthesis in the methanogenic archaeon *Methanococcus maripaludis*. J Biol Chem **285:**31923-9.

15. **Ma, K., and M. W. Adams.** 2001. Ferredoxin:NADP oxidoreductase from *Pyrococcus furiosus*. Methods Enzymol **334:**40-5.

16. **Ma, K., and M. W. Adams.** 1994. Sulfide dehydrogenase from the hyperthermophilic archaeon *Pyrococcus furiosus*: a new multifunctional enzyme involved in the reduction of elemental sulfur. J Bacteriol **176:**6509-17.

17. **Ma, K., R. N. Schicho, R. M. Kelly, and M. W. Adams.** 1993. Hydrogenase of the hyperthermophile *Pyrococcus furiosus* is an elemental sulfur reductase or sulfhydrogenase: evidence for a sulfur-reducing hydrogenase ancestor. Proc Natl Acad Sci U S A **90:**5341-4.

18. **Miller, R. E., and E. R. Stadtman.** 1972. Glutamate synthase from *Escherichia coli*. An iron-sulfide flavoprotein. J Biol Chem **247:**7407-19.

19. **Santangelo, T. J., L. Cubonova, and J. N. Reeve.** 2011. Deletion of alternative pathways for reductant recycling in *Thermococcus kodakarensis* increases hydrogen production. Mol Microbiol **81:**897-911.

20. **Sapra, R., K. Bagramyan, and M. W. Adams.** 2003. A simple energy-conserving system: proton reduction coupled to proton translocation. Proc Natl Acad Sci U S A **100:**7545-50.

21. **Schut, G. J., S. D. Brehm, S. Datta, and M. W. Adams.** 2003. Whole-genome DNA microarray analysis of a hyperthermophile and an archaeon: *Pyrococcus furiosus* grown on carbohydrates or peptides. J Bacteriol **185:**3935-47.

22. **Schut, G. J., S. L. Bridger, and M. W. Adams.** 2007. Insights into the metabolism of elemental sulfur by the hyperthermophilic archaeon *Pyrococcus furiosus*: characterization of a coenzyme A- dependent NAD(P)H sulfur oxidoreductase. J Bacteriol **189:**4431-41.

23. **Schut, G. J., J. Zhou, and M. W. Adams.** 2001. DNA microarray analysis of the hyperthermophilic archaeon *Pyrococcus furiosus*: evidence for a new type of sulfur-reducing enzyme complex. J Bacteriol **183:**7027-36.

24. **Silva, P. J., E. C. van den Ban, H. Wassink, H. Haaker, B. de Castro, F. T. Robb, and W. R. Hagen.** 2000. Enzymes of hydrogen metabolism in *Pyrococcus furiosus*. Eur J Biochem **267:**6541-51.

25. **Strand, K. R., C. Sun, T. Li, F. E. Jenney, Jr., G. J. Schut, and M. W. Adams.** 2010. Oxidative stress protection and the repair response to hydrogen peroxide in the hyperthermophilic archaeon *Pyrococcus furiosus* and in related species. Arch Microbiol **192:**447-59.

26. **Williams, E., T. M. Lowe, J. Savas, and J. DiRuggiero.** 2007. Microarray analysis of the hyperthermophilic archaeon *Pyrococcus furiosus* exposed to gamma irradiation. Extremophiles **11:**19-29.

27. **Yang, H., G. L. Lipscomb, A. M. Keese, G. J. Schut, M. Thomm, M. W. Adams, B. C. Wang, and R. A. Scott.** 2010. SurR regulates hydrogen production in *Pyrococcus furiosus* by a sulfur-dependent redox switch. Mol Microbiol **77:**1111-22.

Table 3.1. *P. furiosus* strains constructed and/or used in this study.

Strain[a]	Genotype	Deleted ORF(s)[b]	Source or Reference
COM1 (MW00002)	Δ*pyrF*	PF1114	(13)
NSR1 (MW00010)	Δ*pyrF* Δ*nsr*	PF1114, PF1186	This work
MBX1 (MW00011)	Δ*pyrF* Δ*mbxL*	PF1114, PF1442	This work
COM1c (MW00003)	Δ*pyrF*::*pyrF*	None[c]	This work
SIP1 (MW00012)	Δ*pyrF* Δ*sipA*::P_{gdh} *pyrF*	PF2025	This work

[a] MW strain codes in parentheses are lab strain designations.
[b] ORF, open reading frame.
[C] Restored.

Figure 3.1. Effect of S^0 availability on the growth of NSR1 and MBX1. Cultures were grown in 100 ml bottles stirred at 98°C with 5 g/L maltose, 0.5 g/L yeast extract, and 20 µM uracil. Cell growth was monitored by assaying total cell protein at each time point. Top. Maltose only. Bottom. Maltose + 2 g/L S^0. COM1 (closed circles), NSR1 (open squares), and MBX1 (open triangles).

FIGURE 3.1

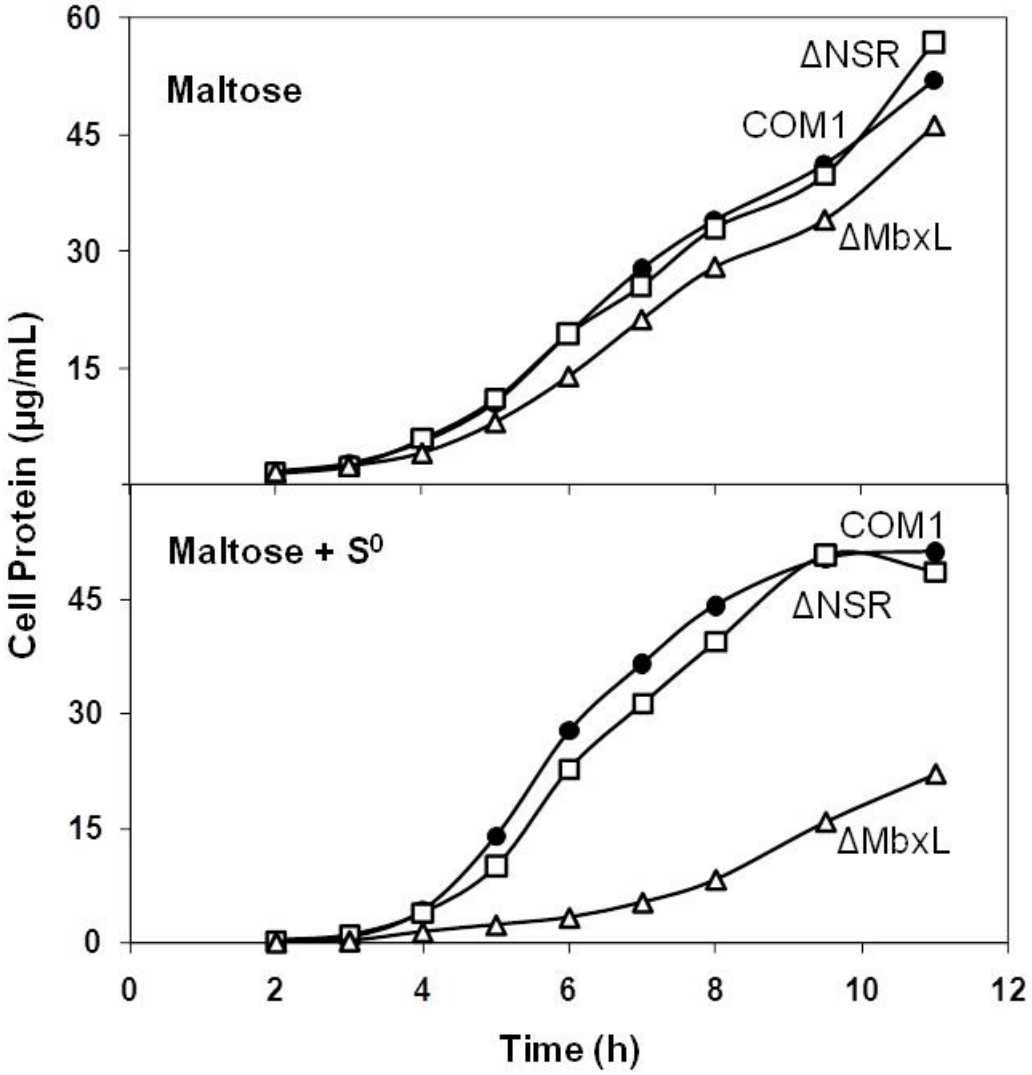
Maltose
ΔNSR
COM1
ΔMbxL
Maltose + S0
COM1
ΔNSR
ΔMbxL
Cell Protein (µg/mL)
Time (h)
0
15
30
45
60
0
2
4
6
8
10
12

Figure 3.2. Effect of S^0 availability on the growth of SIP1. Cultures were grown in 100 ml bottles stirred at 98°C with 5 g/L maltose and 0.5 g/L yeast extract. Cell growth was monitored by assaying total cell protein at each time point. Top. Maltose only. Bottom. Maltose + 2 g/L S^0. COM1c (closed squares) and SIP1 (open circles).

FIGURE 3.2

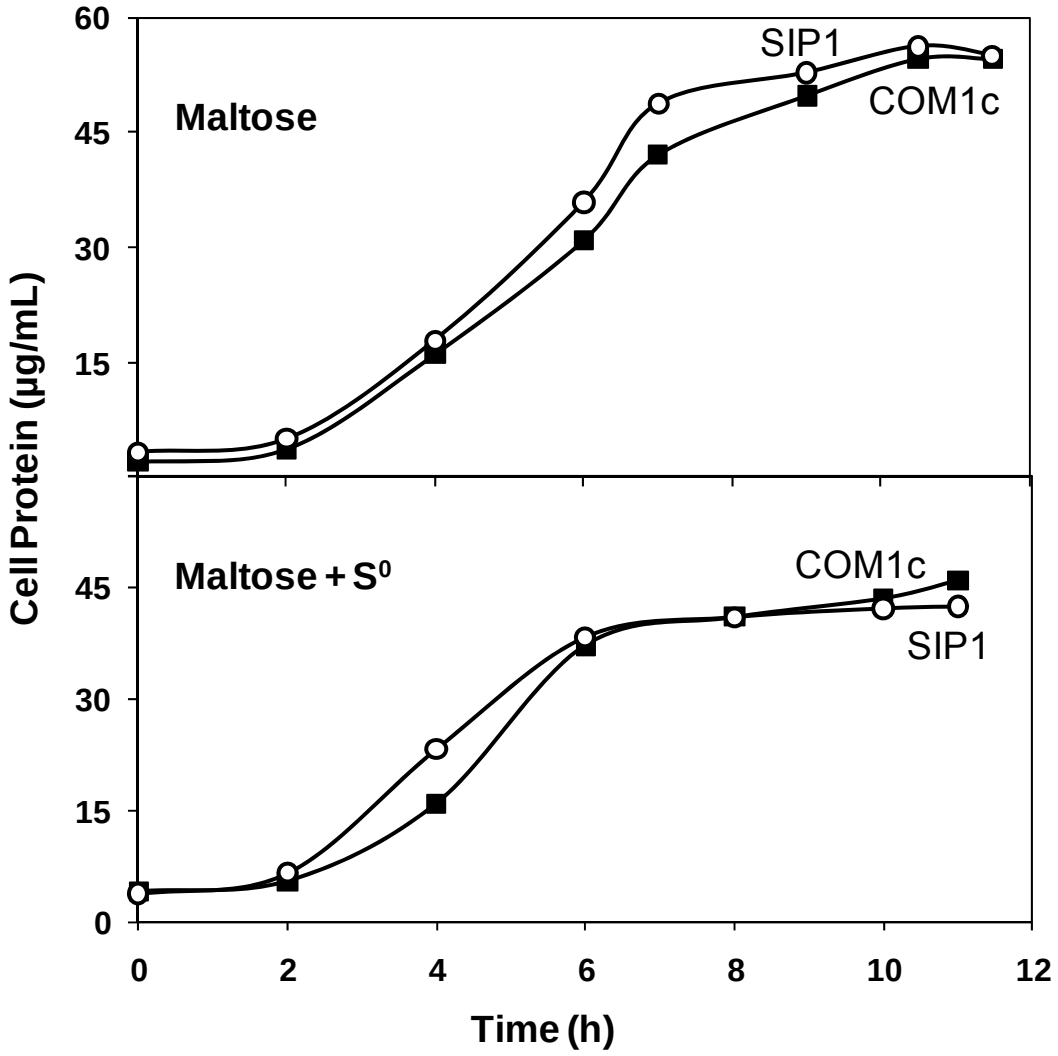
Maltose
SIP1
COM1c
Maltose + S0
COM1c
SIP1
Cell Protein (µg/mL)
Time (h)
0
15
30
45
60
0
2
4
6
8
10
12

Figure 3.3. Effect of S^0 addition on the growth of NSR1, MBX1 and SIP1. Kinetic growth curves of deletion strains compared to control strains designated in Table 3.1. Cultures were grown in 100 ml bottles stirred at 98°C with 5 g/L maltose and 0.5 g/L yeast extract prior to the addition of 2 g/L S^0 (as indicated by arrow). Cell growth was monitored by assaying total cell protein at each time point. Top. 20 µM uracil was added to the growth of COM1 (closed circles), NSR1 (open squares), MBX1 (open triangles). Bottom. COM1c (closed squares) and SIP1 (open circles).

FIGURE 3.3

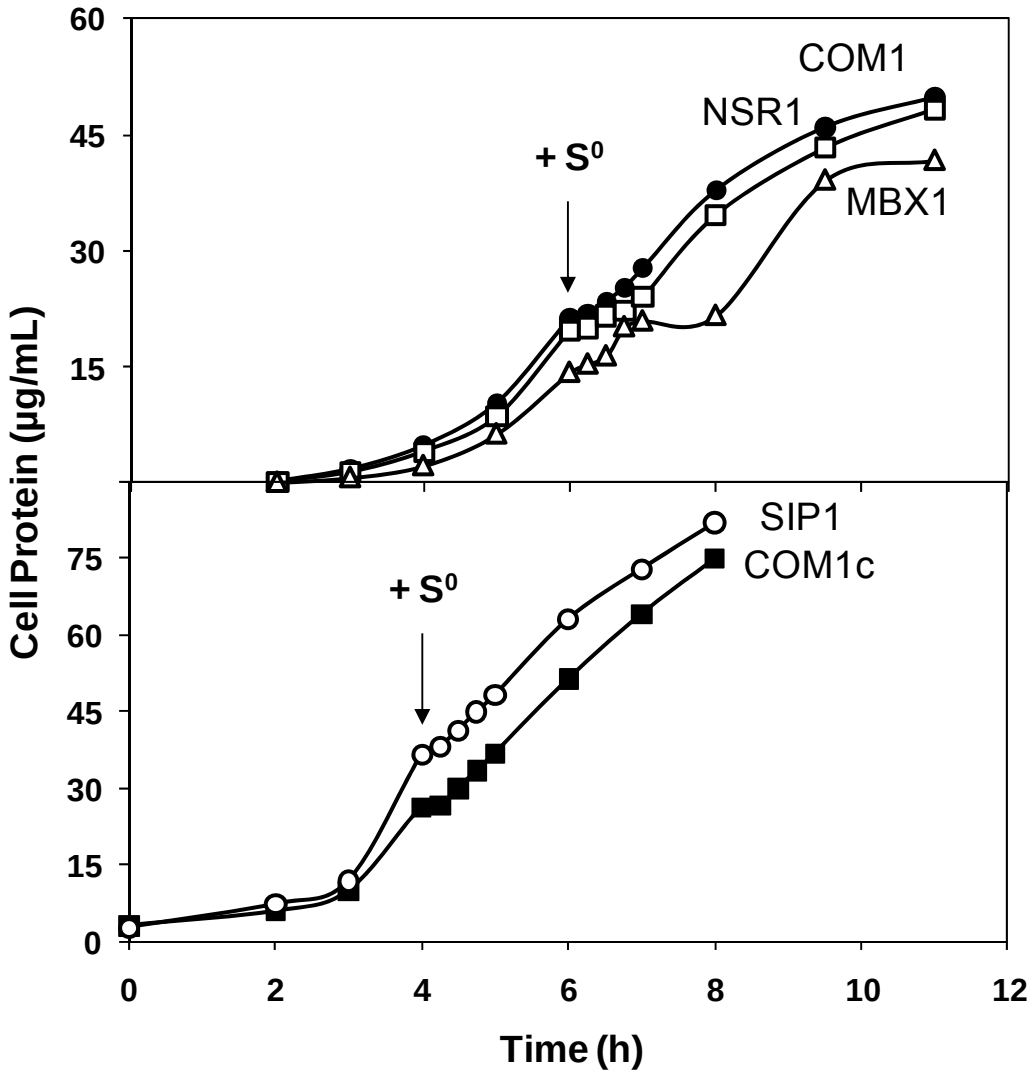
60
45
30
15
COM1
NSR1
MBX1
+ S0
Cell Protein (µg/mL)
75
60
45
30
15
0
SIP1
COM1c
+ S0
0
2
4
6
8
10
12
Time (h)

Figure 3.4. Quantitative RT-PCR of select S^0 response genes. Total RNA was prepared from COM1, NSR1 and MBX1 cells harvested before and 30 min after S^0 addition (2 g/L). For gene clusters of interest, the first gene in the operon was selected for analysis. Constitutively expressed gene PF0971 (*por* gamma subunit) was used as a control. Ratio of change in gene expression within 30 min of S^0 addition in deletion strains (open bars) compared to the appropriate control strains (closed bars). A. COM1 (closed bars) and NSR1 (open bars). B. COM1 (closed bars) and MBX1 (open bars). Single asterisk (*) indicates QPCR confirmation of deleted gene product. Double asterisks (* *) indicates an increase in gene expression of *mbxA* (PF1453) was observed in MBX1; however, no gene product was observed for the deleted L-subunit (PF1442).

FIGURE 3.4

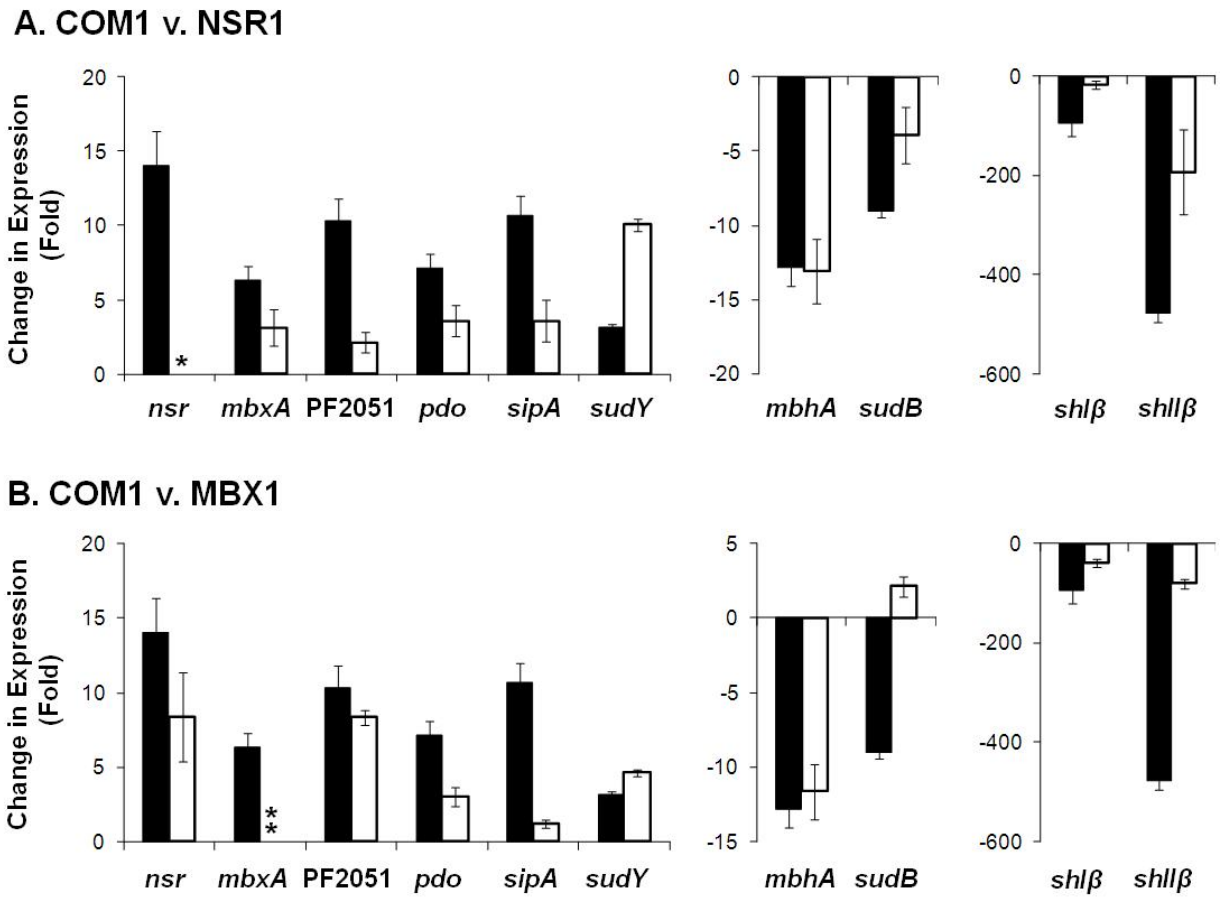
A. COM1 v. NSR1
Change in Expression (Fold)
20
15
10
5
0
*
nsr
mbxA
PF2051
pdo
sipA
sudY
0
-5
-10
-15
-20
mbhA
sudB
0
-200
-400
-600
shlβ
shllβ
B. COM1 v. MBX1
Change in Expression (Fold)
20
15
10
5
0
**
nsr
mbxA
PF2051
pdo
sipA
sudY
5
0
-5
-10
-15
mbhA
sudB
0
-200
-400
-600
shlβ
shllβ

Figure 3.5. Proposed physiological roles of S^0 reduction in *P. furiosus*: bioenergetics and FeS metabolism. MBX, membrane-bound oxidoreductase complex; NSR, NADPH sulfur oxidoreductase; SipA, sulfur-induced protein A; SurR, S^0-response regulator; SuDH I and II, sulfide dehydrogenase I and II; Fd, ferredoxin; PS, polysulfide; H_2S, hydrogen sulfide; CoASH, co-enzyme A; NSR1, deletion strain lacking NSR. The precise mechanisms by which PS interacts with SurR and SipA is involved in FeS metabolism are not clear.

FIGURE 3.5

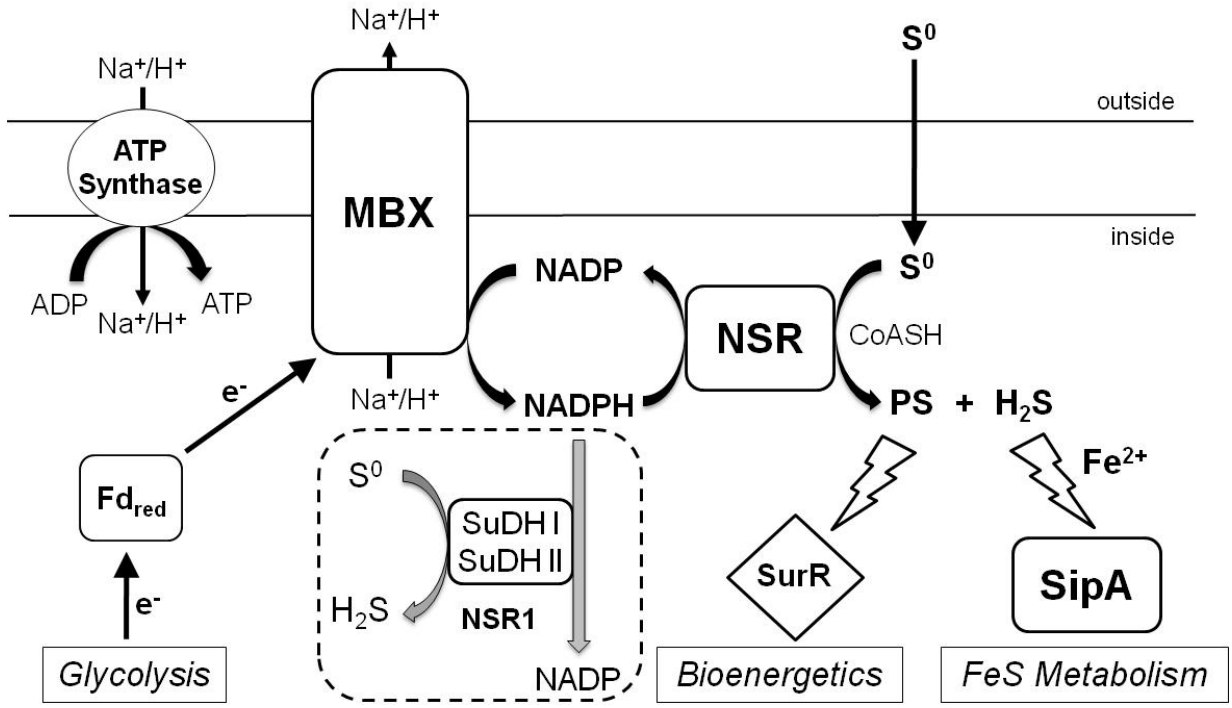
Na+/H+
Na+/H+
S0
outside
ATP Synthase
MBX
inside
ADP
Na+/H+
ATP
NADP
S0
NSR
CoASH
e-
Na+/H+
NADPH
PS + H2S
Fe2+
Fdred
S0
SuDH I
SuDH II
SurR
SipA
e-
H2S
NSR1
Glycolysis
NADP
Bioenergetics
FeS Metabolism

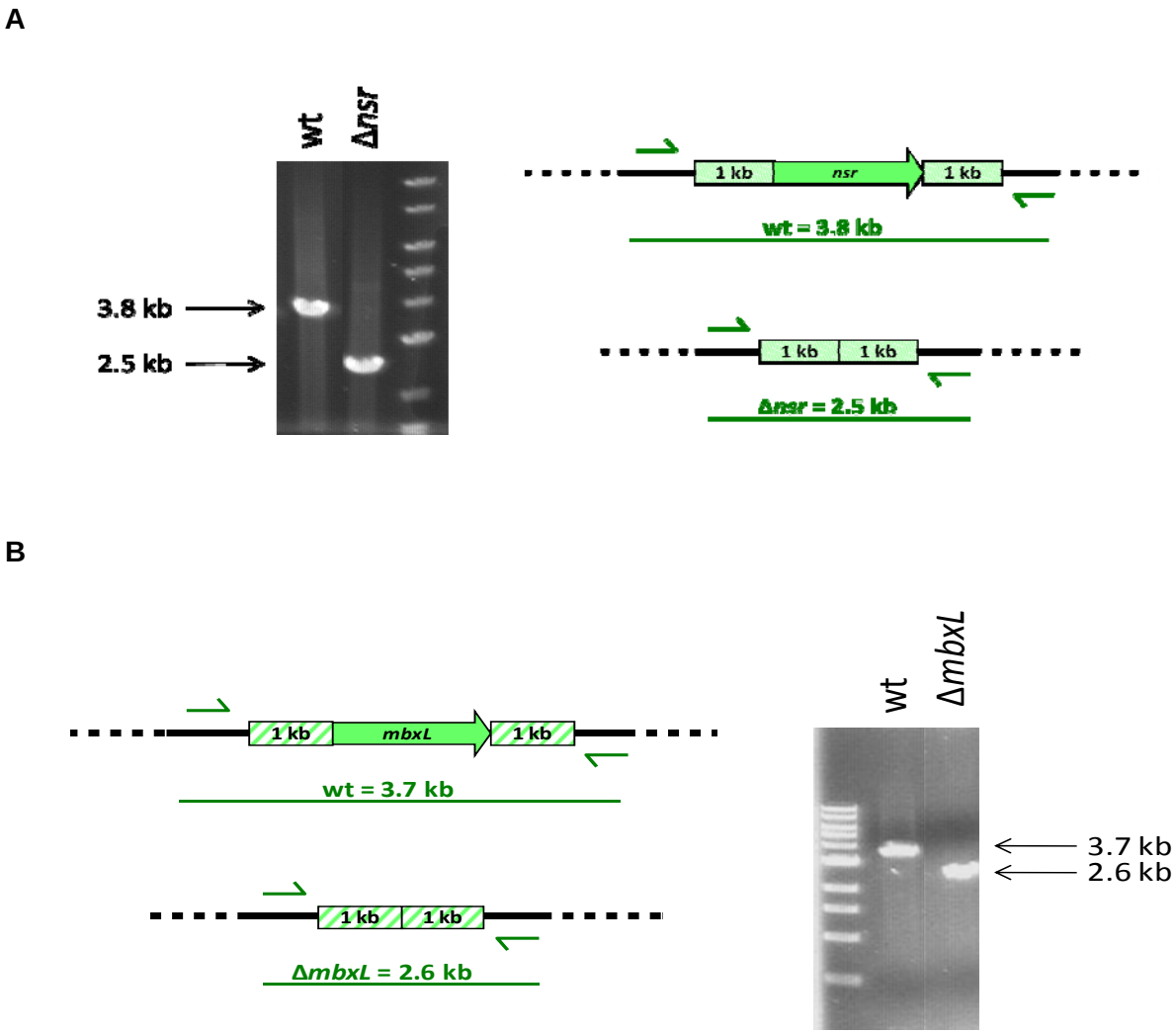

Figure S3.1. PCR confirmation of gene deletions *nsr* and *mbxL*. PCR confirmation of the *nsr* deletion (A, top) was obtained using primers KS023 and KS024, where the parent strain yielded a product of approximately 3.8 kb and the NSR1 strain a product of 2.5 kb. PCR confirmation of the *mbxL* deletion (B, bottom) was obtained using primers KS053MBXconF, where the parent strain yielded a product of approximately 3.7 kb and the ΔMbxL strain a product of 2.6 kb. PCR products obtained from the deletion strains were sequenced for further confirmation (data not shown).

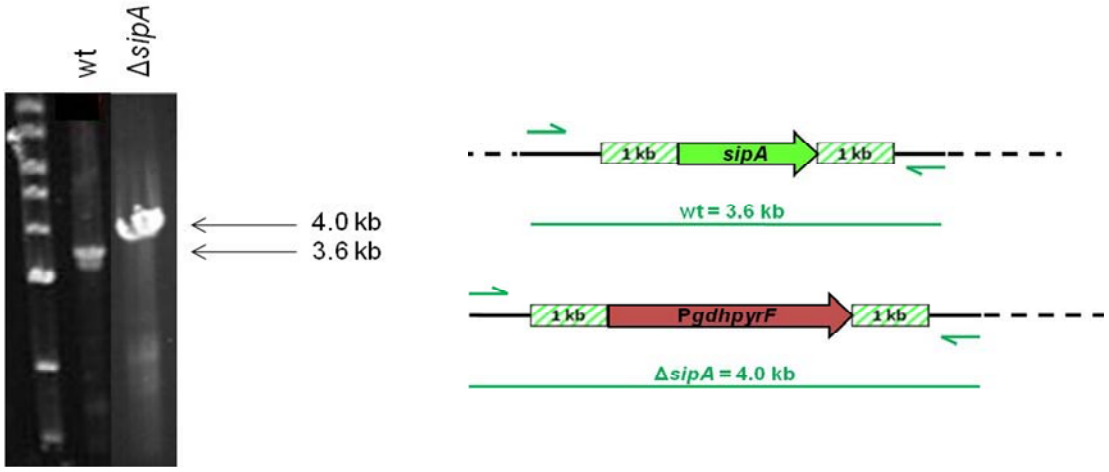

Figure S3.2. Confirmation of the *sipA* marker replacement deletion. Confirmation of the Δ*sipA* deletion was performed by PCR analysis using primers MD01 and MD014. The parent strain yielded a product of approximately 3.6 kb and the SIP1 strain a product of 4.0 kb. The latter was further confirmed by restriction enzyme digestion with both XbaI and EcoRI, giving products as expected (data not shown).

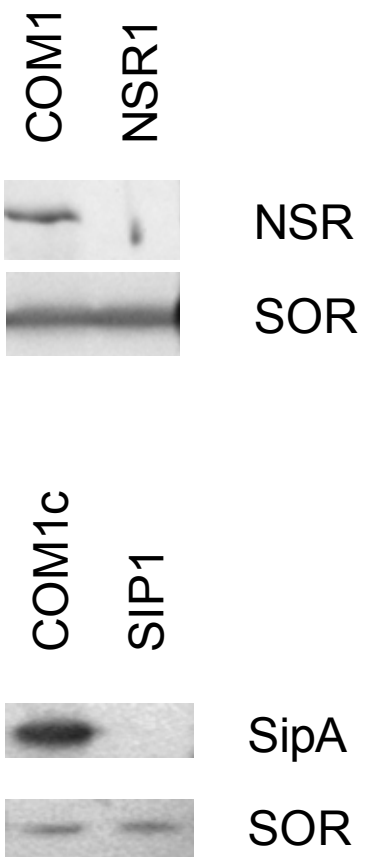

Figure S3.3. Western blot confirmation of NSR1 and SIP1 following S^0 addition. Polyclonal antibodies to NSR and SipA were generated against recombinant protein with an N-terminal His6 tag that was produced in *Escherichia coli* and purified in the presence of 6 M guanidinium chloride (Research Animal Resources Facility, Athens, GA). These and the polycolonal antibody to *P. furiosus* superoxide reductase ([SOR] a gift from Frank Jenney, Philadelphia College of Osteopathic Medicine, Suwanee, GA) were purified from serum using a protein A column (GenScript, Piscataway, NJ). Western blot analyses were performed on cell extracts prepared from cells harvested 30 min after S^0 addition (2g/L) with SOR used as a loading control.

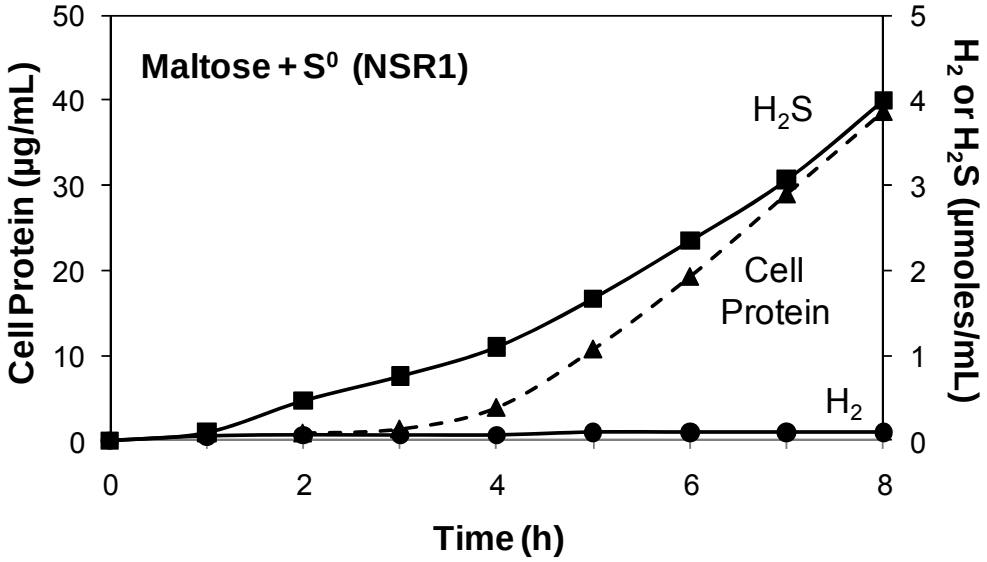

Figure S3.4. H_2S is produced during growth of NSR1 in the presence of S^0. 100 ml bottle cultures stirred at 98°C with 5 g/L maltose, 0.5 g/L yeast extract, 20 µM uracil, and 2 g/L S^0. Samples of headspace gas and media were transferred to secondary assay vials at each point for subsequent hydrogen gas and sulfide analyses, and cell growth was monitored by assaying total cell protein. Cell growth (closed triangles/dotted line), hydrogen gas (closed circles), and hydrogen sulfide (closed squares).

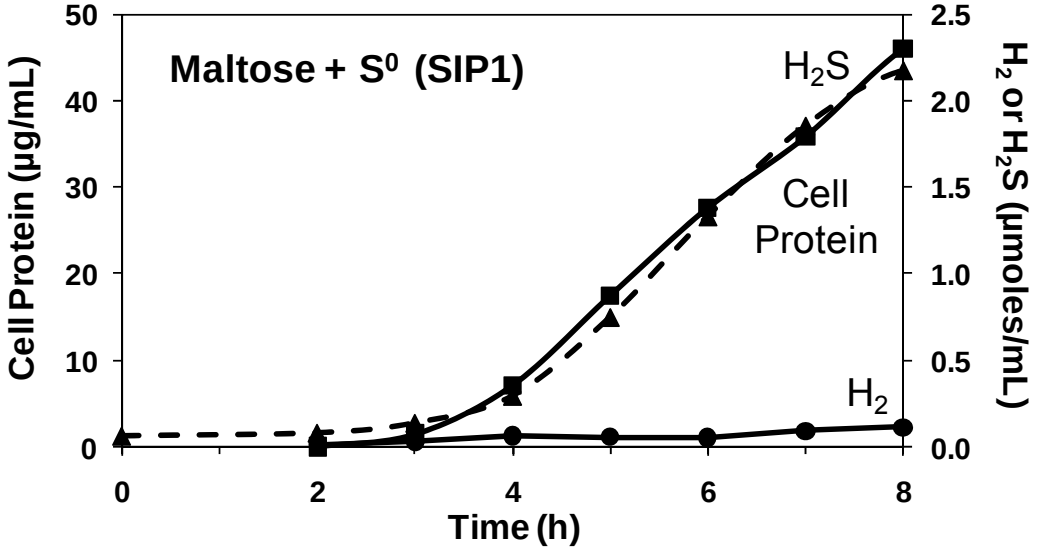

Figure S3.5. H_2S production follows growth of SIP1 in the presence of S^0. 100 ml bottle cultures stirred at 98°C with 5 g/L maltose, 0.5 g/L yeast extract, and 2 g/L S^0. Samples of headspace gas and media were transferred to secondary assay vials at each point for subsequent hydrogen gas and sulfide analyses, and cell growth was monitored by assaying total cell protein. Cell growth (closed triangles/dotted line), hydrogen gas (closed circles), and hydrogen sulfide (closed squares).

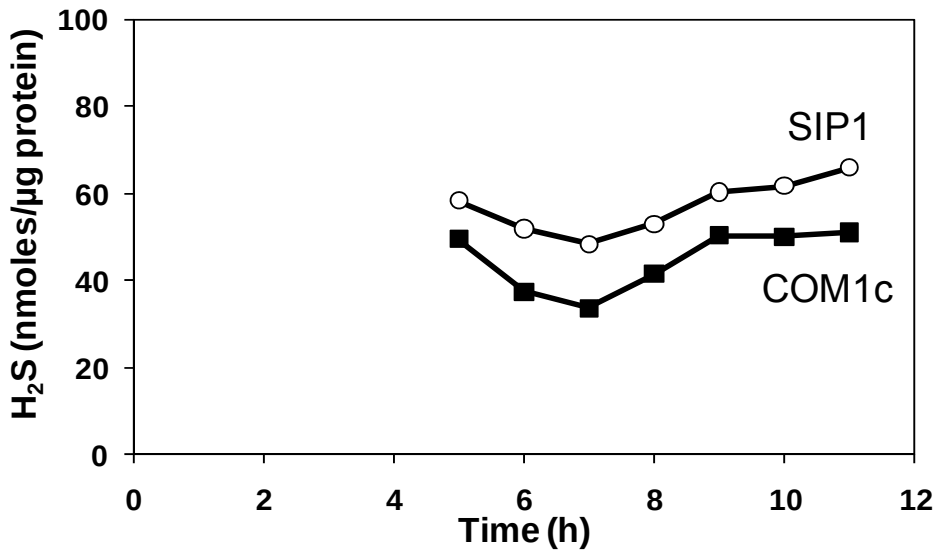

Figure S3.6. Amount of sulfide generated per unit protein in COM1c and SIP1. Cultures were grown in 100 ml bottles stirred at 98°C with 5 g/L maltose, 0.5 g/L yeast extract and 2 g/L S^0. Total cell protein and sulfide production were determined at each time point. COM1c (closed squares), SIP1 (open circles).

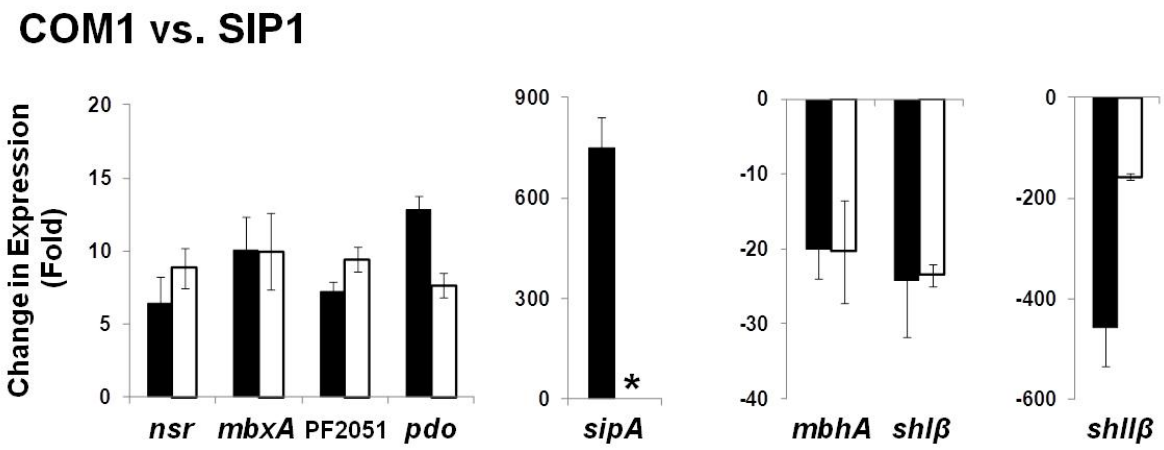

Figure S3.7. Quantitative RT-PCR of Select S^0 Response Genes in SIP1. Total RNA was prepared from COM1c and SIP1 cells harvested before and 30 min after S^0 addition (2 g/L). For gene clusters of interest, the first gene in the operon was selected for analysis. Constitutively expressed gene PF0971 (*por* gamma subunit) was used as a control. Ratio of change in gene expression within 30 min of S^0 addition in SIP1 (open bars) compared to the control strain COM1c (closed bars). Asterisk (*) indicates QPCR confirmation of deleted gene product.

CHAPTER 4

TRANSCRIPTIONAL ANALYSES OF THE *PYROCOCCUS FURIOSUS* DELETION STRAINS COM1 AND NSR1 USING WHOLE GENOME DNA MICROARRAYS

ABSTRACT

Characterization of genetically modified *Pyrococcus furiosus*, COM1, the genetically-tractable strain, and NSR1, the CoA-dependent NADPH sulfur oxidoreductase (NSR) deletion strain, have been described in Chapters 2 and 3, respectively. In order to further investigate the physiological role of NSR in *P. furiosus* in both the presence and absence of S^0, DNA microarrays were used to analyze both the primary response to S^0 addition (within 10 minutes) in NSR1 and transcriptional differences between NSR1 and COM1 during non-S^0 growth on maltose. Overall, the primary response to S^0 in NSR1 included less genes involved in hydrogen and sulfur metabolism compared to wild type, supporting a role for NSR in modulating transcriptional control by the S^0 response regulator, SurR. In addition, *P. furiosus* appears to be more sensitive to S^0 addition in the absence of NSR, as genes involved in both oxidative stress and nucleotide metabolism are up-regulated as part of the primary response to S^0 in NSR1. Surprisingly, the absence of NSR in non-S^0 (maltose) grown cells had a dramatic affect on the expression of genes encoding proteins involved in α- and β-glucan metabolism and transport which are inconsistent with previously reported responses to α- vs. β-substrate glycoside linkages. Key enzymes appear to be two NADPH-dependent alcohol dehydrogenases, AdhA and AdhB, which are co-expressed with β-glucan utilization genes. These results suggest that NSR not only produces H_2S but also maintains the thiol-redox balance of the cell and thereby indirectly modulates transcriptional control via thiol-based regulators like SurR.

INTRODUCTION

Pyrococcus furiosus is a model hyperthermophilic archaeon that grows optimally near 100°C (7). It utilizes both α- and β-linked di- and oligosaccharides and peptides as substrates for growth and produces organic acids such as acetate, CO_2 and H_2. When elemental sulfur (S^0) is present, hydrogen sulfide (H_2S) is produced instead of H_2 (1, 7, 36). The cytoplasmic enzyme responsible for CoA-dependent NADPH-linked S^0 reduction in *P. furiosus*, NSR, has been identified and purified from native S^0-grown cell extracts (36). Transcriptional analyses revealed NSR to be one of two key enzymes significantly up-regulated as part of the primary response to S^0 addition within 10 minutes (36). The expression of almost all of the primary S^0-response genes are thought to be regulated by the S^0-response regulator, SurR (20), which causes the up-regulation of genes involved in S^0 metabolism and down-regulation of those involved in H_2 metabolism.

Recent development of a genetics system for *P. furiosus* was based on the isolation of a variant in the lab strain population, which was highly efficient for the uptake and recombination of exogenous DNA (21). This genetically-tractable strain of *P. furiosus*, designated COM1, is a uracil auxotroph (ΔpyrF) and has been used to generate both marked and markerless deletions of a number of genes including PF1186, which encodes for NSR. Termed NSR1, biochemical and growth analyses carried out with the NSR deletion strain (Chapter 3) in the presence and absence of S^0 revealed a non-essential role for NSR in S^0 reduction (4). NSR1 grew well on maltose with S^0 and without S^0, and produced comparable amounts of sulfide as the parent strain (COM1). Unlike NSR1, characterization of the MBX1 deletion strain (membrane-bound oxidoreductase; (34)) clearly demonstrated that MBX plays a critical role in S^0 reduction and energy conservation (4). Limited transcriptional analysis of only ten select genes in NSR1 suggested a compensatory role for two NADPH-dependent SudDH enzymes in S^0 reduction and a potential regulatory role for NSR in producing intracellular sulfur species that contribute to the SurR transcriptional response.

The complete genome sequence of the COM1 strain has been determined (Chapter 2) and revealed a surprisingly large number of changes compared to that of the *P. furiosus* NCBI reference sequence (32), including chromosomal rearrangements, deletions, and single base changes in both coding and potential regulatory regions (5). Insertion sequence (IS) elements were shown to play a significant role in the evolution of the COM1 strain resulting in the direct deletion or insertional inactivation of thirteen genes. In addition, another seven genes were predicted to be non-functional due to chromosomal deletion and another 102 of the 2134 predicted gene products were different at the protein-level in COM1. Collectively, all of these genomic changes potentially impact cellular functions including carbohydrate, peptide and nucleotide metabolism, DNA repair, CRISPR-associated defense, transcriptional regulation, membrane transport and low temperature growth in COM1. However, in spite of all the genomic changes only a few phenotypic differences could be observed in COM1 compared to its parental strain and a *P. furiosus* DSMZ strain. It is expected that the same genomic changes are present in the NSR1 daughter strain, in addition to the targeted deletion of PF1186 (*nsr*).

The purpose of this work was to investigate transcriptional differences in both of the mutant strains of *P. furiosus* discussed in Chapters 2 and 3. Specifically, DNA microarrays were used to analyze both the primary response to S^0 addition (within 10 minutes) in NSR1 and the transcriptional differences between NSR1 and its parental strain, COM1, during non-S^0 growth on maltose.

MATERIALS AND METHODS

Strains and growth conditions.

P. furiosus strains used in this work are NSR1 (Δ*nsr*; (4)) and COM1 (Δ*pyrF*; (21)). All strains were grown as previously reported (1) with maltose (5 g/L) and yeast extract (0.5 g/L), and uracil (20 μM) was added to the growth media of the auxotrophic strains (COM1 and NSR1). To obtain RNA for microarray analyses, cultures were grown in a 20 L fermentor (1) and samples

(2 L each) were removed during mid-log phase growth. For the NSR1 S^0 switch, samples were removed before and 10 min after the addition of S^0 (2 g/L) as previously described (36).

RNA isolation and DNA microarray analyses.

Total RNA was isolated from *P. furiosus* cells using two acid-phenol extractions (37), Turbo DNase (Ambion® Cat# AM2238) treatment (30 min, 37°C), and Absolutely RNA Miniprep kit (Stratagene® Cat# 400800). Design and construction of the PCR product based DNA microarrays contained the predicted 2,192 open reading frames (ORFs) in the annotated genome of *P. furiosus* (30) as previously described (37). RNA samples were fluorescently labeled using the ULYSIS Alexa Fluor® Nucleic Acid labeling kits (Invitrogen Cat# U21660, U21654, U21652) and purified using Micro Bio-Spin® columns (Bio-Rad Cat# 732-6250). Labeled RNA was dried under vacuum and rehydrated in 1-2 µl of nuclease free water prior to being mixed with hybridization solution. RNA-DNA hybridization experiments (55°C for ~15 hrs) were performed using DIG Easy Hyb Solution (Roche Cat# 11 603558 001), Hybridization Chamber II (Corning® Cat# 40080), and M Series Lifterslip™ (ThermoScientific Cat# 60I-M-5439-001-LS). Post-hybridization washing was performed using the Universal Hybridization Kit (Corning Pronto!™ Cat# 40030). Fluorescence intensities for the Alexa dyes were measured as described previously (37). Signal intensities were quantified and normalized using ScanArray Express software (PerkinElmer). The $\log_2$ ratio values represent an average of two hybridization experiments using RNA derived from a single culture of the *P. furiosus* strain.

RESULTS

RNA-DNA microarray hybridization analyses.

For each experiment in this study, RNA samples were directly labeled and hybridized to a DNA microarray composed of PCR products that represent 2,065 annotated *P. furiosus* ORFs (37). This RNA-DNA hybridization method differs from previously published array data (35-38, 42) where cDNA was prepared from RNA samples and DNA-DNA hybridizations were performed.

In order to determine the efficacy of this approach, numerous control experiments were performed including side-by-side comparison of RNA/DNA-DNA hybridizations where the results showed a very high degree of correlation in gene expression profiles (data not shown). In addition, to determine the standard deviation (log_2 signal intensity ratios) for the average of each ORF represented under the RNA-DNA hybridization conditions, *P. furiosus* RNA samples derived from two cultures grown under identical conditions (NSR1, t=0) were differentially labeled and hybridized to the same slide. As shown in Figure 4.1, the normalized signal intensities for all ORFs vary less than 2-fold as indicated by the light blue diagonal dotted lines.

Primary S^0 response in the NSR1 strain.

Within 10 minutes of the addition of S^0 to a growing culture of NSR1 the expression of a total of 48 genes are significantly ($\geq$ 3-fold) up- or down-regulated (Figure 4.2). As shown in Table 4.1, of the 24 up-regulated genes, only one gene encoding protein disulfide oxidoreductase (PDO; (8)) was previously identified as being part of the primary S^0 response in *P. furiosus* (36). The other 23 ORFs in NSR1 that are immediately up-regulated in response to S^0 addition encode for some proteins originally observed in the secondary response to S^0 (within 30 minutes; (36)) including the branched chain amino acid biosynthetic enzymes (PF0935-42). Additional biosynthesis related proteins include: serine/threonine (PF1053-56), and methionine (PF1266-69), asparagine synthetase A (PF1951), and phosphoenolpyruvate carboxylase (PF1975). The remaining six genes encode for proteins involved with nucleotide metabolism, oxidative stress and two with unknown function: ribonucleotide reductase (RNR; (31)), anaerobic ribonucleotide triphosphate reductase (PF1971), peroxiredoxin (PF1033), and hypothetical proteins (PF0101 and PF0934). Of these peroxiredoxin and PF0101 were previously reported as being part of the peroxide stress response in *P. furiosus* (38). Similarly, of the 24 genes significantly down-regulated within 10 minutes of S^0 addition in NSR1 (Table 4.2), two key S^0 metabolism gene clusters including the soluble hydrogenase II (SHII; (25)) and the membrane-bound hydrogenase (MBH; (34)), and two genes of unknown function were previously reported as

primary S^0 response genes (36). The other genes in NSR1 that are immediately down-regulated after S^0 addition include aldehyde:ferredoxin oxidoreductase (AOR; (28)), ferredoxin:NADPH oxidoreductase I beta (FNOR I; (22)), sarcosine oxidase alpha (PF1795), a predicted heme biosynthesis protein (PF0647), and three hypothetical proteins (PF1390, PF1481, and PF1488). Of these FNOR I was previously reported as being part of the secondary response to S^0 (36).

Transcriptional Differences between NSR1 and COM1 during growth on Maltose.

To further investigate the physiological role of NSR in *P. furiosus*, both the NSR1 deletion strain and its parental COM1 strain were grown on maltose in the absence of S^0 for direct comparison of gene expression profiles under hydrogen producing growth conditions. As shown in Figure 4.3, a total of 48 genes in NSR1 are differentially expressed ($\geq$ 3-fold) compared with COM1 under the same growth conditions. Surprisingly, of the 17 genes more highly expressed in NSR1 during growth on maltose (α-linked sugar), 12 of them encode for proteins associated with β-linked sugar catabolism and transport (Table 4.3). These genes are clustered into three regions on the chromosome and include β-glucosidase (CelB; (12)), two alcohol dehydrogenases (AdhA and AdhB; (23, 40)), beta-1,3-lamarinase (LamA; (9)), beta-mannosidase (BmnA; (3)), a β-glucan (cellobiose) transport system (CbtA-F; (15)), and a transporter predicted to be involved in the uptake of chitobiose (β-linked glucosamine; (39)). As shown in Figures 4.4A and B, these regions contain divergently oriented genes and the majority have been shown to be coordinately expressed in the presence of β-glucan sugars including: *celB*, *adhA*, *adhB*, and *lamA* (41), and *cbtA* and *cbtB* (15), respectively. The remaining five genes encode for a predicted heme biosynthesis protein (PF0647) and four hypothetical proteins (PF0546, PF0934, PF1452, and PF1455). As shown in Table 4.4, the 28 genes less highly expressed in NSR1 compared with COM1 encode for proteins involved with α-glucan sensing, α-linked oligosaccharide transport, peptide catabolism and transport, hydrogen metabolism, and various stress responses. For example, alpha amylase (PF0477; (35)),

maltodextrin transporter (Mal-II; (16)), glutamate dehydrogenase (GDH; (13)), oligopeptide transporter (PF0191-94), soluble hydrogenase I (SHI; (24)), ribonucleotide reductase (RNR; (31)), alkyl hydroperoxide reductase (PF0722), peroxiredoxin (PF1033), and S^0 induced protein A (SipA; (37)).

DISCUSSION

Initial characterization of the NSR1 deletion strain revealed probable regulatory roles for NSR in modulating both the primary and secondary responses to S^0 in *P. furiosus* (4). In order to further elucidate the role of NSR in the metabolic shift from hydrogen to sulfur metabolism (via SurR) the same DNA microarray approach as reported for wild type *P. furiosus* was employed (36). With the exceptions of PDO, SHII and MBH, these results differ from the distinct SurR-mediated (20) primary S^0 response which included the key S^0 responsive proteins, MBX, SHI, and putative transcriptional regulators PF2051-52 (36). These results support a role for NSR in modulating the activity of SurR via its redox-dependent DNA-binding. Within only 10 minutes of S^0 addition, hydrogenase proteins would still be present including SHI, SHII, and MBH. It has been shown that S^0 inhibits the activities of both SHI and MBH *in vitro* (G. Schut, personal communication); however, SHI also is capable of NADPH-dependent S^0 reduction and is hence why its function as a hydrogenase is abolished in the presence of S^0. It is therefore likely that SHI would immediately start reducing S^0 to H_2S upon addition. Characterization of the MBX1 deletion strain revealed not only a vital role for MBX in both S^0 reduction and energy conservation in the presence of S^0, but also showed that like NSR1, the SurR transcriptional response to S^0 was greatly reduced in MBX1. This observation suggested a cooperative relationship between NSR and MBX, and it was postulated that the activity of NSR is dependent on MBX (presumably Fd-linked NADP reduction). However, it cannot be ruled out that MBX is the primary S^0-reducing enzyme because all attempts to measure an activity of MBX *in vitro* have been unsuccessful. In the absence of S^0, SurR acts as a repressor of sulfur metabolism

genes (ie. *nsr* and *mbx*) by binding to the promoter and presumably blocking transcription machinery. Therefore when S^0 becomes available, a non NSR-dependent mechanism must also be present for the oxidation/deactivation of SurR in the switch from H_2 to S^0 metabolism. These results indicate that the SurR transcriptional response to S^0 is not dependent on the activity of NSR, but that its activity expedites the cells response to S^0 by influencing the redox state of the cytoplasm.

The results of the primary S^0 response also indicate that *P. furiosus* undergoes a "S^0 stress" response in the absence of NSR where genes that have been previously observed as being part of either peroxide- or cold-induced shock in *P. furiosus* (38, 42) are up-regulated > 3-fold within 10 minutes of S^0 addition. These genes encode for enzymes responsible for both nucleotide synthesis and peroxide reduction, namely ribonucleotide reductase, anaerobic ribonucleotide triphosphate reductase, and peroxiredoxin. These results appear to be consistent with the oxygen sensitivity phenotype reported for a mutant strain of *T. kodakarensis*, ΔTK1481, which is an NAD(P)H oxidase homolog of NSR (14). Therefore, NSR appears to not only function in sulfur metabolism but may also have a detoxification role in helping remove certain oxidized sulfur species from the cytoplasm that may cause damage to nucleic acids and/or FeS cluster containing proteins.

In the absence of S^0, transcriptional differences between NSR1 and its parental strain COM1 appear to be consistent with some type of regulatory affect involving carbohydrate sensing and/or a redox imbalance in NSR1. During growth on the α-linked disaccharide maltose, twelve genes encoding β-linked sugar (cellobiose and chitobiose) catabolism and transport proteins are more than 6 to 30-fold higher expressed than in COM1, and the α-glucan sensing amylase and (α-glucan) maltodextrin transporter are more than 3 to 5-fold less highly expressed than in COM1. These results are inconsistent with the previously reported transcriptional responses to substrate glycoside linkage (i.e. maltose vs. cellobiose) in *P. furiosus*, where ORFs involved in β-glucan utilization and transport were highly expressed under

cellobiose-grown conditions and α-glucan under maltose-grown conditions, respectively (6). As shown in Figure 4.5, there is no theoretical difference in the oxidation/reduction equivalents or energy yield associated with the utilization of α- versus β-linked sugars; however, a previous work comparing growth on cellobiose and maltose indicated dramatically different impacts on bioenergetics and on H_2 production by *P. furiosus*. Specifically, on cellobiose 75% of the sugar was converted to acetate and H_2 whereas only 50% of the maltose was converted (6). It was suggested that maltose cultures may have a bottleneck leading to lower protein and H_2 production, whereas the coordinated expression of the two alcohol dehydrogenases (AdhA and AdhB) during growth on cellobiose alleviates the bottleneck in energy metabolism and detoxifies the cytoplasm by removing acetaldehyde generated from pyruvate by POR (6). *In vitro*, NADPH-dependent oxidoreductases, AdhA and B have been shown to act on a wide range of substrates in both oxidative and reductive reactions; however, their physiological substrates are unclear (23, 40). It is possible that these alcohol dehydrogenases could be disposing of excess reductant (NADPH) and producing alcohol in the NSR1 strain.

In *P. furiosus*, two transcriptional regulators have been shown to be involved in α-sugar sensing, namely, TrmB, a multifunctional repressor specific for both the trehalose and maltose (TM) system (Mal-I operon) and the maltodextrin (MD) system (Mal-II operon) (17), and a TrmB-like protein, TrmBL1, that has been shown to be a global regulator for MD transport as well as for glycolytic and gluconeogenic enzymes (18). A third TrmB-like protein, TrmBL2, has only been preliminarily examined and does not appear to be able to bind sugar; however, it has been shown to recognize the MD promoter (17). It has been speculated that TrmBL2 may follow a similar mechanism to that of the *E. coli* maltose system, and interact with the regulatory domain in the ABC subunits of the TM and MD transporters in *P. furiosus*. Together these results indicate that at a minimum the MD promoter alone has three regulators. To date, no studies have been reported on transcriptional regulators involved in β-sugar sensing; however, given the complexity arising from dual promoter specificity and multiplicity of sugar effectors (both

activation and repressing (19)) in α-glucan regulation, it will be challenging to dissect which potential regulators could be affecting the gene expression profile observed for NSR1 during growth on maltose. It is also possible that the regulation pattern observed is not directly carbohydrate related, but instead a mechanism to dispose of excess reductant (NADPH) in the cell through coordinated expression of the alcohol dehydrogenase genes. These dramatic regulatory effects also call into question what the functions of the uncharacterized regulatory targets of SurR might be, and if additional secondary regulators under the control of SurR (e.g. PF2051; (20)) are also affected in NSR1.

Collectively, these results taken together with previous reports of predicted physiological functions for the protein encoded by PF1186 (NSR (4, 36) and CoADR (10, 11)) have lead to a newly proposed name for this protein, NADPH-dependent redox sensor (NRS), and a model for its role in sensing and maintaining the redox state of the cytoplasm in *P. furiosus*. In this model NRS reduces CoA-polysulfane sulfur species (derived from abiotic reaction with S^0) at the expense of NADPH and concurrently produces intracellular H_2S (Figure 4.6). Analogous to bacterial species that lack glutathione, CoA is thought to be the alternative low-molecular-weight (LMW) thiol acting as an intracellular redox buffer in *P. furiosus* (11). Greater than 450 μM of free CoA thiol has been measured in non-S^0 grown cell extracts; whereas when cells were grown with S^0, total CoA levels almost doubled and about half was found to be in the disulfide form (CoA-S-S-CoA) (11). Therefore, similarly to the non-enzymatic reaction of glutathione with S^0 (33), it is likely that CoA abiotically reacts with S^0 (S_8 ring) to form monoorganylpolysulfane compounds ($CoAS_nH$, n>1), bisorganylpolysulfanes ($CoAS_nCoA$, n>2), CoA disulfides (CoA-S-S-CoA) and some H_2S in the cytoplasm of *P. furiosus*. Given that NRS has been shown to act as a CoA disulfide reductase (CoADR; (10)) it would make sense that if oxidized CoA-sulfur species were not properly reduced in the NSR1 strain (ΔPF1186), it would disturb the redox balance of the cell and lead to oxidative damage of nucleic acids and other cellular components; however, it is not known what range of CoA-sulfur species are physiological substrates for NRS.

Based on the sluggish response of NSR1 (and MBX1) to the addition of S^0 in growth curves and the muted SurR transcriptional response to S^0 in the mutant strains, it is predicted that abiotically generated CoA-sulfur species in the cytoplasm must not be as good of oxidants for SurR (presumably longer CoA-polysulfane chains), and that NRS readily reduces these molecules to smaller chains (potentially CoA-disulfides) rendering them better effectors for SurR. In this scheme, it is still plausible that other promiscuous sulfur reducing enzymes (ie. SuDHs and SHs) could be compensating for NRS activity in the NSR1 strain.

In summary, the NADPH-dependent redox sensory protein, NRS, is proposed to be involved in maintaining the redox state of the cytoplasm in *P. furiosus* by reducing oxidized CoA-polysulfide species derived from the abiotic reaction with S^0 and producing H_2S (Figure 4.6). The precise physiological role of MBX is still unknown; however it clear that MBX plays a critical role in both S^0 reduction and energy conservation. It is conceivable that MBX is the primary S^0-reducing enzyme or that it (or a FNOR type enzyme) provides the source of electrons (in form of NADPH) for NRS, which catalyzes the reduction of CoA-polysulfide species (and CoA disulfide) ultimately to CoA and H_2S. Oxidized CoA-sulfur species are thought to be the *in vivo* effectors of SurR (mediating transcriptional control of primary S^0 response genes and potentially secondary regulators under its control) and imaginably other yet to be discovered thiol-based regulators. SipA *(*secondary S^0 response) is thought to utilize H_2S generated during S^0 reduction by NRS (formerly NSR) in the biosynthesis of FeS clusters.

REFERENCES

1. **Adams, M. W., J. F. Holden, A. L. Menon, G. J. Schut, A. M. Grunden, C. Hou, A. M. Hutchins, F. E. Jenney, Jr., C. Kim, K. Ma, G. Pan, R. Roy, R. Sapra, S. V. Story, and M. F. Verhagen.** 2001. Key role for sulfur in peptide metabolism and in regulation of three hydrogenases in the hyperthermophilic archaeon *Pyrococcus furiosus*. J Bacteriol **183:**716-24.
2. **Andreotti, G., M. V. Cubellis, G. Nitti, G. Sannia, X. Mai, M. W. Adams, and G. Marino.** 1995. An extremely thermostable aromatic aminotransferase from the hyperthermophilic archaeon *Pyrococcus furiosus*. Biochim Biophys Acta **1247:**90-6.
3. **Bauer, M. W., E. J. Bylina, R. V. Swanson, and R. M. Kelly.** 1996. Comparison of a beta-glucosidase and a beta-mannosidase from the hyperthermophilic archaeon *Pyrococcus furiosus*. Purification, characterization, gene cloning, and sequence analysis. J Biol Chem **271:**23749-55.
4. **Bridger, S. L., S. M. Clarkson, K. Stirrett, M. B. DeBarry, G. L. Lipscomb, G. J. Schut, J. Westpheling, R. A. Scott, and M. W. Adams.** 2011. Deletion strains reveal metabolic roles for key elemental sulfur-responsive proteins in *Pyrococcus furiosus*. J Bacteriol **193:**6498-504.
5. **Bridger, S. L., W. A. Lancaster, F. L. Poole, 2nd, G. J. Schut, and M. W. Adams.** Genome Sequencing of a Genetically-Tractable *Pyrococcus furiosus* Strain Reveals a Highly Dynamic Genome. J Bacteriol**:**(*in submission*).
6. **Chou, C. J., K. R. Shockley, S. B. Conners, D. L. Lewis, D. A. Comfort, M. W. Adams, and R. M. Kelly.** 2007. Impact of substrate glycoside linkage and elemental sulfur on bioenergetics of and hydrogen production by the hyperthermophilic archaeon *Pyrococcus furiosus*. Appl Environ Microbiol **73:**6842-53.

7. **Fiala, G., and K. Stetter.** 1986. *Pyrococcus furiosus* sp. nov. represents a novel genus of marine heterotrophic archaebacteria growing optimally at 100°C. Arch Microbiol **145:**56-61.

8. **Guagliardi, A., D. de Pascale, R. Cannio, V. Nobile, S. Bartolucci, and M. Rossi.** 1995. The purification, cloning, and high level expression of a glutaredoxin-like protein from the hyperthermophilic archaeon *Pyrococcus furiosus*. J Biol Chem **270:**5748-55.

9. **Gueguen, Y., W. G. Voorhorst, J. van der Oost, and W. M. de Vos.** 1997. Molecular and biochemical characterization of an endo-beta-1,3- glucanase of the hyperthermophilic archaeon *Pyrococcus furiosus*. J Biol Chem **272:**31258-64.

10. **Harris, D. R., D. E. Ward, J. M. Feasel, K. M. Lancaster, R. D. Murphy, T. C. Mallet, and E. J. Crane, 3rd.** 2005. Discovery and characterization of a Coenzyme A disulfide reductase from *Pyrococcus horikoshii*. Implications for this disulfide metabolism of anaerobic hyperthermophiles. FEBS J **272:**1189-200.

11. **Hummel, C. S., K. M. Lancaster, and E. J. Crane, 3rd.** 2005. Determination of coenzyme A levels in *Pyrococcus furiosus* and other Archaea: implications for a general role for coenzyme A in thermophiles. FEMS Microbiol Lett **252:**229-34.

12. **Kengen, S. W., E. J. Luesink, A. J. Stams, and A. J. Zehnder.** 1993. Purification and characterization of an extremely thermostable beta-glucosidase from the hyperthermophilic archaeon *Pyrococcus furiosus*. Eur J Biochem **213:**305-12.

13. **Klump, H., J. Di Ruggiero, M. Kessel, J. B. Park, M. W. Adams, and F. T. Robb.** 1992. Glutamate dehydrogenase from the hyperthermophile *Pyrococcus furiosus*. Thermal denaturation and activation. J Biol Chem **267:**22681-5.

14. **Kobori, H., M. Ogino, I. Orita, S. Nakamura, T. Imanaka, and T. Fukui.** 2010. Characterization of NADH oxidase/NADPH polysulfide oxidoreductase and its unexpected participation in oxygen sensitivity in an anaerobic hyperthermophilic archaeon. J Bacteriol **192:**5192-202.

15. **Koning, S. M., M. G. Elferink, W. N. Konings, and A. J. Driessen.** 2001. Cellobiose uptake in the hyperthermophilic archaeon *Pyrococcus furiosus* is mediated by an inducible, high-affinity ABC transporter. J Bacteriol **183:**4979-84.

16. **Koning, S. M., W. N. Konings, and A. J. Driessen.** 2002. Biochemical evidence for the presence of two alpha-glucoside ABC-transport systems in the hyperthermophilic archaeon *Pyrococcus furiosus*. Archaea **1:**19-25.

17. **Lee, S. J., C. Moulakakis, S. M. Koning, W. Hausner, M. Thomm, and W. Boos.** 2005. TrmB, a sugar sensing regulator of ABC transporter genes in *Pyrococcus furiosus* exhibits dual promoter specificity and is controlled by different inducers. Mol Microbiol **57:**1797-807.

18. **Lee, S. J., M. Surma, S. Seitz, W. Hausner, M. Thomm, and W. Boos.** 2007. Characterization of the TrmB-like protein, PF0124, a TGM-recognizing global transcriptional regulator of the hyperthermophilic archaeon *Pyrococcus furiosus*. Mol Microbiol **65:**305-18.

19. **Lee, S. J., M. Surma, S. Seitz, W. Hausner, M. Thomm, and W. Boos.** 2007. Differential signal transduction via TrmB, a sugar sensing transcriptional repressor of *Pyrococcus furiosus*. Mol Microbiol **64:**1499-505.

20. **Lipscomb, G. L., A. M. Keese, D. M. Cowart, G. J. Schut, M. Thomm, M. W. Adams, and R. A. Scott.** 2009. SurR: a transcriptional activator and repressor controlling hydrogen and elemental sulphur metabolism in *Pyrococcus furiosus*. Mol Microbiol **71:**332-49.

21. **Lipscomb, G. L., K. Stirrett, G. J. Schut, F. Yang, F. E. Jenney, Jr., R. A. Scott, M. W. Adams, and J. Westpheling.** 2011. Natural competence in the hyperthermophilic archaeon *Pyrococcus furiosus* facilitates genetic manipulation: construction of markerless deletions of genes encoding the two cytoplasmic hydrogenases. Appl Environ Microbiol **77:**2232-8.

22. **Ma, K., and M. W. Adams.** 2001. Ferredoxin:NADP oxidoreductase from *Pyrococcus furiosus*. Methods Enzymol **334:**40-5.

23. **Ma, K., and M. W. Adams.** 1999. An unusual oxygen-sensitive, iron- and zinc-containing alcohol dehydrogenase from the hyperthermophilic archaeon *Pyrococcus furiosus*. J Bacteriol **181:**1163-70.

24. **Ma, K., R. N. Schicho, R. M. Kelly, and M. W. Adams.** 1993. Hydrogenase of the hyperthermophile *Pyrococcus furiosus* is an elemental sulfur reductase or sulfhydrogenase: evidence for a sulfur-reducing hydrogenase ancestor. Proc Natl Acad Sci U S A **90:**5341-4.

25. **Ma, K., R. Weiss, and M. W. Adams.** 2000. Characterization of hydrogenase II from the hyperthermophilic archaeon *Pyrococcus furiosus* and assessment of its role in sulfur reduction. J Bacteriol **182:**1864-71.

26. **Mai, X., and M. W. Adams.** 1994. Indolepyruvate ferredoxin oxidoreductase from the hyperthermophilic archaeon *Pyrococcus furiosus*. A new enzyme involved in peptide fermentation. J Biol Chem **269:**16726-32.

27. **Mai, X., and M. W. Adams.** 1996. Purification and characterization of two reversible and ADP-dependent acetyl coenzyme A synthetases from the hyperthermophilic archaeon *Pyrococcus furiosus*. J Bacteriol **178:**5897-903.

28. **Mukund, S., and M. W. Adams.** 1991. The novel tungsten-iron-sulfur protein of the hyperthermophilic archaebacterium, *Pyrococcus furiosus*, is an aldehyde ferredoxin oxidoreductase. Evidence for its participation in a unique glycolytic pathway. J Biol Chem **266:**14208-16.

29. **Oslowski, D. M., J. H. Jung, D. H. Seo, C. S. Park, and J. F. Holden.** 2011. Production of hydrogen from alpha-1,4- and beta-1,4-linked saccharides by marine hyperthermophilic Archaea. Appl Environ Microbiol **77:**3169-73.

30. **Poole, F. L., 2nd, B. A. Gerwe, R. C. Hopkins, G. J. Schut, M. V. Weinberg, F. E. Jenney, Jr., and M. W. Adams.** 2005. Defining genes in the genome of the hyperthermophilic archaeon *Pyrococcus furiosus*: implications for all microbial genomes. J Bacteriol **187:**7325-32.

31. **Riera, J., F. T. Robb, R. Weiss, and M. Fontecave.** 1997. Ribonucleotide reductase in the archaeon *Pyrococcus furiosus*: a critical enzyme in the evolution of DNA genomes? Proc Natl Acad Sci U S A **94:**475-8.

32. **Robb, F. T., D. L. Maeder, J. R. Brown, J. DiRuggiero, M. D. Stump, R. K. Yeh, R. B. Weiss, and D. M. Dunn.** 2001. Genomic sequence of hyperthermophile, *Pyrococcus furiosus*: implications for physiology and enzymology. Methods Enzymol **330:**134-57.

33. **Rohwerder, T., and W. Sand.** 2003. The sulfane sulfur of persulfides is the actual substrate of the sulfur-oxidizing enzymes from *Acidithiobacillus* and *Acidiphilium spp*. Microbiology **149:**1699-710.

34. **Sapra, R., M. F. Verhagen, and M. W. Adams.** 2000. Purification and characterization of a membrane-bound hydrogenase from the hyperthermophilic archaeon *Pyrococcus furiosus*. J Bacteriol **182:**3423-8.

35. **Schut, G. J., S. D. Brehm, S. Datta, and M. W. Adams.** 2003. Whole-genome DNA microarray analysis of a hyperthermophile and an archaeon: *Pyrococcus furiosus* grown on carbohydrates or peptides. J Bacteriol **185:**3935-47.

36. **Schut, G. J., S. L. Bridger, and M. W. Adams.** 2007. Insights into the metabolism of elemental sulfur by the hyperthermophilic archaeon *Pyrococcus furiosus*: characterization of a coenzyme A- dependent NAD(P)H sulfur oxidoreductase. J Bacteriol **189:**4431-41.

37. **Schut, G. J., J. Zhou, and M. W. Adams.** 2001. DNA microarray analysis of the hyperthermophilic archaeon *Pyrococcus furiosus*: evidence for a new type of sulfur-reducing enzyme complex. J Bacteriol **183:**7027-36.

38. **Strand, K. R., C. Sun, T. Li, F. E. Jenney, Jr., G. J. Schut, and M. W. Adams.** 2010. Oxidative stress protection and the repair response to hydrogen peroxide in the hyperthermophilic archaeon *Pyrococcus furiosus* and in related species. Arch Microbiol **192:**447-59.

39. **Tanaka, T., T. Fukui, H. Atomi, and T. Imanaka.** 2003. Characterization of an exo-beta-D-glucosaminidase involved in a novel chitinolytic pathway from the hyperthermophilic archaeon *Thermococcus kodakaraensis* KOD1. J Bacteriol **185:**5175-81.

40. **van der Oost, J., W. G. Voorhorst, S. W. Kengen, A. C. Geerling, V. Wittenhorst, Y. Gueguen, and W. M. de Vos.** 2001. Genetic and biochemical characterization of a short-chain alcohol dehydrogenase from the hyperthermophilic archaeon *Pyrococcus furiosus*. Eur J Biochem **268:**3062-8.

41. **Voorhorst, W. G., Y. Gueguen, A. C. Geerling, G. Schut, I. Dahlke, M. Thomm, J. van der Oost, and W. M. de Vos.** 1999. Transcriptional regulation in the hyperthermophilic archaeon *Pyrococcus furiosus*: coordinated expression of divergently oriented genes in response to beta-linked glucose polymers. J Bacteriol **181:**3777-83.

42. **Weinberg, M. V., G. J. Schut, S. Brehm, S. Datta, and M. W. Adams.** 2005. Cold shock of a hyperthermophilic archaeon: *Pyrococcus furiosus* exhibits multiple responses to a suboptimal growth temperature with a key role for membrane-bound glycoproteins. J Bacteriol **187:**336-48.

Table 4.1. ORFs whose expression is up-regulated ≥ 3-fold as part of the primary response (within 10 minutes) to S^0 in the NSR1 deletion strain.

ORF Number	Description[a]	Average Intensity Ratio ($log_2 \pm SD$)[b]	Change in Expression (Fold)[c]
PF0094[d]	[protein disulfide oxidoreductase, PDO (8)]	1.6 ± 0	3.1
PF0101	conserved hypothetical protein	2.1 ± 0.2	4.2
PF0440	[ribonucleotide reductase, RNR (31)]	2.3 ± 1	5.1
PF0934	hypothetical protein	1.8 ± 0.1	3.5
Branched amino acid biosynthesis			
PF0935	acetolactate synthase	2.4 ± 0.1	5.4
PF0936	ketol-acid reductoisomerase	2.5 ± 0.2	5.7
PF0937	2-isopropylmalate synthase	2.4 ± 0.1	5.3
PF0938	3-isopropylmalate dehydratase large	2 ± 0.2	4.1
PF0939	3-isopropylmalate dehydratase, small	1.7 ± 0.1	3.3
PF0940	3-isopropylmalate dehydrogenase	2.2 ± 0.1	4.6
PF0941	alpha-isopropylmalate synthase	2.1 ± 0.1	4.4
PF0942	dihydroxy-acid dehydratase	1.9 ± 0.2	3.8
PF1033	peroxiredoxin	2.5 ± 0.1	5.8
Serine/threonine biosynthesis			
PF1053	aspartate kinase	1.9 ± 0.7	3.8
PF1054	homoserine kinase	2.3 ± 0	5.0
PF1055	threonine synthase	2.2 ± 0.1	4.6
PF1056	aspartate-semialdehyde dehydrogenase	2.2 ± 0	4.6
Methionine biosynthesis			
PF1266	cystathione gamma lyase	2.9 ± 0.1	7.6
PF1267	conserved hypothetical protein	2.6 ± 0.4	6.1
PF1268	5-methyltetrahydropteroyltriglutamate-homocysteine S-methyltransferase	2.9 ± 0.2	7.7
PF1269	methionine synthase	2.6 ± 0	6.0
PF1951	asparagine synthetase A	1.7 ± 0.1	3.3
PF1971	anaerobic ribonucleoside triphosphate reductase	1.7 ± 0.1	3.2

PF1975	phosophoenolpyruvate carboxylase	1.6 ± 0	3.1

[a] ORF descriptions are NCBI gene names (no brackets) and literature cited ([ ]).
[b] Intensity ratio is expressed as a $\log_2$ value so that the standard deviation (SD) can be given.
[c] Average (n-fold) change in signal intensity.
[d] *P. furiosus* (wild type) primary S^0 response genes (36).

Table 4.2. ORFs whose expression is down-regulated ≥ 3-fold as part of the primary response (within 10 minutes) to S^0 in the NSR1 deletion strain.

ORF Number	Description[a]	Average Intensity Ratio (log_2 ± SD)[b]	Change in Expression (-Fold)[c]
PF0346	[aldehyde:ferredoxin oxidoreductase, AOR (28)]	-3.3 ± 0.1	9.9
PF0647	heme biosynthesis protein	-2 ± 0.2	3.9
PF0736[d]	hypothetical protein	-2.7 ± 0.4	6.6
PF0736.1n[d]	hypothetical protein	-3.1 ± 0.1	8.8
PF1328	[ferredoxin:NADPH oxidoreductase I beta (22)]	-2.2 ± 0.2	4.5
[Soluble Hydrogenase II, SHII (25)][d]			
PF1329	hydrogenase II beta	-2.1 ± 0.3	4.2
PF1330	hydrogenase II gamma	-2 ± 0.5	3.9
PF1331	hydrogenase II delta	-1.7 ± 0.1	3.2
PF1332	hydrogenase II alpha	-1.8 ± 0.3	3.6
PF1390	hypothetical protein	-1.7 ± 0.1	3.2
[Membrane-bound hydrogenase, MBH (34)][d]			
PF1423	MbhA	-3 ± 0.3	8.2
PF1424	MbhB	-2.5 ± 0.2	5.8
PF1425	MbhC	-2.8 ± 0.2	6.7
PF1427	MbhE	-2.2 ± 0.2	4.5
PF1428	MbhF	-2.5 ± 0.2	5.7
PF1430	MbhH	-2.7 ± 0.3	6.6
PF1431	MbhI	-2.2 ± 0.3	4.7
PF1433	MbhK	-1.9 ± 0.1	3.7
PF1434	MbhL	-2.5 ± 0.2	5.7
PF1435	MbhM	-2.5 ± 0.1	5.9
PF1436	MbhN	-2.2 ± 0.1	4.5
PF1481	conserved hypothetical protein	-1.6 ± 0.2	3.0
PF1488	conserved hypothetical protein	-1.7 ± 0.1	3.2
PF1795	sarcosine oxidase alpha	-1.9 ± 0.1	3.8

[a-d] See Table 4.1 for details

Table 4.3. ORFs whose expression is ≥ 3-fold higher in maltose grown NSR1 cells than maltose grown COM1 cells.

ORF Number	Description[a]	Average Intensity Ratio ($log_2 \pm SD$)[b]	Difference in Expression (Fold)[c]
[β-glucan utilization]			
PF0073	[beta-glucosidase, CelB (12)]	3.8 ± 0.1	13.9
PF0074	[alcohol dehydrogenase, short chain, AdhA (40)]	4.9 ± 0.3	30.7
PF0075	[alcohol dehydrogenase, AdhB (23)]	4.4 ± 0.2	20.8
PF0076	[beta-1,3-laminarinase, LamA (9)]	2.9 ± 0.2	7.4
PF1208	[beta-mannosidase (3)]	3 ± 0.1	7.9
[β-linked glucosamine transporter (chitobiose) (39)]			
PF0360	oligopeptide ABC transporter	3.4 ± 0.1	10.2
PF0361	oligopeptide ABC transporter	2.6 ± 0.1	6.3
[β-glucan transporter (15)]			
PF1209	[cellobiose binding protein (CbtA)]	4.1 ± 0.7	17.2
PF1210	[cellobiose transporter, permease subunit (CbtB]	3.9 ± 0	15.1
PF1211	[cellobiose transporter, permease subunit (CbtC)]	3.3 ± 0.1	9.9
PF1212	[cellobiose transporter, ATP binding subunit (CbtD)]	3.7 ± 0.1	12.6
PF1213	[cellobiose transporter, ATP binding subunit (CbtF)]	2.8 ± 0.1	6.9
Unknown			
PF0546	conserved hypothetical protein	1.7 ± 0.3	3.3
PF0647	heme biosynthesis protein	1.6 ± 0.2	3.0
PF0934	hypothetical protein	2.1 ± 0.1	4.3
PF1454	conserved hypothetical protein	1.7 ± 0.1	3.2
PF1455	conserved hypothetical protein	1.7 ± 0.1	3.3

[a-c] See Table 4.1 for details

Table 4.4. ORFs whose expression is ≥ 3-fold lower in maltose grown NSR1 cells than maltose grown COM1 cells.

ORF Number	Description[a]	Average Intensity Ratio ($log_2 \pm SD$)[b]	Difference in Expression (-Fold)[c]
Peptide Metabolism			
PF0121	[aromatic aminotransferase I, AroAT I (2)]	-2.6 ± 0.1	6.0
PF0532	[acetyl-CoA synthetase II alpha (27)]	-1.6 ± 0.1	3.0
PF0533	[indolepyruvate oxidoreductase alpha (26)]	-1.8 ± 0.1	3.5
PF0534	[indolepyruvate ferredoxin oxidoreductase beta (26)]	-1.6 ± 0.1	3.1
PF1341	glycine cleavage system aminomethyltransferase T	-1.7 ± 0.2	3.3
PF1602	[glutamate dehydrogenase, GDH (13)]	-2.2 ± 0.3	4.5
PF1999	glycine dehydrogenase subunit 1	-2.1 ± 0	4.2
Oligopeptide Transporter			
PF0191	oligopeptide transport system permease	-1.8 ± 0.1	3.4
PF0192	oligopeptide transport permease appc	-2.1 ± 0.1	4.3
PF0193	ABC transport ATP binding protein	-2.2 ± 0.1	4.6
PF0194	dipeptide ABC transporter ATP-binding protein	-1.7 ± 0.1	3.2
PF0477	alpha amylase	-2 ± 0.1	4.1
[Soluble Hydrogenase I, SHI (24)]			
PF0891	hydrogenase I beta	-2.4 ± 0.2	5.2
PF0892	hydrogenase I gamma	-2.6 ± 0	6.1
PF0893	hydrogenase I delta	-2.5 ± 0.2	5.6
PF0894	hydrogenase I alpha	-2.9 ± 0.2	7.3
[α-Glucan Sensing Amylase (35)]			
PF0477	alpha amylase	-2 ± 0.1	4.1
[(α-Glucan) Maltodextrin transporter (16)]			
PF1933	sugar transport ATP-hydrolyzing	-2.4 ± 0.1	5.2
PF1934	conserved hypothetical protein	-2.2 ± 0.1	4.5
PF1935	amylopullulanase	-1.6 ± 0.7	3.1
PF1936	malg-like sugar transport inner membrane protein	-2.5 ± 0.2	5.8

PF1937	malf-like sugar transport inner membrane protein	-2.3 ± 0.1	5.0
PF1938	[maltodextrin binding protein]	-2.4 ± 0.1	5.4
Nucleotide Metabolism			
PF0440	[ribonucleotide reductase, RNR (31)]	-2.5 ± 0.2	5.6
Oxidative Stress Response			
PF0722	alkyl hydroperoxide reductase	-1.7 ± 0.1	3.3
PF1033	peroxiredoxin	-2.1 ± 0.1	4.4
PF2025	[sulfur- induced protein A, SipA (37)]	-2 ± 0.1	4.1
Unknown			
PF0101	conserved hypothetical protein	-1.7 ± 0	3.3
PF0531	cobalamin biosynthesis protein	-1.9 ± 0.1	3.7

[a-c] See Table 4.1 for details

Figure 4.1. Scatterplot of normalized microarray signal intensities of control samples. *P. furiosus* RNA samples derived from two cultures grown under identical conditions (NSR1, t=0) were differentially labeled (Alexa 647 and 594) and hybridized to the same slide to determine the standard deviation (log_2 signal intensity ratios) for the average of each ORF represented under the RNA-DNA hybridization conditions used in this study. Signal intensities for all ORFs vary less than 2-fold as indicated by the light blue diagonal dotted lines.

FIGURE 4.1

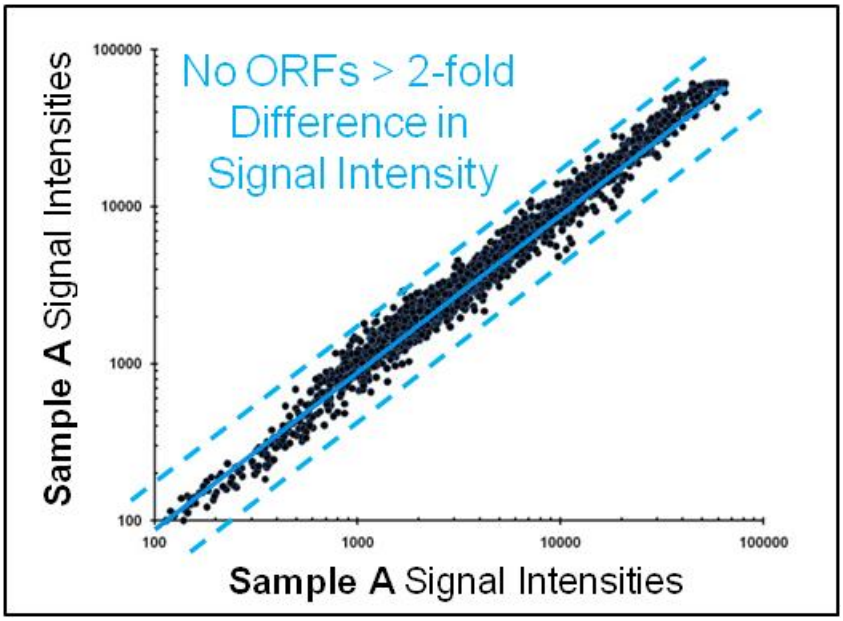
No ORFs > 2-fold Difference in Signal Intensity
Sample A Signal Intensities
100000
10000
1000
100
100
1000
10000
100000
Sample A Signal Intensities

Figure 4.2. Scatterplot of the normalized microarray signal intensities for primary S^0 response in the *P. furiosus* NSR1 mutant. A 15-liter culture of NSR1 was grown with maltose (5 g/L) and yeast extract (0.5 g/L), and S^0 (2 g/L) was added in mid-log phase. RNA samples were prepared from cells harvested just before (t=0) and 10 minutes after (t=10) S^0 addition and labeled with Alexa dyes 647 and 594, respectively. Red and green lines indicate the 3-fold up- and down-regulated cut-offs, respectively.

FIGURE 4.2

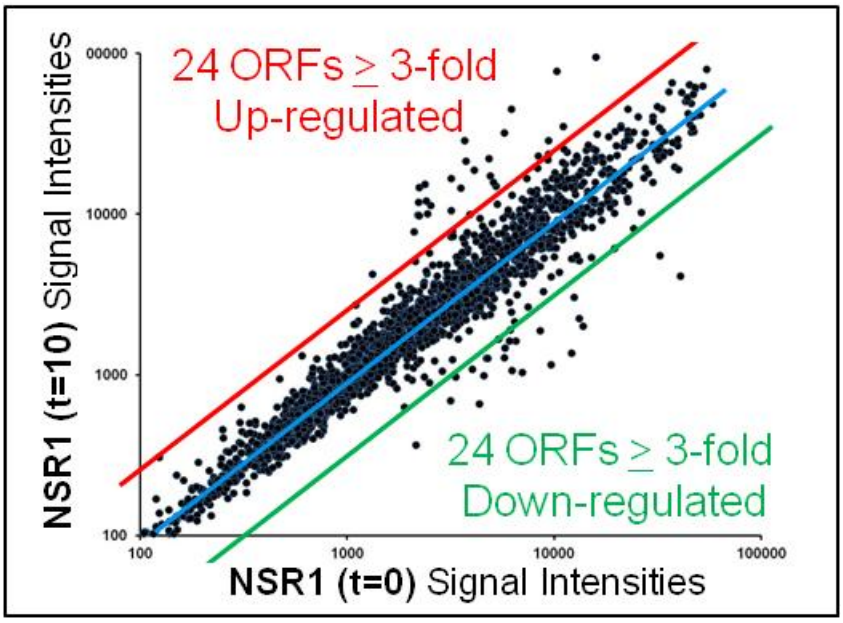
24 ORFs ≥ 3-fold
Up-regulated
24 ORFs ≥ 3-fold
Down-regulated
NSR1 (t=10) Signal Intensities
NSR1 (t=0) Signal Intensities
00000
10000
1000
100
100
1000
10000
100000

Figure 4.3. Scatterplot of normalized microarray signal intensities for the comparison of *P. furiosus* NSR1 mutant and COM1 parental strain. A 15-liter culture of each strain was grown with maltose (5 g/L) and yeast extract (0.5 g/L). RNA samples were prepared from cells harvested at mid-log phase and labeled with Alexa dyes 647 and 594, respectively. 17 ORFs were expressed significantly higher (≥ 3-fold, red) and 28 significantly lower (≥ 3-fold, green) in NSR1 than COM1.

FIGURE 4.3

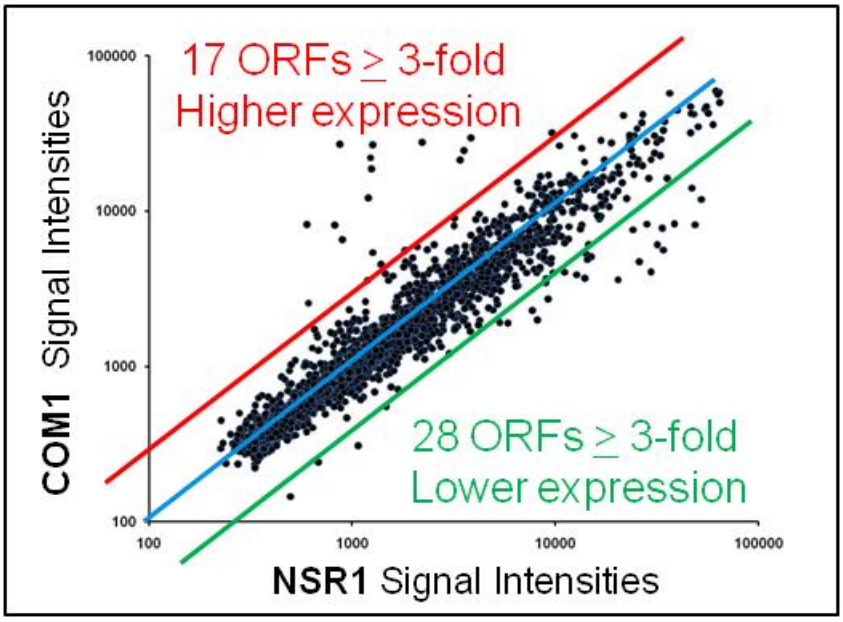
17 ORFs ≥ 3-fold
Higher expression
28 ORFs ≥ 3-fold
Lower expression
COM1 Signal Intensities
NSR1 Signal Intensities
100000
10000
1000
100
100
1000
10000
100000

Figure 4.4. Divergently oriented genes associated with β-linked glucan utilization in *P. furiosus*. Genome organization of ten genes whose expression is significantly higher in maltose-grown NSR1 cells compared to COM1. (A) *celB* (β-glucosidase) is divergently oriented from the *lamA* operon encoding *adhA* (alcohol dehydrogenase A, short chain), *adhB* (alcohol dehydrogenase B, iron-dependent), and *lamA* (β-1,3-endoglucanase). The intergenic region (red) between *celB* and *adhA* has been mapped and transcription initiation starts sites have been analyzed (41). (B) *bmnA* (β-mannosidase) is divergently oriented from the cellobiose ABC transport system (*cbtA*-*F*). The intergenic region (dotted line) between *bmnA* and *cbtA* has not been characterized (15). Genes whose expression has been biochemically shown to be β-glucan dependent are shaded in grey (15, 41).

FIGURE 4.4

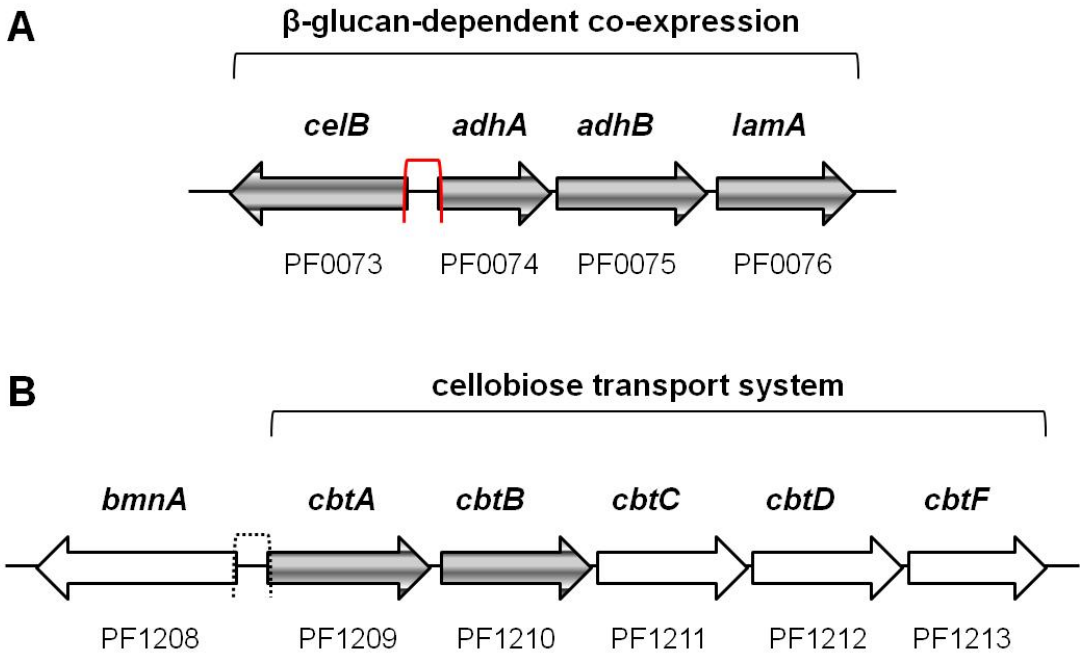
A
β-glucan-dependent co-expression
celB
adhA
adhB
lamA
PF0073
PF0074
PF0075
PF0076
B
cellobiose transport system
bmnA
cbtA
cbtB
cbtC
cbtD
cbtF
PF1208
PF1209
PF1210
PF1211
PF1212
PF1213

Figure 4.5. Model of α- and β-linked sugar utilization in *P. furiosus*. The redox balance and ATP produced is per glucose molecule. The proteins and pathways are as follows: 1, cellobiose ABC transporter (PF1209-13) 2, Mal-I ABC transporter (PF1739-41, PF1744); 3, Mal-II ABC transporter (PF1933, PF1936-38); 4, β-glucosidase (PF0073); 5, α-glucosidase (PF0132); 6, cyclomaltodextrinase (PF1939); 7, ADP-dependent hexokinase (PF0312); 8, α-glucan phosphorylase (PF1535); 9, modified Embden-Meyerhof pathway; 10, pyruvate oxidoreductase (PF0965-67); 11, acetyl-CoA synthetase (PF1540); Fd, electron carrier ferredoxin (PF1909). Modified from (29).

FIGURE 4.5

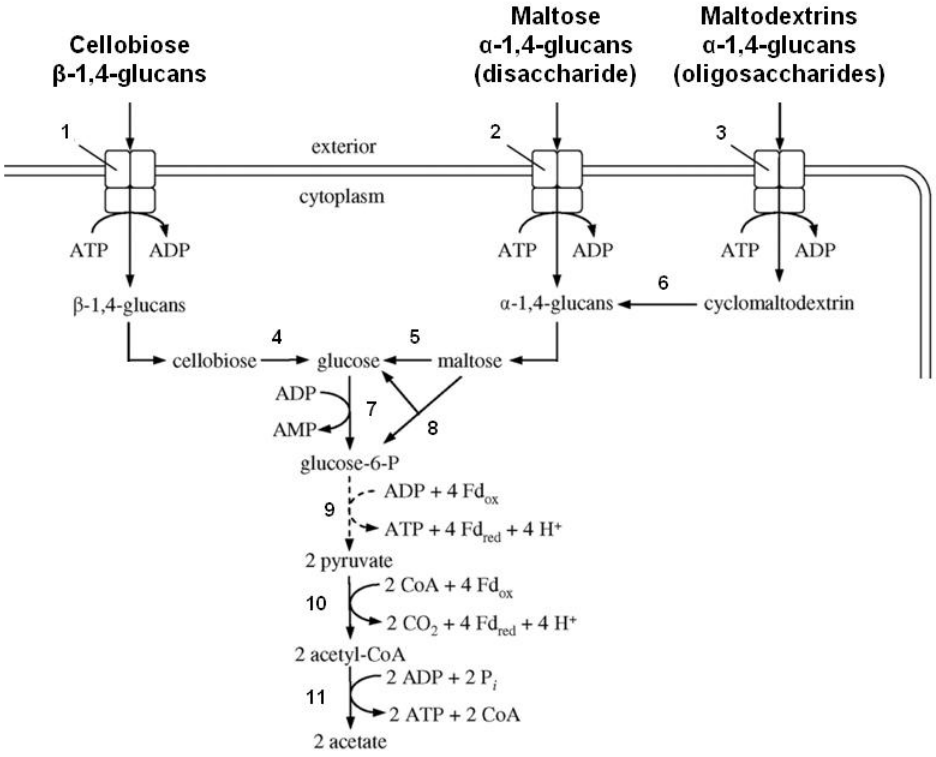
Cellobiose
β-1,4-glucans
Maltose
α-1,4-glucans
(disaccharide)
Maltodextrins
α-1,4-glucans
(oligosaccharides)
1
2
3
exterior
cytoplasm
ATP
ADP
ATP
ADP
ATP
ADP
β-1,4-glucans
α-1,4-glucans
6
cyclomaltodextrin
4
5
cellobiose
glucose
maltose
ADP
AMP
7
8
glucose-6-P
9
ADP + 4 Fdox
ATP + 4 Fdred + 4 H+
2 pyruvate
10
2 CoA + 4 Fdox
2 CO2 + 4 Fdred + 4 H+
2 acetyl-CoA
11
2 ADP + 2 Pi
2 ATP + 2 CoA
2 acetate

Figure 4.6. Proposed physiological role of NRS (formerly NSR) in *P. furiosus*: NAD(P)H-dependent redox sensor. MBX, membrane-bound oxidoreductase complex; NRS, NADPH redox sensor (this work); NSR, NADPH S^0-oxidoreductase (36); CoADR, CoA disulfide reductase (10); CoASH, co-enzyme A (red); CoA-S-S_x-CoA, CoA polysulfide (ox); CoA-S-S-CoA, CoA disulfide (ox); SurR, S^0 response regulator; SipA, sulfur-induced protein A, FNOR, ferredoxin NADP oxidoreductase; S^0, elemental sulfur; H_2S, hydrogen sulfide, Fd, ferredoxin. Solid black arrows indicate characterized functions, whereas grey or dotted arrows indicate proposed functions or interactions.

FIGURE 4.6

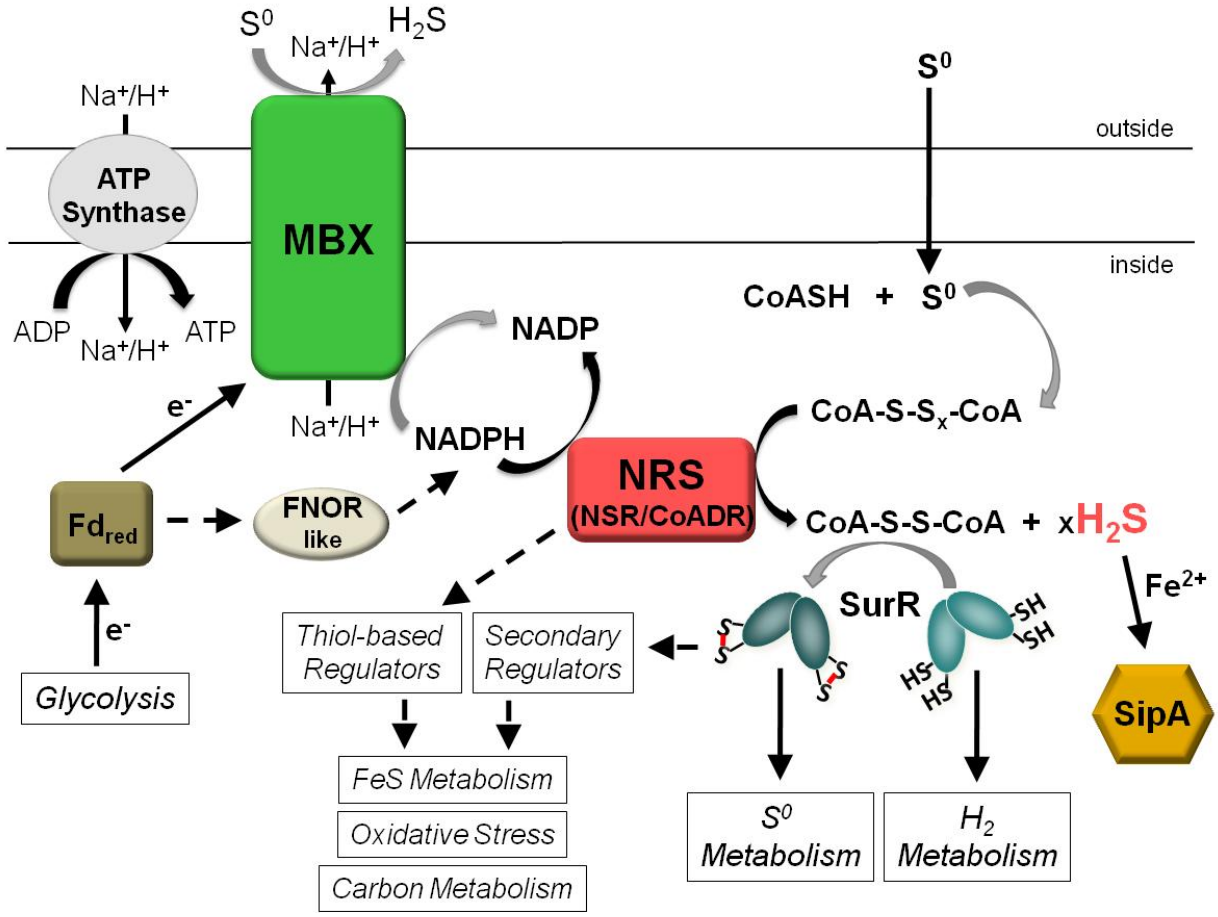
S0
Na+/H+
H2S
Na+/H+
ATP Synthase
MBX
S0
outside
inside
ADP
Na+/H+
ATP
CoASH + S0
NADP
e-
Na+/H+
NADPH
CoA-S-Sx-CoA
NRS
(NSR/CoADR)
Fdred
FNOR like
CoA-S-S-CoA + xH2S
Fe2+
e-
SurR
Thiol-based Regulators
Secondary Regulators
Glycolysis
SipA
FeS Metabolism
Oxidative Stress
Carbon Metabolism
S0 Metabolism
H2 Metabolism

CHAPTER 5

DISCUSSION

The mechanism of S^0 reduction by members of the hyperthermophilic heterotrophic *Thermococcales* has been unraveled over the last few years through key comparative biochemical, transcriptional, and genetic studies with *Pyrococcus furiosus* in both the presence and absence of S^0. The availability of the highly efficient genetic system in *P. furiosus* has vastly improved our ability to study this model hyperthermophilic archaeon. The work presented here described the genome sequencing of the genetically-tractable strain, COM1, and the biochemical characterization of deletion strains of key sulfur responsive proteins, namely MBX1, NSR1 and SIP1. These studies have not only provided a complete molecular template for future genetic manipulations using the COM1 strain, but also provided insights into potential factors involved in its remarkable DNA uptake and recombination abilities, and improved our understanding of the physiological roles of both MBX and NSR in the metabolism of *P. furiosus*. This chapter will summarize the major findings in this work and suggest future directions.

COMPETENCE IN COM1

As described in Chapter 2, one significant difference between the COM1 *P. furiosus* strain and both the lab strain population from which it was selected (Parent) and DSMZ type strains are their ability to be genetically manipulated. It is presumed that one or more of the genomic differences revealed by the comparison of the COM1 genome sequence with the NCBI reference sequence may be responsible for its high efficiency of transformation and recombination (3). However, given the large number of genes disrupted in COM1 (122 genes, Figure S2.1) and the fact that more than half of them encode for conserved hypothetical

proteins (56 genes), determining which genes affect competence will not be an easy task. One strategy for narrowing down the list of potential targets would be to utilize the whole genome DNA microarray to obtain a global view of transcriptional differences between the Parent and or DSMZ type strain and the COM1 strain. However, particular care would have to be taken in analyzing the resulting data considering the known chromosomal deletions, rearrangements, and potential regulatory regions that have been affected.

The CRISPR-Cas system is the most well characterized defense system against invasion by foreign nucleic acids in both archaea and bacteria (6, 15). As mentioned in Chapter 2, it is one of the most obvious targets potentially involved in conferring competence in COM1. Five of the CRISPR-associated (Cas) proteins (8) including: Cas6 and its homolog Cas6-2 (PF1131 and PF0393, respectively), Cmr1-1 and its homolog Cmr1-2 (PF1130 and PF0352, respectively) and Cas5t (PF1121) have been disrupted in COM1. It is plausible that Cas6, Cmr1-1, and Cas5t are still functional in COM1, as the disruptions affecting these proteins are characterized as minor since their translated products are greater than 90% identical to the NCBI reference sequence, whereas the disruptions to both Cas6-2 and Cmr1-2 result in major differences in the translated protein product and are therefore thought to be non-functional in the COM1 strain. The gene encoding Cas6-2 is disrupted by an IS element (781 bp insertion within the ORF) and results in a premature stop (~51 bp into the ORF), whereas Cmr1-2 is disrupted at the translation level due to a single base deletion resulting in a frameshift and ~50% longer protein product (3). In *P. furiosus*, Cas6 has been shown to recognize and cleave foreign RNA that match spacer sequences present in the host's CRISPR loci (4, 8); however, its homolog Cas6-2 has yet to be characterized and it is unclear whether this protein might be involved in a foreign DNA recognition system.

Other disrupted genes in COM1 that could also play role in DNA uptake and/or recombination efficiency include twenty or more predicted integral membrane proteins and/or transporters, which could affect membrane integrity thereby facilitating DNA uptake, and

numerous proteins involved in DNA replication, transcription, and repair. Table 5.1 contains a sub-set of all the disrupted genes in COM1 that fall into one of these categories and are therefore potentially involved in conferring competence. Future studies to determine if any of these potentially disrupted proteins play a role in conferring competence will involve further genetic manipulations with the COM1 strain by restoring the targeted genes to the non-competent parent and demonstrating loss of transformation ability.

PHYSIOLOGICAL ROLE OF MBX

The first evidence demonstrating that MBX plays a critical role in energy conserving S^0 reduction came from the work presented herein (Chapter 3), where growth of the MBX deletion strain, MBX1, was significantly hindered in the presence of S^0 and little if any sulfide, but much more acetate (per unit protein) was produced in MBX1 compared to the parental strain (2). As shown in Figure 3.5, MBX is predicted to conserve energy through an ion gradient by oxidizing ferredoxin and reducing NADP, which serves as the electron donor for NSR to reduce S^0 to H_2S. However, the actual physiological role of MBX is still unclear because we have not been unable to demonstrate ferredoxin-dependent reduction of NADP in S^0-grown membranes *in vitro*. In addition, attempts to measure direct ferredoxin-dependent S^0 reduction by MBX were also unsuccessful. Given the previous success of using non S^0-grown membranes (inverted vesicles) to demonstrate activity of the highly homologous MBH (17), it calls into question why no activity can be measured for MBX. Does the complication arise from contamination of other cellular proteins, loss of critical subunits during cell fractionation, membrane protein stability, loss of cofactor, or something else? Utilizing the *P. furiosus* genetic system, a recombinant strain has recently been constructed that expresses an affinity-tagged MBH (Chandrayan, S., and McTernan, T., unpublished data). The resulting protein complex has been successfully solubilized from *P. furiosus* membranes and purified in an active form. Therefore, using the methods developed for MBH, a recombinant strain should be constructed to express an affinity-

tagged MBX. The only difference strain would be that cells will have to be grown in the presence of S^0. The availability of an affinity-tagged form of MBX should facilitate ease of purification and hopefully lead to a measurable catalytic activity without the complications of background activities in a cell-free extract.

NSR ACTIVITIES

NSR was originally described as a highly active CoA-dependent NADPH elemental sulfur oxidoreductase (18). Natively purified from peptides sulfur grown *P. furiosus* extracts to heterogeneity over four sequential anaerobic column chromatography steps, the protein encoded by PF1186 displayed the highest activity every reported for any sulfur reductase type enzyme system (approximately 100 units/mg). The standard NSR assay mixture contained 50 mM phosphate buffer pH (7.0), 10 mM NAD(P)H, 6.4 g/L (w/v) colloidal sulfur, and 200 μM coenzyme A (CoASH), where one unit of NSR catalyzed the production of 1 μmole of H_2S per minute. NSR was shown to specifically require CoASH as a cofactor, as it could not be replaced by dephospho- or desulfo-CoA, or by glutathione or coenzyme M (18). Also, based on its similarity to a closely characterized homolog, PH0572 from *P. horikoshii* that was predicted to function as NAD(P)H-dependent CoA disulfide reductase (CoADR), NSR was also assayed for CoADR activity. The results indicated that while NSR could catalyze CoADR activity (6.0 μmole CoA-S-S-CoA reduced/min/mg), that the specific activities were 20-fold lower than the enzyme exhibited for sulfur reduction, and therefore the CoADR activity was thought to represent only the half reaction of its true physiological function, CoA-dependent sulfur reduction (18). In addition, NSR was shown to utilize CoA disulfide (CoA-S-S-CoA) as a cofactor in the sulfur reductase assay; however the activities were about 50% lower than with CoASH. In total, NSR was shown to catalyze the CoA-dependent reduction of three sulfur substrates: elemental sulfur (S^0, yellow powder), colloidal sulfur (fine brownish powder) and polysulfide prepared by dissolving S^0 powder in an aqueous sulfide solution (13). The best substrate appeared to be

colloidal sulfur generated from polysulfide, as it lead to an almost 2-fold increase in activity compared to elemental and colloidal sulfur powders (18). However, given the CoASH-dependence of the reaction and the easy by which sulfur species make and break bonds, it is possible that polysulfide derivatives of CoASH were being generated *in vitro*. Therefore, it is unknown what the physiological sulfur substrate is for NSR.

NSR, SURR, COENZYME A, AND REDOX

In addition to being characterized as a highly active sulfur reductase, the gene encoding NSR, PF1186, was shown to be one of only 19 ORFs (within 5 gene clusters) immediately up-regulated (> 3-fold) within ten minutes of adding S^0 to a growing culture of *P. furiosus* and thus categorized as a primary S^0 response gene (18). The S^0-response regulator, SurR, is thought to regulate expression of almost all of the primary S^0-response genes (including *nsr*) as their upstream regions contain the SurR DNA recognition site (11). The DNA-binding activity of SurR has been shown to be redox-dependent, whereby oxidation of cysteine residues in the CxxC motif induce conformation change that eliminates sequence-specific binding (20). The predicted *in vivo* oxidants present within *P. furiosus* cells after S^0 addition are thought to be S^0-derived species such as colloidal S^0 in the form of short chains of S^0, or polysulfide (20).

Transcriptional analyses (both targeted qRT-PCR and DNA microarray studies, Chapters 3 and 4, respectively) analyzing the primary S^0-response of the NSR deletion strain, NSR1, revealed a probable role for NSR in mediating transcriptional control of the SurR regulon, as the overall SurR-mediated S^0 response was significantly muted (Tables 4.1 and 4.2 and Figure 3.4; (2)) compared to previously reported expression changes in *P. furiosus* (18). Collectively, these results taken together with previously measured CoA-disulfide reductase activity (9, 18) and a demonstration that oxidized and reduced CoA species are present in the cytoplasm of S^0-grown *P. furiosus* (10), lead to the prediction that a product of NSR (presumably

an oxidized CoA-sulfur species) is at least in part responsible for the oxidation and transcriptional deactivation of SurR *in vivo* (Figure 4.6).

Further, the newly proposed name for NSR, NADPH-dependent redox sensor (NRS), is based on its predicted analogy to glutathione reductase (16) in maintaining the redox balance of the cytoplasm in *P. furiosus* by reducing oxidized CoA-sulfur species at the expensive of NADPH. Like bacterial species that lack glutathione, CoA is thought to be the alternative low-molecular-weight (LMW) thiol acting as an intracellular redox buffer in *P. furiosus* (10). Therefore in addition to producing H_2S, NRS is thought to play a detoxification role in helping remove oxidized CoA-sulfur species from the cytoplasm that may cause damage to nucleic acids and/or FeS cluster containing proteins. Potential support for this theory was also obtained from transcriptional analyses, where genes previously reported to be involved in peroxide-or cold-induced shocks in *P. furiosus* were up-regulated as part of the primary response to S^0 in NSR1 (Table 4.1). These "S^0 stress" response genes encode for enzymes responsible for both nucleotide synthesis and peroxide reduction, namely ribonucleotide reductase, anaerobic ribonucleotide triphosphate reductase, and peroxiredoxin. This observed stress response could be similar to "disulfide stress" described in other prokaryotes and eukaryotes, where the redox balance of the cell (ie. the ratio of reduced:oxidized intracellular thiol) is shifted due to a depletion or modification to the thiol pool (1).

Further studies utilizing the NSR1 deletion strain could be carried out to determine if the absence of NSR does in fact affect the ratio of oxidized to reduced CoA sulfur species in the cytoplasm. Highly sensitive HPLC separation methods for this analysis have already been developed for wild-type *P. furiosus*, which utilize a thiol-reactive fluorescent probe, monobromobimane (mBBr), to label cell extracts (10). In addition to determining the physiologically relevant CoA-sulfur species in the cytoplasm of *P. furiosus* (in the presence and absence of NSR), *in vitro* transcription assays could be carried out to determine if oxidized CoA-sulfur species are indeed relevant effector molecules for the deactivation of SurR. Freshly

precipitated colloidal S^0 (100-500 μM) has been shown to completely eliminate the specific redox-dependent DNA-binding activity of SurR (20). Therefore, using a known regulatory target, such as the *mbh* promoter, electronmobility shift assays (EMSA) should be carried out with CoA-sulfur species including: CoASH (control), CoA disulfide, and potentially longer CoA polysulfide species if they are stable in solution. Results of these studies should shed light on the potential relevance of a CoA (and its oxidized derivatives) contributing to the intracellular redox environment of *P. furiosus*. Also, the NSR1 strain should be assessed for other redox stress related phenotypes, such as exposure to reactive oxygen species.

ADDITIONAL DELTION STRAINS RELATED TO SULFUR METABOLISM

Based on the initial biochemical and transcriptional studies identifying NSR as the primary S^0 reducing enzyme in *P. furiosus* (18), it was quite surprising that characterization of the NSR deletion strain, NSR1, revealed a non-essential role for NSR in S^0 reduction (2). As shown in Figure 3.1, the NSR1 strain grew well in both the presence and absence of S^0 and produced similar amounts of H_2S as the control strain. The only minor growth defect appeared to be a slight lag (15-30 minutes) in growth following S^0 addition in sulfur switch cultures (Figure 3.3). These results posed a fundamental question as to what reduces S^0 in the absence of NSR? As alluded to above, and given the degree of homology between MBX and MBH, MBX is an obvious candidate; however since no activity has ever been shown this still remains unknown. It is postulated that the enzymes SuDH I (7, 13) and its homolog SuDH II (7) (also referred to in the literature as FNOR; (12, 13)) may compensate in the absence of NSR, as SuDH I has been previously shown to catalyze the NADPH-dependent reduction of S^0 *in vitro* and their expression is differentially regulated in the NSR1 strain compared to the parent. Therefore, the next step in determining what other enzymes are reducing S^0 in the absence of NSR is to delete the genes encoding these potential compensatory S^0 reducing enzymes in the NSR1 strain. Deletion

strains Δ*nsr* Δ*suDHI*, Δ*nsr* Δ*suDHII*, and Δ*nsr* Δ*suDHI* Δ*suDHII* should be constructed and screened for their abilities to grow with S^0 and produce H_2S should be compared.

PHYSIOLOGICAL RELVANCE OF β-GLUCAN EXPRESSION IN NSR1

Dramatic transcriptional differences between NSR1 and COM1 were observed in the absence of S^0 during growth on the α-linked sugar maltose (Tables 4.3 and 4.4). Genes encoding β-glucan utilization and transport were more than 6 to 30-fold higher expressed in NSR1 than in COM1, where as α-glucan utilization and transport genes were more than 3 to 5-fold less highly expressed in NSR1 than in COM1. These results were somewhat puzzling, as it has been shown in wild-type *P. furiosus* that ORFs involved in β-glucan utilization and transport are highly expressed under cellobiose-grown conditions and α-glucan under maltose-grown conditions, respectively (5). It is thought that these high levels of β-glucan gene expression in NSR1 are not directly carbohydrate related, but instead a mechanism to dispose of excess reductant (NADPH) in the cell through the coordinated expression of two alcohol dehydrogenase genes (AdhA and AdhB; (14, 19)). Both enzymes have been natively purified from *P. furiosus* and shown to act on a wide range of substrates, with a preference for the reducing aldehydes (pyruvaldehyde and phenylacetaldehyde) to alcohols, while simultaneously disposing of excess reducing equivalents and removing toxic aldehydes from the cytoplasm. Therefore, future studies should first address whether a 20-30-fold excess of alcohols are produced by the NSR1 strain compared with the COM1 strain, and if the specific activates of these Adh enzymes are also markedly higher. In addition, if in fact there is an excess of reducing equivalents in the form of NADPH in NSR1 cells, this too should be measured by comparing the ratios of NADPH to NADP in the parent and deletion strains.

Based on the remarkable coexpression pattern observed for genes encoding β-glucan utilization and transport proteins observed in NSR1, the promoter region between the divergently transcribed (and co-regulated) *celB* and *adhA* genes appear to be an ideal target for

the discovery of one or more key transcription factors that have major effects on the primary metabolism of *P. furiosus*. Using this promoter region as bait, the same DNA-affinity protein capture approach used for the SurR discovery (11) could be employed to identify DNA-binding proteins that are differentially captured from cell extracts grown on maltose (α-glucan) and cellobiose (β-glucan). The sequence of any potential regulators identified could also be analyzed for cysteine residues within putative DNA-binding domains to predict if the discovered regulators might potentially be novel thiol-based redox-dependent switches, like SurR (20).

Table 5.1. Sub-set of disrupted genes in *P. furiosus* COM1 strain (from Table S2.1) potentially involved in conferring competence.

Gene	Gene Annotation[b]	Identical Residues (AA)[i]	Alignment Length (AA)[i]	Identitiy (%)[i]	Operon Position[c]	Location[d]
PF0036	daunorubicin resistance membrane protein	262	263	99.6	2 of 2	mem
PF0054[m]	AsnC family transcriptional regulator	91	155	58.7	6 of 7	cyt
PF0058	dolichol monophosphate mannose synthase	351	352	99.7	1 of 3	mem
PF0067[m]	cobalt transport ABC transporter	157	243	64.6	1 of 2	mem
PF0085	DNA helicase	1274	1355	94	1 of 2	cyt
PF0352[m]	[CRISPR-associated protein, Cmr1-2 (21)]	189	451	41.9		cyt
PF0357	dipeptide-binding protein	630	631	99.8	1 of 7	mem
PF0360	oligopeptide ABC transporter	323	324	99.7	4 of 7	cyt
PF0393[k]	[CRISPR-associated protein, Cas6-2 (21)]	11	241	4.6		cyt
PF0407[k]	<carboxypeptidase-like, regulatory domain>	14	607	2.3	1 of 2	mem
PF0429[k]	proline permease	195	493	39.6		mem
PF0509	integral membrane glycosyltransferase	673	707	95.2	2 of 4	mem
PF0524[m]	<ribbon-helix-helix (Met_repress_like)>	57	72	79.2	1 of 4	cyt
PF0552	arsenical-resistance protein acr3	363	399	91		mem
PF0572	dna2-nam7 helicase family protein	654	655	99.8		cyt
PF0592	ATP-dependent RNA helicase	866	867	99.9	5 of 6	cyt
PF0621	<winged helix-turn-helix transcription repressor DNA-binding>	255	283	90.1	2 of 2	exc

PF0710[m]	<transcription repressor DNA-binding>	79	157	50.3	3 of 3	cyt
PF0777[m]	hypothetical protein	191	215	88.8		mem
PF0782	<polysaccharide biosynthesis protein>	107	109	98.2	1 of 2	mem
PF0823[k]	<multi antimicrobial extrusion protein (MatE)>	115	472	24.4	1 of 2	mem
PF0872	<circadian clock protein KaiC/DNA repair protein RadA>	115	125	92	3 of 3	cyt
PF0921	ABC transporter	285	305	93.4	1 of 5	cyt
PF0933	DNA repair helicase Rad3	626	647	96.8	3 of 3	cyt
PF1075[m]	hypothetical protein	3	219	1.4		mem
PF1120	ATP-dependent RNA helicase	723	724	99.9	3 of 4	cyt
PF1121	[CRISPR-associated protein, Cas5t (21)]	229	230	99.6	4 of 4	cyt
PF1130	[CRISPR-associated protein, Cmr1-1 (21)]	325	338	96.2	7 of 7	cyt
PF1131	[CRISPR-associated protein, Cas6 (21)]	263	264	99.6		cyt
PF1168	[5’ to 3’ exonuclease, NurA (23)]	450	451	99.8	6 of 7	exc
PF1206[m]	<nucleic acid-binding, PIN, PH0500>	15	156	9.6	1 of 3	cyt
PF1238	ABC transporter	622	632	98.4	2 of 2	cyt
PF1249[l]	ABC transporter	0	0	0	1 of 2	cyt
PF1252[l]	hypothetical protein	0	0	0	2 of 2	mem
PF1254[l]	sodium dependent transporter	270	578	46.7	1 of 2	mem
PF1259	hypothetical protein	106	107	99.1	3 of 3	mem
PF1494	hypothetical protein	190	193	98.4		mem
PF1573[n]	<peptidase U62, modulator of DNA gyrase>	455	455	100	1 of 2	cyt
PF1603[k]	Na antiporter	185	427	43.3	1 of 3	mem
PF1624	hypothetical protein	174	175	99.4		mem

PF1725	DNA primase	422	452	93.4	2 of 2	cyt
PF1748 [m]	system permease, ABC transporter	321	543	59.1	4 of 6	mem
PF1749 [m]	sulfate transport membrane protein	10	228	4.4	5 of 6	mem
PF1882	cell division protein CDC48	795	796	99.9		cyt
PF1902	DNA repair helicase	444	447	99.3		cyt

[b] Annotations are NCBI gene names (no brackets) and literature cited ([ ]), except for hypothetical genes, where the best IPR (< >) match is given if available.
[c] Operon predictions from (55) based on NCBI reference sequence.
[d] Predicted cellular location based on predicted TMDs, proteins with >= 2 TMDs classified as membrane (mem), proteins with <2 TMDs and a predicted signal peptide using SignalP with the gram-positive model >= 0.6 are classified as extracellular (exc), and proteins with <2 TMDs and no predicted signal peptide are classified as cytoplasmic (cyt).
[l] Based on Needleman-Wunsch global alignment with NCBI reference sequence.
[k] Genes affected by IS activity (Table 2.2).
[l] Additional large chromosomal deletions (Table 2.3).
[m] Major protein-level genome differences, < 90% identity (Table 2.4).

REFERENCES

1. **Antelmann, H., and J. D. Helmann.** 2011. Thiol-based redox switches and gene regulation. Antioxid Redox Signal **14:**1049-63.
2. **Bridger, S. L., S. M. Clarkson, K. Stirrett, M. B. DeBarry, G. L. Lipscomb, G. J. Schut, J. Westpheling, R. A. Scott, and M. W. Adams.** 2011. Deletion strains reveal metabolic roles for key elemental sulfur-responsive proteins in *Pyrococcus furiosus*. J Bacteriol **193:**6498-504.
3. **Bridger, S. L., W. A. Lancaster, F. L. Poole, 2nd, G. J. Schut, and M. W. Adams.** Genome Sequencing of a Genetically-Tractable *Pyrococcus furiosus* Strain Reveals a Highly Dynamic Genome. J Bacteriol**:**(*in submission*).
4. **Carte, J., N. T. Pfister, M. M. Compton, R. M. Terns, and M. P. Terns.** 2010. Binding and cleavage of CRISPR RNA by Cas6. RNA **16:**2181-8.
5. **Chou, C. J., K. R. Shockley, S. B. Conners, D. L. Lewis, D. A. Comfort, M. W. Adams, and R. M. Kelly.** 2007. Impact of substrate glycoside linkage and elemental sulfur on bioenergetics of and hydrogen production by the hyperthermophilic archaeon *Pyrococcus furiosus*. Appl Environ Microbiol **73:**6842-53.
6. **Garrett, R. A., G. Vestergaard, and S. A. Shah.** 2011. Archaeal CRISPR-based immune systems: exchangeable functional modules. Trends Microbiol **19:**549-56.
7. **Hagen, W. R., P. J. Silva, M. A. Amorim, P. L. Hagedoorn, H. Wassink, H. Haaker, and F. T. Robb.** 2000. Novel structure and redox chemistry of the prosthetic groups of the iron-sulfur flavoprotein sulfide dehydrogenase from *Pyrococcus furiosus*; evidence for a [2Fe-2S] cluster with Asp(Cys)3 ligands. J Biol Inorg Chem **5:**527-34.
8. **Hale, C. R., P. Zhao, S. Olson, M. O. Duff, B. R. Graveley, L. Wells, R. M. Terns, and M. P. Terns.** 2009. RNA-guided RNA cleavage by a CRISPR RNA-Cas protein complex. Cell **139:**945-56.

9. **Harris, D. R., D. E. Ward, J. M. Feasel, K. M. Lancaster, R. D. Murphy, T. C. Mallet, and E. J. Crane, 3rd.** 2005. Discovery and characterization of a Coenzyme A disulfide reductase from *Pyrococcus horikoshii*. Implications for this disulfide metabolism of anaerobic hyperthermophiles. Febs J **272:**1189-200.

10. **Hummel, C. S., K. M. Lancaster, and E. J. Crane, 3rd.** 2005. Determination of coenzyme A levels in *Pyrococcus furiosus* and other Archaea: implications for a general role for coenzyme A in thermophiles. FEMS Microbiol Lett **252:**229-34.

11. **Lipscomb, G. L., A. M. Keese, D. M. Cowart, G. J. Schut, M. Thomm, M. W. Adams, and R. A. Scott.** 2009. SurR: a transcriptional activator and repressor controlling hydrogen and elemental sulphur metabolism in *Pyrococcus furiosus*. Mol Microbiol **71:**332-49.

12. **Ma, K., and M. W. Adams.** 2001. Ferredoxin:NADP oxidoreductase from *Pyrococcus furiosus*. Methods Enzymol **334:**40-5.

13. **Ma, K., and M. W. Adams.** 1994. Sulfide dehydrogenase from the hyperthermophilic archaeon *Pyrococcus furiosus*: a new multifunctional enzyme involved in the reduction of elemental sulfur. J Bacteriol **176:**6509-17.

14. **Ma, K., and M. W. Adams.** 1999. An unusual oxygen-sensitive, iron- and zinc-containing alcohol dehydrogenase from the hyperthermophilic archaeon *Pyrococcus furiosus*. J Bacteriol **181:**1163-70.

15. **Makarova, K. S., D. H. Haft, R. Barrangou, S. J. Brouns, E. Charpentier, P. Horvath, S. Moineau, F. J. Mojica, Y. I. Wolf, A. F. Yakunin, J. van der Oost, and E. V. Koonin.** 2011. Evolution and classification of the CRISPR-Cas systems. Nat Rev Microbiol **9:**467-77.

16. **Masip, L., K. Veeravalli, and G. Georgiou.** 2006. The many faces of glutathione in bacteria. Antioxid Redox Signal **8:**753-62.

17. **Sapra, R., K. Bagramyan, and M. W. Adams.** 2003. A simple energy-conserving system: proton reduction coupled to proton translocation. Proc Natl Acad Sci USA **100:**7545-50.

18. **Schut, G. J., S. L. Bridger, and M. W. Adams.** 2007. Insights into the metabolism of elemental sulfur by the hyperthermophilic archaeon *Pyrococcus furiosus*: characterization of a coenzyme A- dependent NAD(P)H sulfur oxidoreductase. J Bacteriol **189:**4431-41.

19. **van der Oost, J., W. G. Voorhorst, S. W. Kengen, A. C. Geerling, V. Wittenhorst, Y. Gueguen, and W. M. de Vos.** 2001. Genetic and biochemical characterization of a short-chain alcohol dehydrogenase from the hyperthermophilic archaeon *Pyrococcus furiosus*. Eur J Biochem **268:**3062-8.

20. **Yang, H., G. L. Lipscomb, A. M. Keese, G. J. Schut, M. Thomm, M. W. Adams, B. C. Wang, and R. A. Scott.** 2010. SurR regulates hydrogen production in *Pyrococcus furiosus* by a sulfur-dependent redox switch. Mol Microbiol **77:**1111-22.

APPENDIX A

INSIGHTS INTO THE METABOLISM OF ELEMENTAL SULFUR BY THE HYPERTHERMOPHILIC ARCHAEON *PYROCOCCUS FURIOSUS*: CHARACTERIZATION OF A COENZYME A-DEPENDENT NAD(P)H SULFUR OXIDOREDUCTASE[3]

[3] Schut, G.J., S.L. Bridger and M.W. Adams. 2007. *J Bacteriol.* 189(12):4431-4441.
Reprinted here with permission from the American Society for Microbiology.

ABSTRACT

The hyperthermophilic archaeon, *Pyrococcus furiosus*, uses carbohydrates as a carbon source and produces acetate, CO_2 and H_2 as end products. When S^0 is added to a growing culture, within 10 min the rate of H_2 production rapidly decreases and H_2S is detected. After one hour cells contain high NADPH- and coenzyme A-dependent S^0 reduction activity (0.7 units/mg, 85°C) located in the cytoplasm. The enzyme responsible for this activity was purified to electrophoretic homogeneity (specific activity, 100 units/mg) and is termed NAD(P)H elemental sulfur oxidoreductase (NSR). NSR is a homodimeric flavoprotein (Mr 100 kDa) and is encoded by PF1186. This was previously assigned to an enzyme that reduces coenzyme A disulfide, which is a side-reaction of NSR. Whole genome DNA microarray and quantitative PCR analyses showed that the expression of NSR is up-regulated up to 7-fold within 10 min of S^0 addition. This primary response to S^0 also involves the up-regulation (> 16-fold) of a 13 gene cluster encoding a membrane-bound oxidoreductase (MBX). MBX is proposed replace the homologous 14 gene cluster that encodes the ferredoxin-oxidizing, H_2-evolving membrane-bound hydrogenase (MBH), which is down-regulated >12-fold within 10 min of S^0 addition. Although an activity for MBX could not be demonstrated, it is proposed to conserve energy by oxidizing ferredoxin and reducing NADP, which is used by NSR to reduce S^0. A secondary response to S^0 is observed 30 min after S^0 addition and includes the up-regulation of genes encoding proteins involved in amino acid biosynthesis and iron metabolism, as well as two so-called sulfur-induced proteins, termed SipA and SipB. This novel S^0-reducing system involving NSR and MBX is so far unique to the heterotrophic Thermococcales, and is in contrast to the cytochrome- and quinone-based S^0-reducing system in autotrophic archaea and bacteria.

INTRODUCTION

The hyperthermophilic archaea are a group of microorganisms that grow optimally at temperatures of 80°C and above (48). Most of these microorganisms utilize elemental sulfur (S^0) as a terminal electron acceptor and reduce it to H_2S (17, 19). Those that use molecular H_2 as the electron donor, such as *Thermoproteus tenax* and *Acidianus ambivalens*, are thought to have a respiratory system analogous to that found in mesophilic S^0-reducing bacteria such as *Wolinella succinogenes*, where S^0 reduction is accomplished by a membrane-bound respiratory system (17). On the other hand, the mechanism of S^0 reduction by the heterotrophic hyperthermophilic archaea, such as *Pyrococcus* and *Thermococcus* species, is completely unknown. These organisms grow by fermentation with peptides as the carbon source and most of them appear to be obligately dependent on S^0 for optimal growth (48). The exceptions are those that are able to grow by fermentation of carbohydrates, such as *Pyrococcus furiosu*s, which grows equally well with or without S^0 (9). Herein we have exploited this property to investigate the mechanism by which this prototypical heterotrophic hyperthermophile reduces S^0 to H_2S.

P. furiosus utilizes a range of both simple and complex carbohydrates and converts them to acetate, CO_2, H_2 and, if S^0 is present, to H_2S. Its glycolytic pathway has been extensively studied and served as one of the model systems for elucidating the modified Embden Meyerhof pathway in archaea (39, 40, 51). The key feature of this pathway is that the classical enzymes glyceraldehyde-3-phosphate dehydrogenase (GAPDH) and phosphoglycerate kinase (PGK) are replaced by a single ferredoxin-linked enzyme, glyceraldehyde-3-phosphate ferredoxin oxidoreductase (GAPOR, EC. 1.2.1.-). This converts glyceraldehyde-3-phosphate to glycerate-3-phosphate without the generation of ATP (51). Consequently, only ferredoxin serves as the electron acceptor in glycolysis and no NAD(P)H is formed. The reason for this became apparent when a membrane bound hydrogenase was discovered in *P. furiosus* which evolved H_2 from reduced ferredoxin in an energy-conserving

manner via a proton motive force (41). The other oxidation step in the conversion of glucose to acetate is also coupled to the reduction of ferredoxin, and this is catalyzed by pyruvate ferredoxin oxidoreductase (POR) (4). Hence, in the production of acetate from glucose, all of the reductant is generated as reduced ferredoxin. Its oxidation via the membrane-bound hydrogenase is thought to result in the conservation of energy equivalent to 1.2 ATP per glucose (41). Two cytoplasmic hydrogenases have also been characterized from *P. furiosus* (29) but these use NADPH, rather than ferredoxin, as the electron carrier and their functions in fermentative metabolism are unclear. It is possible that one or both serve to recycle the H_2 produced by the membrane bound enzyme to generate NADPH for biosynthesis(29, 47).

In *P. furiosus* and related heterotrophic *Thermococcocales*, S^0 reduction, like H_2 production, was proposed to be a mechanism for disposing of excess reductant (9, 43). H_2 production is now regarded as an energy conserving process (41) but it is not known if this is also true of S^0 reduction. The S^0 reduction system of the mesophilic bacterium *Wolinella succinogenes* is generally accepted as a model system for anaerobic S^0 respiration in which H_2S producion is coupled to energy conservation (17). *W. succinogenes* uses H_2 or formate as the electron donor and their oxidation is linked through cytochrome *b* and quinones to a membrane bound, molybdopterin-containing sulfur reductase (8). A similar S^0-reducing respiratory system has been characterized in other autotrophs, including the hyperthermophilic bacterium *Aquifex aeolicus* (13) and the hyperthermoacidophilic archaeon *A. ambivalens* (27), and it appears to be present in the H_2-oxidizing hyperthermophilic archaea, *Pyrodictium brockii* (36) and *Pyrodictium abyssi* (24).

P. furiosus and the other heterotrophic hyperthermophilic archaea seem to have a different mechanism for S^0 reduction than that found in the autotrophic species. The available genome sequences of three *Pyrococcus* and one *Thermococcus* species (7, 11, 23, 38) do not contain obvious homologs of the molybdenum-containing sulfur reductase of *W. succinogenes* or *A. ambivalens* (2). There are also no reports of the presence of quinones or cytochromes in

these organisms. Three enzymes from *P. furiosus* have been previously reported to possess S^0 reductase activity *in vitro*, the two cytosolic hydrogenases (29) and a sulfide dehydrogenase (30). However, both the activity and the expression of the two hydrogenases dramatically decreased in cells grown in the presence of S^0 (1, 46). Similarly, the sulfide dehydrogenase is now thought to function *in vivo* as a ferredoxin:NADPH oxidoreductase (FNOR) (28), and the expression of its genes is related to the carbon source rather than S^0 (44). Consequently, none of these three enzymes is likely to play a role in S^0 reduction *in vivo*.

In a previous study with *P. furiosus,* the effect of S^0 on the expression of a selected group of genes (271) was investigated using a targeted DNA microarray by comparing cells grown for many generations (as batch cultures) in the presence or absence of S^0 (46). While a significant number of genes were affected, including those encoding the two cytoplasmic hydrogenases (which were down-regulated in S^0-grown cells), this study was limited by a) the small number of genes analyzed, and b) batch-grown cells, where regulated genes involved in the primary metabolism of S^0 could not be distinguished from those causing secondary or other effects. In the present work, the primary response of *P. furiosus* to S^0 has been investigated using a kinetic approach, where S^0 is added to a log-phase culture, and changes in gene expression are analyzed using a complete genome DNA microarray. In addition, the enzyme responsible for NAD(P)H-linked S^0 reduction was characterized independently by biochemical approaches and the up-regulation of the gene encoding it (PF1186) was shown to be a component of the primary response of *P. furiosus* to S^0 addition.

MATERIALS AND METHODS

Growth conditions.

P. furiosus (DSM 3638) was grown in the presence and absence of S^0 with maltose as the primary carbon source. The growth medium was the same as previously reported (1) except that the yeast extract was 1.0 g/L and cysteine (3 mM) was the reducing agent (Na_2S was not

added). Growth experiments to determine the effects of S^0 addition were carried out in 100 ml serum bottles with 50 ml stirred (300 rpm) cultures or in a 20-L custom fermentor (1). Cultures were grown until they reached mid-log phase (0.8 x 10^8 cells/ml) and S^0 (J. T. Baker, Phillipsburg, NJ) was added to a final concentration of 5 and 2 g/L, respectively. To prepare cell extracts, cells were rapidly cooled by pumping the culture from the 20-L fermentor through a glass cooling coil, the cells were collected by centrifugation (10,000 x *g*, 10 min) and were fractionated as previously described (1). Approximately 7 L of the culture was harvested before (time zero) and one hr after S^0 addition. To obtain RNA for microarray and QPCR analyses, samples (2 L) were removed from the fermentor before and at various time points after the addition of sulfur, and were cooled in ice and fractionated as described previously (46).

Gas analyses.

Using the 100 ml cultures, samples (500 µl each) were taken from the liquid and headspace and these were injected into 10 ml anaerobic vials containing an inner reaction vial (500 µl eppendorf tube) surrounded by 0.1 M NaOH (1 ml) to capture H_2S. Sulfuric acid (100 µl of 2.0 M) was added to the inner vial to release acid-labile sulfide from the liquid culture. H_2S production was measured in the NaOH phase of the double vial system using the methylene blue assay (6). H_2 gas was detected in the headspace of the vials using a gas chromatograph (Shimadzu GC-8A). The Bradford method was used to estimate protein concentration in harvested cells using bovine serum albumin as a standard (5).

Enzyme assays.

Intact *P. furiosus* cells were harvested from fermentor mid-log phase cultures by centrifugation (10,000 x *g*, 10 min) and were gently resuspended in fresh growth medium without S^0 or maltose to a final protein concentration of ~15 mg/ml. The production of H_2 and H_2S by intact cells using maltose (50 mM) as the source of reductant was measured in the 10 ml double vial system described above containing 0.1 M NaOH (1 ml). The inner reaction vial (500 µl) contained the reaction mixture (100 µl) including 12.8 g/L colloidal sulfur (Fluka, Milwaukee, WI)

where indicated. NAD(P)H-dependent elemental sulfur oxidoreductase (NSR) activity was measured using the same double vial system. The standard NSR assay mixture (50 µl) contained 50 mM phosphate buffer pH (7.0), 10 mM NAD(P)H, 6.4 g/L (w/v) colloidal sulfur, and 200 µM coenzyme A (CoASH). The mixture was incubated 5 min at 85°C, the reaction was stopped and H_2S was released by the addition to the reaction mixture of 100 µl 2 M H_2SO_4 and quantitated as described above. One unit of NSR catalyzed the production of 1 µmole of H_2S per min under these conditions. Ferredoxin-linked H_2S production was measured by the same method except that NADPH was omitted and the electron donor was ferredoxin reduced by the pyruvate ferredoxin oxidoreductase (POR) of *P. furiosus.* The 50 µl assay mixture contained 50 mM phosphate buffer (pH 7.0), 10 mM pyruvate, 1 mM CoASH, 5 mM ADP, 10 µg ml^{-1} POR, 10 µM ferredoxin, and 6.4 g/L colloidal sulfur. The addition of ADP allows the acetyl CoA that is generated by the POR reaction to be utilized by acetyl CoA synthetase (present in the cell-extract) thereby preventing accumulation of acetyl CoA. The reaction mixture was incubated at 85°C for 10 min and H_2S formation was determined as described above. The kinetic analyses were carried out under the same conditions except that NADPH, NADH, CoASH and CoA disulfide concentrations were varied as indicated. POR and ferredoxin were purified from *P. furiosus* as described previously (45). Polysulfide was prepared as described previously (30) and the final concentration in the assay mixture was 11 mM. NAD(P)H, CoASH, CoASSCoA, CoMSH, glutathione, and dephospho- and desulfo-CoA were purchased from Sigma (St Louis, MO).

RNA extraction and DNA microarray analyses.

Total RNA was extracted from cell-free extracts of *P. furiosus* using acid-phenol (46) and stored at -80°C until needed. The design and construction of DNA microarrays containing all of the predicted 2,192 open reading frames (ORFs) in the annotated genome of *P. furiosus* (37), preparation of cDNA from the RNA samples, and hybridization experiments, were all performed as previously described (46). Fluorescently-labeled cDNA was prepared using the ARES DNA

labeling kit (Molecular Probes, Eugene, OR). The resulting amine-modified cDNA was purified using a QIAquick PCR Purification Kit (Qiagen, Valencia, CA) according to the manufacturer's instructions except that the wash buffer was replaced with 75% (v/v) ethanol and the cDNA was eluted with 45 µl of distilled water and dried under vacuum. The amine-modified cDNA was labeled with Alexa dye 488, 546, 594 or 647 (Molecular Probes) according to the manufacturer's instructions. The labeled cDNA was purified using the QIAquick PCR Purification Kit (Qiagen) and dried under vacuum. Differentially-labeled cDNAs derived from *P. furiosus* cells grown in the absence of S^0 or from cell harvested at various times after S^0 addition (up to 60 min) were pooled, hybridized to the DNA microarray, and the fluorescence intensities for the Alexa dyes were measured as described previously (46). For the microarray experiments, each $\log_2$ value represents an average of two hybridization experiments performed in triplicate using cDNA derived from two different cultures of *P. furiosus*. The $\log_2$ ratios were subjected to an unpaired *t*-test function with two-tailed distribution to get the raw p-values. The raw p-values were subjected to a family-wise error rate (FWER) correction using the Holm's step-down (18) procedure to give final *P*-values. All microarray data is deposited in the NCBI GEO database (ref. GPL4688).

Quantitative PCR.

RNA was isolated as described above and further purified twice using the Absolutely RNA clean up kit (Stratagene, La Jolla, CA) with an intermediate DNase (Ambion, Austin, TX) treatment (30 min, 37°C). cDNA was then prepared as described previously (53). The genes PF1186, PF2051, PF2052, PF1441-PF1453, PF1423-PF1436 and PF2025 were selected for study and the constitutively-expressed gene encoding the POR gamma subunit (PF0971) was selected as a control. Primers for the genes were designed using the program Array Designer v.1.16 (Premier Biosoft International, Palo Alto, CA). All QPCR experiments were carried out using an Mx3000P instrument (Stratagene) using the Brilliant SYBR Green QPCR mastermix

(Stratagene). The comparative cycle threshold (C_T) method was used to analyze the resulting data (Applied Biosystems, Bulletin #2), which are expressed as $\log_2$ fold change ($\Delta\Delta C_t$).

Purification of NSR from *P. furiosus*.

Frozen *P. furiosus* cell paste (100 g) grown on peptides in the presence of S^0 (50) were lysed anaerobically by osmotic shock in 200 ml of 50 mM Tris-HCl (pH 8.0) under argon followed by sonication (Branson Sonifier, 10 min, power setting 4). The cell-free extract (CE) was centrifuged at 120,000 x *g* for 1 hr to fractionate the soluble, cytoplasmic (CT), from the insoluble, membrane (M) fraction. NSR was purified from the cytoplasmic fraction by anaerobic multistep chromatography using an Akta Basic (GE Healthcare, Piscataway, NY). Unless otherwise stated, 50 mM Tris-HCl (pH 8.0) buffer was used and all column chromatography materials were obtained from GE Health Care. The cytoplasmic fraction (340 ml, 5243 mg, 5774 units) was loaded onto a DEAE-Sepharose column (150 ml) at a flow rate of 15 ml min^{-1}. The column was washed with 2 column volumes (CV) of buffer, and eluted with a NaCl gradient (0 - 1.0 M) over 20 CV. NSR eluted as 200-290 mM NaCl was applied to the column. Fractions with the highest specific activity were pooled (330 ml, 1046 mg, 3815 units) and, after diluting with an equal volume of buffer, were loaded onto a Blue Sepharose column (40 ml) at a flow rate of 15 ml min^{-1}, washed with 2 CV, and eluted with a linear gradient of NaCl (0 – 2.0 M over 20 CV) NSR eluted as broad peak between 0.5-1.9 M NaCl. Active fractions were pooled (275 ml, 198 mg, 2163 units), diluted 3-fold with buffer, and loaded onto a Hydroxyapatite (HAP, BioRad) column (40 ml) at a flow rate of 10 ml min^{-1}, and washed with 10 CV of buffer containing 5 mM phosphate (pH 7.4). Some of the activity (254 ml, 33 mg, 491 units) eluted during the wash and was purified separately while the remainder (75 ml, 39 mg, 577 units) eluted when 129-162 mM phosphate was applied as part of a linear gradient of phosphate (5 - 500 mM in 18 CV). The active fractions from the wash and gradient elution steps were pooled separately, and each was diluted with an equal volume of 2.0 M $(NH_4)_2SO_4$ in 50 mM Tris (pH 8.0) and loaded onto a Phenyl Sepharose HP column (20 ml) at a flow rate of 10 ml min^{-1}. The

column was washed with 2 CV of 1.0 M $(NH_4)_2SO_4$ in 50 mM Tris (pH 8.0), and eluted with decreasing concentrations of $(NH_4)_2SO_4$ (1.0 - 0 M over 20 CV). NSR activity was eluted as 575 - 465 mM $(NH_4)_2SO_4$ was applied. The two NSR samples (11 ml, 3 mg, 317 units; and 12 ml, 2.3 mg, 224 units) from the Phenyl Sepharose columns were concentrated separately using a Q-Sepharose FF column (5 ml) and each was loaded onto a Bioscale Q5 column (Biorad, Hercules, CA). NSR activity eluted as 130-150 mM NaCl was applied. The two NSR samples were indistinguishable by SDS-gel analysis and specific activity and were combined to yield 2.0 mg with a total activity of 221 units.

Purification of recombinant NSR.

To clone the gene encoding NSR (PF1186), *att*B-PCR primers were designed based on the Gateway™ Cloning Technology (Invitrogen) with a TEV protease cleavage site two residues upstream of the start site on N-terminus. The forward and reverse primers were: CTTACAAGTTTGTACAAAAAAGCAGGCTTAGAAAACCTGTATTTTCAGGGAGGAGAAAAGA AAAGGTAGTCATAAT and CTTACCACTTTGTACAAGAAAGCTGGGTGTCACAAAACCCTG GCGAGGAC, respectively. Pfu polymerase (Stratagene) was used to amplify the gene of interest from *P. furiosus* genomic DNA and the resulting PCR product was purified using a QIAquick PCR Purification Kit (Qiagen). This was cloned into the destination vector pDEST C1 containing a 6X His-tag, according the manufacturer's protocols (Invitrogen). This destination vector was then transformed into the expression strain of *E. coli* BL21(DE3)pRIL (Stratagene). These were grown aerobically on 2XYT medium in 2.8-L fernbach flasks (1L medium) at 37°C for 6 hrs shaking at 200 rpm before induction with 1 mM isopropyl-beta-D-thiogalactopyranoside (IPTG). After 16 hr at 16°C, cells were harvested (10,000 x *g*, 20 min), resuspended in 100 ml 50 mM Tris-HCl (pH 7.4), degassed under argon and frozen at -20°C. All purification procedures were carried out under anaerobic conditions and all chemicals were acquired from Sigma (St. Louis, MO). Frozen cells (28 g, wet weight) were thawed in the presence of

lysozyme (200 μg ml^{-1}), DNaseI (5 μg ml^{-1}), and PMSF (1 mM) and incubated with shaking at 37°C for 1 hr. The cell extract was sonicated (Branson Sonifier, 10 min, power setting 4), incubated at 80°C for 30 min and then centrifuged (40,000 x *g* for 45 min) to remove denatured proteins. The heat-treated cytoplasmic extract (108 ml, 206 mg) containing 1,650 units of NSR activity was loaded onto a 12 ml Ni-NTA drip column (HIS-Select Nickel Affinity Gel, Sigma) equilibrated with 50 mM Tris-HCl (pH 8.0) containing 0.5 M NaCl. NSR was eluted with 300 mM imidazole in the same buffer. The eluted His-tagged NSR protein (20 ml, 31 mg, 1352 units) was incubated at 23°C for 3 hrs with AcTEV™ Protease according the manufacturer's protocols (Invitrogen), diluted 30-fold in 50 mM Tris-HCl (pH 8.0), and loaded onto the second Ni-NTA column. Protease cleaved NSR, without the N-terminal His-tag, (97 ml, 14.6 mg, 1443 units) did not bind to the column while residual His-tagged protein (18.6 ml, 14.9 mg, 1044 units) was eluted with imidazole as described above. Both proteins were concentrated separately using a Q-sepharose HP column (5 ml), where purified recombinant non-tagged NSR (10 mg, 1672 units) and His-tag NSR (12.5 mg, 1400 units) was obtained.

Other Methods.

SDS-PAGE analysis of purified NSR was performed using 4-20% Long Life Gels (Life Therapeutics, Australia) with a Tris-Hepes buffer system. Samples were heated at 100°C for 10 minutes prior to loading. Gel filtration chromatography was performed using a Superdex S-200 column (320 ml, GE Healthcare) equilibrated with 50 mM Tris-HCl buffer (pH 8.0) containing 300 mM NaCl. MALDI (matrix assisted laser desorption ionization) was performed on Bruker Autoflex (TOF) mass spectrometer. SDS-PAGE gel bands of purified NSR were excised, destained and dehydrated with 50 % acetonitrile in 50 mM NH_4HCO_3 and then digested with 15 μl of 10 μg/ml trypsin for 16 hr. Peptides were then extracted from the gel slice by three 15 min washes (once with 50 mM NH_4HCO_3, and twice with 75 % acetonitrile, 0.5 % TFA). Peptides were purifed using NuTip C-18 tips (Glygen Corp., Columbia, MD) and spotted (1μl, containing

α-cyano-4-hydroxycinnamic acid) directly on MALDI plate. Data analysis was performed in Protein Prospector v 3.2.1 using MS-Fit (http://prospector.ucsf.edu/).

RESULTS

Effects of S^0 on H_2 and H_2S production by intact cells.

P. furiosus has been known to reduce S^0 to H_2S since its discovery (9). Under the growth conditions used here, the amount of H_2S produced by cells grown for many generations in the presence S^0 is comparable to the amount of H_2 produced (per amount of cell protein) by cells grown without S^0 (see Supplementary Figures SA1 and SA2) and cells produce insignificant amounts of the other gas (H_2 in the presence of S^0 or H_2S in the absence of S^0). Both sulfide and hydrogen production rates were closely correlated with cell density, although some abiotic production of sulfide was apparent at the early stage of growth (Figure SA1). This is consistent with the results from a control experiment using the same S^0-containing medium but lacking cells, which showed that sulfide, was produced abiotically, reaching a concentration of approximately 0.5 mM after 1 hr incubation (data not shown). The effect of adding S^0 to a growing *P. furiosus* culture is shown in Figure A1. Within 10 min, H_2S can be detected and the rate of production rapidly increases in parallel with cell growth. Conversely, the rate of H_2 production decreases to almost zero within 1 hr after S^0 addition. Clearly, *P. furiosus* prefers to use S^0 as an electron acceptor rather than protons, and it rapidly adapts when S^0 becomes available. In addition, when S^0 is added, cell growth (as measured by total cellular protein) appears to stall for approximately 20 min before growth is coupled to H_2S production. This suggests that a dramatic physiological response occurs within minutes of S^0 addition.

To determine if the decrease in H_2 production by whole cells upon S^0 addition was related to an effect of S^0 on hydrogenase activity *in vivo*, cells were harvested before and 1 hr after S^0 addition, resuspended in fresh media, and intact cell H_2 production was measured using maltose as the source of reductant. As shown in Figure A2A, both cell types exhibited high H_2

production activities showing that even after 1 hr exposure to S^0, cells contained comparable amounts of the H_2-producing, membrane-bound hydrogenase. Surprisingly, however, when the same assays were conducted with S^0 added to the assay mixture (Figure A2B), H_2 production was clearly inhibited in both cell types. Under these conditions, both cell types have high S^0 reduction activities (Figure A2C). Consequently, growing cells exposed to S^0 for 1 hr, as illustrated in Figure A1, have high hydrogenase activity but do not produce H_2 since reductant is channeled preferentially to S^0. Such cells therefore produce H_2S rather than H_2 due to changes in the pathway of electron flow rather than to the absence or presence of key enzymes. The enzyme primarily responsible for S^0 reduction is discussed below.

Elemental sulfur reductase activities in cell-free extracts.

Cell-free extracts were prepared from intact cells harvested before and 1 hr after addition of S^0 (see Figure A1). Attempts were made to measure S^0 reductase activity using either *P. furiosus* ferredoxin (reduced by *P. furiosus* POR) or NAD(P)H as the electron donor using cell-free extracts and using the cytoplasmic and membrane fractions after a 100,000 x *g* centrifugation step. Sodium dithionite and reduced dyes such as benzyl viologen and methyl viologen could not be used in these assays as they readily reduce S^0 abiotically. Significant ferredoxin-linked S^0 reductase activity could not be measured (above the background) in any fraction, even though cell-free extracts and the membrane fraction exhibited ferredoxin-linked H_2 production (data not shown, see (42)). These results are in contrast to those obtained using the assays described above with intact cells where S^0 reductase activity, as well as hydrogenase activity, was measured using maltose as the electron donor.

In contrast to ferredoxin-linked activity, NADPH-dependent S^0 reductase activity was readily measured in cell-free extracts and in the cytosolic fraction, but not in the membranes. As shown in Figure A3, the activity was greatly stimulated by the addition of CoASH to give a specific activity in the cytoplasm of 0.7 units/mg. The enzyme responsible for the activity was purified from the cytoplasm using anaerobic column chromatography. Only one peak of this

NADPH- and CoASH-dependent activity eluted from the first chromatography column, together with a minor CoASH-independent peak of NADPH-linked S^0-reducing activity, which was due to FNOR (28). The primary S^0-reducing enzyme was purified by three subsequent chromatography steps to a specific activity in S^0 reduction of approximately 100 units/mg, which represented a greater than 140-fold purification compared to the cell-free extract. This NADPH elemental sulfur oxidoreductase, or NSR, has the highest activity reported for any sulfur reductase type enzyme system (13, 30, 33). The purified NSR preparation gave rise to a single protein band when analyzed by SDS-polyacrylamide electrophoresis (Figure SA3) and this corresponded to a molecular weight of approximately 50 kDa. The apparent mass of the holoenzyme from analytical gel filtration was approximately 100 kDa, suggesting that NSR is a homodimer (data not shown). Analysis of the SDS-gel band by trypsin digestion/MS revealed that NSR corresponds to PF1186 (43% coverage), which is predicted to encode a protein of 48,720 Da, in agreement with the biochemical analyses of NSR.

The recombinant form of NSR (rNSR) with an N-terminal His tag was obtained by expression of PF1186 in *E. coli.* The enzyme was purified anaerobically by following its NADPH- and CoASH-dependent S^0 reductase activity. The purified preparation gave rise to a single band after electrophoretic analysis (Figure SA3) and it eluted as an apparent homodimer after analytical gel filtration (data not shown). Purified rNSR had a specific activity of 112 unit/mg in the standard NSR assay. Although the sulfur reductase activity of NSR requires anaerobic conditions (the product sulfide is oxidized by oxygen), neither the native nor recombinant enzymes were oxygen-sensitive (no loss of activity after exposure to air for 16 hr at 23°C), and the two forms had very similar kinetic properties with respect to NADPH and CoASH. The calculated apparent K_m (and V_{max}) values (for the native enzyme) were 8.5 mM (225 units/mg, using 200 μM CoASH) and 18 μM (271 units/mg, using 10 mM NADPH), for NADPH and CoASH, respectively. It should be noted, however, that the enzyme did not exhibit linear kinetics with respect to NADPH as substrate (Supplementary Figure SA4), and this issue is discussed

further below. The native and recombinant enzymes also utilized NADH and CoA disulfide (CoA-SS-CoA) as substrates, although the activities were about 50% lower (data not shown). The calculated apparent K_m (and V_m) values (for the native enzyme) were 3.3 mM (143 units/mg, using 200 μM CoASH) and 10 μM (147 units/mg, using 10 mM NAPDH) for NADH and CoA-SS-CoA, respectively. Colloidal sulfur at a concentration of 6.4 g/L was used in these assays and this appeared to be saturating. Approximately half-maximal activity was measured using 0.64 g/L of colloidal sulfur.

In the NSR assays the rate of sulfide production from colloidal sulfur was linear (up to 10 min) suggesting that this is the true substrate for the enzyme. A lag phase in sulfide production would be expected if polysulfide, which is generated by the reaction of sulfide with elemental sulfur, was the substrate for NSR. Accordingly, less than a 2-fold increase in activity was observed, both at pH 7.0 and 9.0, when polysulfide (11 mM) was used as the substrate, compared to using elemental sulfur (6.4 g/l). Polysulfide is stable only at pH ≥ 8 and readily dissociates to colloidal sulfur and sulfide at neutral pH (14). A much greater stimulation of activity would be observed if polysulfide were the preferred substrate, particularly at the higher pH. Presumably, the colloidal sulfur generated from polysulfide is a better substrate for NSR than the elemental sulfur typically added to the assay mixture (leading to ~ 2-fold increase in activity). The pH optimum for sulfide production (pH 6.5, data not shown) is also consistent with elemental sulfur rather than polysulfide being the substrate of NSR. Given the CoASH-dependence of the reaction, it is possible that polysulfide derivatives of CoASH are generated during catalysis, and this is currently under investigation.

PF1186 is a member of a large family of FAD-dependent pyridine nucleotide-disulphide oxidoreductases (InterPro IPR013027). Accordingly, both native and recombinant forms of NSR were yellow in color and exhibited a UV/visible spectrum characteristic of flavoprotein (A_{460}/A_{280} = 0.13 for the native enzyme). PF1186 and its homolog (PH0572) from *P. horikoshii* were previously proposed to function as NAD(P)H-dependent coenzyme A disulfide reductases

(CoDRs) and the recombinant form of the *P. horikoshii* enzyme was characterized (15). The aerobically-purified *P. horikoshii* CoDR apoprotein was reconstituted with FAD and had a specific activity for coenzyme A disulfide (CoA-S-S-CoA) reduction of approximately 8.3 μmole/min/mg (at 75°C) using NADPH as the electron donor. The reported K_m value for CoA-S-S-CoA (30 μM) is comparable to what was found (10 μM) in the present study using *P. furiosus* NSR in the S^0 reduction assay, although the K_m-value for NADPH and *P. horikoshii* CoDR (< 9μM, (15)) is three orders of magnitude lower that what was determined with *P. furiosus* NSR (8.5 mM). The reason for this discrepancy is discussed below. It should be noted that for the *P. furiosus* enzyme, the specific activity for CoA-S-S-CoA reduction (6.0 μmole CoA-S-S-CoA reduced/min/mg) is about 20-fold lower than the activity that this enzyme exhibits in the S^0 reduction assay. A second discrepancy is that *P. horikoshii* CoADR was reported to be a homotetramer (198 kDa (15)). This is in contrast to results presented here for *P. furiosus* NSR (92% sequence identity), which indicate that it is a homodimer. It was also reported that CoADR activity could not be purified from *P. furiosus* (15), but this attempt utilized cells grown in the absence of S^0. Such cells would be expected to have a much lower content of the product of PF1186, according to the data presented in Figure A2, a conclusion supported by the molecular analyses described below.

These results therefore suggest that the previously reported CoADR activity of the PF1186 homolog (in *P. horikoshii*) represents only the half reaction of its true physiological function, which is now proposed to be CoASH-dependent S^0 reduction. Purified *P. furiosus* NSR did not reduce S^0 to H_2S in detectable amounts in the absence of CoASH (or CoA-S-S-CoA), and this cofactor could not be replaced by dephospho- or desulfo-CoA, nor by glutathione or the methanogenic cofactor coenzyme M. The K_m value for CoASH (10 μM) is much lower than the intracellular concentration in *P. furiosus* (860 μM, (20)) indicating that NSR would normally be saturated. The affinity of *P. furiosus* NSR for NADPH (K_m 8.5 mM) is surprisingly low, however, given the intracellular nicotinamide nucleotide concentration in *P. furiosus* (0.5

mM: (34)). This high apparent K_m value for NADPH may be related to the proposed mechanism of NADPH oxidation by NSR. *P. horikoshii* CoADR (15) is thought to react with two NADPH molecules, one to reduce the active site Cys (from the sulfenic acid derivative) to give the reduced enzyme ("EH_2", which could react with CoA-S-S-CoA generating CoASH), and one to produce the EH_2NADPH active state (in which the FAD remains oxidized). Consequently, the prior kinetic analyses (15) might have only measured the first reaction, while the S^0 reduction reaction reported herein measures the second reaction. This would explain the difference in the kinetic constants for NADPH between this study and the earlier one (15), the non-linear kinetics observed for S^0 reduction (Supplementary Figure SA4) and the apparent high K_m value for NADPH. A detailed study of the mechanism of S^0 reduction by NSR is currently underway. Suffice to say that since NSR only contains one cysteinyl residue, it is feasible that CoASH provides the active site with a second thiol group to enable the two electron reduction of S^0, where the resulting disulfide is reduced by NADPH. Consequently, the ability of NSR to reduce CoA-S-S-CoA appears to be an artifactual side-reaction of the catalytic mechanism and is not thought to have any physiological relevance.

Transcriptional Analyses.

Growth studies showed that *P. furiosus* has a rapid response to the addition of S^0, with H_2S detected within 10 min and a pause in growth for approximately 20 min (Figure A1). Transcriptional analyses of the complete genome (2,192 ORFs, (37)) were therefore conducted on RNA extracted from cells harvested 10, 20, 30 and 60 min after S^0 addition. In spite of the apparent dramatic physiological response (Figure A1), only 19 ORFs were significantly up-regulated more than 3-fold ($p < 0.05$) within 10 min of adding S^0, and a total of 34 were down-regulated. These ORFs are shown in Tables A1 and A2, respectively, together with those that are part of corresponding and potentially-regulated operons. The regulation of these 34 ORFs is proposed to represent the primary response to S^0. QPCR analyses were carried out with selected key ORFs to assess the validity of the DNA microarray data and the results (Figure A4)

are discussed below. In analyzing the data, advantage was taken of the availability of the genome sequences of three other members of the Thermococcales, *Pyrococcus abyssi, P. horikoshii* and *Thermococcus kodakaraensis* (7, 11, 23). All three utilize S^0 and it is assumed that they use the same mechanism as that of *P. furiosus.* Therefore, if a S^0-regulated ORF in *P. furiosus* is not conserved in the other three species, this calls into question a direct role in primary S^0 metabolism.

The Primary Response to S^0 (Up-regulated ORFs).

Within 10 min of the addition of S^0 to a growing culture of *P. furiosus,* the expression of the gene encoding NSR (PF1186) was up-regulated by 3.7 fold according to the DNA microarray (Table A1) and by 7.0-fold using QPCR analysis (Figure A4). These data are consistent with NSR playing a key and primary role in the response of *P. furiosus* to S^0. As shown in Table A1, of the remaining 18 ORFs whose expression is immediately up-regulated upon S^0 addition, 13 of them are arranged as a gene cluster, PF1441-PF1453. QPCR shows that they are up-regulated by an average of 16-fold (Figure A4). This 13-ORF cluster was previously proposed to encode a second membrane bound hydrogenase, MBX, as it shows high sequence identity and conservation of gene order with the 14 ORFs (MBH) that encode the membrane-bound hydrogenase (42). However, MBX lacks two key residues that coordinate the NiFe catalytic site of the hydrogenase (47). Moreover, the up-regulation of MBX is a primary response to S^0, and it has been previously shown that cells grown for multiple generations with S^0 lack significant hydrogenase activity (1), in further support of the contention that MBX is not a hydrogenase. Accordingly, the 14 ORFs that encode MBH, in addition to the 8 ORFs that encode the two cytoplasmic hydrogenases I and II, are dramatically down-regulated within 10 min of S^0 addition (Table A2 and Figure A4). These data therefore indicate that, as a primary response to S^0, the MBX cluster replaces the homologous MBH cluster (Figure A4). Both the Mbh and Mbx operons are highly conserved, in both sequence and in gene order, in *P. horikoshii*, *P. abyssi*

and *T. kodakaraensis* (49), in agreement with the proposed metabolic importance of these complexes in S^0 and H_2 metabolism.

MBH and MBX are part of the NADH dehydrogenase complex I/hydrogenase family which includes NADH:quinone oxidoreductases (NUO or complex I), F_{420} quinone oxidoreductases and energy-converting hydrogenases (Ech) (10, 16). These complexes consist of a core of six homologous subunits and through evolution and recruitment of additional subunits diverged into complexes with different physiological functions (10). For example, the core enzymes of MBH and MBX (MbxH, J-N and MbhH, J-N, respectively) are supplemented with six subunits of a ubiquitous family of cation/proton antiporters (49). Previous studies have shown that MBH is an energy conserving complex in which the oxidation of ferredoxin and the reduction of protons is coupled to the generation of a proton motive force (41). MBH lacks homologs of the NADH- and flavin-binding subunits (NuoEFG) of the typical complex I (10, 16) and couples the oxidation of ferredoxin, rather than NADH, to proton pumping and in this case H_2 production. The remarkable gene conservation and sequence similarity between MBH and MBX suggests that they have very similar functions.

As illustrated in Figure A5, MBX is proposed, like MBH, to oxidize ferredoxin and to conserve energy by pumping protons. The question then becomes, what entity does MBX reduce that ultimately leads to S^0 reduction? The most logical explanation is that MBX reduces NADP and NADPH is reoxidized by NSR as S^0 is reduced to H_2S (Figure A5). However, we were unable to measure ferredoxin-dependent reduction of NADP or of S^0 using a membrane preparation obtained from *P. furiosus* cells harvested from 10 to 60 min after S^0 addition or using cells grown for many generations with S^0. Since the amount of S^0 reduced by growing *P. furiosus* cells approximates the amount of H_2 produced on cellular protein basis (see Supplementary Figure SA2), it would seem likely that MBX and MBH conserve comparable amounts of energy during growth with and without S^0, respectively, and that most, if not all, of reductant used to reduce S^0 flows through MBX. We speculate that our inability to measure an

activity associated with MBX is due to instability of the complex. In this regard, it should be noted that MBH readily loses its ability to use ferredoxin as an electron donor during membrane fractionation (42, 47). Similarly, bacterial complex I has yet to be isolated as an intact complex (54). Attempts to stabilize *P. furiosus* MBX are in progress.

In addition to NSR and MBX, the DNA microarray data (Table A1) show that the expression of the gene encoding a glutaredoxin-like protein termed protein disulfide oxidoreductase (PDO (12, 25)), PF0094, is up-regulated almost 4-fold as part of the primary response to S^0 (Table A1). A specific role for PF0094 as a PDO in *P. furiosus* has yet to be established. It has been proposed that in *Pyrococcus* species PDO is reduced by a thioredoxin reductase (PF1442, (22)) and that it could be an electron carrier for ribonucleotide reductase (PF0440, (3)). However, neither PF1442 nor PF0440 were part of the primary response to S^0, although their expression was up-regulated 60 min after S^0 addition (by 2.3- and 3.8-fold, respectively, data not shown). Since homologs of PDO and thioredoxin reductase (and RNR) are widespread throughout the archaea, including those that do not utilize S^0 (25, 35) it would seem unlikely that PDO has a specific role in reducing S^0. To investigate this, the recombinant form of PF0094 was obtained using published procedures (12). However, the purified protein had no effect on the S^0-reduction activity of purified NSR activity or the ability of *P. furiosus* membranes to couple ferredoxin oxidation to the reduction of NADP or S^0 (data not shown).

In addition to NSR, MBX and PDO, there are only four other ORFs that are significantly up-regulated within 10 min of S^0 addition (Table A1), and these appear to be present as two operons. PF2051 and PF2052 are both annotated as transcriptional regulators but only PF2051 contains regulatory domains (IPR001845), while PF2052 contains a NTP pyrophosphohydrolase domain (IPR004518). Both ORFs most likely form an operon as their sequences overlap by 22 nt, and this synteny is conserved in the genome sequences of the other three Thermococcales. It is possible that these regulators play a key role in the primary response to S^0, although the nature of the effector is unknown. The other two ORFs that are

regulated, PF0261 and PF0262, overlap by 12 nt. PF0262 shows homology to multi drug efflux systems (IPR001036) while PF0261 has a nucleic acid binding fold (IPR008994). Homologs of both ORFs are found in the genomes of the other two *Pyrococcus* species but not in the genome sequence of *T. kodakaraensis*, so their role in S^0 metabolism is unclear.

The Primary Response to S^0 (Down-regulated ORFs).

The most striking feature of the list of 34 ORFs whose expression is down-regulated within 10 min of S^0 addition (Table A2) is that 22 of them encode the structural genes of the three hydrogenases and another involves hydrogenase maturation. It was known that cells grown for many generations with S^0 contain only very low hydrogenase activity (1), and it is now apparent that the biosynthesis of all three hydrogenases is rapidly curtailed within minutes of S^0 addition, indicating a complete shut down at the genetic level of H_2 metabolism in the presence of S^0 (Table A2 and Figure A4). Cells continue to produce H_2 for 2 hrs or so after S^0 addition (Figure A1) due to the existing hydrogenase protein in the cell, but by 1 hr the rate is <10% of the rate of H_2S production, and eventually no H_2 is produced. The small amount of H_2 subsequently consumed (Figure A1) may reflect a differential stability between the membrane-bound hydrogenase (less stable) and the cytoplasmic enzymes, which are proposed to consume H_2 and reduce NADP (29). The hydrogenase genes are well conserved within the Thermococcales, although hydrogenase II, whose exact function is unknown, is absent from *P. horikoshii* and *T. kodakaraensis* (29).

It is difficult to rationalize the roles of the remaining 11 ORFs that are part of the primary response to S^0 (Table A2), particularly when not all of them are conserved in the other three Thermococcales. PF0450 encodes a putative glutamine synthetase but it was not regulated in cells grown for many generations with S^0 (46) and why it is affected so quickly after S^0 addition is puzzling. While PF0450 has homologs in the other sequenced Thermococcales, this is not the case for the other S^0-responsive ORFs, suggesting that they may not be playing essential roles in S^0 metabolism. PF0528-PF0531 appears to form an operon and is annotated as a

cobalt transporter. This operon is conserved in *T. kodakaraensis* but not in *P. horikoshii* or *P. abyssi*. Similarly, PF1621 contains a fibronectin-like fold (IPR008957) but has a homolog only in *T. kodakaraensis.* Since *P. horikoshii* and *P. abyssi* do not utilize sugars like *P. furiosus* and *T. kodakaraensis*, perhaps the latter two ORF systems are involved in sugar metabolism. PF0925-PF0926 are predicted to contain a radical SAM domain but close homologs are absent from *P. horikoshii*, *P. abyssi* and *T. kodakaraensis*. PF0736 and PF0736.1 are hypothetical ORFs on opposing strands and show little sequence similarity to any protein in the NCBI database (2). PF0913 is a homolog of subunit E of formylmethanofuran dehydrogenase, an enzyme found in methanogens, but this is not the catalytic subunit and its function is unknown (52).

The Secondary Response to S^0.

The ORFs that are up-regulated only 10 min after S^0 addition are assumed to represent the primary response and all remain up-regulated at 30 min. At this time, an additional 27 ORFs are more than 3-fold up-regulated (or are part of a potentially-regulated operon) and these appear to represent a secondary response to S^0 (Table A3). This is supported by the fact that most of them (15 of 27) are involved in metabolism of glutamate or branched chain amino acids. PF0204-PF206 and PF1852 are potentially involved in glutamate biosynthesis (21, 44) and these might compensate for down-regulation (by 4.1-fold) of the ORF that encodes glutamate dehydrogenase (data not shown), although why is not clear. Three ORFs involved in iron metabolism are also up-regulated by S^0 (Table A3). Presumably, the production of intracellular sulfide (by cytoplasmic NSR) might lead to insoluble iron sulfides and ORFs involved in ferrous iron transport (PF0857) and iron-sulfur cluster biosynthesis (PF1285, PF1286) are up-regulated in response to the products of S^0 reduction.

In a previous study (46) involving cells grown for many generations with S^0, two highly-regulated S^0-dependent ORFs were characterized as “sulfur induced proteins” A and B (SipA and SipB). We were surprised to find that these are part of the secondary, rather than the primary response to S^0, although the response is quite dramatic and appears to represent an

on/off switch. By QPCR analysis, SipA and SipB are up-regulated over 400-fold and 26-fold, respectively, 30 mins after S^0 addition (Figure A4). They are conserved in the four Thermococcales whose genomes have been sequenced, but their physiological function still remains a mystery. A potential transcription factor, PF0986, which is up-regulated 30 min after S^0 addition might be involved in coordinating the secondary responses to S^0. PF0986 is a homolog of the characterized TFIIS in *Methanococcus thermolithotrophicus,* which is involved in RNA proofreading (26) . PF0986 is potentially in an operon with PF0984, a small 59 residue protein, both of which are conserved in the sequenced Thermococcales (2). However, the relationship of these ORFs to transcriptional regulation and S^0 metabolism is not clear at this point.

In conclusion, while the addition of S^0 to a culture of *P. furiosus* cells causes growth to stall indicating a large metabolic shift (Figure A1), only two key enzymes were identified, MBX and NSR, that appear to be directly involved in S^0 reduction. As shown in Figure A5, MBX and NSR are proposed to be the key enzymes responsible for the reoxidation of ferredoxin and NAD(P)H, respectively. Another primary response to S^0 availability is the concomitant shut-down of H_2 metabolism, resulting in the preferential transfer of reducing equivalents to the reduction of S^0 rather than protons (Figure A5). This novel S^0-reducing system involving NSR and MBX is so far unique to the heterotrophic Thermococcales, and contrasts with the cytochrome- and quinone-based S^0-reducing system in autotrophic archaea (and bacteria). Future research will focus on elucidating the precise role of MBX and the mechanism of S^0 reduction by NSR.

ACKNOWLEDGEMENTS

This research was funded by grants (FG05-95ER20175 and FG02-05ER15710) from the Department of Energy. We thank Peter S. Horanyi for providing the pDEST C1 Gateway expression vector, Cindy Lim for preliminary QPCR studies, Scott D. Hamilton-Brehm for

assistance in constructing the microarrays, Frank E. Jenney, Jr. and Angeli L. Menon for many helpful discussions, and Farris L. Poole II for bioinformatics analyses.

REFERENCES

1. **Adams, M. W. W., J. F. Holden, A. L. Menon, G. J. Schut, A. M. Grunden, C. Hou, A. M. Hutchins, F. E. Jenney, Jr., C. Kim, K. Ma, G. Pan, R. Roy, R. Sapra, S. V. Story, and M. F. Verhagen.** 2001. Key role for sulfur in peptide metabolism and in regulation of three hydrogenases in the hyperthermophilic archaeon *Pyrococcus furiosus*. J. Bacteriol. **183:**716-24.
2. **Altschul, S. F., T. L. Madden, A. A. Schaffer, J. Zhang, Z. Zhang, W. Miller, and D. J. Lipman.** 1997. Gapped BLAST and PSI-BLAST: a new generation of protein database search programs. Nucleic Acids Res **25:**3389-402.
3. **Arner, E. S., and A. Holmgren.** 2000. Physiological functions of thioredoxin and thioredoxin reductase. Eur J Biochem **267:**6102-9.
4. **Blamey, J. M., and M. W. Adams.** 1993. Purification and characterization of pyruvate ferredoxin oxidoreductase from the hyperthermophilic archaeon *Pyrococcus furiosus*. Biochim Biophys Acta **1161:**19-27.
5. **Bradford, M. M.** 1976. A rapid and sensitive method for the quantitation of microgram quantities of protein utilizing the principle of protein-dye binding. Anal Biochem **72:**248-54.
6. **Chen, J. S., and L. E. Mortenson.** 1977. Inhibition of methylene blue formation during determination of the acid-labile sulfide of iron-sulfur protein samples containing dithionite. Anal Biochem **79:**157-65.
7. **Cohen, G. N., V. Barbe, D. Flament, M. Galperin, R. Heilig, O. Lecompte, O. Poch, D. Prieur, J. Querellou, R. Ripp, J. C. Thierry, J. Van der Oost, J. Weissenbach, Y. Zivanovic, and P. Forterre.** 2003. An integrated analysis of the genome of the hyperthermophilic archaeon *Pyrococcus abyssi*. Mol Microbiol **47:**1495-512.

8. **Dietrich, W., and O. Klimmek.** 2002. The function of methyl-menaquinone-6 and polysulfide reductase membrane anchor (PsrC) in polysulfide respiration of *Wolinella succinogenes*. Eur J Biochem **269:**1086-95.

9. **Fiala, G., and K. O. Stetter.** 1986. *Pyrococcus furiosus* sp-nov represents a novel genus of marine heterotrophic archaebacteria growing optimally at 100-degrees C. Arch. Microbiol. **145:**56-61.

10. **Friedrich, T., and D. Scheide.** 2000. The respiratory complex I of bacteria, archaea and eukarya and its module common with membrane-bound multisubunit hydrogenases. FEBS Lett **479:**1-5.

11. **Fukui, T., H. Atomi, T. Kanai, R. Matsumi, S. Fujiwara, and T. Imanaka.** 2005. Complete genome sequence of the hyperthermophilic archaeon *Thermococcus kodakaraensis* KOD1 and comparison with Pyrococcus genomes. Genome Res **15:**352-63.

12. **Guagliardi, A., D. de Pascale, R. Cannio, V. Nobile, S. Bartolucci, and M. Rossi.** 1995. The purification, cloning, and high level expression of a glutaredoxin-like protein from the hyperthermophilic archaeon *Pyrococcus furiosus*. J Biol Chem **270:**5748-55.

13. **Guiral, M., P. Tron, C. Aubert, A. Gloter, C. Iobbi-Nivol, and M. T. Giudici-Orticoni.** 2005. A membrane-bound multienzyme, hydrogen-oxidizing, and sulfur-reducing complex from the hyperthermophilic bacterium *Aquifex aeolicus*. J Biol Chem **280:**42004-15.

14. **Gun, J., A. D. Modestov, A. Kamyshny, D. Ryzkov, V. Gitis, A. Goifman, O. Lev, V. Hultsch, T. Grischek, and E. Worch.** 2004. Electrospray ionization mass spectrometric analysis of aqueous polysulfide solutions. Microchimica Acta **146:**229-237.

15. **Harris, D. R., D. E. Ward, J. M. Feasel, K. M. Lancaster, R. D. Murphy, T. C. Mallet, and E. J. Crane, 3rd.** 2005. Discovery and characterization of a Coenzyme A disulfide

reductase from *Pyrococcus horikoshii*. Implications for this disulfide metabolism of anaerobic hyperthermophiles. Febs J **272:**1189-200.

16. **Hedderich, R., and L. Forzi.** 2005. Energy-converting [NiFe] hydrogenases: more than just H_2 activation. J Mol Microbiol Biotechnol **10:**92-104.
17. **Hedderich, R., O. Klimmek, A. Kroger, R. Dirmeier, M. Keller, and K. O. Stetter.** 1999. Anaerobic respiration with elemental sulfur and disulfides. Fems Microbiol. Rev. **22:**353-381.
18. **Holm, S.** 1979. A simple sequentially rejective multiple test procedure. Scand. J. Statist. **6:**65-70.
19. **Huber, R., H. Huber, and K. O. Stetter.** 2000. Towards the ecology of hyperthermophiles: biotopes, new isolation strategies and novel metabolic properties. FEMS Microbiol Rev **24:**615-23.
20. **Hummel, C. S., K. M. Lancaster, and E. J. Crane, 3rd.** 2005. Determination of coenzyme A levels in *Pyrococcus furiosus* and other Archaea: implications for a general role for coenzyme A in thermophiles. FEMS Microbiol Lett **252:**229-34.
21. **Jongsareejit, B., R. N. Rahman, S. Fujiwara, and T. Imanaka.** 1997. Gene cloning, sequencing and enzymatic properties of glutamate synthase from the hyperthermophilic archaeon *Pyrococcus sp*. KOD1. Mol Gen Genet **254:**635-42.
22. **Kashima, Y., and K. Ishikawa.** 2003. A hyperthermostable novel protein-disulfide oxidoreductase is reduced by thioredoxin reductase from hyperthermophilic archaeon *Pyrococcus horikoshii*. Arch Biochem Biophys **418:**179-85.
23. **Kawarabayasi, Y., M. Sawada, H. Horikawa, Y. Haikawa, Y. Hino, S. Yamamoto, M. Sekine, S. Baba, H. Kosugi, A. Hosoyama, Y. Nagai, M. Sakai, K. Ogura, R. Otsuka, H. Nakazawa, M. Takamiya, Y. Ohfuku, T. Funahashi, T. Tanaka, Y. Kudoh, J. Yamazaki, N. Kushida, A. Oguchi, K. Aoki, and H. Kikuchi.** 1998. Complete

sequence and gene organization of the genome of a hyper-thermophilic archaebacterium, *Pyrococcus horikoshii* OT3. DNA Res **5:**55-76.

24. **Keller, M., and R. Dirmeier.** 2001. Hydrogen-sulfur oxidoreductase complex from *Pyrodictium abyssi*. Methods Enzymol **331:**442-51.

25. **Ladenstein, R., and B. Ren.** 2006. Protein disulfides and protein disulfide oxidoreductases in hyperthermophiles. Febs J **273:**4170-85.

26. **Lange, U., and W. Hausner.** 2004. Transcriptional fidelity and proofreading in Archaea and implications for the mechanism of TFS-induced RNA cleavage. Mol Microbiol **52:**1133-43.

27. **Laska, S., F. Lottspeich, and A. Kletzin.** 2003. Membrane-bound hydrogenase and sulfur reductase of the hyperthermophilic and acidophilic archaeon *Acidianus ambivalens*. Microbiology **149:**2357-71.

28. **Ma, K., and M. W. Adams.** 2001. Ferredoxin:NADP oxidoreductase from *Pyrococcus furiosus*. Methods Enzymol **334:**40-5.

29. **Ma, K., and M. W. Adams.** 2001. Hydrogenases I and II from *Pyrococcus furiosus*. Methods Enzymol. **331:**208-16.

30. **Ma, K., and M. W. Adams.** 1994. Sulfide dehydrogenase from the hyperthermophilic archaeon *Pyrococcus furiosus*: a new multifunctional enzyme involved in the reduction of elemental sulfur. J Bacteriol **176:**6509-17.

31. **Ma, K., R. N. Schicho, R. M. Kelly, and M. W. Adams.** 1993. Hydrogenase of the hyperthermophile *Pyrococcus furiosus* is an elemental sulfur reductase or sulfhydrogenase: evidence for a sulfur-reducing hydrogenase ancestor. Proc Natl Acad Sci U S A **90:**5341-4.

32. **Ma, K., R. Weiss, and M. W. Adams.** 2000. Characterization of hydrogenase II from the hyperthermophilic archaeon *Pyrococcus furiosus* and assessment of its role in sulfur reduction. J Bacteriol **182:**1864-71.

33. **Ng, K. Y., R. Sawada, S. Inoue, K. Kamimura, and T. Sugio.** 2000. Purification and some properties of sulfur reductase from the iron-oxidizing bacterium *Thiobacillus ferrooxidans* NASF-1. J Biosci Bioeng **90:**199-203.

34. **Pan, G., M. F. Verhagen, and M. W. Adams.** 2001. Characterization of pyridine nucleotide coenzymes in the hyperthermophilic archaeon *Pyrococcus furiosus*. Extremophiles **5:**393-8.

35. **Pedone, E., D. Limauro, R. D'Alterio, M. Rossi, and S. Bartolucci.** 2006. Characterization of a multifunctional protein disulfide oxidoreductase from *Sulfolobus solfataricus*. Febs J **273:**5407-20.

36. **Pihl, T. D., L. K. Black, B. A. Schulman, and R. J. Maier.** 1992. Hydrogen-oxidizing electron transport components in the hyperthermophilic archaebacterium *Pyrodictium brockii*. J Bacteriol **174:**137-43.

37. **Poole, F. L., 2nd, B. A. Gerwe, R. C. Hopkins, G. J. Schut, M. V. Weinberg, F. E. Jenney, Jr., and M. W. Adams.** 2005. Defining genes in the genome of the hyperthermophilic archaeon *Pyrococcus furiosus*: implications for all microbial genomes. J Bacteriol **187:**7325-32.

38. **Robb, F. T., D. L. Maeder, J. R. Brown, J. DiRuggiero, M. D. Stump, R. K. Yeh, R. B. Weiss, and D. M. Dunn.** 2001. Genomic sequence of hyperthermophile, *Pyrococcus furiosus*: implications for physiology and enzymology. Methods Enzymol **330:**134-57.

39. **Ronimus, R. S., and H. W. Morgan.** 2003. Distribution and phylogenies of enzymes of the Embden-Meyerhof-Parnas pathway from archaea and hyperthermophilic bacteria support a gluconeogenic origin of metabolism. Archaea **1:**199-221.

40. **Sakuraba, H., and T. Ohshima.** 2002. Novel energy metabolism in anaerobic hyperthermophilic archaea: A modified Embden-Meyerhof pathway. J. Biosci. Bioeng. **93:**441-448.

41. **Sapra, R., K. Bagramyan, and M. W. Adams.** 2003. A simple energy-conserving system: proton reduction coupled to proton translocation. Proc Natl Acad Sci U S A **100:**7545-50.

42. **Sapra, R., M. F. Verhagen, and M. W. W. Adams.** 2000. Purification and characterization of a membrane-bound hydrogenase from the hyperthermophilic archaeon *Pyrococcus furiosus*. J. Bacteriol. **182:**3423-8.

43. **Schicho, R. N., K. Ma, M. W. Adams, and R. M. Kelly.** 1993. Bioenergetics of sulfur reduction in the hyperthermophilic archaeon *Pyrococcus furiosus*. J Bacteriol **175:**1823-30.

44. **Schut, G. J., S. D. Brehm, S. Datta, and M. W. Adams.** 2003. Whole-genome DNA microarray analysis of a hyperthermophile and an archaeon: *Pyrococcus furiosus* grown on carbohydrates or peptides. J Bacteriol **185:**3935-47.

45. **Schut, G. J., A. L. Menon, and M. W. W. Adams.** 2001. 2-ketoacid oxidoreductases from *Pyrococcus furiosus* and *Thermococcus litoralis*. Methods Enzymol. **331:**144-58.

46. **Schut, G. J., J. Zhou, and M. W. W. Adams.** 2001. DNA microarray analysis of the hyperthermophilic archaeon *Pyrococcus furiosus*: evidence for a new type of sulfur-reducing enzyme complex. J. Bacteriol. **183:**7027-36.

47. **Silva, P. J., E. C. van den Ban, H. Wassink, H. Haaker, B. de Castro, F. T. Robb, and W. R. Hagen.** 2000. Enzymes of hydrogen metabolism in *Pyrococcus furiosus*. Eur. J. Biochem. **267:**6541-51.

48. **Stetter, K. O.** 1996. Hyperthermophilic procaryotes. Fems Microbiol. Rev. **18:**149-158.

49. **Swartz, T. H., S. Ikewada, O. Ishikawa, M. Ito, and T. A. Krulwich.** 2005. The Mrp system: a giant among monovalent cation/proton antiporters? Extremophiles **9:**345-54.

50. **Verhagen, M. F., A. L. Menon, G. J. Schut, and M. W. Adams.** 2001. *Pyrococcus furiosus*: large-scale cultivation and enzyme purification. Methods Enzymol **330:**25-30.

51. **Verhees, C. H., S. W. Kengen, J. E. Tuininga, G. J. Schut, M. W. Adams, W. M. De Vos, and J. Van Der Oost.** 2003. The unique features of glycolytic pathways in Archaea. Biochem J **375:**231-46.

52. **Vorholt, J. A., M. Vaupel, and R. K. Thauer.** 1996. A polyferredoxin with eight [4Fe-4S] clusters as a subunit of molybdenum formylmethanofuran dehydrogenase from *Methanosarcina barkeri*. Eur J Biochem **236:**309-17.

53. **Weinberg, M. V., G. J. Schut, S. Brehm, S. Datta, and M. W. Adams.** 2005. Cold shock of a hyperthermophilic archaeon: *Pyrococcus furiosus* exhibits multiple responses to a suboptimal growth temperature with a key role for membrane-bound glycoproteins. J Bacteriol **187:**336-48.

54. **Yagi, T., and A. Matsuno-Yagi.** 2003. The proton-translocating NADH-quinone oxidoreductase in the respiratory chain: the secret unlocked. Biochemistry **42:**2266-74.

Table A1. ORFs whose expression is up-regulated within 10 min after the addition of elemental sulfur to growing *P. furiosus* cells.

ORF	Description[a]	Fold change[b]
PF0094	Protein disulfide oxidoreductase (12)	3.7
[UNKNOWN TRANSPORTER]		
PF0261[c]	[Nucleic acid-binding, OB-fold]	3.5
PF0262[c]	[Acriflavin resistance protein]	2.9
PF1186	NAD(P)H sulfur reductase (this work)	3.7
[MEMBRANE BOUND OXIDOREDUCTASE] (42)		
PF1441	Mbx N	4.3
PF1442	Mbx L	5.0
PF1443	Mbx K	ND
PF1444	Mbx J	8.7
PF1445	Mbx M	4.6
PF1446	Mbx H	5.5
PF1447	Mbx H	6.0
PF1448	Mbx G	6.9
PF1449	Mbx F	4.7
PF1450	Mbx D	8.0
PF1451	Mbx C	8.6
PF1452	Mbx B	9.2
PF1453	Mbx A	12
[TRANSCRIPTIONAL REGULATORS]		
PF2051	[Bacterial regulatory protein, ArsR]	6.5
PF2052	[Uncharacterised conserved protein]	5.6

[a] The ORF description is derived from the best hit in the Interpro database (http://www.ebi.ac.uk/interpro/), given within square brackets, or is from the indicated reference where there are experimental data to support the ORF assignment (given without brackets). Potential operons and their potential functions are indicated in bold.
[b] All fold-changes are statistically significant (p-value <0.05) unless indicated. ND not determined.
[c] No homolog present in the genome sequence of *T. kodakaraensis*.

Table A2. ORFs whose expression is down-regulated within 10 min after the addition of elemental sulfur to growing *P. furiosus* cells.

ORF	Description[a]	Fold change[b]
PF0450	[Glutamine synthetase, catalytic region]	4.2
[COBALT TRANSPORT]		
PF0529[d]	[Cobalt transport protein (CbiQ)]	5.1
PF0530[d]	[Conserved hypothetical protein]	2.6
PF0531[d]	[Cobalamin (vitamin B12) biosynthesis CbiM]	5.6
PF0559	[Hydrogenase maturation protein HypF]	6.3
PF0736[e]	[Conserved hypothetical protein]	5.0
PF0736.1[e]	[Conserved hypothetical protein]	4.1
HYDROGENASE I (31)		
PF0891	Hydrogenase I beta	4.4
PF0892	Hydrogenase I gamma	4.9
PF0893	Hydrogenase I delta	4.0
PF0894	Hydrogenase I alpha	2.9
PF0913[c]	[Formylmethanofuran dehydrogenase, subunit E]	6.1
PF0915	[Cytochrome c biogenesis protein]	3.0
[UNKNOWN]		
PF0925[f]	[Radical SAM]	9.4
PF0926[f]	[Conserved hypothetical protein]	10.2
HYDROGENASE II[g] (32)		
PF1329	Hydrogenase II beta	11.3
PF1330	Hydrogenase II gamma	7.8
PF1331	Hydrogenase II delta	10.0
PF1332	Hydrogenase II alpha	4.4
MEMBRANE BOUND HYDROGENASE (42)		
PF1423	Mbh A	4.4
PF1424	Mbh B	7.2
PF1425	Mbh C	6.5
PF1426	Mbh D	8.0
PF1427	Mbh E	6.8

PF1428	Mbh F	6.7
PF1429	Mbh G	ND
PF1430	Mbh H	5.2
PF1431	Mbh I	5.7
PF1432	Mbh J	ND
PF1433	Mbh K	4.0
PF1434	Mbh L	3.7
PF1435	Mbh M	2.5
PF1436	Mbh N	2.4
PF1621[d]	[Fibronectin, type III-like fold]	4.2

[a] See Table A1.
[b] All fold-changes are statistically significant (p-value <0.05) unless indicated. ND not determined.
[c] No homolog present in *T. kodakaraensis*.
[d] No homologs in *P. horikoshii* and *P abyssi*.
[e] Unique to *P. furiosus*.
[f] No homologs in *T. kodakaraensis*, *P. horikoshii* and *P abyssi***.**
[g] No homologs in *T. kodakaraensis* and *P. horikoshii*

Table A3. ORFs whose expression is up-regulated within 30 min after the addition of elemental sulfur to growing *P. furiosus* cells.

ORF	Description[a]	Fold change[b]
[GLUTAMATE BIOSYNTHESIS]		
PF0204[f]	[Glutamate synthase, large subunit]	4.0
PF0205[f]	[Ferredoxin-dependent glutamate synthase]	2.8
PF0206[f]	[Glutamate synthase, large subunit region 3]	3.2
PF0686[e]	[hypothetical protein]	3.1
PF0704	[Protein of unknown function DUF302]	3.1
PF0857	[Ferrous iron transport protein B, N-terminal]	3.2
[BRANCHED CHAIN AMINO ACID BIOSYNTHESIS]		
PF0935	[Acetolactate synthase, large subunit]	4.6
PF0936	[Acetohydroxy acid isomeroreductase]	4.7
PF0937	[Pyruvate carboxyltransferase]	5.0
PF0938	[3-isopropylmalate dehydratase large subunit]	3.5
PF0939	[3-isopropylmalate dehydratase small subunit]	4.3
PF0940	[Isocitrate/isopropylmalate dehydrogenase]	3.7
PF0941	[2-isopropylmalate/homocitrate synthase]	3.1
PF0942	[6-phosphogluconate dehydratase]	3.2
[TRANSCRIPTION FACTOR]		
PF0984	[hypothetical protein]	3.3
PF0986	[Transcription factor TFIIS]	3.4
[IRON SULFUR CLUSTER ASSEMBLY]		
PF1285[f]	[SufBD]	2.3
PF1286[f]	[SufBD]	3.2
[BRANCHED CHAIN AMINO ACID BIOSYNTHESIS]		
PF1678	[Alpha-isopropylmalate/homocitrate synthase]	5.2
PF1679	[3-isopropylmalate dehydratase large subunit]	6.9
PF1680	[3-isopropylmalate dehydratase small subunit]	4.9
[RIBOSOME]		
PF1823	[Ribosomal L23 protein]	2.6
PF1824	[Ribosomal protein L4/L1e]	4.0

PF1852	[Glutamate synthase (21)]	3.4
[Sulfur Induced Proteins (46)]		
PF2025	SipA	9.3
PF2026	SipB	6.5
PF2029	[hypothetical protein]	3.7

[a-f] See Table A1 and A2 for details.

Figure A1. Effect of S^0 availability on growth of and the production of H_2 and H_2S by *P. furiosus*. Elemental sulfur (S^0, 5 g/L) was added (as indicated by the arrow) to a stirred maltose grown culture (100 ml). Samples for total cell protein (dotted line, closed diamonds), H_2 production (open circles) and H_2S production (open squares) were taken at the indicated times.

FIGURE A1

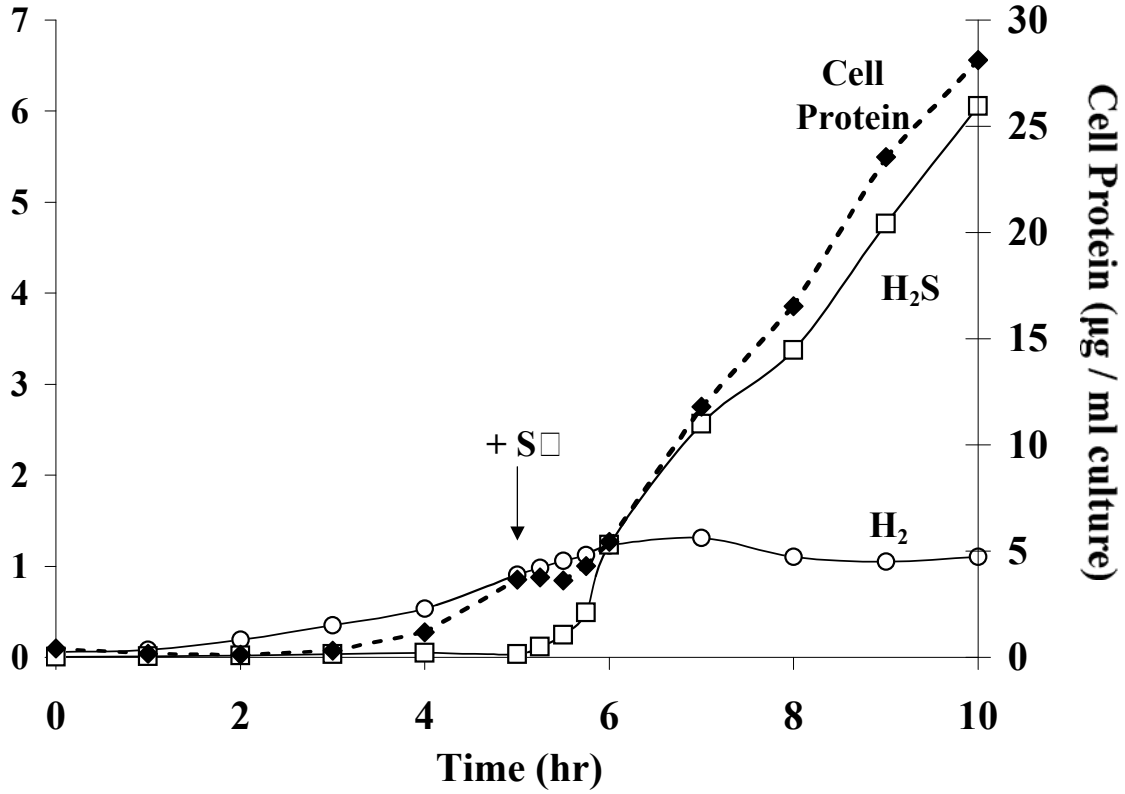
7
6
5
4
3
2
1
0
30
25
20
15
10
5
0
0
2
4
6
8
10
Time (hr)
Cell Protein (μg / ml culture)
Cell Protein
H2S
H2
+ S□

Figure A2. Effect of elemental sulfur on H_2 and H_2S production using intact *P. furiosus* cells. Cells were harvested from a maltose-grown culture before (white bar) and 1 hr after (gray bar) the addition of S^0. Cells were resuspended in fresh media (lacking S^0 or maltose) and their ability to produce H_2 was measured using maltose as the electron donor in the absence (A) and presence (B) of S^0 (colloidal sulfur, 12.8 g/L) in the assay medium. In the case where S^0 was present, the ability of the intact cells to produce H_2S (C) was also measured in the same assay vial.

FIGURE A2

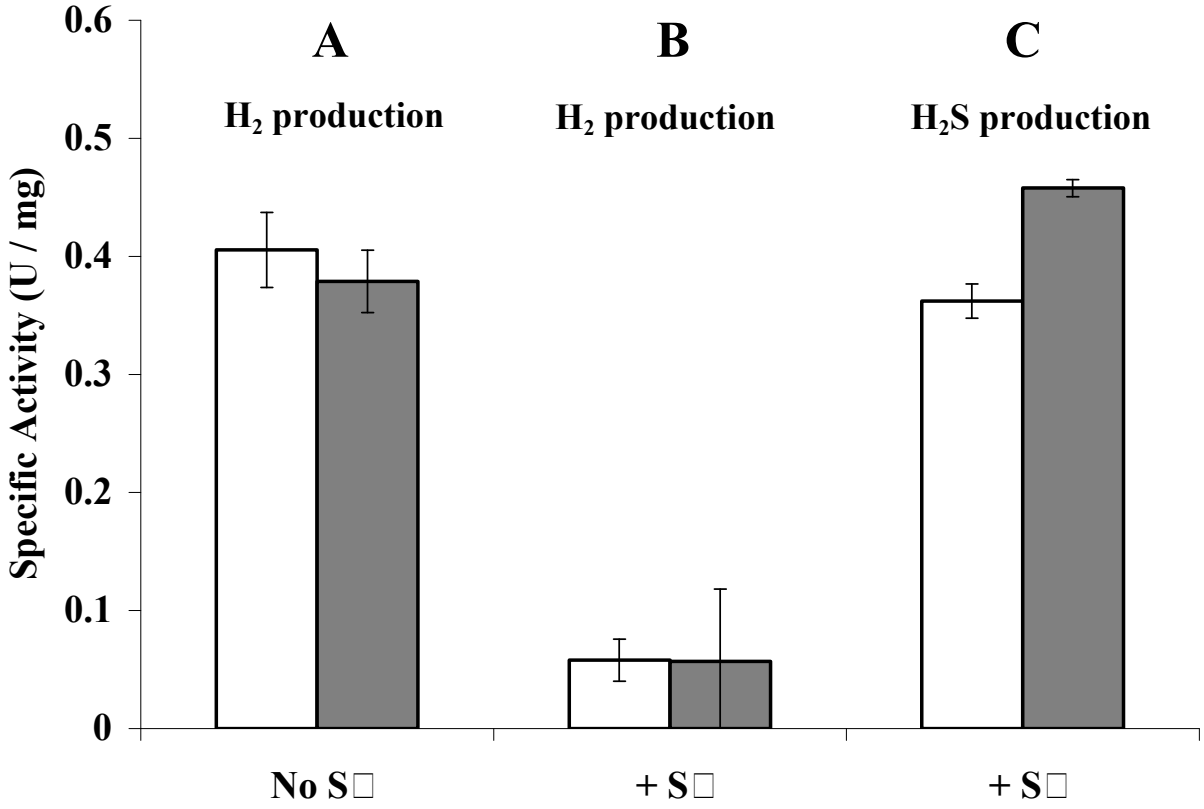
A
B
C
H2 production
H2 production
H2S production
Specific Activity (U / mg)
0.6
0.5
0.4
0.3
0.2
0.1
0
No S□
+ S□
+ S□

Figure A3. NADPH- and CoASH-dependent S^0 reductase activities in cellular fractions of *P. furiosus*. The cells were obtained from a maltose-grown culture prior to (no S^0, white bars) and 1 hr after (S^0/1hr) the addition of S^0 (gray bars). The fractions are cell-free extract (CE), cytoplasm (CT, supernatant after 1 hour at 120,000 x *g*) and membrane (M, pellet after 1 hour 120,000 x *g*). Elemental sulfur reductase activity is expressed as units/mg.

FIGURE A3

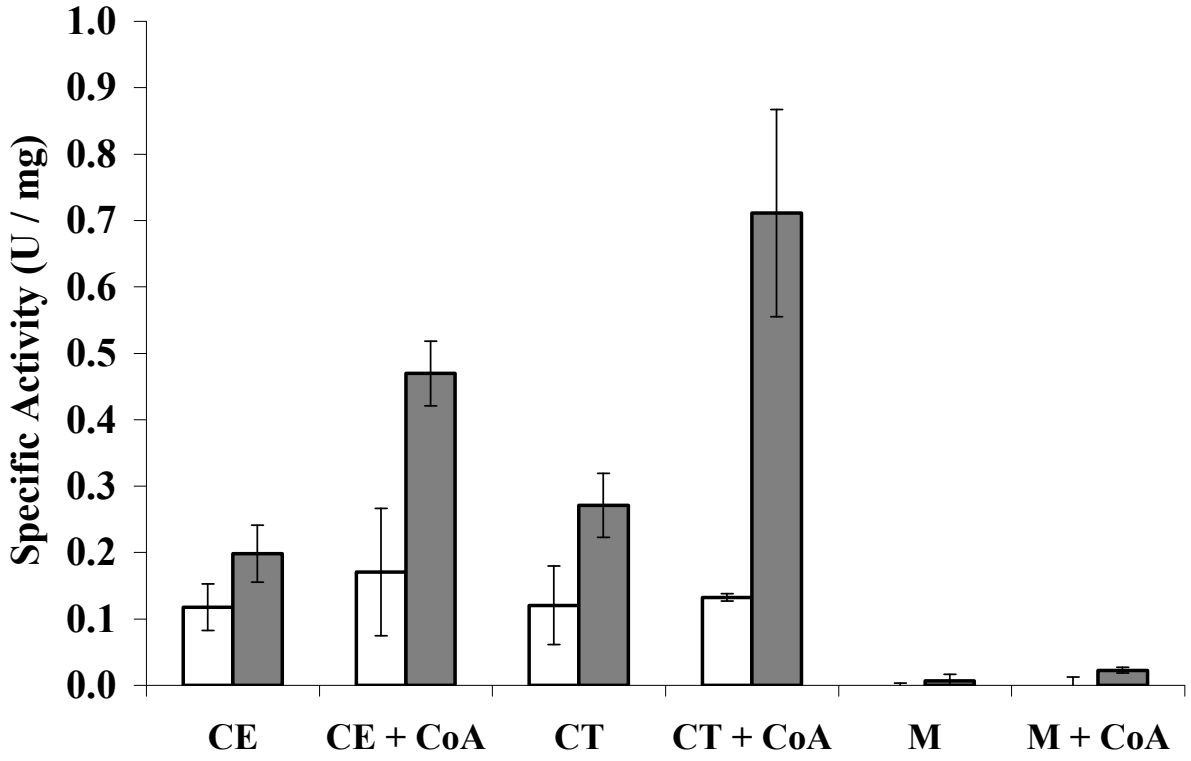
Specific Activity (U / mg)
1.0
0.9
0.8
0.7
0.6
0.5
0.4
0.3
0.2
0.1
0.0
CE
CE + CoA
CT
CT + CoA
M
M + CoA

Figure A4. Real time PCR analysis of the effect of S^0 addition on the transcription of key genes. A 15 liter *P. furiosus* culture was grown with maltose as the carbon source and S^0 was added in mid log phase. RNA samples were prepared at 0, 10, 20, 30, and 60 min after S^0 addition. The genes are: NSR (PF1186, open circles), MBH (PF1423-1436, closed squares), MBX (PF1441-1453, closed triangles), SipA (PF2025, closed diamonds), and putative regulators (PF2051 and PF2052, open squares). In the case of potential co-regulated operons, the average response of all ORFs within the operon was plotted.

FIGURE A4

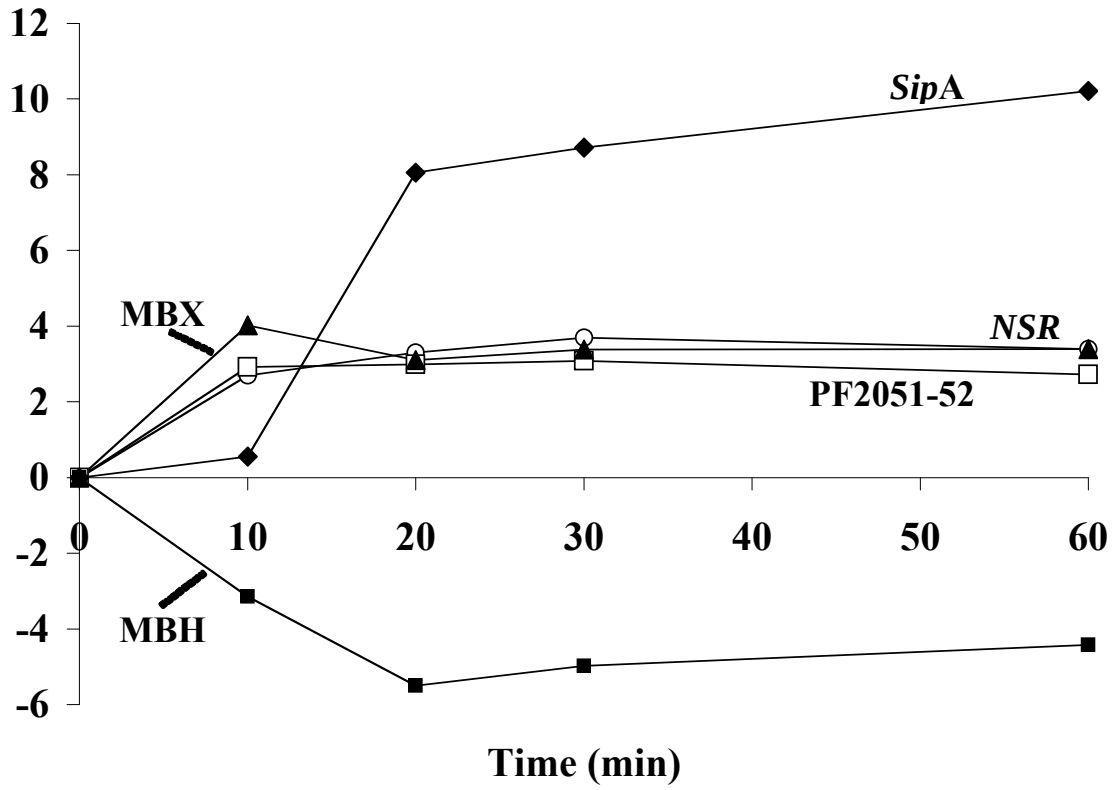
12
10
8
6
4
2
0
-2
-4
-6
0
10
20
30
40
50
60
Time (min)
SipA
NSR
PF2051-52
MBX
MBH

Figure A5. Proposed pathways of electron flow in *Pyrococcus furiosus* in the presence and absence of S^0. The abbreviations are: Fd, ferredoxin; MBH, membrane bound hydrogenase; MBX, membrane bound oxidoreductase; NSR, CoASH-depdendent NAD(P)H elemental sulfur reductase.

FIGURE 2.5

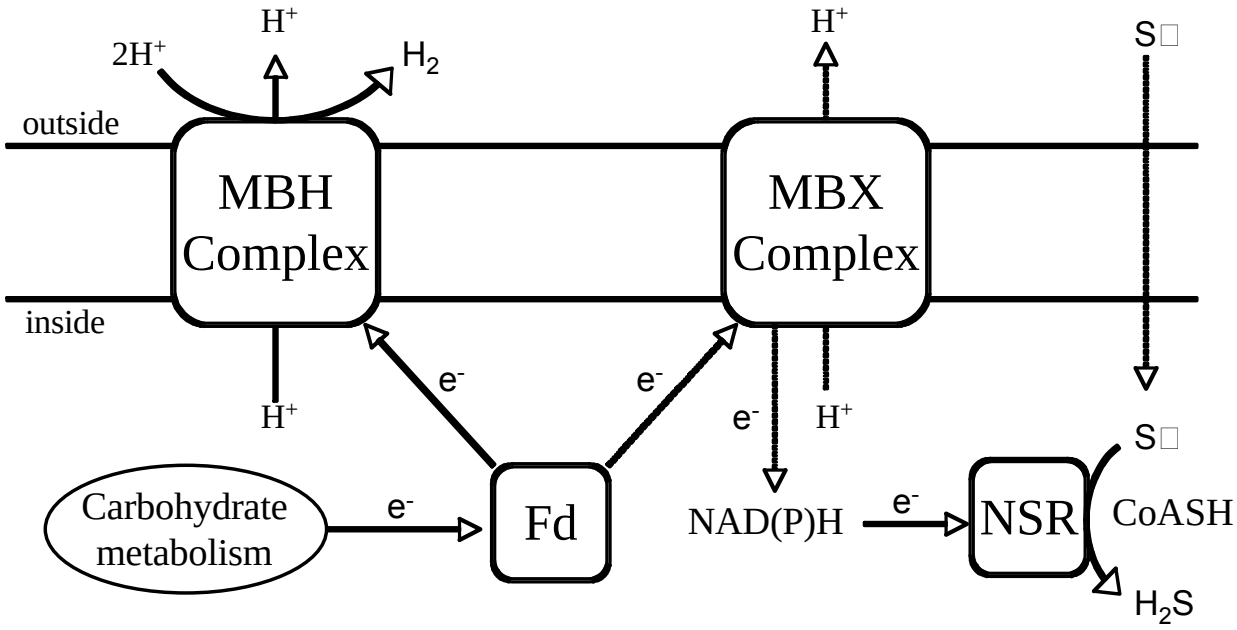
H+
2H+
H2
H+
S
outside
MBH
Complex
MBX
Complex
inside
H+
e-
e-
e-
H+
S
Carbohydrate
metabolism
e-
Fd
NAD(P)H
e-
NSR
CoASH
H2S

SUPPLEMENTAL MATERIAL

Table SA1. ORFs whose expression is significantly (p-value<0.05) down-regulated within 30 min after the addition of elemental sulfur to growing cells of *P. furiosus*.

ORF	Description	Expression change (fold)
[Unknown transporter]		
PF0004	[hypothetical protein]	3.7
PF0005	[ABC transporter related]	4.0
PF0121	Aromatic aminotransferase (1)	7.1
PF0164	[Aminotransferase, class V]	3.2
PF0289	[Phosphoenolpyruvate carboxykinase (2)]	3.2
PF0346	Aldehyde ferredoxin oxidoreductase (9)	5.3
PF0477	Alpha amylase (4)	4.0
[Aromatic amino acid degradation]		
PF0532	Acetyl-CoA synthetase II (3)	3.3
PF0533	Indole pyruvate Fd:oxidoreductase beta (8)	3.1
PF0534	Indole pyruvate Fd:oxidoreductase alpha (8)	2.4
PF0547	[Cobalamin synthesis protein/P47K]	4.7
PF0552	[Bile acid:sodium symporter]	5.8
PF0580	[IMP dehydrogenase/GMP reductase]	3.6
PF0581	[IMP dehydrogenase/GMP reductase]	2.9
PF0602	[FMN-binding split barrel]	3.3
PF0613	[Fructose 1,6-bisphosphatase (10)]	4.0
PF0846	[TatD-related deoxyribonuclease]	3.3
PF0915	[Cytochrome c biogenesis protein, transmembrane region]	3.1
PF0924	[hypothetical protein]	3.0
PF0927	[Nucleotide binding protein, PINc]	3.2
PF0928	[(Trans)glycosidases]	4.8
[3-hydroxy-3-methylglutaryl-CoA-synthase related]		
PF0972	[3-hydroxy-3-methylglutaryl-CoA-synthase, archaeal]	5.9
PF0973	[Thiolase]	6.3

PF0974	[Protein of unknown function DUF35]	6.6
PF0975	[Peptidase M52, hydrogen uptake protein]	3.1
PF1013	[Hypothetical protein]	6.5
[Unknown carbohydrate binding]		
PF1109	[APHP (CARDB)]	2.4
PF1110	[Carbohydrate-binding family 9, cellobiose dehydrogenase cytochrome]	3.5
[Oxidative stress related]		
PF1195	[Ferritin/ribonucleotide reductase-like]	4.3
PF1196	[Rubrerythrin]	3.8
PF1197	NAD(P)H rubredoxin:oxidoreductase (7)	3.5
[Proline metabolism]		
PF1245	[BFD-like [2Fe-2S]-binding region]	3.3
PF1246	[FAD dependent oxidoreductase]	2.3
Ferredoxin NAD(P)H:oxidoreductase (6)		
PF1327	Ferredoxin NAD(P)H:oxidoreductase alpha	4.4
PF1328	Ferredoxin NAD(P)H:oxidoreductase beta	3.8
PF1333	PfkB (PfkB)	3.0
[Thiamine metabolism]		
PF1336	[Permease for cytosine/purines, uracil, thiamine, allantoin]	6.3
PF1337	[TENA/THI-4 protein]	5.1
PF1338	[TENA/THI-4 protein]	4.4
PF1339	[Protein of unknown function DUF257]	2.8
PF1340	[von Willebrand factor, type A]	2.8
PF1341	[Glycine cleavage T protein]	3.5
PF1421	[Aminotransferase class-III]	3.9
PF1481	[OsmC-like protein]	3.9
PF1482	[ThiamineS]	3.3
PF1497	Alanine aminotransferase (13)	3.0
PF1532	NAD(P)H oxidase (12)	4.0
PF1602	Glutamate dehydrogenase (11)	4.1
PF1687	[Corticotropin-releasing factor, CRF]	3.1
Aromatic amino acid biosynthesis		

PF1692	[Dehydroquinase class I]	3.4
PF1693	[Shikimate/quinate 5-dehydrogenase]	2.1
PF1702	[Aminotransferases class-I pyridoxal-phosphate-binding site]	2.9
PF1703	[NAD(P)-binding Rossmann-fold domains)	3.0
PF1705	[Tryptophan synthase, alpha chain]	4.2
PF1706	[Tryptophan synthase, beta chain and related]	4.9
PF1707	[Ribulose-phosphate binding barrel]	5.8
PF1708	[WD-40 repeat]	6.1
PF1709	[Anthranilate synthase component I and chorismate binding protein]	6.7
PF1710	[Glycosyl transferase, family 3]	4.5
PF1711	[Indole-3-glycerol phosphate synthase]	5.6
Proline metabolism		
PF1795	[2Fe-2S ferredoxin, iron-sulfur binding site]	2.8
PF1796	[4Fe-4S ferredoxin, iron-sulfur binding]	2.7
PF1797	[BFD-like [2Fe-2S]-binding region]	3.6
PF1798	[FAD dependent oxidoreductase]	1.6
PF1853	[Glucose/ribitol dehydrogenase]	3.5
Maltose transporter II (5)		
PF1933	ATP-binding protein (MalK)	3.0
PF1934	Amylopullulanase*	4.0
PF1935	Amylopullulanase	4.4
PF1936	Permease (MalG)	4.2
PF1937	Permease (MalF)	5.4
PF1938	Maltose binding protein (MaLE)	3.5
Glycine metabolism		
PF1999	[Glycine cleavage system P-protein]	6.0
PF2000	[Glycine cleavage system P-protein]	5.8

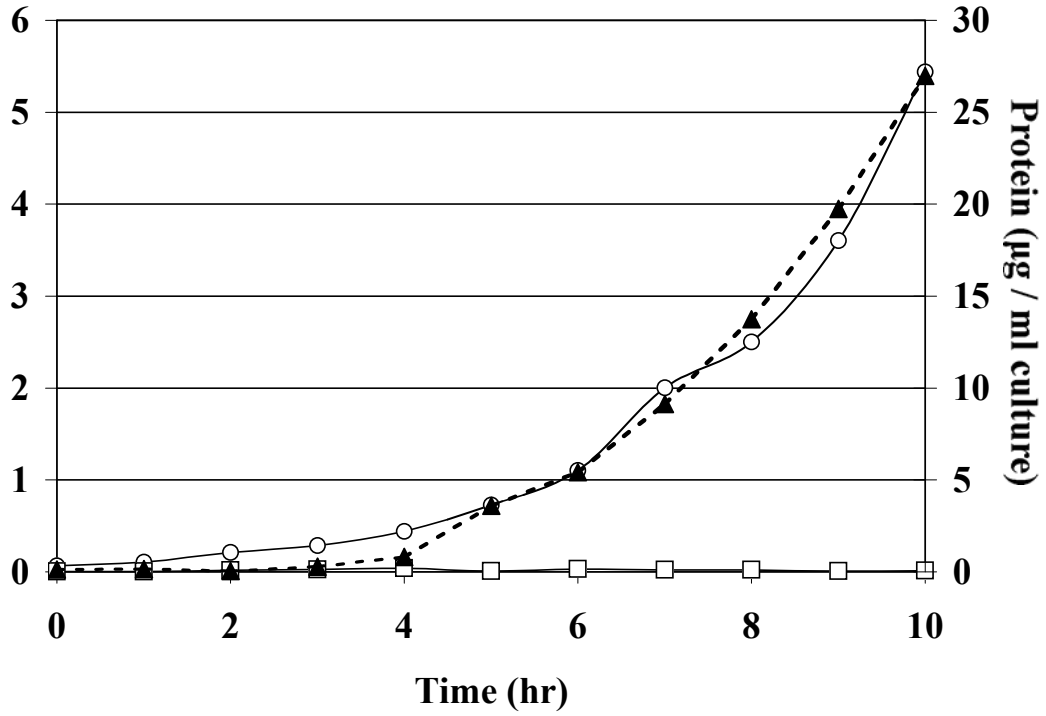

Figure SA1. H_2/H_2S production in *P. furiosus* during growth on maltose without S^0. Samples for total cell protein (dotted line, closed triangles), hydrogen production (open circles) and hydrogen sulfide production (open squares) were taken at set intervals.

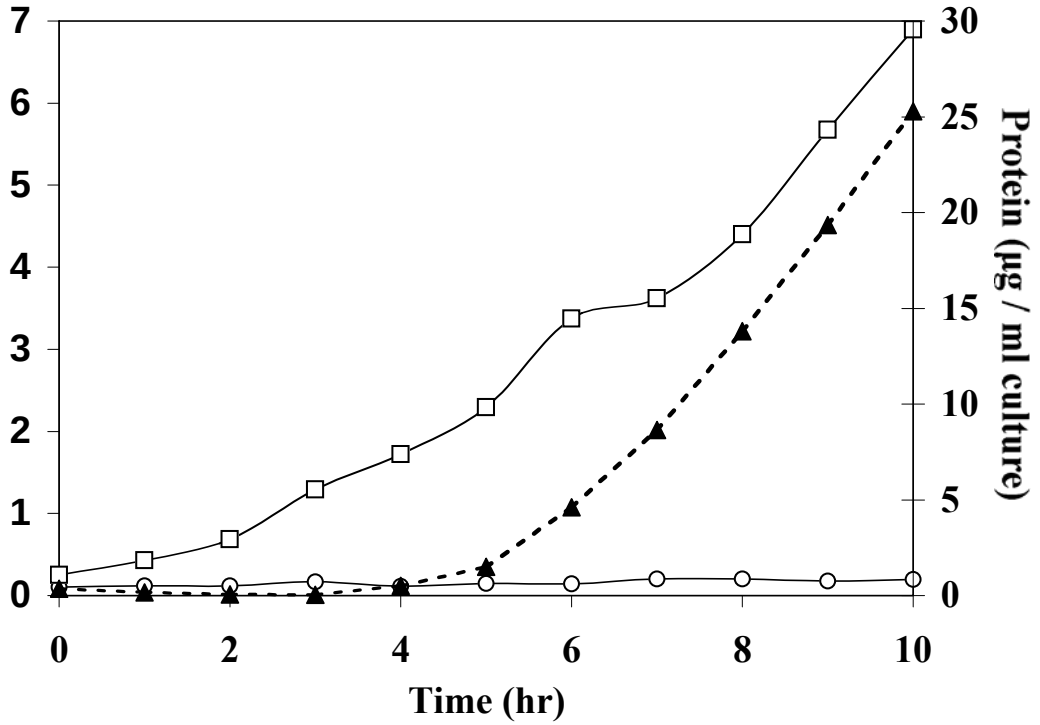

Figure SA2. H_2/H_2S production in *P. furiosus* during growth on maltose with S^0. Samples for total cell protein (dotted line, closed triangles), hydrogen production (open circles) and hydrogen sulfide production (open squares) were taken as indicated.

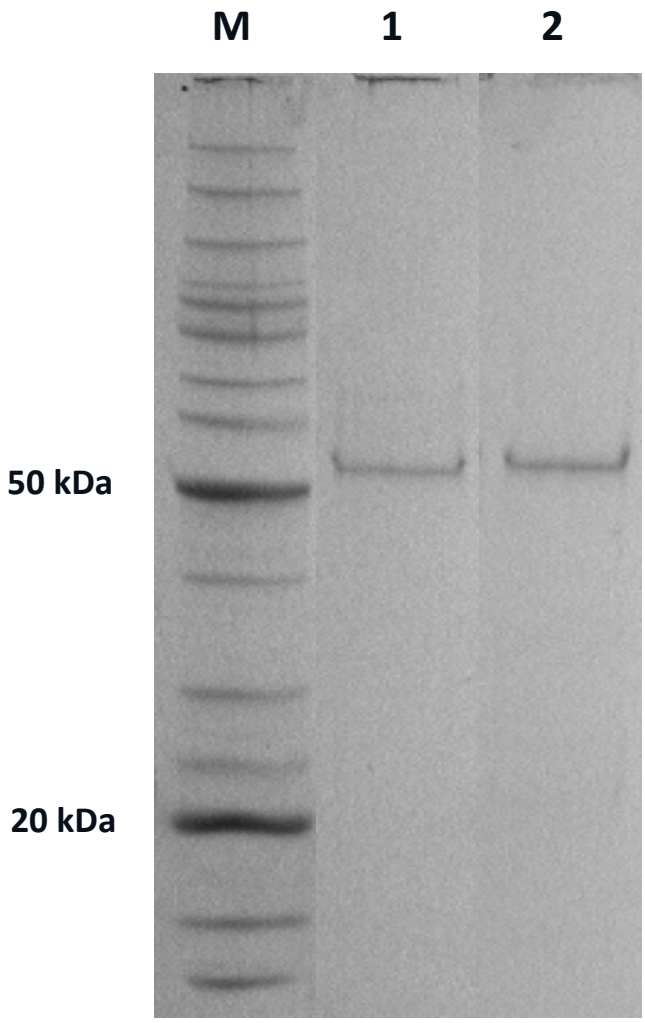

Figure SA3. SDS-PAGE analysis of purified native and recombinant NSR (PF1186). SDS-PAGE analysis (4-20%) of purified native (lane 1) and recombinant (lane 2) NSR, where (M) is the protein standard (Invitrogen BenchMark™ Protein Ladder). The gel was stained with Coomassie Brilliant Blue.

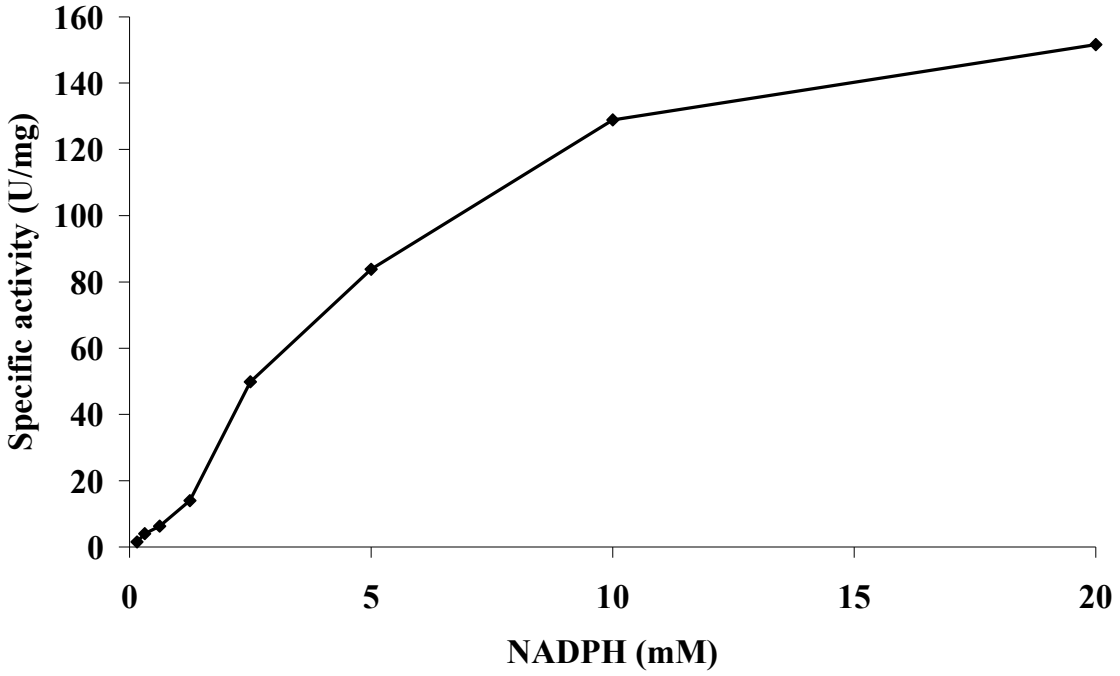

Figure SA4. Kinetic Analysis of NSR using NADPH as the variable substrate. Specific activity is defined as μmole H_2S/mg protein/min.

SUPPLEMENTAL REFERENCES

1. **Andreotti, G., M. V. Cubellis, G. Nitti, G. Sannia, X. Mai, M. W. Adams, and G. Marino.** 1995. An extremely thermostable aromatic aminotransferase from the hyperthermophilic archaeon *Pyrococcus furiosus*. Biochim Biophys Acta **1247:**90-6.
2. **Fukuda, W., T. Fukui, H. Atomi, and T. Imanaka.** 2004. First characterization of an archaeal GTP-dependent phosphoenolpyruvate carboxykinase from the hyperthermophilic archaeon *Thermococcus kodakaraensis* KOD1. J Bacteriol **186:**4620-7.
3. **Hutchins, A. M., J. F. Holden, and M. W. W. Adams.** 2001. Phosphoenolpyruvate synthetase from the hyperthermophilic archaeon *Pyrococcus furiosus*. J. Bacteriol. **183:**709-15.
4. **Jorgensen, S., C. E. Vorgias, and G. Antranikian.** 1997. Cloning, sequencing, characterization, and expression of an extracellular alpha-amylase from the hyperthermophilic archaeon *Pyrococcus furiosus* in *Escherichia coli* and *Bacillus subtilis*. J Biol Chem **272:**16335-42.
5. **Koning, S. M., W. N. Konings, and A. J. Driessen.** 2002. Biochemical evidence for the presence of two alpha-glucoside ABC-transport systems in the hyperthermophilic archaeon *Pyrococcus furiosus*. Archaea **1:**19-25.
6. **Ma, K., and M. W. Adams.** 2001. Ferredoxin:NADP oxidoreductase from *Pyrococcus furiosus*. Methods Enzymol **334:**40-5.
7. **Ma, K., and M. W. Adams.** 1999. A hyperactive NAD(P)H:Rubredoxin oxidoreductase from the hyperthermophilic archaeon *Pyrococcus furiosus*. J Bacteriol **181:**5530-3.
8. **Mai, X., and M. W. Adams.** 1996. Purification and characterization of two reversible and ADP-dependent acetyl coenzyme A synthetases from the hyperthermophilic archaeon *Pyrococcus furiosus*. J Bacteriol **178:**5897-903.

9. **Mukund, S., and M. W. Adams.** 1991. The novel tungsten-iron-sulfur protein of the hyperthermophilic archaebacterium, *Pyrococcus furiosus*, is an aldehyde ferredoxin oxidoreductase. Evidence for its participation in a unique glycolytic pathway. J Biol Chem **266:**14208-16.

10. **Rashid, N., H. Imanaka, T. Kanai, T. Fukui, H. Atomi, and T. Imanaka.** 2002. A novel candidate for the true fructose-1,6-bisphosphatase in archaea. J Biol Chem **277:**30649-55.

11. **Robb, F. T., J. B. Park, and M. W. Adams.** 1992. Characterization of an extremely thermostable glutamate dehydrogenase: a key enzyme in the primary metabolism of the hyperthermophilic archaebacterium, *Pyrococcus furiosus*. Biochim Biophys Acta **1120:**267-72.

12. **Ward, D. E., C. J. Donnelly, M. E. Mullendore, J. van der Oost, W. M. de Vos, and E. J. Crane, 3rd.** 2001. The NADH oxidase from *Pyrococcus furiosus*. Implications for the protection of anaerobic hyperthermophiles against oxidative stress. Eur J Biochem **268:**5816-23.

13. **Ward, D. E., S. W. Kengen, J. van Der Oost, and W. M. de Vos.** 2000. Purification and characterization of the alanine aminotransferase from the hyperthermophilic archaeon *Pyrococcus furiosus* and its role in alanine production. J Bacteriol **182:**2559-66.